Thesis

Nonequilibrium quantum many-body phenomena in Floquet systems

Kaoru Mizuta

January, 2022

Abstract

Periodically-driven (Floquet) systems are one of the most important classes in nonequilibrium physics, which are modulated periodically in time. They have various realizations, such as materials under laser light and AMO (atomic, molecular and optical) systems. In addition, due to their time-dependency, they can host various quantum phenomena inherent in nonequilibrium beyond conventional equilibrium physics. Floquet systems also enable the control of materials by periodic drive, which is called "Floquet engineering." These various platforms, nonequilibrium properties, and applications have brought extremely rapid growth of Floquet systems during the past decade, giving fundamental comprehension of nonequilibrium physics and technical developments related to optical devices, quantum simulations, and quantum computation.

One of the most significant interests in Floquet systems in recent years may be :

What kinds of nonequilibrium phenomena take place when nonequilibrium properties inherent in Floquet systems and quantum many-body properties induced by interactions coexist ?

As mentioned before, nonequilibrium properties are keys for Floquet systems to surpass conventional equilibrium setups. A representative example is an anomalous Floquet topological insulator, in which a winding number, emerging from the breakdown of the conventional band picture in static systems, characterizes topological natures. On the other hand, quantum many-body properties bring various basic but nontrivial phenomena in condensed matter physics, well-known for crystals, ferro- or antiferro-magnets, and superconductors. Thus, Floquet systems with the interplay of nonequilibrium and quantum many-body properties, dubbed *Floquet many-body systems*, are intriguing fields lying in the frontier of nonequilibrium condensed matter physics.

Unfortunately, there exists a notorious problem called *heating problem*, which is believed to valid for nonintegrable closed Floquet many-body systems from some numerical studies. Briefly speaking, the heating problem dictates that any nonintegrable closed Floquet systems always relax to featureless states after a long time as a result of *Floquet Eigenstate Thermalization Hypothesis* (Floquet-ETH). Does this immediately mean that Floquet many-body systems host no interesting nonequilibrium phenomena ? The answer is actually no, as a series of recent studies have revealed various stimulating many-body phenomena in Floquet setups. We should explore several directions to realize nontrivial phenomena that overcome the heating problem as follows:

1. Ordered and topological phases on quasi-steady states in intermediate time regime
2. Ordered and topological phases in localized Floquet many-body systems
3. Nonequilibrium dynamics and steady states in dissipative Floquet many-body systems

Each of the fields 1., 2., and 3. breaks some part of the assumptions, "after a long time," "nonintegrable," and "closed" in the heating problem (or Floquet-ETH) respectively, thereby enabling its own nontrivial physics. Simultaneously, we should note that the heating problem (or Floquet-ETH) is merely an empirical law confirmed by some numerical simulations. Therefore, it is nontrivial whether the heating problem completely prohibits steady states other than featureless thermal ones. To be precise, it is also a significant question whether there exist

4. Athermal steady states in nonintegrable closed Floquet many-body states

as opposed to featureless thermal steady states expected from the heating problem.

In this thesis, we focus on nontrivial nonequilibrium dynamics and steady states in Floquet many-body systems, which cover the above fields 1., 3., and 4., as follows:

Resonant prethermal phases and resonant Floquet engineering (Chapter 2) — The high-frequency regime, where the local energy scale of the Hamiltonian is much smaller than the driving frequency, can host nontrivial quantum many-body phenomena during their quasi-steady states before heating to featureless steady states. However, in the high-frequency regime, the stroboscopic dynamics of Floquet systems completely corresponds to that of static local Hamiltonians, indicating the absence of unique nonequilibrium properties in this regime. In our study, we consider a hybrid regime, where high-frequency drives and resonant drives having comparable energy scale to the frequency coexist. Compared to the high-frequency regime, this hybrid regime can host unique nonequilibrium phenomena such as prethermal discrete time crystals. We construct a perturbative method to analyze their quasi-steady states with emergent unitary symmetries and prethermal discrete time crystals. Furthermore, we also propose a new protocol for Floquet engineering, with which we can simultaneously control phases and symmetries by resonant drives.

Emergent non-Markovianity in dissipative Floquet systems (Chapter 3) — We consider dissipative Floquet many-body systems which break the assumption "closed" in Floquet-ETH. They are typically described by Floquet-Lindblad equations when we assume Markovianity. While they are expected to host athermal steady states by avoiding the heating problem, their universal nature has remained a mystery because of their complexity caused by the coexistence of periodic drives, interactions, and dissipation. In our study, we focus on the high-frequency regime, and uncover that dissipative Floquet many-body systems universally show emergent non-Markovianity due to the spread of interactions. This result indicates that dissipative Floquet systems have no counterparts in dissipative static systems under Markovianity even in the high-frequency regime, in contrast to closed Floquet systems which have no unique nonequilibrium effect compared to static systems in the same regime.

Exact Floquet quantum many-body scars under Rydberg blockade (Chapter 4) — Floquet-ETH is just an empirical law confirmed by some numerical simulations. It is a crucial and fundamental question whether nontrivial athermal steady states appear in Floquet many-body systems satisfying all the assumptions of Floquet-ETH, "nonintegrability," "isolation," and "infinite lifetime." In our study, we tackle this question by constructing a counter example of Floquet-ETH, called Floquet quantum many-body scars. We consider a one-dimensional system with extremely strong repulsive interactions, recently observed in Rydberg atoms experiments. By exploiting a binary drive composed of two static Hamiltonians showing static quantum many-body scars, our model shows athermal persistent oscillations under some special initial states, while all the other initial states relax to infinite-temperature states. This anomalous behavior dependent on the initial conditions contradicts the consequence of Floquet-ETH or the heating problem, and exemplifies a novel nonequilibrium phenomena in nonintegrable closed Floquet many-body systems.

Contents

List of publications

Papers related to the thesis

1. **Kaoru Mizuta**, Kazuaki Takasan, and Norio Kawakami
High-frequency expansion for Floquet prethermal phases with emergent symmetries: Application to time crystals and Floquet engineering
Physical Review B **100**, 020301(R) (2019)

2. **Kaoru Mizuta**, Kazuaki Takasan, and Norio Kawakami
Floquet engineering of topological phases protected by emergent symmetries under resonant drives
Physical Review A **100**, 052109 (2019)

3. **Kaoru Mizuta**, Kazuaki Takasan, and Norio Kawakami
Exact Floquet quantum many-body scars under Rydberg blockade
Physical Review Research **2**, 033284 (2020)

4. **Kaoru Mizuta**, Kazuaki Takasan, and Norio Kawakami
Breakdown of Markovianity by interactions in stroboscopic Floquet-Lindblad dynamics under high-frequency drive
Physical Review A **103**, L020202 (2021)

Papers not included in the thesis

5. **Kaoru Mizuta**, Kazuaki Takasan, Masaya Nakagawa, and Norio Kawakami
Spatial-Translation-Induced Discrete Time Crystals
Physical Review Letters **121**, 093001 (2018)

6. Ken Mochizuki, **Kaoru Mizuta**, and Norio Kawakami
Fate of topological edge states in disordered periodically driven nonlinear systems
Physical Review Research **3**, 043112 (2021)

7. **Kaoru Mizuta**, Mikiya Fujii, Shigeki Fujii, Kazuhide Ichikawa, Yukihiro Okuno, and Yuya O. Nakagawa
Deep variational quantum eigensolver for excited states and its application to quantum chemistry calculation of periodic materials
Physical Review Research **3**, 043121 (2021)

Chapter 1

Introduction

1.1 Floquet systems

Floquet systems are one of the classes of nonequilibrium systems, driven periodically in time. In the case of quantum systems isolated from environments, they are described by time-dependent Schrödinger equation:

$$i\frac{d}{dt}\left|\psi(t)\right\rangle = H(t)\left|\psi(t)\right\rangle, \quad H(t) = H(t+T). \tag{1.1}$$

Here, a quantum state $|\psi(t)\rangle$ is an element of a Hilbert space $\mathcal{H}$ with the normalization $\langle\psi(t)|\psi(t)\rangle = 1$, and a time-periodic Hamiltonian $H(t)$ is a linear map from $\mathcal{H}$ to $\mathcal{H}$. Throughout this thesis, we set the Planck constant as $\hbar = 1$ and consider a finite-dimensional Hilbert space $\mathcal{H}$.

The center of today's condensed matter physics is static or equilibrium systems dominated by a time-independent Hamiltonian H. They are described by well-established theories for time-independent Schrödinger equation or the equilibrium partition function $Z = \mathrm{Tr}[\exp(-\beta H)]$. The difference between conventional equilibrium systems and Floquet systems is just the time-dependency, but this is essential for Floquet systems to have unique nonequilibrium phenomena due to the absence of energy conservation and the breakdown of statistical physics for equilibrium. The time-periodicity of Floquet systems is also important in that it gives simple but various experimental platforms and works as discrete time translation symmetry inherent in time-dependent systems. Floquet systems have experienced the rapid growth both in theories and experiments during the past decade, and have attracted much interest compared to conventional equilibrium systems and other nonequilibrium systems, mainly due to the following characteristics of Floquet systems.

Various platforms for Floquet systems

There are several experimental platforms rapidly developing in recent years for Floquet systems. They directly realize time-periodic Hamiltonians, or indirectly provide Floquet systems by realizing unitary dynamics equivalent to that in Floquet systems.

Solid materials under laser light.— The first typical platform for Floquet systems is materials coupled with classical light. Let us consider a material described by a tight-binding Hamiltonian

$$H = \sum_{\vec{k}\in G} \varepsilon_{\vec{k}} c^\dagger_{\vec{k}} c_{\vec{k}}, \quad G: \text{ reciprocal lattice}, \tag{1.2}$$

for the undriven case. When we shine classical laser light described by the time-periodic gauge field $\vec{A}(t) = \vec{A}(t+T)$, the time-periodic Hamiltonian is obtained by

$$H(t) = \sum_{\vec{k}\in G} \varepsilon_{\vec{k}-\vec{A}(t)} c^\dagger_{\vec{k}} c_{\vec{k}}, \tag{1.3}$$

dubbed Pieres substitution. Recent typical experimentally-realized examples are two-dimensional materials, such as graphene [1], under circularly-polarized light.

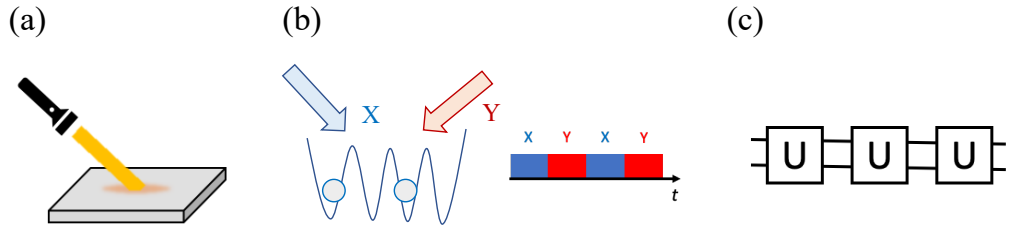

Figure 1.1: Various platforms for Floquet systems. (a) Laser-irradiated materials. (b) Artificial quantum systems under alternating pulse. (c) Quantum walk and quantum circuits.

Artificial quantum systems under periodic switching.— We can generate the time-periodicity with the period T by the following Hamiltonians:

$$H(t) = \begin{cases} H_1 & 0 = T_0 \le \tilde{t} < T_1 \\ H_2 & T_1 \le \tilde{t} < T_2 \\ \vdots & \\ H_n & T_{n-1} \le \tilde{t} < T_n = T \end{cases} \tag{1.4}$$

with $\tilde{t} = (t \mod T)$ and a set of static Hamiltonians $\{H_j\}_{j=1}^n$. Experimentally, they can be realized by alternate sequential pulse (See Fig. 1.1). Such non-smooth modulation is generally easy to implement highly-tunable artificial quantum systems such as trapped ions [2], cold atoms [3], photonic waveguides [4, 5]. In these setups, the time evolution operator over one period T (called Floquet operator later) is simply represented by

$$U_f = U_n U_{n-1} \dots U_2 U_1, \quad U_i = e^{-iH_j(T_j - T_{j-1})}, \tag{1.5}$$

with a set of unitary operators $\{U_j\}_{j=1}^n$.

Quantum walk and quantum circuits.— Quantum walk is an extended version of the classical random walk, which allows the superposition at different sites. The state at time $t \in \mathbb{Z}$ is given by $|\psi(t)\rangle = \sum_{x,\sigma} \alpha_{x,\sigma}(t) |x, \sigma\rangle$ ($\alpha_x(t) \in \mathbb{C}$) with discrete spatial coordinate x and internal degrees of freedom σ. Its dynamics with the probability conservation is described as

$$|\psi(t)\rangle = U^t |\psi(0)\rangle, \quad U\text{: unitary.} \tag{1.6}$$

Typically, the unitary evolution U is experimentally implemented by optical elements in optical systems, and is composed of the following operations for one-dimensional systems with $\sigma = \pm$ [6, 7]:

$$C(\theta) = \sum_{x,\sigma} e^{i\theta\sigma} |x, \sigma\rangle \langle x, \sigma| \text{ : Coin operator with tunable } \theta \in \mathbb{R}, \tag{1.7}$$

$$S^{\pm} = \sum_{x} (|x \pm 1, \pm\rangle \langle x, \pm| + |x, \mp\rangle \langle x, \mp|) \text{ : Shift operator.} \tag{1.8}$$

Thus, quantum walk is often discussed as Floquet systems, in that U and its components $\{C(\theta), S^{\pm}\}$ respectively correspond to U_f and $\{U_j\}_j$ in Eq. (1.5).

Quantum circuits are one of the models for quantum computation. The quantum state defined on multiple qubits are transformed by a set of unitary gates:

$$|\psi_{\text{output}}\rangle = u_n u_{n-1} \dots u_2 u_1 |\psi_{\text{input}}\rangle. \tag{1.9}$$

A set of unitary gates $\{u_j\}_j$ is often chosen from elementary gates acting on single qubit (Pauli gates etc.) and two qubits (CNOT gate etc.). When the series $\{u_j\}_j$ has some time-periodicity given as $u_{j+k} = u_j$ for a certain $k \in \mathbb{N}$, the quantum circuit is analysed as a Floquet system with the correspondence of $U = u_k u_{k-1} \dots u_1$ and U_f [See Eq. (1.5)]. Even in the absence of

such time periodicity, we can obtain some insight from Floquet analysis with relating the whole gate $U = u_n \dots u_1$ to U_f. Quantum circuits are experimentally implemented in artificial quantum circuits such as superconducting qubits, photonic systems and trapped ions [8, 9, 10]. When we remember the underlying Hamiltonians of these setups, quantum circuits often become equivalent to the quantum systems described in the previous paragraph, given by Eq. (1.5). In that sense, Floquet analysis on quantum circuits seems to be natural.

Novel nonequilibrium phenomena inherent in Floquet systems

What makes Floquet systems attractive seems to be their novel nonequilibrium phenomena prohibited in static or equilibrium systems. Various interesting physics in Floquet systems comes from the time-dependency of their Hamiltonians. This implies the absence of energy conservation, as we can imagine from the fact that light irradiation does not conserve energy. Thus, energy eigenvalues and energy eigenstates of Hamiltonians become ill-defined in Floquet systems. As discussed later in Section 1.2.1, Floquet systems are characterized by quasienergy and a Floquet eigenstate of certain time evolution operators (Floquet operators), which can show anomalous behaviors that energy eigenvalues and energy eigenstates in static systems cannot mimic.

A prototypical example of unique nonequilibrium phases is an anomalous Floquet topological phase [11]. A topological phase in static systems is a phase of matter characterized by the topology of their static Hamiltonians H [12]. It is robust against any local perturbation as long as the gap of H is maintained. If the robustness is present only under some symmetries, the phase is called a symmetry-protected topological (SPT) phase. In Floquet systems, the gap of energy eigenvalues is replaced by that of quasienergy eigenvalues. Quasienergy has periodicity of $2\pi/T$ unlike energy in static systems (See Section 1.2.1), thereby enabling the nontrivial winding in the quasienergy direction. This plays a role of a topological index unique to Floquet systems, and for instance, Floquet systems can host unique two-dimensional Chern insulators with the vanishing Chern numbers, which is topologically nontrivial due to the nonzero winding number [13]. The periodicity of quasienergy also provides an emergent symmetric point at quasienergy $\varepsilon = \pm\pi/T$ in addition to $\varepsilon = 0$ under some symmetries such as a particle-hole symmetry (PHS). This provides a unique SPT phase accompanied by a topologically-protected gapless excitation appearing at $\varepsilon = \pm\pi/T$, dubbed Majorana π mode (MPM) [14], while static systems host a Majorana zero mode (MZM), appearing at $\varepsilon = 0$. In terms of deformation of Hamiltonians $H(t)$, Floquet systems can be classified by the topology of their effective Hamiltonians, which is time-independent, or that of their time evolution operators [15]. This difference results in various manifestations of Floquet topological phases including the above examples.

We also note that various symmetries brought by the time-dependency are resources for interesting physics in Floquet systems. The time-periodicity of Hamiltonians, $H(t) = H(t+T)$, can be interpreted as a discrete time-translation symmetry (TTS). Thus, we can expect spontaneous symmetry breaking (SSB) for it. As a matter of fact, the ordered phases brought by spontaneous breaking of a discrete TTS are known as discrete time crystals (DTCs) [16]. The no-go theorem for static systems with local interactions ensures that spontaneous breaking of a continuous TTS is absent in ground states and thermal equilibrium states [17], and hence time crystals are referred to as novel nonequilibrium phases (See Section 1.3.5 for the detail). Furthermore, we can define various symmetries combined with the time-dependency other than a discrete TTS. For instance, the symmetries generated by the combination of the time translation and the spatial symmetry operations are known as dynamical symmetries, which includes Floquet nonsymmorphic symmetries. Such symmetries inherent in Floquet systems lead to Floquet topological phases protected by the time-glide symmetries, which is composed of the half-period time translation and the spatial rotation [18, 19], and selection rules for optical responses such as high-harmonic generation [20, 21].

Control of phases of matter in nonequilibrium setups (Floquet engineering)

The other interesting aspect of Floquet systems is the control of materials by periodic drives, dubbed *Floquet engineering*. With the usage of Floquet theory discussed later, the stroboscopic dynamics of Floquet systems, the dynamics at $t = mT$ ($m = 0, 1, 2, \dots$) can be described by a static Hamiltonian H_{eff}, called the effective Hamiltonian. Floquet engineering aims to reproduce dynamics or steady states under a preferable static Hamiltonian H by tuning the periodic drive $H(t)$ so that the effective Hamiltonian H_{eff} becomes the preferable one H.

Floquet engineering is widely utilized both in artificial quantum systems and materials. For instance, in cold atoms which are typically charge-neutral, we can realize a Hamiltonian involving artificial gauge fields by exploiting the optical lattice shaking as a periodic drive [22]. This technique is actually used for realizing the Haldane model [23], which is usually difficult due to the sublattice-dependent gauge fields. Another important example is a light-induced phase transition in solid materials, which employs the coupling between electrons and time-periodic gauge fields like Eq. (1.3). For instance, we can realize topological phase transitions in graphene by shining circularly-polarized light, which are theoretically proposed in 2009 [24] and experimentally observed in 2020 [1]. Recently, Floquet engineering with high-frequency light has been extensively explored such as laser-induced topological superconductivity [25, 26], as the development of a powerful tool for the effective Hamiltonian, called the high-frequency expansions [See Section 1.2.3].

1.2 Floquet theory

In this section, we introduce a mathematical framework, Floquet theory, to tackle quantum physics in Floquet systems. The terminology *Floquet theory* is named after a French mathematician Gaston Floquet in the 19-th century. Floquet theory, which was constructed before the birth of quantum physics, provides information about solutions of generic linear differential equations whose coefficients are periodic in some parameters. Nowadays, Floquet theory is widely used in the context of quantum physics described by time-dependent Schrödinger equation with time-periodic Hamiltonians — Floquet systems. We briefly discuss Floquet theory developed in the context of quantum physics below.

1.2.1 Floquet theorem

Here, we introduce Floquet theorem, which identifies the solutions of time-periodic Schödinger equations. In generic time-dependent Schrödinger equation, the solution is given by

$$|\psi(t)\rangle = U(t,0)\,|\psi(0)\rangle\,, \quad U(t,t') = \mathcal{T}\exp\left\{-i\int_{t'}^{t} H(\tilde{t})d\tilde{t}\right\}, \tag{1.10}$$

where $\mathcal{T}$ denotes the time-ordered product. By using the time-periodicity, the following theorem is obtained.

Theorem 1.2.1. (Floquet theorem)
Let us consider time-periodic Schr̈odinger equation,

$$i\frac{d}{dt}\,|\psi(t)\rangle = H(t)\,|\psi(t)\rangle\,, \quad H(t) = H(t+T). \tag{1.11}$$

Then, the solutions are always written in the following form:

$$|\psi(t)\rangle = \sum_n c_n e^{-i\varepsilon_n t}\,|\phi_n(t)\rangle\,, \quad |\phi_n(t+T)\rangle = |\phi_n(t)\rangle\,. \tag{1.12}$$

Here, the coefficients $c_n \in \mathbb{C}$ are determined by the initial condition as $c_n = \langle\phi_n(0)|\psi(0)\rangle$. The real numbers ε_n, called *quasienergy*, are eigenvalues of an effective Hamiltonian H_{eff} given by

$$H_{\text{eff}} = -\frac{i}{T}\log U_f, \quad U_f = \mathcal{T}\exp\left\{-i\int_0^T H(t)dt\right\}. \tag{1.13}$$

Proof

The unitary operator U_f, defined by Eq. (1.13), is always written in the spectral decomposition as

$$U_f = \sum_n e^{-i\varepsilon_n T}\,|\phi_n(0)\rangle\,\langle\phi_n(0)|\,, \tag{1.14}$$

where $|\phi_n(0)\rangle$ is an eigenstate of U_f. By setting $t = t_0 + mT$ $(m = 0, 1, 2, \ldots)$, the solution of Eq. (1.11) becomes

$$\begin{aligned} |\psi(t)\rangle &= U(t_0 + mT, t_0)(U_f)^m |\psi(0)\rangle = U(t_0, 0) \sum_n e^{-i\varepsilon_n mT} |\phi_n(0)\rangle \langle\phi_n(0)|\psi(0)\rangle \\ &= \sum_n c_n e^{-i\varepsilon_n(t_0+mT)} (e^{i\varepsilon_n t_0} U(t_0, 0) |\phi_n(0)\rangle) \end{aligned} \tag{1.15}$$

When we define the Floquet states by $|\phi_n(t)\rangle = e^{i\varepsilon_n t_0} U(t_0, 0) |\phi_n(0)\rangle$, they satisfy the time-periodicity as

$$|\phi_n(t + T)\rangle = e^{i\varepsilon_n(t_0+T)} U(t_0, 0) U_f |\phi_n(0)\rangle = |\phi_n(t)\rangle . \tag{1.16}$$

This completes the proof of Floquet theorem, Eq. (1.12). □

Terminology

The complex values ε_n and the time-periodic states $|\phi_n(t)\rangle$ in Eq. (1.12) are called quasienergy and Floquet states respectively. Here, the Floquet states composes a orthornormal basis for the Hilbert space $\mathcal{H}$ in that

$$\langle\phi_n|\phi_{n'}\rangle_{\mathrm{T}} \equiv \frac{1}{T} \int_0^T dt \, \langle\phi_n(t)|\phi_{n'}(t)\rangle = \delta_{nn'}. \tag{1.17}$$

Floquet theorem dictates that the solution is always written by the superposition of $e^{-i\varepsilon_n t} |\phi_n(t)\rangle$.

The time evolution operator over one period T is called Floquet operator, given as U_f. The first role of U_f is to provide quasienergy ε_n. It has a spectral decomposition

$$U_f = \sum_n e^{-i\varepsilon_n T} |\phi_n(0)\rangle \langle\phi_n(0)| , \tag{1.18}$$

giving the quasienergy. We note that the Floquet operator depends on the choice of the time origin t_0 (sometimes referred as Floquet gauge), since $U(T, 0)$ is not equal to $U(t_0 + T, t_0)$ in general. However, since Floquet operators in different gauges are connected by unitary transformation as

$$U_f^{t_0} \equiv U(t_0 + T, t_0) = U(t_0 + T, T) U(T, 0) U^{-1}(t_0, 0) = U(t_0, 0) U_f U^{-1}(t_0, 0), \tag{1.19}$$

the quasienergy ε_n does not depend on the gauge t_0.

The second important role of the Floquet operator U_f is to provide the stroboscopic dynamics of quantum states $|\psi(mT)\rangle$ $(m = 0, 1, 2, \ldots)$. By using the time-periodicity and the effective Hamiltonian introduced by Eq. (1.13), we obtain

$$|\psi(mT)\rangle = \sum_n c_n e^{-i\varepsilon_n mT} |\phi_n(0)\rangle = (U_f)^m |\psi(0)\rangle = e^{-iH_{\mathrm{eff}} mT} |\psi(0)\rangle . \tag{1.20}$$

The time evolution at any time $t = t_0 + mT$ $(0 \leq t_0 < T)$ is always decomposed into the stroboscopic dynamics $(U_f)^m$ and the microscopic dynamics $U(t_0, 0)$ as $U(t, 0) = U(t_0, 0)(U_f)^m$. The stroboscopic dynamics describes characteristic long-term behaviors of Floquet systems, confirming the importance of U_f or H_{eff}. Therefore, physics in Floquet systems often focus on the stroboscopic dynamics, so we do in this thesis.

We also note that the effective Hamiltonian H_{eff} plays a role of a static Hamiltonian in time-independent systems as Eq. (1.20). Analysis of H_{eff} as a static Hamiltonian gives the properties of Floquet systems. In fact, Floquet engineering aims to reproduce a preferable time-independent system by the effective Hamiltonian H_{eff}.

Quasi-energy periodicity and Relation to Bloch theorem

Each solution of the time-periodic Schrödinger equation satisfies

$$e^{-i\varepsilon_n t} |\phi_n(t)\rangle = e^{-i(\varepsilon_n + l\omega)t} |\tilde{\phi}_n(t)\rangle , \qquad |\tilde{\phi}_n(t)\rangle \equiv e^{il\omega t} |\phi_n(t)\rangle = |\tilde{\phi}_n(t + T)\rangle \tag{1.21}$$

with $l \in \mathbb{Z}$. It dictates that $\{\varepsilon_n, |\phi_n(t)\rangle\}$ and $\{\varepsilon_n + l\omega, |\tilde{\phi}_n(t)\rangle\}$ give the identical solution, regarded as the quasienergy periodicity. We can also see this behavior as the choice of branch for the

logarithm appearing in Eq. (1.13). In order to avoid considering the identical solutions by different quasienergy, we generally consider $\varepsilon \in [-\pi/T, \pi/T)$, which is called the first Brillouine zone (BZ).

Floquet theorem for time-periodic systems is completely parallel to well-known Bloch theorem for spatially-periodic systems. Bloch theorem says that the eigenstates of a static Hamiltonian $H(x)$ satisfying $H(x) = H(x+L)$ is given by $e^{-ik_n x}|u_n(x)\rangle$ with $|u_n(x)\rangle = |u_n(x+L)\rangle$. This is a counterpart of Eq. (1.12) in Floquet systems. The quasienergy periodicity in Floquet systems corresponds to that of the wavenumber k_n, which gives the first BZ $k_n \in [-\pi/L, \pi/L)$.

1.2.2 Formulation in Sambe space

Here, we introduce another formulation of Floquet systems based on the Fourier space in time, called *Sambe space*. Using Floquet theorem, the independent solution of time-periodic Schrödinger equation satisfies

$$i\frac{d}{dt}\left(e^{-i\varepsilon_n t}|\phi_n(t)\rangle\right) = H(t)e^{-i\varepsilon_n t}|\phi_n(t)\rangle\,. \tag{1.22}$$

We define the Fourier transformation in time by

$$H(t) = \sum_{l\in\mathbb{Z}} H_l e^{-il\omega t}, \quad |\phi_n(t)\rangle = \sum_{l\in\mathbb{Z}} |\phi_n^{(l)}\rangle\, e^{-il\omega t} \tag{1.23}$$

with $\omega = 2\pi/T$ based on the periodicity $H(t+T) = H(t)$ and $|\phi_n(t+T)\rangle = |\phi_n(t)\rangle$. By substituting Eq. (1.23) into Eq. (1.22), we obtain

$$\sum_{l\in\mathbb{Z}} (\varepsilon_n + l\omega)e^{-il\omega t}|\phi_n^{(l)}\rangle = \sum_{l,l'\in\mathbb{Z}} H_{l'}|\phi_n^{(l)}\rangle\, e^{-i(l'+l)\omega t}. \tag{1.24}$$

By performing the inverse Fourier transformation, this becomes equivalent to the following equation:

$$\mathscr{H}|\Phi_n\rangle = \varepsilon_n|\Phi_n\rangle\,, \tag{1.25}$$

with

$$\mathscr{H} = \begin{pmatrix} \ddots & & & & & & \\ & H_0-2\omega & H_{+1} & H_{+2} & H_{+3} & H_{+4} & \\ & H_{-1} & H_0-\omega & H_{+1} & H_{+2} & H_{+3} & \\ & H_{-2} & H_{-1} & H_0 & H_{+1} & H_{+2} & \\ & H_{-3} & H_{-2} & H_{-1} & H_0+\omega & H_{+1} & \\ & H_{-4} & H_{-3} & H_{-2} & H_{-1} & H_0+2\omega & \\ & & & & & & \ddots \end{pmatrix}, \qquad |\Phi_n\rangle = \begin{pmatrix} \vdots \\ |\phi_n^{(2)}\rangle \\ |\phi_n^{(1)}\rangle \\ |\phi_n^{(0)}\rangle \\ |\phi_n^{(-1)}\rangle \\ |\phi_n^{(-2)}\rangle \\ \vdots \end{pmatrix}. \tag{1.26}$$

Floquet state $|\phi_n(t)\rangle$ has one-to-one correspondence with the vector $|\Phi_n\rangle$ in an infinite-dimensional space called Sambe space. Thus, Eq. (1.25) suggests that solving time-periodic Schrödinger equation is equivalent to solving the eigenvalue problem of the time-independent hermitian operator $\mathscr{H}$ on Sambe space.

We note that, while the time-dependency disappears in Eq. (1.25), the difficulty itself does not alter from Eq. (1.11) in general due to the infinite dimensionality of Sambe space. However, this formalism sometimes make use of physical intuitions and approximations based on them. Let us regard each Fourier component $|\phi_n^{(-l)}\rangle$ as a state dressed with l photons. Then, the Hamiltonian $\mathscr{H}$ describes a set of duplicated systems with different number of photons (See Fig. 1.2). The diagonal term $H_0 + l\omega$ represents the energy of the l-photon-dressed states. The off-diagonal term $H_{\Delta l}$ ($\Delta l \in \mathbb{Z}$) plays a role of couplings with pairs of states having different photon numbers by Δl.

1.2.3 High-frequency expansions

Here, we consider the effective Hamiltonian H_{eff}, given by Eq. (1.13). While it enables analysis of Floquet systems based on a static Hamiltonian, it is too difficult to obtain its explicit form due to the existence of time-ordered product and the logarithm of operators. Possible ways to

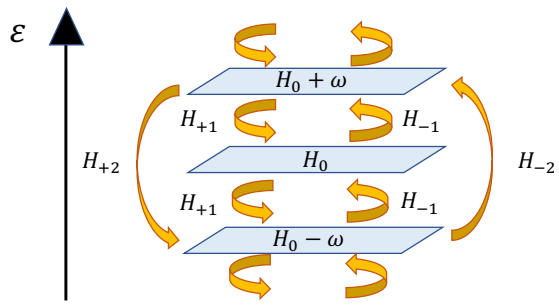

Figure 1.2: Intuitive picture of Floquet systems in Sambe space. Floquet systems are equivalent to an infinite series of static systems having l photons, described by $H_0 + l\omega$, with the coupling by the time-dependent terms $H_{\pm l'}$. The van Vleck expansions or the Brillouin-Wigner expansions intuitively give the effective Hamiltonian for the 0-photon state in the high-frequency regime.

obtain H_{eff} is considering some limiting parameter regimes and performing some approximations. The important parameter here is the ratio of the frequency $\omega = 2\pi/T$ to the energy scale of the Hamiltonian $H(t)$.

Let us consider a parameter regime where the frequency ω is much larger than the energy scale of $H(t)$, called *high-frequency regime*. In this regime, we can apply perturbative expansions in the small parameter $||H(t)||/\omega$, where $||\quad||$ denotes the operator norm. The result for H_{eff} is known as Floquet-Magnus expansions below.

Remark. (Floquet-Magnus expansion)
For a time-periodic Hamiltonian $H(t)$ with the period T, we define the n-th order Floquet-Magnus expansion H^n_{FM} $(n = 0, 1, 2, \dots)$ by

$$H^n_{\text{FM}} = \sum_{m=0}^{n} H^{(m)}_{\text{FM}}, \tag{1.27}$$

with each m-th order term $H^{(m)}_{\text{FM}}$ given by

$$\begin{aligned} H^{(m)}_{\text{FM}} &= \sum_{\sigma} (-1)^{m-\tilde{\theta}(\sigma)} \frac{\tilde{\theta}(\sigma)!(m-\tilde{\theta}(\sigma))!}{m!(m+1)^2 i^m T} \\ &\quad \times \int_0^T dt_{m+1} \dots \int_0^{t_2} dt_1 [H(t_{\sigma(m+1)}), [H(t_{\sigma(m)}), \dots, [H(t_{\sigma(2)}), H(t_{\sigma(1)})] \dots]], \\ \tilde{\theta}(\sigma) &\equiv \sum_{k=1}^{m} \theta(\sigma(k+1) - \sigma(k)), \quad \theta(x)\text{: a step function.} \end{aligned} \tag{1.28}$$

Here, σ represents the permutation of $\{1, 2, \dots, m+1\}$ [27, 28]. Then, the effective Hamiltonian H_{eff} defined by Eq. (1.13) is approximated as

$$H_{\text{eff}} = H^n_{\text{FM}} + O\left(||H(t)|| \cdot r^{n+1}\right), \quad r = \frac{||H(t)||}{\omega}, \tag{1.29}$$

for the sufficiently small dimensionless parameter r.

We note several points on Floquet-Magnus expansions. First, they are not always convergent, that is, the perturbative expansion Eq. (1.27) has a finite convergence radius $r_c > 0$ in the ratio r. Although the exact value of r_c is still unclear, several mathematical analysis has revealed $r_c = O(1)$. When we consider quantum many-body systems under periodic drives, the energy scale of $||H(t)||$ is typically proportional to the system size L, making the ratio r larger than r_c. This means that Floquet-Magnus expansions become divergent and the approximation is no longer

valid in generic Floquet many-body systems. However, as we will see later in Section 1.3.4, when we consider Floquet many-body systems only with local interactions, Floquet-Magnus expansions $H^n_{\rm FM}$ are still meaningful for the dynamics despite their divergence.

Second, we can also provide Floquet-Magnus expansions by using the Fourier components given by

$$H_l = \frac{1}{T}\int_0^T H(t)e^{il\omega t}dt. \tag{1.30}$$

After some simple calculations, we obtain each m-th order term by

$$H^{(0)}_{\rm FM} = H_0, \qquad H^{(1)}_{\rm FM} = \sum_{m\neq 0}\frac{[H_{-m},H_m]}{2m\omega} + \sum_{m\neq 0}\frac{[H_m,H_0]}{m\omega},\dots \tag{1.31}$$

Finally, Floquet-Magnus expansion depends on the time origin t_0 due to the change of the Floquet operator. With explicitly writing the t_0-dependence, the Floquet-Magnus expansion $H^n_{\rm FM}[t_0]$ approximates the effective Hamiltonian $H_{\rm eff}[t_0] = (i/T)\log U_f^{t_0}$ with $U_f^{t_0} = U(t_0+T,t_0)$. It is proven that we can remove the Floquet gauge dependence by a unitary transformation as

$$H_{\rm eff}[t_0] = e^{-iK[t_0]}H'_{\rm eff}\,e^{iK[t_0]}. \tag{1.32}$$

The effective Hamiltonian $H'_{\rm eff}$ becomes gauge-dependent while $K[t_0]$, called a kick operator, is t_0-dependent with satisfying $K[t_0+T] = K[t_0]$. Since the time evolution operator becomes

$$(U_f^{t_0})^m = e^{-iH_{\rm eff}[t_0]mT} = e^{-iK[t_0]}e^{-iH'_{\rm eff}mT}e^{iK[t_0]}, \tag{1.33}$$

$H'_{\rm eff}$ and $K[t_0]$ respectively represent the macroscopic dynamics and the gauge-dependent microscopic dynamics. We can also apply perturbative expansions to the gauge-independent effective Hamiltonian $H'_{\rm eff}$ and the kick operator $K[t_0]$, dubbed van Vleck expansions.

Remark. (van Vleck expansion)
For a time-periodic Hamiltonian $H(t)$ with the period T, we define the n-th order van Vleck effective Hamiltonian $H^n_{\rm vV}$ and kick operator $K^n_{\rm vV}[t_0]$ $(n=0,1,2,\dots)$ by

$$H^n_{\rm vV} = \sum_{m=0}^{n} H^{(m)}_{\rm vV}, \qquad K^n_{\rm vV}[t_0] = \sum_{m=0}^{n} K^{(m)}_{\rm vV}[t_0], \tag{1.34}$$

where each m-th order term is given by

$$\begin{aligned}
H^{(0)}_{\rm vV} &= H_0, \quad H^{(1)}_{\rm vV} = \sum_{m\neq 0}\frac{[H_{-m},H_m]}{2m\omega}, && (1.35)\\
H^{(2)}_{\rm vV} &= \sum_{m\neq 0}\frac{[[H_{-m},H_0],H_m]}{2m^2\omega^2} + \sum_{m\neq 0}\sum_{n\neq 0,m}\frac{[[H_{-m},H_{m-n}],H_n]}{3mn\omega^2}, && (1.36)\\
&\vdots\ , \\
iK^{(0)}_{\rm vV}[t_0] &= -\sum_{m\neq 0}\frac{V_m}{m\omega}, && (1.37)\\
iK^{(1)}_{\rm vV}[t_0] &= \sum_{m\neq 0}\sum_{n\neq 0,m}\frac{[H_m,H_{m-n}]}{2mn\omega^2} + \sum_{m\neq 0}\frac{[H_m,H_0]}{m^2\omega^2}, && (1.38)\\
&\vdots\ .
\end{aligned}$$

Then, for the sufficiently small $r = ||H(t)||/\omega$, the effective Hamiltonian is approximated by

$$H_{\rm eff}[t_0] = e^{-iK^n_{\rm vV}[t_0]}H^n_{\rm vV}e^{iK^n_{\rm vV}[t_0]} + O(||H(t)||\cdot r^{n+1}). \tag{1.39}$$

When we set $t_0 = 0$, this reproduces the Floquet-Magnus expansion up to the order of $O(r^n)$.

Floquet-Magnus expansions and van Vleck expansions both give the approximate dynamics of Floquet systems. The former becomes important when we consider the real-time dynamics from a certain initial state, since the Floquet gauge is specified by $t_0 = 0$. On the other hand, when we consider quasi-steady states in the high-frequency regimes, the latter is often used to capture the gauge-independent properties of the quasi-steady states.

We also introduce a property of van Vleck expansions for later convenience. As described in Eqs. (1.35) and (1.36), each m-th order term $H_{\rm vV}^{(m)}$ is composed of the $(m+1)$-th order products,

$$H_{l_1} H_{l_2} \dots H_{l_{m+1}}, \tag{1.40}$$

by expanding all the commutators. Here, we use the gauge-independence of the van Vleck expansions. If we change the time origin from 0 to t_0, the Fourier component H_l changes to $H_l^{t_0}$, given by

$$H_l^{t_0} = \frac{1}{T}\int_0^T H(t+t_0)e^{il\omega t}dt = e^{-il\omega t_0}H_l. \tag{1.41}$$

Each term given by Eq. (1.40) is transformed to

$$H_{l_1}^{t_0} H_{l_2}^{t_0} \dots H_{l_{m+1}}^{t_0} = \exp\left(-i\omega t_0 \sum_{i=1}^{m+1} l_i\right) H_{l_1} H_{l_2} \dots H_{l_{m+1}}. \tag{1.42}$$

This should be the same as Eq. (1.40) for any t_0 due to the gauge-independence of $H_{\rm vV}^n$, and hence we obtain the following result.

Remark. (Gauge-independence of van Vleck expansion)
Each m-th order term in van Vleck expansions $H_{\rm vV}^n$ $(0 \le m \le n)$ is composed of the $(m+1)$-th order products like

$$H_{l_1} H_{l_2} \dots H_{l_{m+1}}. \tag{1.43}$$

Then, the gauge-independence of $H_{\rm vV}^n$ results in

$$\sum_{i=1}^{m+1} l_i = 0 \qquad \text{for any } m. \tag{1.44}$$

As discussed in Sambe formalism in Section 1.2.2, H_l represents the l-photon absorption or emission process. Equation (1.44) indicates that only the processes satisfying the conservation of the photon number have an effect on the gauge-independent part of Floquet dynamics. To be precise, each m-th order term represented by Eq. (1.44) captures a process where a certain dressed state gets back to the original space after repeating l_i-photon absorption or emission (See Fig. 1.2).

We can also derive the perturbative theory based on Sambe formalism. In the high-frequency regime $\omega \gg ||H(t)||$, we can focus on the space dressed with no photon ($l = 0$) and regard the other dressed spaces ($l \neq 0$) as an environment since the energy scale of each space, ω, is much larger than the couplings H_l in the Hamiltonian $\mathscr{H}$ [Eq. (1.25)]. By applying the conventional perturbation theory of static Hamiltonian, we obtain the effective Hamiltonian for each space with the fixed photon number given by

$$H_{\rm BW}^n = H_0 + \sum_{m\neq 0} \frac{H_{-m}H_m}{m\omega} + \left(\sum_{m,l\neq 0} \frac{H_{-m}H_{m-l}H_l}{ml\omega^2} + \sum_{m\neq 0} \frac{H_{-m}H_m H_0}{m^2\omega^2}\right) + \dots + H_{\rm BW}^{(n)}, \tag{1.45}$$

up to the n-th order. This is called Brillouine-Wigner expansion. The higher order terms capture the process in which a state with the certain photon number travels other dressed spaces and finally goes back to the original space via photon absorption and emission. Although the physical sense of $H_{\rm BW}$ is similar to that of van Vleck expansions,we note that $H_{\rm BW}$ does not approximate the dynamics. Nowadays, Brillouine-Wigner expansions are proven to be related to other high-frequency expansions (Floquet-Magnus, van Vleck) via non-unitary transformations [29].

1.3 Steady states in closed static and Floquet many-body systems

One of the today's central questions in quantum physics is what kind of phenomena can take place in quantum many-body systems. In this section, we introduce the generic properties of the dynamics in closed quantum many-body systems, that is, the solutions of Schrödinger equation under a many-body Hamiltonian. The key notion in this section is Floquet eigenstate thermalization hypothesis (Floquet-ETH), which we should overcome for realizing nontrivial quantum many-body phenomena in Floquet systems. For the clear description and the comparison with time-independent cases, we begin with discussion on static quantum many-body systems.

1.3.1 Eigenstate thermalization hypothesis (ETH)

Here, we focus on a closed quantum many-body system described by time-independent Schrödinger equation,

$$i\frac{d}{dt}\left|\psi(t)\right\rangle = H\left|\psi(t)\right\rangle. \tag{1.46}$$

We assume that a system is defined on a lattice Λ with the size $|\Lambda| = L$, and that the many-body Hamiltonian H is bounded, which means $||H|| < \infty$ (bosonic systems with the limited occupation at each site, fermionic systems, or spin systems).

In generic quantum systems coupled to a huge external bath, as we intuitively expect, any initial state arrives at a thermal equilibrium state after a sufficiently long time. From this fact, it has been one of the central questions whether there exists relaxation or some steady state in isolated quantum many-body systems obeying Schrödinger equation. Some analytical and numerical studies have shown that generic nonintegrable many-body systems generally relax to thermal equilibrium states even in isolated cases while integrable and many-body localized (MBL) systems avoid thermalization. They have also conjectured that what distinguishes them is the eigenstate thermalization hypothesis (ETH), which is expected to be valid only for nonintegrable systems. We discuss integrablity of quantum many-body systems and ETH below, and MBL is discussed in Section 1.3.5.

Integrability and Nonintegrability

Integrability characterizes conserved quantities of Hamiltonians, which seem to play a crucial role on the dynamics. We call a many-body Hamiltonian H integrable if it has a macroscopic number ($\sim O(L)$) of conserved quantities, and we call nonintegrable otherwise. The simplest examples for integrable Hamiltonians is non-interacting Hamiltonians and their corresponding ones connected via some transformations. For instance, the one-dimensional transverse-field Ising Hamiltonian, given by

$$H_{\mathrm{TFIM}} = J\sum_i \sigma_i^z\sigma_{i+1}^z + h\sum_i \sigma_i^x, \tag{1.47}$$

is integrable since it is equivalent to free-fermionic systems via Jordan-Wigner transformation. Another nontrivial example of integrable Hamiltonians is the one-dimensional XXZ Hamiltonian, given by

$$H_{\mathrm{XXZ}} = \sum_i \left\{J_\perp(\sigma_i^x\sigma_{i+1}^x + \sigma_i^y\sigma_{i+1}^y) + J_z\sigma_i^z\sigma_{i+1}^z\right\}. \tag{1.48}$$

This model is exactly solvable and proven to have an extensive number of conserved quantities with the usage of Bethe ansatz [30]. On the other hand, as an example of nonintegrable Hamiltonians, the one-dimensional XYZ model under a magnetic field, given by

$$H_{\mathrm{XYZ},h} = \sum_i (J_X\sigma_i^x\sigma_{i+1}^x + J_Y\sigma_i^y\sigma_{i+1}^y + J_Z\sigma_i^z\sigma_{i+1}^z) + h\sum_i \sigma_i^z, \tag{1.49}$$

is rigorously proven to have no local conserved quantities [31]. We note that rigorous judgment on the integrability and the nonintegrability is generally difficult. For the integrability, we should exactly solve the model and identify its conserved quantities in some way. The nonintegrability is further difficult since we should prove the absence of local conserved quantities. While generic

interacting models, in which we cannot naively find a set of conserved quantities (i.e. non-fine-tuned Hamiltonians), are expected to be nonintegrable, the rigorous proof on the nonintegrability is limited to specific models such as $H_{\mathrm{XYZ},h}$ [31].

However, we can numerically test the integrability and nonintegrability based on the energy spectrum of a many-body Hamiltonian [32, 33]. Let E_n denote the n-th smallest eigenvalue of H ($n = 0, 1, \ldots, \dim(\mathcal{H}) - 1$), and define the level spacing s_n and the level spacing ratio r_n by

$$s_n = E_{n+1} - E_n, \quad r_n = \min\left(\frac{s_n}{s_{n+1}}, \frac{s_{n+1}}{s_n}\right). \tag{1.50}$$

In generic many-body systems, the tendency of adjacent energy eigenvalues avoiding the degeneracy, called the level repulsion, is expected to vary depending on their integrability. The statistics of $\{s_n\}_n$ or $\{r_n\}_n$ measures the repulsion of the energy eigenvalues. When the Hamiltonian H is integrable, the eigenvalue E_n is composed of independent contributions of a macroscopic number of conserved quantities, implying the absence of the level repulsion. Thus, in integrable systems, the level spacing $\{s_n\}_n$ is expected to have the probability distribution of the Poisson statistics,

$$P(s) \propto e^{-s/\langle s_n\rangle_n}, \tag{1.51}$$

where $\langle s_n\rangle_n$ denotes the mean value of s_n. This gives the averaged value of the level spacing ratio,

$$r \equiv \langle r_n\rangle_n \simeq 0.386, \tag{1.52}$$

providing a simple diagnosis for integrable systems.

On the other hand, generic nonintegrable systems, without a macroscopic number of local conserved quantities, host the level repulsion. Their Hamiltonians behave like a random hermitian matrix from the Gaussian ensemble, with reflecting their hermiticity and symmetry. When the nonintegrable Hamiltonian does not respect any symmetry, the level statistics $\{s_n\}_n$ is expected to obey the Wigner-Dyson distribution for the Gaussian Unitary Ensemble (GUE), given by

$$P(s) \propto \left(\frac{s}{\langle s_n\rangle_n}\right)^2 \exp\left(-\frac{4s^2}{\pi\langle s_n\rangle_n^2}\right), \quad r \equiv \langle r_n\rangle_n \simeq 0.603. \tag{1.53}$$

In the presence of the time-reversal symmetry, that is, if there exists a certain unitary operator $U_{\mathcal{T}}$ satisfying

$$U_{\mathcal{T}} H^* U_{\mathcal{T}}^\dagger = H, \tag{1.54}$$

the level statistics behaves like that of the Gaussian Orthogonal Ensemble (GOE). As a result, a time-reversal symmetric nonintegrable Hamiltonian gives the level statistics obeying the Wigner-Dyson distribution,

$$P(s) \propto \frac{s}{\langle s_n\rangle_n} \exp\left(-\frac{\pi s^2}{4\langle s_n\rangle_n^2}\right), \quad r \equiv \langle r_n\rangle_n \simeq 0.536. \tag{1.55}$$

We can numerically test the integrability by fully diagonalizing the Hamiltonian H and checking its level statistics $\{s_n\}_n$ or $\{r_n\}_n$, which can be visualized as Fig. 1.3.

Eigenstate thermalization hypothesis

Now, let us consider the long-time dynamics of closed quantum many-body systems, that is the Schödinger solution $|\psi(t)\rangle = e^{-iHt}|\psi(0)\rangle$ for the sufficiently large time t and size L. The quantum state $|\psi(t)\rangle$ itself cannot reach a thermal equilibrium state, since the latter one is a mixed state while $|\psi(t)\rangle$ is a pure state at any time. We note that this does not prohibit the existence of relaxation in closed systems.

We characterize the relaxation from the viewpoint of indistinguishability in local observables. We define the equivalence of a pure state $|\psi\rangle$ and a mixed state ρ by

$$\langle\psi|O|\psi\rangle \simeq \mathrm{Tr}[O\rho], \tag{1.56}$$

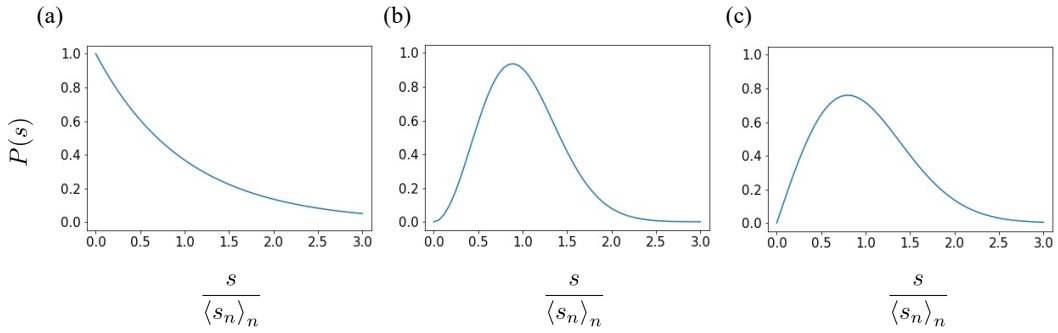

Figure 1.3: Level statistics $\{s_n\}$ in static Hamiltonians. (a) Poisson statistics, given by Eq. (1.51). It appears in integrable and many-body localized systems. (b) Wigner-Dyson statistics for random matrices from Gaussian Unitary Ensemble, Eq. (1.53). It appears in nonintegrable systems without TRS. (c) Wigner-Dyson statistics for random matrices from Gaussian Orthogonal Ensemble, Eq. (1.55). It appears in nonintegrable systems with TRS.

for any local observable O, which acts in a nontrivial way simultaneously on at-most $O(1)$ sites. In terms of the long-time dynamics of closed systems, we are interested in

$$\overline{\langle O \rangle} \equiv \lim_{\tau \to \infty} \frac{1}{\tau} \int_0^\tau \langle \psi(t)|O|\psi(t)\rangle \, dt, \tag{1.57}$$

which represents the infinite-time average of a local observable $O(t) = \langle \psi(t)|O|\psi(t)\rangle$. Whether $O(t)$ reaches a constant steady-state value at $t \to \infty$ is diagnosed by its fluctuation in time,

$$\overline{\langle (\Delta O)^2 \rangle} \equiv \lim_{\tau \to \infty} \frac{1}{\tau} \int_0^\tau \langle \psi(t)|O|\psi(t)\rangle^2 \, dt - \left(\lim_{\tau \to \infty} \frac{1}{\tau} \int_0^\tau \langle \psi(t)|O|\psi(t)\rangle \, dt \right)^2. \tag{1.58}$$

We refer to that the quantum many-body state $|\psi(t)\rangle$ equilibrates if $\overline{\langle (\Delta O)^2 \rangle} \ll ||O||$ for any local observable O. In addition, if the steady-state value $\overline{\langle O \rangle}$ corresponds to the thermal equilibrium value $\langle O \rangle_{\rm eq}$ with satisfying $\overline{\langle (\Delta O)^2 \rangle} \ll ||O||$, we call it the thermalization in isolated setups.

The existence of thermalization generally depends on the integrability of the system. In integrable or MBL systems, a macropic number of conserved or quasi-conserved quantities prevent the state from relaxing to equilibrium. On the other hand, some numerical and experimental studies have verified that nonintengrable systems generally host thermalization from any initial state [34, 35, 36, 37, 38] (See Refs. [39, 40, 41] for review). They have also conjectured that the difference comes from the following hypothesis, dubbed Eigenstate thermalization hypothesis (ETH). [1]

[1] Here, we consider the satisfaction of Eq. (1.61) for all the eigenstates $|E_n\rangle$. The statement discussed here is sometimes called "strong ETH" to be distinguished from weak ETH. Weak ETH indicates the satisfaction of Eq. (1.61) for almost all the eigenstates $|E_n\rangle$, and even integrable systems avoiding thermalization can satisfy it [42, 43].

Remark. (Eigenstate thermalization hypothesis, ETH)
Let $|E_n\rangle$ denote the n-th eigenstate of a Hamiltonian H. We consider the microcanonical ensemble value in the energy shell $\Delta(E_n) = [E_n - \Delta E, E_n + \Delta E]$, given by

$$\langle O\rangle_{\rm MC} = {\rm Tr}[O\rho_{\rm MC}], \quad \rho_{\rm MC} = \frac{1}{N_{E_n}} \sum_{m:E_m\in\Delta(E_n)} |E_m\rangle \langle E_m|\,, \tag{1.59}$$

where N_{E_n} denotes the number of the eigenstates in the shell $\Delta(E_n)$. In general, for a local operator O, it corresponds to the canonical ensemble value,

$$\langle O\rangle_{\rm MC} \simeq \langle O\rangle_\beta \equiv {\rm Tr}[O\rho_\beta], \quad \rho_\beta = e^{-\beta H}/{\rm Tr}[e^{-\beta H}], \tag{1.60}$$

with the inverse temperature β determined by $E_n = \langle H\rangle_\beta$. The diagonal ETH (or simply ETH) and off-diagonal ETH are described as follows.

(Diagonal ETH, or simply ETH)
Every eigenstate $|E_n\rangle$ is equivalent to the microcanonical ensemble, that is,

$$\langle E_n|O|E_n\rangle \simeq \langle O\rangle_{\rm MC} \tag{1.61}$$

for a local operator O when the system size L is sufficiently large.

(Off-diagonal ETH)
Off-diagonal matrix elements $\langle E_n|O|E_{n'}\rangle$ $(n \neq n')$ for a local operator O show exponential decay in the system size L,

$$\langle E_n|O|E_{n'}\rangle \simeq \frac{f_O(\bar{E}_{nn'}, \omega_{mn})}{\sqrt{D_{\bar{E}_{mn}}}} R_{nn'}, \quad \bar{E}_{nn'} = \frac{E_n + E_{n'}}{2}, \quad \omega_{nn'} = E_n - E_{n'}. \tag{1.62}$$

with a smooth function $f_O(\bar{E}, \omega)$. The density of states under the Hamiltonian, denoted by $D_{\bar{E}}$, usually shows exponential decay in the size L. The complex random variable $R_{nn'}$, satisfying $R_{nn'} = R^*_{n'n}$, has zero mean and unit variance.

While integrable and MBL systems violate ETH and off-diagonal ETH, it has been conjectured that generic nonintegrable systems satisfy them.

Let us see the relation between ETH and thermalization in closed setups. Keeping the dynamics of nonintegrable systems in mind, we assume (diagonal) ETH, Eq. (1.61). For any inital state in the energy shell at E, given by $|\psi(0)\rangle = \sum_{n:E_n\in\Delta(E)} c_n |E_n\rangle$, the infinite-time mean value of a local observable O becomes

$$\overline{\langle O\rangle} = \lim_{\tau\to\infty} \frac{1}{\tau} \int_0^\tau \sum_{n,n'} c^*_n c_{n'} e^{i(E_n - E_{n'})t} \langle E_n|O|E_{n'}\rangle\, dt. \tag{1.63}$$

Due to the level repulsion in generic nonintegrable systems, it is natural to assume the absence of degeneracy in the spectrum $\{E_n\}_n$. Combining with Eq. (1.61), we obtain

$$\overline{\langle O\rangle} = \sum_n |c_n|^2 \langle E_n|O|E_n\rangle \simeq \langle O\rangle_{\rm MC}\,. \tag{1.64}$$

Therefore, ETH is a sufficient condition for the long-time average of any local observable to approach the microcanonical ensemble value in nonintegrable many-body systems.

Next, we consider the fluctuation $\overline{\langle(\Delta O)^2\rangle}$ to assess the equilibration of the system. Here, we further assume off-diagonal ETH, Eq. (1.62). For the initial state $|\psi(0)\rangle = \sum_{n:E_n\in\Delta(E)} c_n |E_n\rangle$, we can compute the fluctuation as

$$\overline{\langle(\Delta O)^2\rangle} = \sum_{n\neq n'} \sum_{l\neq l'} c^*_n c_{n'} c^*_l c_{l'} \left(\lim_{\tau\to\infty} \frac{1}{\tau} \int_0^\tau dt e^{i(E_n - E_{n'} + E_l - E_{l'})t} \right) \langle E_n|O|E_{n'}\rangle \langle E_l|O|E_{l'}\rangle\,. \tag{1.65}$$

In generic nonintegrable systems, the energy eigenvalues are expected to be placed at random with experiencing the repulsion. This validates the assumption of the non-resonance condition,

$$E_n - E_{n'} = E_{l'} - E_l \neq 0 \quad \text{only when } n = l' \text{ and } n' = l, \tag{1.66}$$

which indicates that any pair of the eigenstates has a different gap. This results in

$$\begin{aligned} \overline{\langle (\Delta O)^2 \rangle} &= \sum_n \sum_{n' \neq n} |c_n|^2 |c_{n'}|^2 |\langle E_n|O|E_{n'}\rangle|^2 \\ &\leq \max_{n \neq n'} |\langle E_n|O|E_{n'}\rangle|^2, \end{aligned} \tag{1.67}$$

where we use the normalization condition $\sum_n |c_n|^2 = 1$ in the last inequality. Considering off-diagonal ETH represented by Eq. (1.61), the fluctuation $\overline{\langle (\Delta O)^2 \rangle}$ rapidly vanishes as $e^{-O(L)}$ with the increasing system size L. As a result, the satisfaction of off-diagonal ETH suggests that generic nonintegrable systems equilibrate, and also relax to thermal equilibrium when combined with the result of ETH.

ETH and off-diagonal ETH are merely a sufficient condition of thermalization and there is no rigorous proof of them for generic nonintegrable systems. However, due to the satisfaction of them and the existence of thermalization for generic nonintegrable systems and the opposite results for integrable and MBL systems, ETH and off-diagonal ETH are considered to be key ingredients for understanding thermalization in closed quantum systems.

Entanglement properties of ergodic systems

Generic nonintegrable systems are believed to satisfy ETH and off-diagonal ETH, thereby hosting relaxation to thermal equilibrium states. Such systems are often referred to as ergodic systems, in analogy with ergodicity in classical systems. Although it is difficult to rigorously judge whether a given quantum system is ergodic, we can numerically test it from the common properties of ergodic systems. As discussed above, the fingerprints of quantum ergodic systems appear in the level repulsion and the level spacing obeying the Wigner-Dyson statistics, which comes from their non-inetgrability. We can detect ergodicity by directly confirming that the matrix elements $\langle E_n|O|E_n\rangle$ correspond to thermal equilibrium values.

We hereby introduce entanglement entropy as another frequently-used signature of ergodicity. We split the whole system Λ by $\Lambda = A \cup B$ with $A \cap B = \phi$, where A and B denote subsystems. For a given quantum state $|\psi\rangle$, we define its entanglement entropy between A and B by

$$S[\psi] = -\mathrm{Tr}[\rho_A[\psi] \log \rho_A[\psi]] = -\mathrm{Tr}[\rho_B[\psi] \log \rho_B[\psi]], \tag{1.68}$$

$$\rho_A[\psi] = \mathrm{Tr}_B[|\psi\rangle\langle\psi|], \quad \rho_B[\psi] = \mathrm{Tr}_A[|\psi\rangle\langle\psi|]. \tag{1.69}$$

While the entanglement entropy measures quantum correlations between the two subsystems, it corresponds to the von Neumann entropy of the reduced density matrix for each subsystem. Let us discuss how the entanglement entropy behaves in generic ergodic systems. Here, we assume the subsystem A is sufficiently large but much smaller compared to the whole system Λ. Then, for any local observable O_A acting only on A, ETH dictates the indistinguishability,

$$\mathrm{Tr}_A[O_A \rho_A[E_n]] = \langle E_n|O_A|E_n\rangle \simeq \mathrm{Tr}[O_A \rho_\beta] \tag{1.70}$$

for every eigenstate $|E_n\rangle$ of the whole Hamiltonian H. If the subsystem A is large enough so that the interactions between A and B at their boundaries can be neglected, the thermal equilibrium value $\mathrm{Tr}[O_A \rho_\beta]$ is approximated by that of the subsystem equilibrium $\rho_\beta^A = e^{-\beta H_A}/\mathrm{Tr}[e^{-\beta H_A}]$. Thus, the equivalence by $\mathrm{Tr}_A[O_A \rho_A[E_n]] \simeq \mathrm{Tr}_A[O_A \rho_\beta^A$ for any O_A suggests $\rho_A[E_n] \simeq \rho_\beta^A$, and hence every eigenstate $|E_n\rangle$ is expected to have the volume-law entanglement entropy,

$$S[E_n] \sim L^d, \tag{1.71}$$

in generic nonintegrable systems satisfying ETH.

We also mention typical behaviors of entanglement dynamics in ergodic systems. We prepare a certain product state $|\psi(0)\rangle$, and track its entanglement entropy $S(t) = S[\psi(t)]$ with $|\psi(t)\rangle =$

$e^{-iHt}|\psi(0)\rangle$. From some numerical simulations on spin systems, it has been conjectured that generic ergodic systems experience ballistic transport of information due to the absence of local conserved quantities, which results in the linear growth, $S(t) \sim t$ [44]. This is in contrast to localized systems, where the local conserved quantities strongly suppress the entanglement growth, as discussed in Section 1.3.5.

1.3.2 Quantum many-body scars (QMBS)

As ETH is referred to as "hypothesis", it has been a fundamental and crucial question whether ETH is genuinely satisfied for any nonintegrable Hamiltonian. Quantum many-body scars (QMBS) have been explored as intriguing nonintegrable models violating ETH since the observation of their athermal behaviors in Rydberg atoms in 2017 [45, 46, 47, 48] (See Refs. [49, 50] for review).

Here, we briefly introduce QMBS based on some initial studies along the Rydberg-atom experiments. Let us consider a one-dimensional Ising spin chain whose Hamiltonian is

$$H_{\mathrm{TFIM}} = J\sum_i \sigma_i^z\sigma_{i+1}^z + h\sum_i \sigma_i^x. \tag{1.72}$$

When the nearest-neighbor interaction J is extremely large compared to h, a pair of neighboring excited states is prohibited and the states are restricted in the Hilbert space

$$\mathcal{H}_{\mathrm{Ryd}} = \mathrm{span}\{P_{\mathrm{Ryd}}|\psi\rangle \mid |\psi\rangle \in \mathcal{H}\}, \quad P_{\mathrm{Ryd}} = \prod_{i=1}^{N-1}\left(\frac{I - |\uparrow\uparrow\rangle\langle\uparrow\uparrow|}{2}\right)_{i,i+1}. \tag{1.73}$$

We can obtain the effective static Hamiltonian in the restricted Hilbert space $\mathcal{H}_{\mathrm{Ryd}}$ by

$$P_{\mathrm{Ryd}}H_{\mathrm{TFIM}}P_{\mathrm{Ryd}} = P_{\mathrm{Ryd}}H_{\mathrm{PXP}}P_{\mathrm{Ryd}} \sim H_{\mathrm{PXP}} \quad (\text{on } \mathcal{H}_{\mathrm{Ryd}}), \tag{1.74}$$

with a so-called PXP Hamiltonian [2],

$$H_{\mathrm{PXP}} = \sum_{i=1}^{N} P_{i-1}\sigma_i^x P_{i+1}, \quad P_i = (I - |\uparrow\rangle\langle\uparrow|)_i. \tag{1.75}$$

The PXP Hamiltonian can be experimentally realized in Rydberg atoms, a cold atomic system which has excited states with a larger quantum number ~ 100. Neighboring atoms in the excited states feel strong repulsive van der Waals interactions, thereby making the restriction to the Hilbert space $\mathcal{H}_{\mathrm{Ryd}}$ (called Rydberg blockade).

From the level statistics, the PXP Hamiltonian H_{PXP} on $\mathcal{H}_{\mathrm{Ryd}}$ is numerically confirmed to be nonintegrable [46]. Nevertheless, opposed to the expectation from ETH that any initial state relaxes to thermal equilibrium, it shows the following dynamics dependent on the initial states:

1. (Exact AKLT (Affleck-Kennedy-Lieb-Tasaki) QMBS) Persistent motion completely avoiding thermalization from the exact QMBS eigenstates $|\Gamma\rangle$ (See Chapter 4 for the detail).
2. (Approximate $\mathbb{Z}_n$ QMBS) Extremely long-term oscillation from the $\mathbb{Z}_n$ states,
$$|\mathbb{Z}_2\rangle = |\uparrow\downarrow\uparrow\downarrow\ldots\rangle, \quad |\mathbb{Z}_3\rangle = |\uparrow\downarrow\downarrow\uparrow\downarrow\downarrow\ldots\rangle, \ldots. \tag{1.76}$$
3. Relaxation to thermal equilibrium from the other initial states

The rigorous analytical calculation confirms the behavior 1. [47], and the experiments in Rydberg atoms observes 2. and 3. [45]. The numerical simulations with some approximations, such as the forward scattering approximation (FSA) [46] and the time-dependent variational principle (TDVP) [48], reproduce all of them, especially explaining the mechanism of 2. As an important signature related to ETH here, the exact QMBS eigenstate $|\Gamma\rangle$ is an athermal eigenstate of H_{PXP}, which means that there exists a local observable O such that

$$\langle\Gamma|O|\Gamma\rangle \neq \langle O\rangle_{\mathrm{MC}}. \tag{1.77}$$

[2] We change the definition of the projection P_0 and P_{L+1} depending on the boundary condition. Under the periodic boundary condition, we choose $P_0 \equiv P_L$ and $P_{L+1} \equiv P_1$. Under the open boundary condition, we choose $P_0 \equiv I_L$ and $P_{L+1} \equiv I_1$.

This indicates the violation of ETH in nonintegrable systems, resulting the completely athermal dynamics 1. The approximately athermal behavior 2. can also attributed to the exact QMBS eigenstate $|\Gamma\rangle$ in that the $\mathbb{Z}_n$ states have large overlap with $|\Gamma\rangle$ and a series of its locally-excited states [47].

Therefore, quantum many-body scars (QMBS), the above athermal behavior from some special scar states in nonintegrable systems, provide a counterexample of ETH, leading to the possibility of another mechanism of thermalization in interacting systems. We note that ETH is still considered to be one of the keys to understanding thermalization, since generic nonintegrable systems in fact satisfy ETH, thereby experiencing thermalization. Even in the exceptional models showing QMBS, the Hamiltonian restricted to the Hilbert space except for the exact QMBS eigenstates satisfies ETH as well as generic nonintegrable models, resulting in the thermal steady state (See 3.).

After the proposal of the PXP model, various types of QMBS have been extensively explored. The first type resembles the PXP model, in which local constraints by projections generate some special QMBS eigenstates [51]. The second type relies on algebraic structures in the restricted Hilbert space [52]. In this type, a series of QMBS eigenstates appears in the restricted space with a tower structure generated by ladder operators. The third type is called Hilbert space shattering [53, 54], in which the coexistence of macroscopic symmetries and locality causes the separation of the whole Hilbert space leading to athermal steady states. Any type of QMBS not only plays a role as counterexamples of ETH, but also provides an insight into many-body Hamiltonian and many-body states, such as the hidden separated structure of the Hilbert space.

1.3.3 Floquet eigenstate thermalization hypothesis (Floquet-ETH)

Let us go back to the discussion on Floquet many-body systems described by

$$i\frac{d}{dt}|\psi(t)\rangle = H(t)|\psi(t)\rangle, \quad H(t) = H(t+T). \tag{1.78}$$

We again assume a system defined on a lattice Λ with the size $|\Lambda| = L$, and the bounded Hamiltonian satisfying $||H(t)|| < \infty$ at any instantaneous time t. We are interested in the stroboscopic dynamics of generic quantum many-body systems, $|\psi(mT)\rangle = (U_f)^m|\psi(0)\rangle$. Particularly, in analogy with closed time-independent systems, it is of central interest whether or not the periodically-driven system relaxes to some steady state, and what characterizes the steady state if true. As well as time-independent cases, the existence of thermalization depends on the integrability for Floquet systems, in which the Floquet version of ETH, "Floquet-ETH", is considered to play a significant role.

Integrability and nonintegrability

We begin with the integrability and the nonintegrability for Floquet many-body systems. In the case of Floquet systems, we focus on the Floquet operator U_f, instead of static Hamiltonians. We call a Floquet system integrable if its Floquet operator U_f has an extensive number of local conserved quantities. We call a Floquet system nonintegrable if the Floquet operator U_f does not have an extensive number of local conserved quantities and the effective Hamiltonian $H_{\text{eff}} = (i/T)\log U_f$ becomes nonlocal. Here, we include the nonlocality of H_{eff} for the nonintegrablity to exclude the cases equivalent to time-independent systems. In nonintegrable Floquet systems, there is no physically meaningful conserved quantity that is macroscopic and local, while nonintegrable static systems possess conserved energy.

As well as static systems, integrability and nonintegrablity in Floquet systems can numerically be detected by level statistics [55]. With the usage of the quasienergy spectrum $\{\varepsilon_n\}_n$, the eigenvalues of the effective Hamiltonian H_{eff}, we define the level spacing r_n by

$$r_n = \min\left(\frac{s_n}{s_{n+1}}, \frac{s_{n+1}}{s_n}\right), \quad s_n = \varepsilon_{n+1} - \varepsilon_n. \tag{1.79}$$

Since the quasienergy near the branch cut occupies only the small fraction of the whole spectrum, the choice of the brunch cut hardly affects its statistics $\{r_n\}_n$. In integrable Floquet systems, the quasienergy does not host the level repulsion, and hence the statistics of its gap is expected to obey Poisson distribution. On the other hand, in nonintegrable Floquet systems, it hosts the level

repulsion with mimicking random matrices. Instead of Gaussian ensemble for random hermitian matrices in static cases, the Floquet operator U_f behaves like a random unitary matrix from Circular Unitary Ensemble (CUE) [without TRS] or Circular Orthogonal Ensemble (COE) [with TRS] . Here, the TRS for Floquet systems is defined by

$$^{\exists}U_{\mathcal{T}} : \text{unitary}, \quad \text{s.t.} \quad U_{\mathcal{T}} U_f^* U_{\mathcal{T}}^\dagger = U_f^\dagger. \tag{1.80}$$

To summarize, the integrability of Floquet systems can be diagnosed by the mean value of the level spacing ratio r_n coming from the different level statistics as follows.

$$r \equiv \langle r_n \rangle_n \simeq \begin{cases} 0.386 & \text{(Integrable cases)} \\ 0.597 & \text{(Nonintegrable cases without TRS)} \\ 0.527 & \text{(Nonintegrable cases with TRS).} \end{cases} \tag{1.81}$$

Floquet-ETH and the heating problem

With the above description for the integrability and nonintegrability in Floquet systems, let us consider how the dynamics of closed Floquet many-body systems behaves. For Floquet systems, we focus on the stroboscopic dynamics described by $|\psi(mT)\rangle = (U_f)^m |\psi(0)\rangle$, and we are interested in the infinite-time average at discrete time,

$$\overline{\langle O \rangle}_{\text{Strobo}} = \lim_{M\to\infty} \frac{1}{M} \sum_{m=0}^{M-1} \langle O(mT) \rangle \,, \tag{1.82}$$

with $\langle O(mT) \rangle \equiv \langle \psi(mT)|O|\psi(mT)\rangle$. The convergence of the observable $\langle O(mT)\rangle$ can be evaluated by the fluctuation,

$$\overline{\langle (\Delta O)^2 \rangle}_{\text{Strobo}} = \lim_{M\to\infty} \frac{1}{M} \sum_{m=0}^{M-1} \langle O(mT) \rangle^2 - \left(\lim_{M\to\infty} \frac{1}{M} \sum_{m=0}^{M-1} \langle O(mT) \rangle \right)^2 . \tag{1.83}$$

When the fluctuation $\overline{\langle (\Delta O)^2 \rangle}_{\text{Strobo}}$ is sufficiently small compared to $||O||^2$, the Floquet system equilibrates after long time. In addition, under the equilibration with $\overline{\langle (\Delta O)^2 \rangle}_{\text{Strobo}} \ll ||O||^2$, we can regard a mixed state ρ_{SS}, which gives $\overline{\langle O \rangle}_{\text{Strobo}} \simeq \text{Tr}[O\rho_{\text{SS}}]$ for any local observable O, as a steady state of the Floquet system. The central questions are whether there exists equilibration in generic Floquet many-body systems, and what characterises the steady state ρ_{SS} then. The latter is rather important in Floquet cases, since generic Floquet systems do not have the energy conservation due to their time-dependency. The thermal equilibrium state ρ_β, Eq. (1.60), becomes ill-defined except for $\beta = 0$ in Floquet cases.

The existence of thermalization depends on the integrability also in Floquet cases. In integrable Floquet systems, a macroscopic number of local conserved quantities again prevent the thermalization. On the other hand, generic nonintegrable Floquet systems are believed to satisfy the Floquet versions of ETH and off-diagonal ETH, while integrable Floquet systems violate them [55, 56]. In a similar way to static cases, they lead to thermailization in nonintegrable Floquet systems from any initial state. We describe them, dubbed Floquet-ETH and off-diagonal Floquet-ETH, and discuss their relation to thermalization in Floquet systems below.

Remark. (Floquet eigenstate thermalization hypothesis, Floquet-ETH)
Let $|\varepsilon_n\rangle$ denote the eigenstate of the Floquet operator U_f with the quasienergy ε_n. We define the infinite-temperature state by

$$\rho_\infty = \lim_{\beta\to 0} \frac{e^{-\beta H}}{\mathrm{Tr}[e^{-\beta H}]} = \frac{I}{\dim(\mathcal{H})}. \tag{1.84}$$

as a thermal equilibrium state at infinite temperature. The state ρ_β is referred to as trivial in that it does not reflect the underlying Hamiltonian $H(t)$ at all. Diagonal Floquet-ETH (or simply Floquet-ETH) and off-diagonal Floquet-ETH are described by the following statements.

(Diagonal Floquet-ETH, or simply Floquet-ETH)
Every eigenstate $|\varepsilon_n\rangle$ is equivalent to the infinite-temperature state, that is,

$$\langle\varepsilon_n|O|\varepsilon_n\rangle \simeq \langle O\rangle_\infty, \quad \langle O\rangle_\infty \equiv \mathrm{Tr}[O\rho_\infty], \tag{1.85}$$

for a local operator O when the system size L is sufficiently large.

(Off-diagonal Floquet-ETH)
Off-diagonal matrix elements $\langle\varepsilon_n|O|\varepsilon_{n'}\rangle$ $(n \neq n')$ for a local operator O show exponential decay in the system size L,

$$\langle\varepsilon_n|O|\varepsilon_{n'}\rangle \simeq \frac{f_O(\omega_{nn'})}{\sqrt{D}} R_{nn'}, \quad \omega_{nn'} = \varepsilon_n - \varepsilon_{n'}, \tag{1.86}$$

with a smooth function $f_O(\omega)$ and $D = \dim(\mathcal{H})$. Here, $R_{nn'}$ denotes a complex random variable with zero mean and unit variance, satisfying $R_{nn'} = R^*_{n'n}$.

While integrable Floquet systems and Floquet-MBL systems (See Section 1.3.5) violate ETH and off-diagonal ETH, it has been conjectured that generic nonintegrable Floquet systems satisfy them.

Let us discuss what Floquet-ETH and off-diagonal Floquet-ETH imply in the dynamics of generic nonintegrable Floquet systems. We consider a generic initial state $|\psi(0)\rangle = \sum_n c_n |\varepsilon_n\rangle$, and we first assume the satisfaction of Floquet-ETH, Eq. (1.85). Then, the infinite-time average of a local observable, given by Eq. (1.82), becomes

$$\overline{\langle O\rangle}_{\mathrm{Strobo}} = \lim_{M\to\infty} \sum_{n,n'} \frac{1}{M} \sum_{m=0}^{M-1} c_n^* c_{n'} e^{i(\varepsilon_n - \varepsilon_{n'})mT} \langle\varepsilon_n|O|\varepsilon_{n'}\rangle . \tag{1.87}$$

We can make the assumption of no degeneracy in the quasienergy $\{\varepsilon_n\}_n$, which naturally comes from the level repulsion in nonintegrable systems. As a result, we obtain

$$\overline{\langle O\rangle}_{\mathrm{Strobo}} = \sum_n |c_n|^2 \langle\varepsilon_n|O|\varepsilon_n\rangle \simeq \frac{1}{\dim(\mathcal{H})}\mathrm{Tr}[O]. \tag{1.88}$$

Therefore, in nonintegrable Floquet systems, Floquet-ETH or Eq. (1.85) is the sufficient condition for the infinite-time average of local observables corresponding to their infinite-temperature values. In other words, after sufficiently long time, any initial state becomes indistinguishable from the trivial infinite-temperature state in its time average.

Whether or not the nonintegrable Floquet systems equilibrate can be determined by the fluctuation $\overline{\langle(\Delta O)^2\rangle}_{\mathrm{Strobo}}$, given by Eq. (1.83). Here, let us assume off-diagonal ETH for the nonintegrable Floquet systems, Eq. (1.86), in a similar way to static systems. Then, we can calculate the fluctuation in time as follows:

$$\overline{\langle(\Delta O)^2\rangle}_{\mathrm{Strobo}} = \sum_{n\neq n'} \sum_{l\neq l'} c_n^* c_{n'} c_l^* c_{l'} \left(\lim_{M\to\infty} \frac{1}{M} \sum_{m=0}^{M-1} e^{i(\varepsilon_n - \varepsilon_{n'} + \varepsilon_l - \varepsilon_{l'})mT} \right) \langle\varepsilon_n|O|\varepsilon_{n'}\rangle \langle\varepsilon_l|O|\varepsilon_{l'}\rangle . \tag{1.89}$$

As a natural assumption in generic nonintegrable systems, we again suppose the non-resonance condition,

$$\varepsilon_n - \varepsilon_{n'} = \varepsilon_{l'} - \varepsilon_l \neq 0 \quad \text{only when } n = l' \text{ and } n' = l. \tag{1.90}$$

We combine this condition with off-diagonal Floquet-ETH, Eq. (1.86), which leads to

$$\begin{aligned} \overline{\langle (\Delta O)^2 \rangle}_{\text{Strobo}} &= \sum_{n \neq n'} |c_n|^2 |c_{n'}|^2 |\langle \varepsilon_n | O | \varepsilon_{n'} \rangle|^2 \\ &\leq \max_{n \neq n'} |\langle \varepsilon_n | O | \varepsilon_{n'} \rangle|^2. \end{aligned} \tag{1.91}$$

Off-diagonal Floquet-ETH, Eq. (1.86), implies the vanishing fluctuation $\overline{\langle (\Delta O)^2 \rangle}_{\text{Strobo}}$ with the growing system size L, representing that the expectation value $\langle O(mT) \rangle$ itself approaches a certain value after sufficiently long time. With the combination of Floquet-ETH, we arrive at the following conjecture in Floquet systems, dubbed *heating problem*.

Remark. (Heating problem)
In generic Floquet many-body systems with no local conserved quantities, any initial state $|\psi(0)\rangle$ is believed to relax to a featureless infinite-temperature state:

$$\langle O(mT) \rangle \simeq \frac{1}{\dim(\mathcal{H})} \text{Tr}[O], \tag{1.92}$$

for sufficiently large time $t = mT$ as a result of Floquet-ETH and off-diagonal Floquet-ETH.

Overcome Floquet-ETH or the heating problem

To summarize, Floquet-ETH (or the heating problem) implies the thermalization of the long-time average $\overline{\langle O \rangle}_{\text{Strobo}}$ (or $\langle O(mT) \rangle$ at late time $t = mT$) to the infinite-temperature value. As well as static systems, Floquet-ETH, off-diagonal Floquet-ETH, and the resulting thermalization are numerically verified [55, 56, 57]. In a particular class of Floquet systems, called dual-unitary quantum circuits [58, 59, 60, 61, 62], the distribution of off-diagonal matrix elements, which appear in off-diagonal Floquet-ETH [See Eq. (1.86)] can be exactly obtained [63]. Taking into account that thermalization is absent in integrable Floquet systems and Floquet-MBL systems violating Floquet-ETH and off-diagonal Floquet-ETH, they are believed to explain thermalization in closed nonintegrable Floquet systems.

What distinguishes Floquet-ETH or the heating problem from their counterparts in static systems, they predict trivial physics in generic Floquet many-body systems. Any local observable in steady states of generic Floquet many-body systems, given by $\text{Tr}[O\rho_\infty]$, does not reflect the Hamiltonian $H(t)$ at all. This comes from the absence of a macroscopic local observable, which is a counterpart of a Hamiltonian H in static systems. Although the effective Hamiltonian H_{eff} is a conserved macroscopic observable in nonintegrable Floquet systems, it gives no physical sense for any local observable O due to its nonlocality.

Quantum many-body phenomena in Floquet systems, which are at the center of this thesis, have been a significant and fundamental field in today's nonequilibrium condensed matter physics. To find out nontrivial phenomena, we should overcome Floquet-ETH or the heating problem and avoid trivial steady states predicted from them. In the following subsections, we introduce some preliminary phenomena avoiding the troubles by Floquet-ETH and the heating problem in some way.

1.3.4 Floquet prethermalization in the high-frequency regime

Floquet-ETH or the heating problem predict trivial inifinite-temperature steady states in generic Floquet many-body systems, but they do not deny the non-triviality in the quasi-steady states. Floquet prethermalization indicates the realization of nontrivial thermal quasi-steady states with sufficiently-long but not infinite lifetime. We note that generic Floquet many-body systems hosting Floquet prethermalization still satisfy Floquet-ETH, and typically show dynamics with multiple equilibrations like Fig. 1.4. The existence of Floquet prethermalization or equivalently the long-lived quasi-steady states is nontrivial. However, it has been proven that Floquet many-body

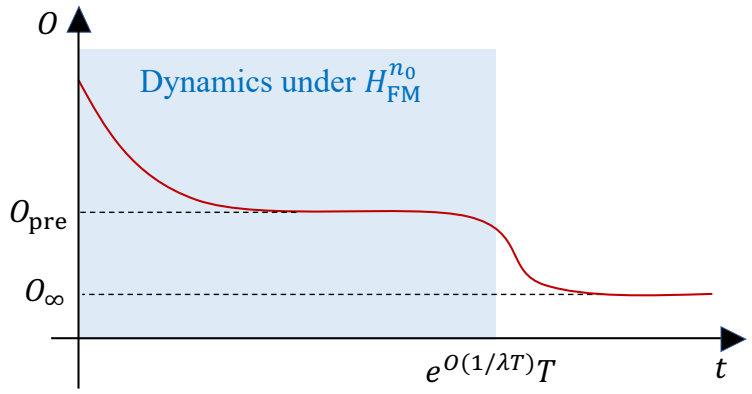

Figure 1.4: Schematic picture of Floquet prethermalization in the high-frequency regime. Dynamics under the time-independent local Hamiltonian $H_{\mathrm{FM}}^{n_0}$ is approximately realized for a sufficiently long time. After that, it is expected to relax to infinite-temperature states due to Floquet-ETH.

systems, where the local energy scale is much smaller than the frequency (the high-frequence regime), can universally host such a phenomenon [28, 64, 65, 66].

To discuss Floquet prethermalization in the high-frequency regime, we first introduce the way to quantitatively evaluate the local energy scale below. We define the locality and the extensiveness as follows.

Definition 1.3.1. (Locality and Extensiveness)
We consider a static Hamiltonian H on a lattice Λ. The Hamiltonian H can be always represented by $H = \sum_{X\subset\Lambda} h_X$, where h_X nontrivially acts just on a domain $X \subset \Lambda$. Then, the locality k and the extensiveness J are defined as follows:

$$H \text{ is } k\text{-local} \quad \Leftrightarrow \quad |X| \le k \text{ for any } X \text{ s.t. } h_X \neq 0, \tag{1.93}$$

$$H \text{ is } J\text{-extensive} \quad \Leftrightarrow \quad \max_{i\in\Lambda}\left(\sum_{X:X\ni i} ||h_X||\right) \le J. \tag{1.94}$$

For a time-periodic Hamiltonian $H(t)$, we define its locality and extensiveness in a similar way. We call $H(t)$ a k-local Hamiltonian when it can be represented as $H(t) = \sum_{X:|X|\le k} h_X(t)$, and call it J-extensive when the maximum of $\sum_{X:X\in i} ||h_X(t)||$ with respect to a site i and time t is bounded by J. We define the local energy scale by $\lambda = 2kJ$.

The k-locality means that a Hamiltonian involves at-most k-body interactions. Using the following inequality

$$||H|| \le \sum_X ||h_X|| \le \sum_{i\in\Lambda}\sum_{X:X\ni i} ||h_X|| \le JL, \tag{1.95}$$

the extensiveness J ($\ge ||H||/L$) gives the maximal energy scale per site, characterizing the local energy scale of a Hamiltonian, $\lambda = 2kJ$. For a simple example described by the one-dimensional long-ranged Hamiltonian

$$H = \sum_{i\neq j} \frac{J_{\mathrm{int}}}{|i-j|^\alpha}\sigma_i^z\sigma_j^z + \sum_i h_x\sigma_i^x, \quad (\alpha > 1), \tag{1.96}$$

we obtain the locality $k = 2$ and the extensiveness $J = 2|J_{\mathrm{int}}|\zeta(\alpha) + |h_x|$ ($\zeta(x)$ is the zeta function). We note that the locality defined here is not related to the range of interactions.

Quasi-steady states and Effective Hamiltonian

We now discuss Floquet prethermalization in the high-frequency regime. We consider a k-local ($k = O(1)$) and J-extensive Hamiltonian $H(t)$ on an L-site lattice Λ. We assume the high-frequency

regime, $JT \ll 1$. Then, as explained below, the following approximation is verified:

$$|\psi(mT)\rangle \simeq e^{-i\tilde{H}_{\rm eff}mT}\,|\psi(0)\rangle\,, \quad t = mT < \tau_c = e^{O(\omega/J)}T, \tag{1.97}$$

with a certain local time-independent Hamiltonian $\tilde{H}_{\rm eff}$. In the exponentially-long time $\tau_c = e^{O(\omega/J)}T$, the stroboscopic dynamics has a macroscopic local conserved quantity $\tilde{H}_{\rm eff}$ just like that in static systems, thereby avoiding the heating. This approximate dynamics under $\tilde{H}_{\rm eff}$ within $t < e^{O(\omega/J)}T$ is called Floquet prethermalization.

Here, we briefly review how the macroscopic local conserved quantity $\tilde{H}_{\rm eff}$ emerges in Floquet prethermalization. Let us consider the effective Hamiltonian $H_{\rm eff} = (i/T)\log U_f$ and the Floquet-Magnus expansion $H^n_{\rm FM}$ [See Eqs. (1.27)-(1.29)], since we are now focusing on the high-frequency regime $JT \ll 1$. We should note that, for generic many-body systems, the perturbative expansion $H^\infty_{\rm FM} = \sum_{m=0}^\infty H^{(m)}_{\rm FM}$ is divergent since the parameter $||H(t)||/\omega \sim JL/\omega$ exceeds the convergence radius $r_c = O(1)$ even in the case of $JT \ll 1$. This means that the Floquet-Magnus expansion is not an asymptotic expansion for the effective Hamiltonian $H_{\rm eff}$, and it seems to have no physical sense. Nevertheless, under the locality and the extensiveness, the Floquet-Magnus expansion is proven to show a convergent behavior up to a certain order. For instance, the first-order term $H^{(1)}_{\rm FM}$ is bounded by

$$\begin{aligned}\left|\left|H^{(1)}_{\rm FM}\right|\right| &= \left|\left|\frac{1}{2iT}\int_0^T dt_1\int_0^{t_1} dt_2[H(t_1),H(t_2)]\right|\right| \\ &\le \frac{1}{2T}\int_0^T dt_1\int_0^{t_1} dt_2 \sum_{X,Y\subset\Lambda} |||[h_X(t_1),h_Y(t_2)]|||\end{aligned} \tag{1.98}$$

Since the integrand is further bounded by

$$\begin{aligned}\sum_{X,Y\subset\Lambda} |||[h_X(t_1),h_Y(t_2)]||| &= 2\sum_{X,Y:X\cap Y\neq\phi} ||h_X(t_1)||\cdot||h_Y(t_2)|| \\ &\le 2\left(\sum_Y\sum_{i\in Y}\sum_{X:X\ni i} + \sum_X\sum_{i\in X}\sum_{Y:Y\ni i}\right)||h_X(t_1)||\cdot||h_Y(t_2)|| \\ &\le 2kJ\sum_X(||h_X(t_1)|| + ||h_X(t_2)||) \le 4kJ^2N,\end{aligned} \tag{1.99}$$

we obtain $\left|\left|H^{(1)}_{\rm FM}\right|\right| \le \lambda T(JL)/4$. This bound is comparably smaller than the expected one, $O(||H(t)||\cdot r) \sim \lambda T(JL)\cdot(N/k)$, obtained from the perturbation parameter $r = ||H(t)||/\omega$ if the locality k is smaller compared to the system size L. In a similar way, Floquet systems with locality and extensiveness have the Floquet-Magnus expansion with suppressed divergence.

Theorem 1.3.2. (FM expansion under locality and extensiveness) [28]
For a k-local and J-extensive Hamiltonian $H(t)$, each m-th order term of its Floquet-Magnus expansion $H^{(m)}_{\rm FM}$, given by Eq. (1.28), has the following upper bound:

$$||H^{(m)}_{\rm FM}||/L \le J^{(m)} \le \frac{(\lambda T)^m}{m+1}m!\cdot J, \tag{1.100}$$

where $J^{(m)}$ is the extensiveness of $H^{(m)}_{\rm FM}$.

Using Stirling's formula $m! \sim (m/e)^m$, this theorem says that the m-th order term $H^{(m)}_{\rm FM}$, which is order of $(m\lambda T/e)^m JN/m$, shows a convergent behavior up to the order $n_0 = O(1/\lambda T)$ ($\gg 1$) satisfying $n_0\lambda T/e \sim 1$. This behavior is in contrast to the divergence of the Floquet-Magnus expansion in generic Floquet many-body systems. In fact, after some discussion based on the locality and the extensiveness, the Floquet-Magnus effective Hamiltonian $H^n_{\rm FM}$ plays a role in giving a macroscopic local quasi-conserved quantity when its convergent behavior is accompanied under $n < n_0 = O(1/\lambda T)$.

Theorem 1.3.3. (Floquet prethermalization) [28]
For a k-local and J-extensive Hamiltonian $H(t)$, we assume $4\lambda T < 1$ with the local energy scale $\lambda = 2kJ$. Then, the Floquet operator U_f is approximated as follows:

$$\left|\left|U_f - e^{-iH_{\rm FM}^{n_0}T}\right|\right| \leq \frac{3}{k}L(\lambda T)2^{-n_0} \tag{1.101}$$

where n_0 is the largest integer that does not exceed $1/(16\lambda T)$. When we truncate it at the order $n \leq n_0$, the bound becomes

$$\left|\left|e^{-iH_{\rm FM}^{n_0}T} - e^{-iH_{\rm FM}^{n}T}\right|\right| \leq 2||H_{\rm FM}^{(n+1)}||T \leq \frac{2(n+1)!}{(n+2)k}L(\lambda T)^{n+2}. \tag{1.102}$$

The right hand side of Eq. (1.101) becomes smaller as the order n increases up to $n_0 = O(1/\lambda T)$. Considering the relation $||(U_f)^m - \exp(-iH_{\rm FM}^{n_0}mT)|| \leq m||U_f - \exp(-iH_{\rm FM}^{n_0}T)||$ and choosing the order n by n_0, the stroboscopic dynamics can be approximated as

$$|\psi(mT)\rangle = (U_f)^m|\psi(0)\rangle = e^{-iH_{\rm FM}^{n_0}mT}|\psi(0)\rangle + mL\cdot e^{O(-1/\lambda T)} \simeq e^{-iH_{\rm FM}^{n_0}mT}|\psi(0)\rangle, \tag{1.103}$$

as long as the time $t = mT$ is smaller than $e^{O(1/\lambda T)}T/L$. This reproduces Eq. (1.97), indicating that the truncated Floquet-Magnus expansion $H_{\rm FM}^{n_0}$ plays a role of a local macroscopic conserved quantity and that the Floquet systems experience the dynamics under $H_{\rm FM}^{n_0}$ during $t < e^{O(1/\lambda T)}T/L$. This lifetime is much larger than the one expected from the convergence radius, $O(T/(\lambda L))$, for many-body systems. Although this theorem says nothing about the dynamics after the prethermal regime, they are expected to host thermalization to infinite temperature due to Floquet-ETH. Thus, the generic dynamics of Floquet many-body systems in the high-frequency regime show multiple relaxations, which can be depicted as Fig. 1.4.

We also note that Eq. (1.102) validates the approximation by the lower-order Floquet-Magnus expansion. The triangle equation with Eqs. (1.101) and (1.102) results in

$$\begin{aligned}\left|\left|U_f - e^{-iH_{\rm FM}^{n}T}\right|\right| &\leq \left|\left|U_f - e^{-iH_{\rm FM}^{n_0}T}\right|\right| + \left|\left|e^{-iH_{\rm FM}^{n_0}T} - e^{-iH_{\rm FM}^{n}T}\right|\right| \\ &\leq \frac{3}{k}L(\lambda T)2^{-n_0} + \frac{2(n+1)!}{(n+2)k}L(\lambda T)^{n+2} \\ &\leq \frac{3}{k}L(\lambda T)2^{-n_0} + \frac{2L}{(n+2)^2k}(n\lambda T)^{n+2}.\end{aligned} \tag{1.104}$$

Since the second term is decreasing function in n when $n \leq O(1/\lambda T) \sim n_0$, the lower-order expansion $H_{\rm FM}^{n}$ ($n \leq n_0$) also plays a role of a macroscopic conserved quantity in the time scale $t \leq (\lambda T)^{-n-2}/L$ for small n.

Floquet engineering

Floquet prethermalization in the high-frequency regime is often used for Floquet engineering, which enables the control of phases of matter in nonequilibrium setups. As discussed above, Floquet systems with the local energy scale $\lambda \ll \omega$ mimic the dynamics under the time-independent local Hamiltonian $H_{\rm FM}^{n}$ during $t \leq e^{O(1/\lambda T)}T$. The truncated Floquet-Magnus expansion $H_{\rm FM}^{n}$ generally includes many-body interactions via commutators, and is expected to become nonintegrable. Thus, by assuming ETH and off-diagonal ETH in static systems [Eqs. (1.61) and (1.62)], any local operator O behaves like

$$\langle O(mT)\rangle \simeq \langle\psi(0)|e^{iH_{\rm FM}^{n}mT}Oe^{-iH_{\rm FM}^{n}mT}|\psi(0)\rangle \simeq {\rm Tr}[O\rho_\beta], \tag{1.105}$$

for sufficiently large time $t = mT$ but smaller than $e^{O(1/\lambda T)}T$. Here, the state ρ_β is the thermal equilibrium state under $H_{\rm FM}^{n}$,

$$\rho_\beta = \frac{e^{-\beta H_{\rm FM}^{n}}}{{\rm Tr}[e^{-\beta H_{\rm FM}^{n}}]}, \tag{1.106}$$

and the effective temperature β is determined by the energy conservation,

$$\langle\psi(0)|H_{\rm FM}^{n}|\psi(0)\rangle = {\rm Tr}[H_{\rm FM}^{n}\rho_\beta]. \tag{1.107}$$

Thus, we can realize a preferable thermal state under the static Hamiltonian $H^n_{\rm FM}$ with finite lifetime $\tau = e^{O(1/\lambda T)}T$. In the context of Floquet engineering, we often use the van Vleck effective Hamiltonian instead of the Floquet-Magnus expansion, since we are interested in quasi-steady state properties independent of the time origin. In that case, we consider a thermal equilibrium state under the static Hamiltonian

$$H^n_{\rm vV} = H_0 + \sum_{m\neq 0} \frac{[H_{-m}, H_m]}{2m\omega} + \ldots + H^{(n)}_{\rm vV}. \tag{1.108}$$

To determine the temperature, we replace the initial state by $e^{iK^n_{\rm vV}[0]}|\psi(0)\rangle$ in Eq. (1.107), which reflects the unitary equivalence between the two expansions Eq. (1.39).

One of the simplest examples is dynamical localization induced by laser light [67, 68, 69]. A one-dimensional fermionic system coupled with linearly-polarized light is typically described by

$$H(t) = -2t\sum_k \sum_{\sigma=\uparrow,\downarrow} \cos(k - A\sin\omega t) c^\dagger_{k,\sigma} c_{k,\sigma} + H_{\rm int}, \tag{1.109}$$

with the vector potential $A(t) = A\sin\omega t$. Here, $H_{\rm int}$ denotes time-independent interactions such as the Hubbard interaction $H_U = U\sum_i c^\dagger_{i,\uparrow}c_{i,\uparrow}c^\dagger_{i,\downarrow}c_{i,\downarrow}$. When the local energy scale of the Hamiltonian $H(t)$ (e.g. $\max(t,U)$ in the case of $H_{\rm int} = H_U$) is much smaller than the frequency ω, the system can be approximated up to the lowest order by

$$H^0_{\rm FM} = -2tJ_0(A)\sum_k \cos(k) c^\dagger_k c_k + U\sum_{k,k',q} c^\dagger_{k+q} c^\dagger_{k'-q} c_{k'} c_k, \tag{1.110}$$

where we employ the formula for the m-th order Bessel function $J_m(A) = \int_0^{2\pi}(d\theta/2\pi)\cos(m\theta - A\sin\theta)$ $(m = 0, 1, 2, \ldots)$. This implies that we can control the hopping $t_{\rm FM}(A) \equiv tJ_0(A)$ by the amplitude of the light. In particular, when we set A around the zeros of the Bessel function $J_0(A)$ $(A \simeq 2.405, 5.520, \ldots)$, the suppressed hopping causes localization, dubbed dynamical localization.

Floquet engineering in Floquet prethermalization under high-frequency drives is now widely discussed in the context of various phenomena (See [70] for review). Recent theoretical studies on Floquet engineering also tell us possibilities of controlling various phenomena, which cover laser-mediated multiferroics [71], laser-induced topological superconductivity [25, 26], and laser-irradiated Kondo effects [72]. While this technique provides a powerful tool to analyze the high-frequency regime, we should note that the stroboscopic dynamics in this regime is completely understood by the time-independent local Hamiltonian $H^n_{\rm FM}$. In other words, closed Floquet systems in the high-frequency regime cannot host unique phenomena in nonequilibrium, such as anomalous Floquet topological phases and discrete time crystals.

1.3.5 Many-body localization and time crystals

Floquet many-body-localized (Floquet-MBL) phases and discrete time crystals (DTCs) are robust nonequilibrium phases realized in Floquet many-body systems. They have a macroscopic number of local quasi-conserved quantities and violate the assumption of Floquet-ETH "nonintegrability", thereby enabling nontrivial phases avoiding thermalization to infinite temperature.

Many-body localization (MBL) and Floquet-MBL

Many-body localization (MBL) is characterized by the emergence of an extensive number of quasi-local conserved quantities under interactions and disorder, forming a robust phase dubbed a MBL phase [32, 73, 74, 75, 76] (See Refs. [77, 78] for review). Quantum many-body systems lying in MBL phases have attracted much attention in that they violate ETH and avoid relaxation to equilibrium states.

Let us begin with the simplest model for MBL phases. We consider a static one-dimensional antiferromagnetic (AFM) Heisenberg model under a disordered magnetic field with $S = 1/2$ [73, 74],

$$H_{\rm MBL} = \sum_i J\vec{\sigma}_i \cdot \vec{\sigma}_{i+1} + \sum_i h_i \sigma^z_i, \quad \vec{\sigma}_i = (\sigma^x_i, \sigma^y_i, \sigma^z_i). \tag{1.111}$$

Here, a real random variable h_i is chosen uniformly from $[-h, h]$. Depending on the strength of disorder h compared to the coupling J, this model lies in either a MBL phase or a delocalized phase, hosting MBL transition between them. When the disorder strength h is smaller than a certain threshold value $h_c \simeq 3.5J$, the model lies in the delocalized phase. In this case, we can numerically confirm that it behaves like usual nonintegrable systems; it experiences the level repulsion leading to the Wigner-Dyson statistics of the level spacing, and it also satisfies ETH. Thus, the system in the delocalized phase experiences thermalization from any initial state.

On the other hand, when the disorder strength is large, $h > h_c$, the system lies in a MBL phase. In this phase, a macroscopic number of quasi-local conserved quantities emergently appear. For the one-dimensional spin chain with $S = 1/2$, such conserved quantities, called local integrals of motion (LIOMs), can be identified by $\{\tau_i^z = U_{\rm local}\sigma_i^z U_{\rm local}^\dagger\}_{i=1}^L$ with a certain local unitary operator $U_{\rm local}$. Each LIOM τ_i^z is localized at the i-th site with exponentially-decaying tails around the i-th site, and satisfies $[\tau_i^z, \tau_j^z] = 0$ and $[\tau_i^z, H_{\rm MBL}] = 0$ for any i, j. This results in the following generic representation of the Hamiltonian in a MBL phase,

$$H_{\rm MBL}[\{\tau_i^z\}] = \sum_i J_i\tau_i^z + \sum_{i,j} J_{ij}\tau_i^z\tau_j^z + \sum_{i,j,k} J_{ijk}\tau_i^z\tau_j^z\tau_k^z + \dots, \tag{1.112}$$

where the coefficients $J_{ij}, J_{ijk}, \dots$ exponentially decay with the distance between each pair of their indices. Emergence of LIOMs brings characteristic properties of MBL phases that distinguishes them from generic integrable or nonintegrable systems. First, every eigenstate of the Hamiltonian $H_{\rm MBL}[\{\tau_i^z\}]$ is given by the simultaneous eigenstate of LIOMs $|\{\tau_i\}_{i=1}^L\rangle$ with the eigenvalue $H_{\rm MBL}[\{\tau_i\}]$, where $\tau_i = \pm 1$ represents the eigenvalue of τ_i^z. Since each LIOM independently contributes to the energy eigenvalue, MBL phases do not host the level repulsion and possesses the level statistics obeying Poisson distribution. Second, each eigenstate $|\{\tau_i\}_{i=1}^L\rangle$ is distinguished from thermal equilibrium states by local observables $\{\tau_i^z\}_{i=1}^z$. This immediately means that MBL systems do not satisfy ETH. Related to the violation of ETH, MBL systems avoid thermalization due to an extensive number of conserved quantities $\{\tau_i^z\}_i$. The third characteristic property of MBL phases appears in entanglement entropy. Each eigenstate $|\{\tau_i\}_{i=1}^L\rangle$ is an approximate product state with local conserved quantities having exponentially-decaying tails. This indicates that each eigenstate of MBL systems has area-law entanglement entropy $S \sim L^{d-1}$. This also provides the characteristic entanglement dynamics of MBL phases, that is, the entanglement of $|\psi(t)\rangle = \exp(-iH_{\rm MBL}t)\,|\psi(0)\rangle$ logarithmically grows in time as $S(t) \propto \log t$ when we prepare a product state $|\psi(0)\rangle$. [3]

Floquet-MBL is the Floquet version of MBL, having an extensive number of quasi-local conserved quantities [79, 80, 81, 82]. One of the most simplest examples for Floquet-MBL phases is realized by the following Hamiltonian on one-dimensional spin chain with $S = 1/2$ [79],

$$H(t) = \begin{cases} \sum_i J\sigma_i^z\sigma_{i+1}^z + \sum_i h_i\sigma_i^z & (0 \le t < T_1) \\ \sum_i J(\sigma_i^x\sigma_{i+1}^x + \sigma_i^y\sigma_{i+1}^y) & (T_1 \le t < T_1 + T_2 = T). \end{cases} \tag{1.113}$$

Here, the random variable h_i, which is uniformly chosen from $[-h, h]$, plays a role of disorder. In the infinite-frequency limit $T \to 0$, this model reproduces the static model Eq. (1.111) since the effective Hamiltonian $H_{\rm eff}$ corresponds to the zeroth-order Floquet-Magnus expansion $H_{\rm FM}^0 = H_{\rm MBL}$, which leads to MBL. When the frequency is finite $T > 0$, thermalization by periodic drive competes with localization by disorder. If the former is dominant, the system lies in an ergodic phase, and hosts thermalization to infinite-temperature as generic nonintegrable Floquet systems. On the other hand, if the latter is dominant (e.g. $T_2 \le T_c \simeq 1$ in the case of $T_1 = 1$, $J = 1/4$, $h = 2.5$), a Floquet-MBL phase is realized, where an extensive number of quasi-local conserved quantities appear. The Floquet operator in Floquet-MBL phases can be written in the form of

$$U_f = \exp(-iTH_{\rm MBL}[\{\tau_i^z\}]) \tag{1.114}$$

with the usage of Eq. (1.112). Importantly, Floquet systems lying in Floquet-MBL phases violate Floquet-ETH, and they can avoid thermalization to trivial infinite-temperature states. By

[3] Integrable systems, which violate ETH, possess the level statistics obeying Poisson statistics as well as MBL systems. Typically, MBL systems can be distinguished from integrable systems by their entanglement nature. When integrable systems can be mapped to free-fermionic systems or can be solved by Bethe ansatz like the XXZ model, wave numbers work as conserved quantities. Since they are not localized in space, typical integrable systems have eigenstates with volume-law entanglement, and host the linear growth in the entanglement dynamics, $S(t) \sim t$.

discussion parallel to MBL phases, Floquet-MBL phases host the characteristic behaviors of MBL phases, such as the level statistics and the entanglement properties.

Since Floquet-ETH or the heating problem predicts trivial steady states in generic interacting Floquet many-body systems, MBL and Floquet-MBL phases are significant ingredients for exploring the interplay of quantum many-body properties and nonequilibrium properties. The first typical example is a discrete time crystal (DTC) phase exploiting MBL, as discussed below. The second one is a Floquet topological phase in interacting systems [83, 84, 85, 86, 87]. It is often discussed upon the existence of Floquet-MBL to avoid trivial Floquet eigenstates, and for instance, two-dimensional class A systems accompanied by Floquet-MBL can host interacting Floquet topological phases characterized by a rational topological number [83]. This is in contrast to static interacting systems where ETH predicts nothing about the gapped ground states and nontrivial topological phenomena in the presence of interactions can be realized without breaking ETH.

Discrete time crystals (DTCs)

Time crystals are one of the ordered phases which spontaneously breaks time translation symmetry (TTS). Time crystals breaking continuous TTS were originally proposed in equilibrium systems as an analogy of crystals spontaneously breaking continuous spatial translation symmetry in 2012 [88], but it was later proven that such continuous time crystals cannot exist in the ground states and the equilibrium states of short-ranged static systems in 2015 [17]. Thus, time crystals are novel ordered phases inherent in nonequilibrium. In particular, Floquet systems have become one of the central platforms for time crystals [16, 89, 90, 91, 92, 93, 94, 95, 96] (See Refs. [97, 98, 99] for review). Such time crystals in Floquet systems are called discrete time crystals (DTCs) since they spontaneously break discrete TTS $H(t) = H(t+T)$.

DTCs are defined by ordered phases showing spontaneous breaking of discrete TTS. To be precise, we call Floquet systems DTCs when an eigenstate of the Floquet operator $|\varepsilon_n\rangle$ has a spatio-temporal long-range order [4]:

$$\lim_{|i-j|\to\infty} |\langle\varepsilon_n|O_iO_j|\varepsilon_n\rangle - \langle\varepsilon_n|O_i|\varepsilon_n\rangle\langle\varepsilon_n|O_j|\varepsilon_n\rangle| = q_0 > 0. \tag{1.115}$$

with a certain local order parameter O_i that satisfies $U_f^\dagger O_i U_f \neq O_i$ and $(U_f^\dagger)^m O_i (U_f)^m = O_i$ ($m \in \mathbb{N}\backslash\{1\}$). When we assume Floquet-ETH or equivalently Eq. (1.85), we obtain $\langle\varepsilon_n|O_iO_j|\varepsilon_n\rangle \sim \langle O_iO_j\rangle_\infty = \langle O_i\rangle_\infty\langle O_j\rangle_\infty \sim \langle\varepsilon_n|O_i|\varepsilon_n\rangle\langle\varepsilon_n|O_j|\varepsilon_n\rangle$ with $\langle O\rangle_\infty \equiv \mathrm{Tr}[O]/\dim(\mathcal{H})$. This indicates the vanishing correlation function in Eq. (1.115), and hence DTCs can appear only when the Floquet systems violate Floquet-ETH.

DTCs, violating Floquet-ETH, are usually realized in Floquet systems accompanied by MBL. Let us consider the simplest case, a kicked Ising chain described by

$$H(t) = \begin{cases} \sum_i (J_i\sigma_i^z\sigma_{i+1}^z + h_i\sigma_i^z) & (0 \le t < \tau) \\ \frac{\pi(1+\varepsilon)}{2(T-\tau)}\sum_i \sigma_i^x & (\tau \le t < T), \end{cases} \tag{1.116}$$

$$U_f = \exp\left(-i\frac{\pi(1+\varepsilon)}{2}\sum_i \sigma_i^x\right)\exp\left(-i\tau\sum_i (J_i\sigma_i^z\sigma_{i+1}^z + h_i\sigma_i^z)\right), \tag{1.117}$$

where J_i and h_i are randomly chosen from $[J_0 - \Delta J, J_0 + \Delta J]$ and $[h_0 - \Delta h, h_0 + \Delta h]$, respectively. When the disorder ΔJ and Δh are strong enough, MBL takes place suggesting the existence of a extensive number of local conserved quantities $\{\tau_i^z = U_{\mathrm{local}}\sigma_i^z U_{\mathrm{local}}^\dagger\}_i$. Then, with the usage of the deformed Pauli operator $\tau_i^x = U_{\mathrm{local}}\sigma_i^x U_{\mathrm{local}}^\dagger$, the Floquet operator U_f is unitarily equivalent to

$$U_f = \left(\prod_i (-i\tau_i^x)\right)\exp(-i\tau H_{\mathrm{MBL}}[\{\tau_i^z\}]), \tag{1.118}$$

[4] This definition of the spatio-temporal order is given in an analogous way to long-range orders in equilibrium systems. Let us consider spontaneous breaking of a certain discrete symmetry generated by g to another discrete symmetry generated by h in equilibrium. Then, the long-range order indicates the existence of a local order parameter O_i satisfying $g^{-1}O_i g \neq O_i$, $h^{-1}O_i h = O_i$, and the non-vanishing correlation function:

$$\lim_{|i-j|\to\infty} |\langle O_iO_j\rangle_{\mathrm{eq}} - \langle O_i\rangle_{\mathrm{eq}}\langle O_j\rangle_{\mathrm{eq}}| = q_0 > 0$$

where $H_{\rm MBL}[\{\tau_i^z\}]$ denotes the MBL Hamiltonian given by Eq. (1.112). Every eigenstate of the Floquet operator U_f is given by

$$|\{\tau_i\}_i,\pm\rangle = \frac{1}{\sqrt{2}}\left(e^{i\tau H^{\rm odd}_{\rm MBL}[\{\tau_i\}]/2}|\{\tau_i\}\rangle \pm e^{-i\tau H^{\rm odd}_{\rm MBL}[\{\tau_i\}]/2}|\{-\tau_i\}\rangle\right), \tag{1.119}$$

$$e^{-iT\varepsilon(\{\tau_i\},\pm)} = \pm e^{i\tau H^{\rm even}_{\rm MBL}[\{\tau_i\}]}. \tag{1.120}$$

Here, τ_i takes ±1 and $|\{\tau_i\}\rangle$ satisfies $\tau_i^z|\{\tau_i\}\rangle = \tau_i|\{\tau_i\}\rangle$. We also give the odd (even) part of the MBL Hamiltonian by $H^{\rm odd(even)}_{\rm MBL}[\{\tau_i^z\}] = (H_{\rm MBL}[\{\tau_i^z\}] \mp H_{\rm MBL}[\{-\tau_i^z\}])/2$. We note that each pair of $|\{\tau_i\}_i,+\rangle$ and $|\{\tau_i\}_i,-\rangle$ has the fixed quasienergy gap π/T. We can choose τ_i^z as a local order parameter that satisfies $(U_f)^\dagger\tau_i^z U_f = -\tau_i^z$, $(U_f^\dagger)^2\tau_i^z(U_f)^2 = \tau_i^z$, and then we find the non-vanishing correlation function for each eigenstate:

$$|\langle\{\tau_i\},\pm|\tau_i^z\tau_j^z|\{\tau_i\},\pm\rangle - \langle\{\tau_i\},\pm|\tau_i^z|\{\tau_i\},\pm\rangle\langle\{\tau_i\},\pm|\tau_j^z|\{\tau_i\},\pm\rangle| = |\tau_i\tau_j| = 1. \tag{1.121}$$

Thus, this system is a DTC. Every eigenstate $|\{\tau_i\},\pm\rangle$ is a superposition of macroscopically different states, dubbed a cat state. Cat states are vulnerable to decoherence, measurement, and infinitesimal perturbations that break the underlying symmetry, and physically unstable. In the actual experiments, we observe physically stable short-range-correlated states, which are superpositions of the eigenstates with the fixed π/T gap:

$$|\{\pm\tau_i\}\rangle \propto |\{\tau_i\},+\rangle \pm |\{\tau_i\},-\rangle. \tag{1.122}$$

Due to the quasienergy gap π/T, the physically stable state $|\{\tau_i\}\rangle$ shows a $2T$-periodic motion,

$$(U_f)^n|\{\tau_i\}\rangle \propto |\{\tau_i\},+\rangle + (-1)^n|\{\tau_i\},-\rangle \propto |\{(-1)^n\tau_i\}\rangle, \tag{1.123}$$

giving a persistent $2T$-periodic oscillation of the order parameter $\langle\tau_i^z(nT)\rangle = (-1)^n\langle\tau_i^z(0)\rangle$. The form of the Floquet operator Eq. (1.118) is maintained under any local perturbation preserving the time-periodicity $H(t) = H(t+T)$ [e.g. ε in Eq. (1.116)] in the presence of MBL. Thus, the $2T$-periodic oscillation of the order parameter, interpreted as spontaneous breaking of discrete TTS $T\mathbb{Z}$ to discrete TTS $NT\mathbb{Z}$, is robust as long as the underlying discrete TTS $T\mathbb{Z}$ is preserved.

In the presence of the generic spatio-temporal order with $m \geq 2$ [See Eq. (1.115)], pairs of m cat states having the fixed gap $2\pi/mT$ appear as the eigenstates of U_f, thereby making a mT-periodic oscillation of the local order parameter in the physically feasible states. We refer to the system having the spatio-temporal order (with $m \geq 2$) robust against any T-periodic local perturbation as a mT-DTC (so the above example is a $2T$-DTC). To summarize, DTCs are physically characterized by the two following phenomena;

1. Existence of a local order parameter $\langle\psi(t)|O|\psi(t)\rangle$, which is mT-periodic but not T-periodic, from a physically-feasible short-range-correlated state $|\psi(0)\rangle$ in $t, L \to \infty$ (time-translation symmetry breaking, TTSB).

2. Robustness of the above behavior against any local T-periodic perturbation in $t, L \to \infty$.

Discrete time-crystalline behaviors were first experimentally observed in trapped ions [95] and diamond NV centers [96], and later in NMR experiments [100, 101]. Although all of them show a $2T$-periodic oscillation robust against a certain perturbation [i.e. ε in Eq. (1.116)], the three-dimensionality and the absence of disorder respectively deny the existence of MBL in the first and third setups [102]. While trapped ions realize a one-dimensional disordered system, MBL seems to be absent due to the lack of disorder in interactions [98]. Thus, the realization of DTCs with the absolute stability brought by MBL is controversial in these prototypical setups. Recently, it has been vigorously discussed to realize DTCs accompanied by MBL in programmable quantum simulators for quantum circuits. In these setups, we can implement tunable disorder and measurements on each qubit, and robustness of DTCs benefits as stability to coherent errors in quantum circuits. After the theoretical proposal on noisy intermediate-scale quantum (NISQ) devices [103], DTCs on superconducting qubits [104, 105, 106] and ^{13}C nuclear spins in diamond [107] were reported.

1.4 Overview of this thesis

At the end of this chapter, we give an overview of this thesis. As discussed so far, Floquet systems have become one of the most important nonequilibrium systems due to their various platforms and phenomena inherent in nonequilibrium. Throughout the thesis, we aim at understanding the fundamental question lying at the center of nonequilibrium condensed matter physics for Floquet systems:

What kind of nonequilibrium phenomena can take place when nonequilibrium properties inherent in Floquet systems and quantum many-body properties induced by interactions coexist ?

Although the theoretical framework of Floquet systems beyond equilibrium seems to easily host unique phenomena, generic Floquet systems suffer from trivial steady states brought by Floquet-ETH: "all the eigenstates of the Floquet operator become equivalent to infinite-temperature states in closed nonintegrable systems." Thus, we should seek for nonequilibrium dynamics or steady states that overcome trivial physics by Floquet-ETH. We expect that a possible direction for nontrivial nonequilibrium phenomena should be to explore outside of Floquet-ETH:

1. Long-lived quasi-steady states of Floquet systems, instead of trivial steady states
2. Integrable or localized Floquet systems, breaking the nonintegrability
3. Dissipative Floquet many-body systems, breaking the isolation

We also note that Floquet-ETH is an empirical law confirmed by experiments and numerical simulations, and hence it is still significant to seek for

4. Nontrivial steady states in closed nonintegrable Floquet systems.

In Section 1.3.5, we briefly review recent development in Floquet-MBL phases and discrete time crystals, which covers 2. We target nonequilibrium phenomena in the other fields 1., 3., and 4.

In Chapter 2, we consider Floquet prethermalization under the resonant and the high-frequency drives, which covers 1. Although the conventional Floquet prethermalization in the high-frequency regime, which we review in Section 1.3.4, enables Floquet engineering, it hosts phenomena having a static counterpart. We clarify the effective Hamiltonian with emergent symmetries for quasi-steady states in the presence of the resonant drive. We also provide its application to the analysis of prethermal discrete time crystals and the resonant Floquet engineering, which enables simultaneous control of symmetry and phases of matter.

In Chapter 3, we consider dissipative Floquet many-body systems in the high-frequency regime, which covers 3. As mentioned above, closed Floquet systems in the high-frequency regime correspond to closed static systems, but its dissipative version of the correspondence is nontrivial. We clarify the breakdown of the correspondence universally caused by interactions, indicating that dissipative Floquet systems can host unique phenomena that have no static counterpart even in the high-frequency regime.

In Chapter 4, we construct a closed nonintegrable Floquet system showing nontrivial steady states, which covers 4. By employing the notion of quantum many-body scars (QMBS) in static systems [See Section 1.3.2], we find athermal and thermal steady states depending on initial states, dubbed Floquet QMBS. We clarify that the model showing Floquet QMBS is a counterexample to Floquet-ETH, and hence the empirical law, Floquet-ETH, is not always true.

Finally, we conclude and summarize this thesis in Chapter 5.

Chapter 2

Resonant prethermal phases and resonant Floquet engineering

In this chapter, we focus on long-lived quasi-steady states in closed Floquet many-body systems. As Floquet-ETH predicts trivial steady states in generic Floquet many-body systems, the quasi-steady states realized before the trivial steady states potentially provide platforms for nontrivial physics of Floquet setups. One of the well-known cases hosting such quasi-steady states is the high-frequency regime, where the local energy scale is much smaller than the frequency. However, it cannot host phenomena inherent in Floquet systems. Nonequilibrium phases of matter such as anomalous Floquet topological phases and discrete time crystals usually take place in the resonant regime, where the local energy scale is comparable to the frequency.

Here, we aim at understanding long-lived quasi-steady states in the resonant regime. We consider generic Floquet many-body systems both in the presence of the resonant and the high-frequency drives, and clarify the effective Hamiltonian which describes their quasi-steady states. Remarkably, the effective Hamiltonian possesses an emergent $\mathbb{Z}_n$-symmetry up to any order of the perturbation theory, different from the conventional high-frequency regime. This result is utilized to explain and analyze discrete-time-crystalline behaviors in quasi-steady states, which are unique to Floquet systems in the resonant regime. We further propose Floquet engineering with the resonant drive, dubbed resonant Floquet engineering. With the usage of the emergent $\mathbb{Z}_n$-symmetry, we can simultaneously control phases and symmetry of the system. As its example, we show the control of topological phases protected by a $\mathbb{Z}_2 \times \mathbb{Z}_2$ symmetry only in the presence of a $\mathbb{Z}_2$ in Floquet setups.

2.1 Prethermal Floquet phases under resonant drives

In this section, we first describe the setup which we target as Floquet systems in the presence of both resonant and high-frequency drives. After that, we derive the effective Hamiltonian describing the sufficiently-long intermediate dynamics in the resonant regime, which is the main result throughout this chapter. Importantly, in contrast to the high-frequency regime in Section 1.3.4, the effective Hamiltonian has a robust emergent $\mathbb{Z}_n$-symmetry up to any perturbation order, leading to prethermal discrete time crystals and Floquet engineering in the following sections.

2.1.1 Setups

Here, we specify Floquet systems under resonant and high-frequency drives throughout this chapter. We consider a time-periodic Hamiltonian $H(t) = H(t+T)$ on a finite lattice Λ. We assume the following three conditions.

1. The time-periodic Hamiltonian $H(t)$ is decomposed as

$$H(t) = H_0(t) + V(t), \tag{2.1}$$

where both $H_0(t)$ and $V(t)$ are time-periodic Hamiltonians with the same period T.

2. (Resonant drive) The Floquet operator under the Hamiltonian $H_0(t)$ gives an onsite $\mathbb{Z}_N$-symmetry operation, that is,

$$^{\exists}N \in \mathbb{N} \quad \text{s. t.} \quad X^N = 1, \quad X = \mathcal{T}\exp\left(-i\int_0^T dt H_0(t)\right). \tag{2.2}$$

3. (High-frequency drive) The time-periodic Hamiltonian $V(t)$ is k-local and J-extensive, defined by Definition 1.3.1.

The condition 1. says that we assign resonant and high-frequency drives to $H_0(t)$ and $V(t)$ respectively. The condition 2. gives restrictions on the drive $H_0(t)$. In order to satisfy Eq. (2.2) for the onsite operator X, the local energy scale of $H_0(t)$ should be given by $\sim 2\pi M/(NT)$ $[M \in \mathbb{Z}]$, comparable to the frequency $\omega = 2\pi/T$. In that sense, $H_0(t)$ gives the resonant drives. The condition 3. dictates that the Hamiltonian $V(t)$ includes at-most k-body interactions with its characteristic energy scale per site, J. This condition is the same as that of Floquet prethermalization in the high-frequency regime (See Section 1.3.4). We refer to $V(t)$ as the high-frequency drive, which typically has a local energy scale smaller than the frequency. If the resonant drive $H_0(t)$ is absent, this setup reproduces the one for the high-frequency regime. Under these conditions, the total Hamiltonian $H(t)$ has local energy comparable to the frequency, and we hereby explore Floquet prethermalization in the resonant regime, which is out of the conventional high-frequency regime.

We note the applicability of the above setup. The strongest restriction is the form of the resonant drive $H_0(t)$ designated by Eq. (2.2). Although it seems to be quite tight, such a form of the resonant drive is often considered in the context of typical nonequilibrium phases of matter inherent in Floquet systems. For instance, in anomalous Floquet topological insulators (AFTIs), unique to the resonant regime, the Floquet operator often becomes or is deformed to a $\mathbb{Z}_N$-symmetry operation. When we adopt such a drive as $H_0(t)$, we can deal with AFTIs under perturbations $V(t)$. Some prototypical examples for two-dimensional systems give $X = 1$ in the square lattice [13, 108] and $X^2 = 1$ in the honeycomb lattice [11, 109]. Another important example for the resonant drive is a sequence of time-periodic pulse, widely used for realizing discrete time crystals (DTCs). When we apply a transverse magnetic field to a spin system with $S = 1/2$ on and off as

$$H_0(t) = \begin{cases} \frac{\pi}{2\tau}\sum_{i=1}^L \sigma_i^x & 0 \le t < \tau \\ 0 & \tau \le t < T, \end{cases} \tag{2.3}$$

we obtain the $\mathbb{Z}_2$ Ising symmetry operation $X = \prod_{i=1}^L(-i\sigma_i^x)$ satisfying $X^2 = 1$ for the even system size L.

We also emphasize the unnecessity of the fine-tuning. When the resonant drive $H_0(t)$ slightly deviates with $X^N \simeq 1$, the assumption seems to be broken by the violation of Eq. (2.2). However, the above setup covers even such situations; Let $H_0'(t) = H_0(t) + \varepsilon(t)$ denote the deviated resonant drive with the small deviation $\varepsilon(t) = \varepsilon(t+T)$. The original one $H_0(t)$ satisfies $X^N = 1$ as Eq. (2.2). By interpreting $H_0(t)$ and $V(t) + \varepsilon(t)$ as the resonant and the high-frequency drives in the deviated Hamiltonian $H(t) = H_0'(t) + V(t)$, all the above conditions are recovered. Thus, we do not need to impose the fine-tuning, that is, the above Floquet setup in the resonant regime is robust against any local perturbation as long as the periodicity is maintained.

Combining the various choice of the resonant drive and the robustness of the conditions, the Floquet systems satisfying Eqs. (2.1) and (2.2) can deal with a wide class of nonequilibrium systems in the resonant regime. It should be noted that they can include unique nonequilibrium phases such as AFTIs and DTCs, while the conventional high-frequency regime always counterparts in static systems (See Section 1.3.4). In the following section, we show that the choice of the resonant drive by Eq. (2.2) enables Floquet prethermalization in the resonant regime, and clarify the effective Hamiltonian for their intermediate dynamics.

2.1.2 Van Vleck expansions with emergent symmetries

Here, we clarify the effective Hamiltonian describing the sufficiently-long intermediate dynamics in the above resonant setup. To this goal, we have two points that should be addressed. First,

it is nontrivial whether there exists such intermediate time scale where Floquet systems under resonant drive can avoid thermalization to infinite temperature. While Floquet prethermalization in the high-frequency regime arises from the mismatch of local energy scale and excitation energy by periodic drive, they are comparable in the resonant regime, which in general leads to quick heating. As we will see later, the choice of resonant drive $H_0(t)$ by Eq. (2.2) enables Floquet prethermalization in the resonant regime. Second, we should identify the characteristics of the approximate Floquet operator or effective Hamiltonian for the intermediate dynamics. In the case of the high-frequency regime, the Floquet operator is approximated by the Floquet-Magnus effective Hamiltonian (See Theorem 1.3.3). In contrast, as we will show below, in the resonant regime, we can obtain the clear description by the van Vleck expansion, dictating that the effective system for the intermediate dynamics acquires an emergent $\mathbb{Z}_N$ symmetry.

Floquet prethermalization in the resonant regime

Let us begin with the existence of Floquet prethermalization in the resonant regime satisfying Eqs. (2.1) and (2.2). Considering that $V(t)$ gives the high-frequency drive with the local energy scale J, we employ the perturbation theory in J/ω. In order to separate the energy scales of $H_0(t)$ and $V(t)$, we consider the rotating frame in $H_0(t)$:

$$\tilde{V}(t) = U_0(t)^\dagger V(t) U_0(t), \quad U_0(t) = \mathcal{T} \exp\left(-i \int_0^t H_0(t) dt\right). \tag{2.4}$$

With the rotating frame, we can derive the following theorem implying Floquet prethermalization.

Theorem 2.1.1. (Floquet prethermalization under resonant drive)
Assume that all the conditions 1.-3. [See Eqs. (2.1) and (2.2)] are satisfied. We define the coarse-grained Floquet operator by

$$U_f^N = U(NT) = (U_f)^N, \tag{2.5}$$

which describes the stroboscopic dynamics with the interval NT. Then, for a sufficiently small period T independent of the system size L, it can be approximated by

$$||U_f^N - e^{-i\tilde{V}_{\rm FM}^{n_0} NT}|| \leq e^{-O(1/(\lambda NT))} L, \tag{2.6}$$

with the Floquet-Magnus expansion $\tilde{V}_{\rm FM}^n$, given by $\tilde{V}(t)$ up to the truncation order $n_0 = O(1/(\lambda NT))$. Furthermore, with the corresponding van Vleck expansion for the lower truncation order $n \leq n_0$, it is also approximated by

$$||U_f^N - e^{-i\tilde{K}_{\rm vV}^n} e^{-i\tilde{V}_{\rm vV}^n NT} e^{i\tilde{K}_{\rm vV}^n}|| \leq e^{-O(1/(\lambda NT))} L + O((\lambda NT)^{n+2}) L. \tag{2.7}$$

Before proving the theorem, we give the explicit formula of the Floquet-Magnus and the van Vleck expansions for $\tilde{V}(t)$. We define the l-th Fourier component of $\tilde{V}(t)$ by

$$\tilde{V}_l = \frac{1}{NT} \int_0^{NT} \tilde{V}(t) e^{il\omega t/N} dt = \frac{1}{NT} \int_0^{NT} U_0(t)^\dagger V(t) U_0(t) e^{il\omega t/N} dt, \tag{2.8}$$

where we have used the period NT for the coarse-grained stroboscopic dynamics. The n-th order Floquet-Magnus expansion is given by

$$\tilde{V}_{\rm FM}^n = \sum_{m=0}^n \tilde{V}_{\rm FM}^{(m)}, \quad \tilde{V}_{\rm FM}^{(0)} = \tilde{V}_0, \quad \tilde{V}_{\rm FM}^{(1)} = N \sum_{l \neq 0} \frac{[\tilde{V}_{-l}, \tilde{V}_l]}{2l\omega} + N \sum_{l \neq 0} \frac{[\tilde{V}_l, \tilde{V}_0]}{l\omega}, \ldots, \tag{2.9}$$

which are obtained by substituting $\tilde{V}(t)$ and NT into $H(t)$ and NT in Eqs. (1.28). In a similar

way, the van Vleck expansion for $\tilde{V}(t)$ is given by

$$\tilde{V}^n_{\rm vV} = \sum_{m=0}^{n} \tilde{V}^{(m)}_{\rm vV}, \quad \tilde{V}^{(0)}_{\rm vV} = \tilde{V}_0, \quad \tilde{V}^{(1)}_{\rm vV} = N\sum_{l\neq 0} \frac{[\tilde{V}_{-l}, \tilde{V}_l]}{2l\omega}, \tag{2.10}$$

$$\tilde{V}^{(2)}_{\rm vV} = N^2 \sum_{m\neq 0} \frac{[[\tilde{V}_{-m}, \tilde{V}_0], \tilde{V}_m]}{2m^2\omega^2} + N^2 \sum_{m\neq 0}\sum_{n\neq 0,m} \frac{[[\tilde{V}_{-m}, \tilde{V}_{m-n}], \tilde{V}_n]}{3mn\omega^2}, \ldots, \tag{2.11}$$

$$\tilde{K}^n_{\rm vV} = \sum_{m=0}^{n} \tilde{K}^{(m)}_{\rm vV}, \quad i\tilde{K}^{(0)}_{\rm vV} = -N\sum_{m\neq 0} \frac{\tilde{V}_m}{m\omega}, \tag{2.12}$$

$$i\tilde{K}^{(1)}_{\rm vV} = N^2 \sum_{m\neq 0}\sum_{n\neq 0,m} \frac{[\tilde{V}_m, \tilde{V}_{m-n}]}{2mn\omega^2} + N^2 \sum_{m\neq 0} \frac{[\tilde{V}_m, \tilde{V}_0]}{m^2\omega^2}, \tag{2.13}$$

$$\begin{aligned} i\tilde{K}^{(2)}_{\rm vV} = & -N^3 \sum_{m\neq 0} \frac{[[\tilde{V}_m, \tilde{V}_0], \tilde{V}_0]}{m^3\omega^3} + N^3 \sum_{m,n\neq 0} \frac{[\tilde{V}_m, [\tilde{V}_{-n}, \tilde{V}_n]]}{4m^2n\omega^3} \\ & -N^3 \sum_{m,n\neq 0} \left(\sum_{l\neq 0,m,n} \frac{[\tilde{V}_n, [\tilde{V}_{l-n}, \tilde{V}_{m-l}]]}{4mnl\omega^3} + \sum_{l\neq 0,m-n} \frac{[\tilde{V}_n, [\tilde{V}_l, \tilde{V}_{m-n-l}]]}{12mnl\omega^3} \right) \\ & -N^3 \sum_{m\neq 0}\sum_{n\neq 0,m} \left(\frac{[[\tilde{V}_n, \tilde{V}_0], \tilde{V}_{m-n}]}{2mn^2\omega^3} + \frac{[[\tilde{V}_n, \tilde{V}_{m-n}], \tilde{V}_0]}{2m^2n\omega^3} \right), \ldots. \end{aligned} \tag{2.14}$$

We prove the theorem with the usage of these expansions in the rotating frame below.

Proof

For the time-periodic Hamiltonian $H(t) = H_0(t) + V(t)$, we consider Schrödinger equation,

$$i\frac{d}{dt}|\psi(t)\rangle = [H_0(t) + V(t)]\,|\psi(t)\rangle\,, \tag{2.15}$$

with the rotating frame by $U_0(t)$ [See Eq. (2.4)]. The state in the rotating frame $|\tilde{\psi}(t)\rangle \equiv U_0(t)^{-1}|\psi(t)\rangle$ obeys

$$\begin{aligned} i\frac{d}{dt}|\tilde{\psi}(t)\rangle &= i\frac{dU_0(t)^{-1}}{dt}|\psi(t)\rangle + U_0(t)^{-1}i\frac{d}{dt}|\psi(t)\rangle \\ &= \tilde{V}(t)\,|\tilde{\psi}(t)\rangle\,. \end{aligned} \tag{2.16}$$

By solving this differential equation, we obtain

$$|\psi(t)\rangle = U_0(t)\,|\tilde{\psi}(t)\rangle = U_0(t)\tilde{U}(t)\,|\psi(0)\rangle\,, \quad \tilde{U}(t) = \mathcal{T}\exp\left(-i\int_0^t \tilde{V}(t)dt\right). \tag{2.17}$$

The condition $X^N = U_0(NT) = 1$ from Eq. (2.2) gives the coarse-grained Floquet operator $U_f^N = \tilde{U}(NT)$.

Let us again focus on Eq. (2.16) in the rotating frame. From Eq. (2.2) and the time-periodicity of $V(t) = V(t+T)$, the rotating-frame Hamiltonian $\tilde{V}(t)$ is NT-periodic, $\tilde{V}(t) = \tilde{V}(t+T)$. Eq. (2.16) can be interpreted as time-dependent Schrödinger equation for a Floquet system with the period NT. In addition, since $\tilde{V}(t)$ is related to the k-local and J-extensive Hamiltonian $V(t)$ [the condition 3.] by the onsite unitary transformation $U_0(t)$ [the condition 2.], $\tilde{V}(t)$ is also a k-local and J-extensive Hamiltonian. Therefore, we can apply Theorem 1.3.3, which dictates Floquet prethermalization in the high-frequency regime. When $\lambda NT < 1/4$ is satisfied with the local energy scale $\lambda = 2kJ$, we obtain the following inequality for the coarse-grained Floquet operator $U_f^N = \tilde{U}(NT)$;

$$||U_f^N - e^{-i\tilde{V}^{n_0}_{\rm FM}NT}|| \leq \frac{3}{k}L(\lambda NT)2^{-n_0} = e^{-O(1/(\lambda NT))}L, \tag{2.18}$$

where n_0 is the largest integer that does not exceed $1/(16\lambda NT)$. This result completes the proof of Eq. (2.6) in the theorem.

Next, we consider the approximation by the van Vleck expansion with the truncation order $n \leq n_0$. Using the triangle inequality,

$$\begin{aligned} ||U_f^N - e^{-i\tilde{K}^n_{\rm vV}} e^{-i\tilde{V}^n_{\rm vV} NT} e^{i\tilde{K}^n_{\rm vV}}|| \quad &\leq \quad ||U_f^N - e^{-i\tilde{V}^{n_0}_{\rm FM} NT}|| + ||e^{-i\tilde{V}^{n_0}_{\rm FM} NT} - e^{-i\tilde{V}^{n}_{\rm FM} NT}|| \\ &\quad + ||e^{-i\tilde{V}^{n}_{\rm FM} NT} - e^{-i\tilde{K}^n_{\rm vV}} e^{-i\tilde{V}^n_{\rm vV} NT} e^{i\tilde{K}^n_{\rm vV}}|| \end{aligned} \tag{2.19}$$

is obtained. The first term of the right hand side is bounded by Eq. (2.18). The second term represents the deviation arising from the replacement of the n_0-th order Floquet-Magnus expansion with the n-th order. Since $\tilde{V}(t)$ is a k-local and J-extensive Hamiltonian with the period NT, we can exploit Theorem 1.3.3 again. This results in the following upper bound on the second term;

$$||e^{-i\tilde{V}^{n_0}_{\rm FM} NT} - e^{-i\tilde{V}^{n}_{\rm FM} NT}|| \leq \frac{2(n+1)!}{(n+2)k} L(\lambda NT)^{n+2} = O((\lambda NT)^{n+2})L. \tag{2.20}$$

The third term comes from the replacement of the Floquet-Magnus expansion by the van Vleck expansion at the n-th order. Since $e^{-i\tilde{V}^{n_0}_{\rm FM} NT}$, $e^{-i\tilde{V}^{n}_{\rm FM} NT}$, and $e^{-i\tilde{K}^n_{\rm vV}} e^{-i\tilde{V}^n_{\rm vV} NT} e^{i\tilde{K}^n_{\rm vV}}$ (at least formally) give the perturbative expansion for the same operator U_f^N, they are equal to one another up to the n-th order. Considering the locality and the extensiveness of $\tilde{V}(t)$, the difference between them is bounded by higher $(n+1)$-th order terms in the local energy scale λNT:

$$||e^{-i\tilde{V}^{n}_{\rm FM} NT} - e^{-i\tilde{K}^n_{\rm vV}} e^{-i\tilde{V}^n_{\rm vV} NT} e^{i\tilde{K}^n_{\rm vV}}|| \leq O((\lambda NT)^{n+2})L. \tag{2.21}$$

We note that the naive perturbation theory predicts the difference of $O((||\tilde{V}(t)||NT)^{n+2}) = O((\lambda LNT)^{n+2})$, which gives a meaningless bound for the large system size L. The locality and extensiveness of $\tilde{V}(t)$ allows much more strict bound given by the above inequality. The derivation of this bound is provided in the appendix for this chapter since it is technical (See Section 2.5). Finally, we obtain Eq. (2.7) by combing Eqs. (2.18)-(2.21). □

Effective Hamiltonian with an emergent symmetry

In Theorem 2.1.1, Eq. (2.6) indicates that the sufficiently-long intermediate dynamics is described by the Floquet-Magnus expansion, avoiding the thermalization to infinite-temperature at least in this time scale. Then, what differs from Floquet prethermalization in the high-frequency regime, which is similarly described by the Floquet-Magnus expansion as Eq. (1.101) ? In fact, we can find the significant difference emerging from the presence of the resonant drive $H_0(t)$ by employing the van Vleck expansion validated by Eq. (2.7) in Theorem 2.1.1. We derive the following theorem on the van Vleck effective Hamiltonian $\tilde{V}^n_{\rm vV}$, which universally characterizes its symmetry.

Theorem 2.1.2. (Emergent $\mathbb{Z}_N$-symmetry in the effective Hamiltonian)
Assume that all the conditions 1.-3. [See Eqs. (2.1) and (2.2)] are satisfied. The van Vleck expansion $\tilde{V}^n_{\rm FM}$, playing a role of the effective Hamiltonian for the intermediate dynamics, respects the $\mathbb{Z}_N$-symmetry X at any truncation order:

$$X^{-1}\tilde{V}^n_{\rm vV} X = \tilde{V}^n_{\rm vV}, \quad X = \mathcal{T}\exp\left(-i\int_0^T H_0(t)dt\right), \quad \text{for any } n. \tag{2.22}$$

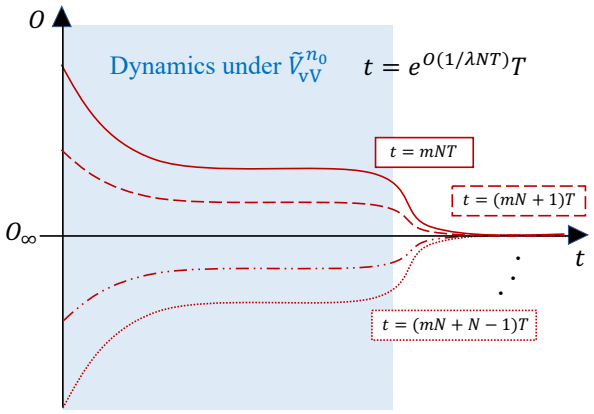

Figure 2.1: Schematic picture of Floquet prethermalization in the resonant regime. Compared to the high-frequency regime in Fig. 1.4, there exist multiple branches of intermediate dynamics and quasi-steady states depending on the time modulo NT. The effective Hamiltonian for the dynamics, $\tilde{V}_{\mathrm{vV}}^{n}$, emergently becomes $\mathbb{Z}_N$-symmetric due to the resonant drive.

Proof

The Fourier component $\tilde{V}_l$, given by Eq. (2.8), can be rewritten as follows:

$$\begin{aligned}\tilde{V}_l &= \frac{1}{NT}\int_0^{NT}\tilde{V}(t)e^{il\omega t/N}dt \\ &= \frac{1}{NT}\sum_{p=0}^{N-1}\int_0^{T}U_0^\dagger(t+pT)V(t)U_0(t+pT)e^{il\omega(t+pT)/N}dt \\ &= \frac{1}{NT}\sum_{p=0}^{N-1}X^{-p}\int_0^{T}\tilde{V}(t)e^{il\omega(t+pT)/N}dt\,X^p. \end{aligned} \tag{2.23}$$

Thus, by using the condition $X^N = 1$, the action of X on the Fourier component is

$$\begin{aligned}X\tilde{V}_l X^{-1} &= \frac{1}{NT}\sum_{p=0}^{N-1}X^{-p+1}\int_0^{T}\tilde{V}(t)e^{il\omega(t+pT)/N}dt\,X^{p-1} \\ &= e^{i2\pi l/N}\tilde{V}_l. \end{aligned} \tag{2.24}$$

When we focus on the n-th order terms of the van Vleck expansion, each term is a product of $n+1$ Fourier components, that is, it is composed of,

$$\tilde{V}_{l_1}\tilde{V}_{l_2}\dots\tilde{V}_{l_{n+1}}. \tag{2.25}$$

From Eq. (2.24), this n-th order term transforms under X as follows,

$$X\tilde{V}_{l_1}\tilde{V}_{l_2}\dots\tilde{V}_{l_{n+1}}X^{-1} = \exp\left(\frac{2\pi i}{N}\sum_{i=1}^{n+1}l_i\right)\tilde{V}_{l_1}\tilde{V}_{l_2}\dots\tilde{V}_{l_{n+1}}. \tag{2.26}$$

As discussed in Section 1.2.3, the van Vleck expansion $\tilde{V}_{\mathrm{vV}}^{n}$ has terms $\tilde{V}_{l_1}\tilde{V}_{l_2}\dots\tilde{V}_{l_{n+1}}$ satisfying $\sum_i l_i = 0$ due to its gauge-independence or its equal photon absorption and emission [See Eq. (1.44)]. Therefore, we obtain the emergent $\mathbb{Z}_N$-symmetry of the van Vleck expansion, $X^{-1}\tilde{V}_{\mathrm{vV}}^{n}X = \tilde{V}_{\mathrm{vV}}^{n}$, for any truncation order n. □

Floquet prethermalization with the emergent symmetry in the resonant regime

Here, we summarize the above theorems and provide their physical interpretation. We consider Floquet many-body systems under the resonant drive $H_0(t)$ in addition to the conventional high-frequency drive $V(t)$. Since the Floquet-Magnus expansion $\tilde{V}_{\mathrm{FM}}^{n_0}$ plays a role of a macroscopic

approximately-conserved quantity from Eq. (2.6), we expect Floquet prethermalization in the resonant regime, avoiding infinite-temperature states for at least $e^{O(1/(\lambda NT))}$ time. Equation (2.7) validates the approximation of the dynamics by

$$|\psi(mNT)\rangle = (U_f^N)^m |\psi(0)\rangle \simeq e^{-i\tilde{K}^n_{\rm vV}} e^{-i\tilde{V}^n_{\rm vV} mNT} e^{i\tilde{K}^n_{\rm vV}} |\psi(0)\rangle \,, \tag{2.27}$$

with the truncation order $n \le n_0 = O(1/(\lambda NT))$. This says that the unitarily-transformed state $e^{i\tilde{K}^n_{\rm vV}} |\psi(t)\rangle$ obeys dynamics under the static Hamiltonian $\tilde{V}^n_{\rm vV}$. Since $\tilde{V}^n_{\rm vV}$ generally has complex terms from commutators in the higher order terms, we naturally assume that it is nonintegrable. With believing ETH in nonintegrable static systems [See Eq. (1.61)], the state $e^{i\tilde{K}^n_{\rm vV}} |\psi(t)\rangle$ is expected to relax to the thermal equilibrium state under $\tilde{V}^n_{\rm vV}$, after the relaxation time $\tau_{\rm pre}$ determined by ETH. In other words, when the time $t = mNT$ is large compared to $\tau_{\rm pre}$ but smaller than the lifetime in which Eq. (2.27) is valid, $\tau = e^{O(1/(\lambda NT))}$, we obtain the quasi-steady states in the intermediate time scale by

$$|\psi(mNT)\rangle \simeq e^{-i\tilde{K}^n_{\rm vV}} \tilde{\rho}_\beta e^{i\tilde{K}^n_{\rm vV}}, \quad \tilde{\rho}_\beta = \frac{e^{-\beta \tilde{V}^n_{\rm vV}}}{{\rm Tr}[e^{-\beta \tilde{V}^n_{\rm vV}}]}, \tag{2.28}$$

where the symbol "$\simeq$" denotes the indistinguishability by any local observable. The effective temperature β is determined by the energy conservation;

$$\langle\psi(0)|e^{-i\tilde{K}^n_{\rm vV}} \tilde{V}^n_{\rm vV} e^{i\tilde{K}^n_{\rm vV}} |\psi(0)\rangle = {\rm Tr}[\tilde{V}^n_{\rm vV} \tilde{\rho}_\beta]. \tag{2.29}$$

While the above equations give the quasi-steady state for the coarse-grained stroboscopic dynamics with the interval NT, the stroboscopic dynamics with the interval T has N branches of quasi-steady states determined by the time modulo NT. The quasi-steady state $\tilde{\rho}_\beta$ for $t = mNT + t_0$ ($t_0 = 0, T, \ldots, (N-1)T$) is obtained by employing $|\psi(t_0)\rangle$ instead of $|\psi(0)\rangle$ in Eq. (2.29). After the sufficient time longer than the lifetime $\tau = e^{O(1/(\lambda NT))}$, all the branches are generally expected to converge to trivial infinite temperature states due to Floquet-ETH (See Section 1.3.3). As a result, we obtain the approximate dynamics of Floquet systems in the resonant regime as described in Fig. 2.1.

Other than the multiple branches of quasi-steady states, we emphasize the essential difference from the high-frequency regime; We can realize the quasi-steady state $\tilde{\rho}_\beta$ under a controlled Hamiltonian with the $\mathbb{Z}_N$-symmetry X, although the original system $H(t)$ does not respect any symmetry except for the discrete time translation symmetry. Furthermore, this emergent $\mathbb{Z}_N$-symmetry is quite robust. As discussed in Section 2.1.1, all the assumptions for the drive are maintained even under local perturbations, and hence the resulting $\mathbb{Z}_N$-symmetry is also maintained. Thus, we can always mimic a $\mathbb{Z}_N$-symmetric static systems by Floquet systems in the resonant regime as long as local perturbations do not break the time periodicity $H(t) = H(t+T)$, in which we refer to the emergent $\mathbb{Z}_N$-symmetry X as "protected by discrete time translation symmetry." At the end of this section, we summarize Floquet prethermalization in the resonant regime, which is the main assertion in this chapter.

Remark. (Floquet prethermalization in the resonant regime)
Consider a Floquet system in the resonant regime driven by the Hamiltonian $H(t) = H_0(t) + V(t)$. We assume that the resonant drive $H_0(t)$ generates a $\mathbb{Z}_N$-symmetry,

$$X^N = 1, \quad X = \mathcal{T} \exp\left(-i \int_0^T dt H_0(t)\right), \tag{2.30}$$

and that the high-frequency drive $V(t)$ has local energy scale λ smaller than the frequency $\omega = 2\pi/T$. Then, its stroboscopic dynamics is approximately dominated by a static Hamiltonian with the emergent $\mathbb{Z}_N$-symmetry;

$$U_f^N = U(NT) \simeq e^{-i\tilde{K}^n_{\rm vV}} e^{-i\tilde{V}^n_{\rm vV} NT} e^{i\tilde{K}^n_{\rm vV}}, \tag{2.31}$$

$$\tilde{V}^n_{\rm vV} = \tilde{V}_0 + N \sum_{l\neq 0} \frac{[\tilde{V}_{-l}, \tilde{V}_l]}{2l\omega} + \ldots + \tilde{V}^n_{\rm vV}, \quad X^{-1}\tilde{V}^n_{\rm vV} X = \tilde{V}^n_{\rm vV}, \tag{2.32}$$

with the truncation order $n \leq O(1/(\lambda NT))$.

2.2 Prethermal discrete time crystals (pDTCs)

We reveal that Floquet systems under the resonant drive generating a $\mathbb{Z}_N$-symmetry can host sufficiently-long intermediate dynamics and quasi-steady states under a static Hamiltonian with the robust $\mathbb{Z}_N$-symmetry by Theorems 2.1.1 and 2.1.2. While Floquet-ETH predicts trivial physics by the heating to infinite temperature in generic Floquet many-body systems (See Section 1.3.3), Floquet prethermalization in the resonant regime can be novel platforms for Floquet many-body physics with a sufficiently-long lifetime. The rest of this chapter is spared to explore the application of this result; what kind of nonequilibrium many-body phenomena can appear in prethermalization of resonant Floquet systems.

While Floquet systems in the high-frequency regime always have counterparts in static systems, the resonant regime is reminiscent of unique nonequilibrium phases of matter such as AFTIs and DTCs. Thus, we can expect that some similar phenomena unique to nonequilibrium can appear in the intermediate dynamics or the quasi-steady states. One of the most intriguing phenomena among them is a discrete time crystalline order in the quasi-steady states, dubbed "prethermal discrete time crystals" (pDTCs). In this section, after describing the definition of pDTCs, we show how Floquet prethermalization in the resonant regime enables the realization of pDTCs.

Definition of pDTCs

Discrete time crystals (DTCs) are nonequilibrium ordered phases which spontaneously break discrete time translation symmetry. As discussed in Section 1.3.5, they are defined by Floquet many-body systems having a non-vanishing spatio-temporal correlation function in the thermodynamic limit, with violating Floquet-ETH. Since DTCs require the spectral splitting of $2\pi/(mT)$, comparable to the frequency, we need resonant drives for the realization.

Floquet many-body systems considered here, satisfying the conditions 1.-3., also lies in the resonant regime. Although they generally satisfy Floquet-ETH and cannot host DTCs in a rigorous sense, we can expect DTC-like behaviors in their quasi-steady states. In the intermediate time scale, they become equivalent to a series of thermal equilibrium states $\tilde{\rho}_\beta(t)$ depending on the time modulo NT, as shown in Fig. 2.1. The quasi-steady states $\tilde{\rho}_\beta$ are determined by Eq. (2.29) with the initial state $|\psi(t \bmod NT)\rangle$. Based on the DTC signatures in Section 1.3.5, we call prethermal discrete time crystals (pDTCs) if they satisfy

1. Existence of a local order parameter $\mathrm{Tr}[O\tilde{\rho}_\beta(t)]$, which is mT-periodic but not T-periodic, from a physically-feasible short-range-correlated state $|\psi(0)\rangle$ for the intermediate time t and the large but finite size L (time-translation symmetry breaking, TTSB).

2. Robustness of the above behavior against any local T-periodic perturbation for the intermediate time t and the large but finite size L.

The first difference between DTCs and pDTCs is that pDTCs can appear only in the intermediate time scale $\tau_{\rm pre} < t < \tau = e^{O(1/(\lambda NT))}T$ due to the lifetime of the quasi-steady states. Second, we should consider the sufficiently-large but finite L in pDTCs. This is because the thermodynamic limit generally causes the breakdown of the quasi-steady states as Eq. (2.6) in Theorem 2.1.1 gives no meaningful bound in $L \to \infty$. Although pDTCs cannot host a genuine long-range order, pDTCs show the same behaviors as DTCs under actual experiments with the limited coherence time and size. As discussed later, pDTCs have an approximately non-vanishing correlation function as long as description by the quasi-steady states is valid, suggesting the presence of the approximate spatio-temporal long-range order .

Effective Hamiltonian for pDTCs

Here, we discuss how Floquet many-body systems in the resonant regime realize pDTCs, or equivalently how Theorems 2.1.1 and 2.1.2 give TTSB and robustness in the quasi-steady states.

Let us consider Floquet systems satisfying the conditions 1.-3. For simplicity, we assume that the resonant drive $H_0(t)$ generates a $\mathbb{Z}_2$-symmetry operation X ($N = 2$). Then, the coarse-grained Floquet operator $U_f^2 = U(2T)$ is well approximated by

$$U_f^2 \simeq e^{-i\tilde{K}^n_{\rm vV}} e^{-2i\tilde{V}^n_{\rm vV}T} e^{i\tilde{K}^n_{\rm vV}}, \tag{2.33}$$

with a proper truncation order n. We choose a local operator O satisfying $X^{-1}OX = -O$, which plays a role of an order parameter for $\mathbb{Z}_2$-symmetry breaking. Then, we have two branches for the expectation value of O in the quasi-steady states;

$$\phi \equiv \langle\psi(2mT)|O|\psi(2mT)\rangle \simeq {\rm Tr}[Oe^{-i\tilde{K}^n_{\rm vV}}\tilde{\rho}_\beta(0)e^{i\tilde{K}^n_{\rm vV}}], \tag{2.34}$$

$$\phi' \equiv \langle\psi((2m+1)T)|O|\psi((2m+1)T)\rangle \simeq {\rm Tr}[Oe^{-i\tilde{K}^n_{\rm vV}}\tilde{\rho}_\beta(T)e^{i\tilde{K}^n_{\rm vV}}], \tag{2.35}$$

where $\tilde{\rho}_\beta(0)$ and $\tilde{\rho}_\beta(T)$ are thermal equilibrium states under $\tilde{V}^n_{\rm vV}$ with the temperatures determined by $e^{i\tilde{K}^n_{\rm vV}}|\psi(0)\rangle$ and $e^{i\tilde{K}^n_{\rm vV}}|\psi(T)\rangle$ respectively.

Next, we seek for the relation between ϕ and ϕ', which should be different in order to host TTSB. By using the description by the rotating frame Eq. (2.4), the Floquet operator U_f is also given by

$$U_f = X\tilde{U}(T), \quad \tilde{U}(T) = \mathcal{T}\exp\left(-i\int_0^T \tilde{V}(t)dt\right). \tag{2.36}$$

Here, the unitary operator $\tilde{U}(T)$ can be regarded as a Floquet operator under the T-periodic Hamiltonian $\tilde{V}(t \bmod T)$. Considering that $\tilde{V}(t \bmod T)$ is also k-local and J-extensive, we can apply Theorem 2.1.1 for Floquet prethermalization in the high-frequency regime. As a result, up to the lowest order, we obtain the approximate Floquet operator by $U_f = X + O(\lambda T)$. This result gives the following approximate relation between ϕ and ϕ';

$$\phi' = \langle\psi(2mT)|U_f^\dagger O U_f|\psi(2mT)\rangle \tag{2.37}$$

$$= \langle\psi(2mT)|X^{-1}OX|\psi(2mT)\rangle + O(\lambda T) \tag{2.38}$$

$$= -\phi + O(\lambda T). \tag{2.39}$$

Therefore, as long as ϕ is a nonzero value larger than $O(\lambda T)$, the system hosts TTSB with a $2T$-periodic oscillation.

On the other hand, $\phi = {\rm Tr}[O\tilde{\rho}_\beta] + O(\lambda T)$ [See Eq. (2.28)] is approximately a thermal equilibrium value under the $\mathbb{Z}_2$-symmetric Hamiltonian $\tilde{V}^n_{\rm vV}$. While the $\mathbb{Z}_2$-symmetry generally predicts the vanishing order parameter, ϕ can be nonzero if the spontaneous breaking of the $\mathbb{Z}_2$-symmetry takes place under $\tilde{V}^n_{\rm vV}$. In other words, we should prepare the initial state $|\psi(0)\rangle$ so that it can provide the temperature lower than the critical value for the spontaneous symmetry breaking (SSB) under the static Hamiltonian $\tilde{V}^n_{\rm vV}$. As a matter of fact, such low-temperature initial states under a $\mathbb{Z}_2$-symmetric Hamiltonian is unstable to dissipation and measurement. They are also vulnerable to infinitesimal perturbations that break the discrete TTS $H(t) = H(t+T)$. In physically-feasible setups, the quasi-steady state becomes a $\mathbb{Z}_2$-symmetry broken state with the nonzero order parameter ϕ, rather than the $\mathbb{Z}_2$-symmetric state $\tilde{\rho}_\beta(0)$ given by Eq. (2.28), thereby allowing the TTSB behavior described in Fig. 2.2 (a).

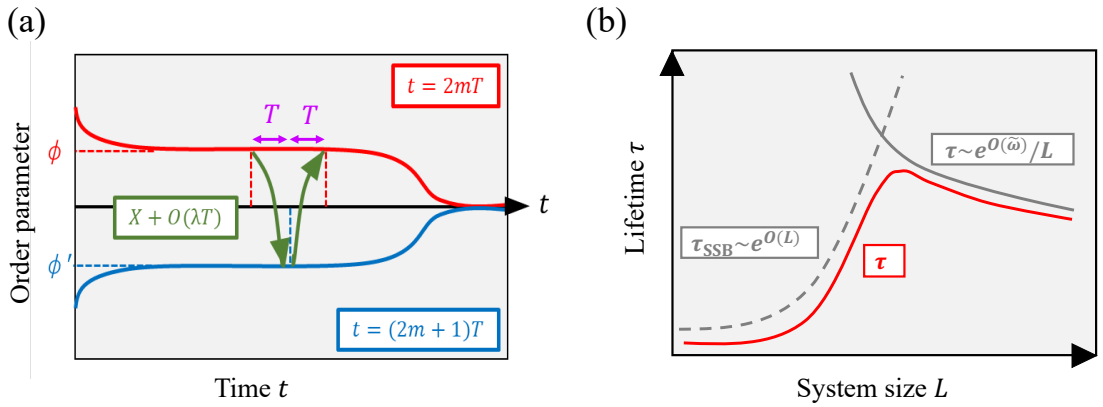

Figure 2.2: (a) Intuitive picture of pDTCs. In the presence of SSB under the $\mathbb{Z}_2$-symmetric Hamiltonian $\tilde{V}^n_{\rm vV}$, the quasi-steady state repeatedly experiences transitions between branches, resulting in the robust nontrivial oscillation. (b) Schematic picture of how the lifetime of pDTCs depends on the system size L. It reflects the lifetime of SSB in finite systems $\tau_{\rm SSB}$, and that of Floquet prethermalization in the resonant regime τ.

We also show the robustness of the above TTSB behavior. We consider a perturbed Floquet system $H_\varepsilon(t) = H_0(t) + V(t) + \varepsilon(t)$ with a local time-periodic perturbation $\varepsilon(t)$ $(= \varepsilon(t+T))$. By regarding $V(t) + \varepsilon(t)$ as the high-frequency drive, we can exploit Theorems 2.1.1 and 2.1.2 again. Then, TTSB in the perturbed Floquet system corresponds to SSB under the $\mathbb{Z}_2$-symmetric Hamiltonian $\tilde{V}^n_{{\rm vV},\varepsilon}$, given by the van Vleck expansion. Considering that SSB defined as phases of matter under the static Hamiltonian $\tilde{V}^n_{\rm vV}$ is generally stable to any local perturbation that preserves the $\mathbb{Z}_2$-symmetry, SSB under $\tilde{V}^n_{{\rm vV},\varepsilon}$ which slightly deviates from $\tilde{V}^n_{\rm vV}$ is maintained. Therefore, the $2T$-periodic oscillation is robust against any local time-periodic perturbation, ensuring the realization of pDTCs.

We finally summarize the result. For generic cases where the resonant drive $H_0(t)$ generates a $\mathbb{Z}_N$-symmetry X $(X^N = 1)$, the effective Hamiltonian $\tilde{V}^n_{\rm vV}$ respects the $\mathbb{Z}_N$-symmetry. The realization of pDTCs can be associated with the effective Hamiltonian as follows.

Remark. (Effective Hamiltonian for pDTCs)
Consider a Floquet system $H(t) = H_0(t) + V(t)$ with the resonant drive $H_0(t)$ generating a $\mathbb{Z}_N$-symmetry X. It can host pDTCs when the $\mathbb{Z}_N$-symmetric effective Hamiltonian $\tilde{V}^n_{\rm vV}$ hosts SSB from the $\mathbb{Z}_N$-symmetry to a $\mathbb{Z}_M$-symmetry (M: a divisor of N) under the temperature determined by the state $e^{i\tilde{K}^n_{\rm vV}}|\psi(0)\rangle$. Then, with the order parameter O for the SSB, $\langle\psi(t)|O|\psi(t)\rangle$ shows a MT-periodic oscillation in the quasi-steady state.

Since the quasi-steady state $\tilde{\rho}_\beta(t)$ corresponds to an ordered state under $\tilde{V}^n_{\rm vV}$, it has the non-vanishing and oscillating correlation function,

$$|{\rm Tr}[O_iO_j\tilde{\rho}_\beta(t)] - {\rm Tr}[O_i\tilde{\rho}_\beta(t)]{\rm Tr}[O_j\tilde{\rho}_\beta(t)]| \simeq q_0 f(t) \tag{2.40}$$

for sufficiently-large $|i-j|$, where $f(t)$ is a mT-periodic function. While this is reminiscent of the spatio-temporal long-range order in DTCs [See Eq. (1.115)], we should note that Floquet prethermalization takes place in finite systems. As the lifetime of SSB under $\tilde{V}^n_{\rm vV}$ and that of Floquet prethermalization are respectively given by $\tau_{\rm SSB} \sim e^{O(L)}$ and $\tau \sim e^{O(1/(\lambda NT))}/L$, the lifetime of pDTCs will become the smaller one of the two, as described in Fig. 2.2 (b).

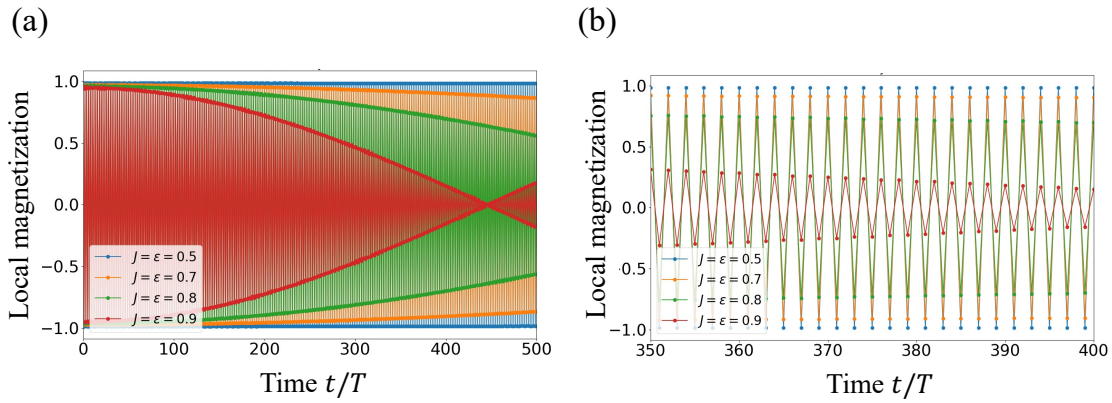

Figure 2.3: Numerical results for the model described by Eqs. (2.41) and (2.42). Each of them is calculated by the exact diagonalization for the finite size $L = 4$. (a,b) Stroboscopic dynamics of the local magnetization $\langle\psi(t)|\,\sigma_i^z\,|\psi(t)\rangle$. The local magnetization oscillates with the period $2T$ in the long transient dynamics.

Minimal model for pDTCs

We provide the simplest model for pDTCs,

$$H_0(t) = \frac{\pi}{2}\sum_{i=1}^{L}\sigma_i^x\sum_{n\in\mathbb{Z}}\delta(t-nT), \tag{2.41}$$

$$V(t) = -J\sum_{i=1}^{L-1}\sigma_i^z\sigma_{i+1}^z + \varepsilon\sin\omega t\sum_{i=1}^{L}\sigma_i^x, \tag{2.42}$$

which describes a one-dimensional Ising chain under periodic pulse. Like Eq. (2.3), the resonant drive $H_0(t)$ generates the $\mathbb{Z}_2$ Ising symmetry operation $X = \prod_{i=1}^{L}(-i\sigma_i^x)$ satisfying X^2. After simple calculation by Eqs. (2.10)-(2.14), we obtain the van Vleck expansion up to the lowest order;

$$\tilde{V}^0_{\mathrm{vV}} = -J\sum_{i=1}^{L-1}\sigma_i^z\sigma_{i+1}^z, \quad \tilde{K}^0_{\mathrm{vV}} = -\frac{\varepsilon T}{4\pi}\sum_{i=1}^{L}\sigma_i^x. \tag{2.43}$$

The effective Hamiltonian $\tilde{V}^0_{\mathrm{vV}}$, corresponding to the one-dimensional Ising Hamiltonian, shows spontaneous breaking of the $\mathbb{Z}_2$ Ising symmetry X only at zero temperature for $J \neq 0$. Thus, in order to observe pDTCs, we should prepare an initial state which gives the zero-temperature quasi-steady states under $\tilde{V}^0_{\mathrm{vV}}$. Such an initial state is spanned by $e^{i\tilde{K}^1_{\mathrm{vV}}}\,|\downarrow\ldots\downarrow\rangle$ and $e^{i\tilde{K}^1_{\mathrm{vV}}}\,|\uparrow\ldots\uparrow\rangle$, where $|\downarrow\ldots\downarrow\rangle$ and $|\uparrow\ldots\uparrow\rangle$ are the two degenerate ground states of $\tilde{V}^0_{\mathrm{vV}}$. However, the superposition of them is physically unstable to observation or decoherence, known as a cat state. Either one of the two states,

$$|\psi(0)\rangle = e^{-i\frac{\varepsilon T}{4\pi}\sum_{i=1}^{L}\sigma_i^x}\,|\downarrow\ldots\downarrow\rangle\,, \quad e^{-i\frac{\varepsilon T}{4\pi}\sum_{i=1}^{L}\sigma_i^x}\,|\uparrow\ldots\uparrow\rangle\,, \tag{2.44}$$

should be prepared as the initial state.

Figure 2.3 shows numerical results for the stroboscopic dynamics of the local magnetization $\langle\psi(t)|\,\sigma_i^z\,|\psi(t)\rangle$ and the lifetime of the oscillation when the initial state $|\psi(0)\rangle$ is $e^{i\tilde{K}1}\,|\uparrow\ldots\uparrow\rangle$. We do not see the first relaxation in Fig. 2.3 since the initial state itself corresponds to the steady state under $\tilde{V}^0_{\mathrm{vV}}$. Figures 2.3 (a) and (b) show the robust $2T$-periodic oscillations of pDTCs, which we can predict from the lowest-order approximation. As the strength JT $(= \varepsilon T)$ increases, the $2T$-periodic oscillation with the amplitude approximately 1 shrinks faster. This behavior can be attributed to the increasing local energy scale $\sim O(J, \varepsilon)$ compared to the frequency ω.

We also compute the lifetime of pDTCs, which gives an estimation for the lifetime of Floquet prethermalization τ. We define the lifetime of pDTCs by the time at which the amplitude of the $2T$-periodic oscillation shrinks to 0.95 times as large as the initial value. Figure 2.4 describes

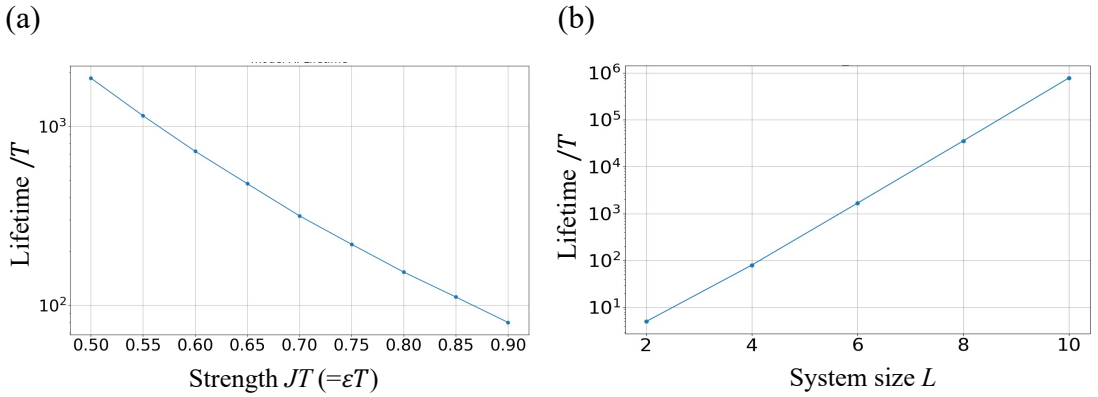

Figure 2.4: (a) Lifetime of pDTCs with the increasing strength JT $(= \varepsilon T)$. The system size is fixed to 4. (b) Lifetime of pDTCs with the increasing system size L with the fixed strength $JT = \varepsilon T = 0.9$. In both cases, the lifetime of pDTCs is defined by the time at which the amplitude of the oscillation in Fig. 2.3 reaches 0.95 times as large as the initial one.

how the lifetime of pDTCs depends on (a) the coupling JT and (b) the system size L. As the lifetime of Floquet prethermalization increases with $\tau = e^{O(1/(\lambda NT))}T$, we confirm from Fig. 2.4 (a) that the lifetime of pDTCs also exponentially grows in $1/(JT) \sim 1/(\lambda NT)$. On the other hand, Fig. 2.4 (b) says that the lifetime of pDTCs exponentially increases in the system size L. This result well matches the behavior for small L in Fig. 2.2 (b), obtained by the lifetime of SSB under the effective Hamiltonian and that of Floquet prethermalization. In order to observe the lifetime inversely-proportional to L, we should compute larger systems in some other ways such as the time-dependent density matrix renormalization group (tDMRG) or the time-evolving block decimation (TEBD) [110, 111, 112].

We demonstrate a driven one-dimensional system here, where the initial states only at zero temperature are available for pDTCs. When we consider higher-dimensional systems, we obtain a series of initial states corresponding to finite temperature, which can host pDTCs. We also discuss how the pDTC behavior can be distinguished from that of DTCs in experiments. DTCs show a robust nontrivial oscillation with infinite lifetime in the genuine steady state under $L \to \infty$. However, due to the experimental limitation of the finite coherence time and the finite size, the DTC behavior has finite lifetime like that of pDTCs. In the case of DTCs accompanied by many-body localization (MBL) [See Section 1.3.5], we can distinguish them from pDTCs by the dependence on the initial states. In DTCs accompanied by MBL, all the Floquet eigenstates have the spatio-temporal long-range orders, indicating that any physically-feasible initial state experiences a robust nontrivial oscillation. On the other hand, pDTCs can host TTSB only when the initial state has low-temperature under the effective Hamiltonian. Thus, by demonstrating the real-time dynamics from different initial states, we can identify DTCs and pDTCs. In fact, while the first experimental observation in trapped ions [95] has been expected to detect DTCs accompanied with MBL due to the one-dimensionality and the randomness, Ref. [98] suggests that it might be attributed to pDTCs because of the absence of TTSB from another initial state.

2.3 Resonant Floquet engineering

Here, we provide the other application of Floquet prethermalization in the resonant regime, dubbed "resonant Floquet engineering." As discussed in Section 1.3.4, Floquet engineering is one of the most intriguing fields as the application of Floquet prethermalization in the high-frequency regime, with which we can control phases of matter by periodic drive such as laser light. This technique is based on the fact that Floquet prethermalization in the high-frequency regime enables a quasi-steady state under the Floquet-Magnus or the van Vleck effective Hamiltonian, which can be modulated by the periodic drive. In a similar way, one can expect that Floquet prethermalization in the resonant regime enables Floquet engineering by exploiting its effective Hamiltonian.

Let us formulate Floquet engineering with the application of Floquet prethermalization in the resonant regime. With the usage of Theorems 2.1.1 and 2.1.2, we summarize resonant Floquet engineering enabled by resonant drives as follows.

Remark. (Resonant Floquet engineering)
We prepare Floquet many-body systems in the resonant regime driven by $H(t) = H_0(t) + V(t)$. We choose the resonant drive $H_0(t)$ so that it can generate a $\mathbb{Z}_N$-symmetry X;

$$X^N = 1, \quad X = \mathcal{T}\exp\left(-i\int_0^T dt H_0(t)\right). \tag{2.45}$$

When we modulate the high-frequency drive $V(t)$ with the local energy scale smaller than the frequency ω, we can control phase of matters in $\mathbb{Z}_N$-symmetric static systems with the Hamiltonian

$$\tilde{V}^n_{\rm vV} = \tilde{V}_0 + N\sum_{l\neq 0}\frac{[\tilde{V}_{-l},\tilde{V}_l]}{2l\omega} + \ldots + \tilde{V}^n_{\rm vV}, \quad X^{-1}\tilde{V}^n_{\rm vV}X = \tilde{V}^n_{\rm vV}, \tag{2.46}$$

by focusing on the coarse-grained dynamics $|\psi(mNT)\rangle$ in the intermediate time regime. The emergent $\mathbb{Z}_N$-symmetry X is robust against any T-periodic local perturbation.

In Floquet engineering only with the high-frequency drive, we can modulate the effective Hamiltonian by the higher-order terms $H^{(m)}_{\rm FM}$ or $H^{(m)}_{\rm vV}$ $(m \geq 1)$. This enables the realization of preferable phenomena under the static Hamiltonian $H^n_{\rm FM}$ or $H^n_{\rm FM}$ even when the undriven Hamiltonian H_0 does not host them. Similarly, resonant Floquet engineering also enables us to modulate the effective Hamiltonian with the higher-order terms $\tilde{V}^{(m)}_{\rm vV}$ $(m \geq 1)$. What distinguishes it from the conventional Floquet engineering is the emergence of the robust $\mathbb{Z}_N$-symmetry X. While the original Hamiltonian $H(t)$ does not necessarily respect the $\mathbb{Z}_N$-symmetry, we can control phases of matter with adding the $\mathbb{Z}_N$-symmetry to the system.

Resonant Floquet engineering by Floquet prethermalization in the resonant regime can be applied to quantum many-body phenomena where symmetries play a significant role. The simplest application is the removal of unpreferable couplings with environments. For instance, let us consider a spin system coupled with a bosonic bath, described by the Hamiltonian;

$$V(t) = \sum_{i=1}^{L}(J\sigma^z_i\sigma^z_{i+1} + h\sigma^x_i) + \gamma\sum_{i=1}^{L}\sigma^z_i(b_i + b^\dagger_i), \tag{2.47}$$

where b_i and $b^\dagger_i$ respectively represent bosonic annihilation and creation operators. We add a periodic pulse to the system, described by the resonant Hamiltonian

$$H_0(t) = \frac{\pi}{2}\sum_{i=1}^{L}\sigma^x_i\sum_{n\in\mathbb{Z}}\delta(t - nT), \tag{2.48}$$

and we assume that only the states with a few bosons are relevant (the Hilbert space has finite dimension). Then, when the local energy scale $\sim \max(J, h, \gamma)$ is small compared to the frequency ω, one can effectively realize the static Hamiltonian,

$$\tilde{V}^n_{\rm vV} = \sum_{i=1}^{L}(J\sigma^z_i\sigma^z_{i+1} + h\sigma^x_i) + \tilde{V}^{(1)}_{\rm vV} + \ldots + \tilde{V}^{(n)}_{\rm vV}, \tag{2.49}$$

which retrieves the asymmetric coupling with the environment. This is reminiscent of the dynamical coupling [113], in which we can retrieve the effect of the coupling with a non-Markovian bath by applying a fast periodic pulse.

Another nontrivial application is the realization and control of symmetry protected topological (SPT) phases. A SPT phase is a kind of topological phases, and has ground state degeneracies robust against any local perturbation only in the presence of certain symmetries. Resonant Floquet

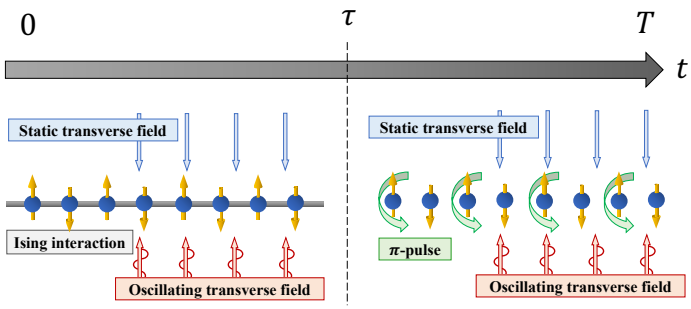

Figure 2.5: Schematic picture of the driving protocol over one period T. The Ising interaction $V_{\rm int}(t)$ [Eq. (2.54)] is uniformly imposed during $0 \le t < \tau$. The resonant drive $H_0(t)$ [Eq. (2.53)], which acts as a π-pulse, is imposed only on the odd sites during $\tau \le t < T$. The oscillating transverse field $V_h(t)$ and the static transverse field V_g [Eq. (2.55)] are both uniformly imposed throughout.

engineering is expected to allow us to manipulate SPT phases even when the required symmetry is absent in the original system. In the rest of this section, we provide a simple example of resonant Floquet engineering for SPT phases.

2.3.1 Model for resonant Floquet engineering

Here, we discuss Floquet systems in the resonant regime, which exemplifies resonant Floquet engineering for SPT phases, and describe how resonant Floquet engineering benefits the control of phases of matter. As the simplest case, we focus on a one-dimensional spin system which becomes equivalent to a spin system hosting SPT phases under a $\mathbb{Z}_2 \times \mathbb{Z}_2$-symmetry. While the SPT phases require a $\mathbb{Z}_2 \times \mathbb{Z}_2$-symmetric system in principle, we aim at constructing a $\mathbb{Z}_2$-symmetric Floquet system hosting them as the nontrivial example of resonant Floquet engineering.

Let us describe the $\mathbb{Z}_2$-symmetric periodically-driven model on a one-dimensional spin chain with $S = 1/2$. We assume that the system size L is a multiple of 4, and impose the open boundary condition (OBC). We give the time-periodic Hamiltonian by

$$H(t) = \begin{cases} J \sum_{j=1}^{L-1} \sigma_j^z \sigma_{j+1}^z + (g + h\cos\omega t) \sum_{j=1}^{L} \sigma_j^x & 0 \le t < \tau \\ \dfrac{\pi}{2(T-\tau)} \sum_{j:\text{odd}} \sigma_i^x + (g + h\cos\omega t) \sum_{j=1}^{L} \sigma_j^x & \tau \le t < T. \end{cases} \tag{2.50}$$

This model respects a global $\mathbb{Z}_2$-symmetry $X_{\rm all}$, represented by

$$X_{\rm all}^{-1} H(t) X_{\rm all} = H(t), \quad X_{\rm all} = \prod_{i=1}^{L} \sigma_i^x. \tag{2.51}$$

The terms in the above Hamiltonian can be separated into resonant and high-frequency drives so that we can grasp Floquet prethermalization in the resonant regime, as follows;

$$H(t) = H_0(t) + V_{\rm int}(t) + V_h(t) + V_g \tag{2.52}$$

$$H_0(t) = \begin{cases} 0 & (0 \le t < \tau) \\ \dfrac{\pi}{2(T-\tau)} \sum_{j:\text{odd}} \sigma_j^x & (\tau \le t < T) \end{cases}, \tag{2.53}$$

$$V_{\rm int}(t) = \begin{cases} J \sum_{j=1}^{L-1} \sigma_j^z \sigma_{j+1}^z & (0 \le t < \tau) \\ 0 & (\tau \le t < T) \end{cases}, \tag{2.54}$$

$$V_h(t) = h\cos\omega t \sum_{j=1}^{L} \sigma_j^x, \quad V_g = g \sum_{j=1}^{N} \sigma_j^x. \tag{2.55}$$

The high-frequency drive $V(t) = V_{\rm int}(t) + V_h(t) + V_g$ is composed of the Ising interactions $V_{\rm int}(t)$, the oscillating transverse field $V_h(t)$, and the static transverse field V_g. The local energy scale of each term in $V(t)$ should be small compared to the frequency ω, which means $\max(J,h,g)/\omega \ll 1$.

On the other hand, the resonant drive $H_0(t)$ represents a sequential pulse of the transverse field, whose Floquet operator X gives the following $\mathbb{Z}_2$-symmetry,

$$X_{\rm odd} = \prod_{i:{\rm odd}} \sigma_i^x. \tag{2.56}$$

Here, we employ the fact that L is a multiple of 4 to erase the phase factor $(-i)^L$. Figure 2.5 schematically depicts how we drive the system. Here, we explore the way to realize and control topological phases protected by the $\mathbb{Z}_2 \times \mathbb{Z}_2$-symmetry generated by $X_{\rm odd}$ and $X_{\rm even}$, where the symmetry operation $X_{\rm even}$ is defined by

$$X_{\rm even} = \prod_{i:{\rm even}} \sigma_i^x = X_{\rm all} X_{\rm odd}^{-1}. \tag{2.57}$$

While a $\mathbb{Z}_2$-symmetric invariant under $X_{\rm all}$ cannot host SPT phases under the $\mathbb{Z}_2 \times \mathbb{Z}_2$-symmetry, resonant Floquet engineering provides a quasi-steady state under the $\mathbb{Z}_2 \times \mathbb{Z}_2$-symmetry generated by $X_{\rm odd}$ and $X_{\rm even}$ by adding the $X_{\rm odd}$-invariance to the system. Thus, even the $\mathbb{Z}_2$-symmetric system under $H(t)$ can be a platform for SPT phases under the $\mathbb{Z}_2 \times \mathbb{Z}_2$-symmetry. Such a control of the symmetry is inherent in resonant Floquet engineering, compared to the conventional Floquet engineering in the high-frequency regime. We concretely discuss what kind of the parameter choice allows nontrivial SPT phases by analyzing the van Vleck effective Hamiltonian.

2.3.2 Realization of SPT phases in quasi-steady states

In this section, we discuss how nontrivial SPT phases are realized in the Floquet system driven by the Hamiltonian Eq. (2.50) or Eq. (2.52). As shown in the beginning of Section 2.3, the quasi-steady state is described by the van Vleck expansion $\tilde{V}^n_{\rm vV}$. Here, we consider up to the second order,

$$\tilde{V}^2_{\rm vV} = \tilde{V}^{(0)}_{\rm vV} + \tilde{V}^{(1)}_{\rm vV} + \tilde{V}^{(2)}_{\rm vV}. \tag{2.58}$$

To evaluate this effective Hamiltonian, we first compute the Fourier components of $\tilde{V}(t)$, the Hamiltonian $V(t) = V_{\rm int}(t) + V_h(t) + V_g(t)$ in the rotating frame. Based on the definition Eq. (2.8),

$$\tilde{V}_0 = g\sum_{j=1}^{L} \sigma_j^x, \quad \tilde{V}_2 = \tilde{V}_{-2} = \frac{h}{2}\sum_{j=1}^{L} \sigma_j^x, \tag{2.59}$$

$$\tilde{V}_l = J\sum_{j=1}^{L-1} \sigma_j^z \sigma_{j+1}^z \frac{e^{il\omega\tau/2}-1}{il\pi} \quad (l:{\rm odd}), \tag{2.60}$$

$$\tilde{V}_l = 0 \quad ({\rm otherwise}). \tag{2.61}$$

Considering $[\tilde{V}_{-l}, \tilde{V}_l] = 0$ for any nonzero integer l, the first order term $\tilde{V}^1_{\rm vV}$, which is given by Eq. (2.10), always vanishes. Thus, the second-order van Vleck expansion becomes

$$\tilde{V}^2_{\rm vV} = g\sum_{j=1}^{L} \sigma_j^x + 4\sum_{m\neq 0} \frac{[[\tilde{V}_{-m}, \tilde{V}_0], \tilde{V}_m]}{2m^2\omega^2} + 4\sum_{m\neq 0}\sum_{n\neq 0,m} \frac{[[\tilde{V}_{-m}, \tilde{V}_{m-n}], \tilde{V}_n]}{3mn\omega^2} \tag{2.62}$$

We assume that the local energy scale of V_g is much smaller than those of $V_{\rm int}(t)$ and $V_h(t)$, that is,

$$\frac{g}{\lambda} = O((\lambda/\omega)^2), \quad \lambda = \max(J,h). \tag{2.63}$$

Then, the second term in Eq. (2.62) is negligible compared to the other terms. In the summation of the third term, the indices m and n satisfying $m-n = \pm 2$ and m:odd have nonzero contributions.

This results in

$$\begin{aligned}\tilde{V}_{\mathrm{vV}}^2 &\simeq g\sum_{j=1}^{L}\sigma_j^x+\frac{4}{3\omega^2}\sum_{m:\mathrm{odd}}\left(\frac{[[\tilde{V}_{-m},\tilde{V}_2],\tilde{V}_{m-2}]}{m(m-2)}+\frac{[[\tilde{V}_{-m},\tilde{V}_{-2}],\tilde{V}_{m+2}]}{m(m+2)}\right)\\ &= g\sum_{j=1}^{L}\sigma_j^x+\frac{2J^2h}{3\omega^2}C\left[\left[\sum_{j=1}^{L-1}\sigma_j^z\sigma_{j+1}^z,\sum_{j=1}^{L}\sigma_j^x\right],\sum_{j=1}^{L-1}\sigma_j^z\sigma_{j+1}^z\right],\end{aligned}\tag{2.64}$$

where the coefficient C is defined by

$$C=\sum_{m:\mathrm{odd}}\frac{(e^{-im\omega\tau/2}-1)(e^{i(m-2)\omega\tau/2}-1)}{m^2(m-2)^2\pi^2}+\sum_{m:\mathrm{odd}}\frac{(e^{-im\omega\tau/2}-1)(e^{i(m+2)\omega\tau/2}-1)}{m^2(m+2)^2\pi^2}.\tag{2.65}$$

With simple analytical calculation, we obtain the commutator in Eq. (2.64) and the coefficient C as follows;

$$\left[\left[\sum_{j=1}^{L-1}\sigma_j^z\sigma_{j+1}^z,\sum_{j=1}^{L}\sigma_j^x\right],\sum_{j=1}^{L-1}\sigma_j^z\sigma_{j+1}^z\right]=-8\left(\sum_{j=1}^{L}\sigma_j^x+\sum_{j=2}^{L-1}\sigma_{j-1}^z\sigma_j^x\sigma_{j+1}^z\right)+4(\sigma_1^x+\sigma_L^x),\tag{2.66}$$

$$C=\frac{1}{4\pi}\{\omega\tau(1+\cos\omega\tau)-2\sin\omega\tau\}.\tag{2.67}$$

When considering SPT phases, the local boundary terms $4(\sigma_1^x+\sigma_L^x)$ are expected to be irrelevant to topological nature coming from the bulk properties. Thus, by neglecting the boundary terms, we arrive at the following effective Hamiltonian

$$\tilde{V}_{\mathrm{vV}}^2 \simeq (g+\gamma)\sum_{j=1}^{L}\sigma_j^x+\gamma\sum_{j=2}^{L-1}\sigma_{j-1}^z\sigma_j^x\sigma_{j+1}^z,\tag{2.68}$$

$$\gamma = \frac{4J^2h}{3\pi\omega^2}\{2\sin\omega\tau-\omega\tau(1+\cos\omega\tau)\}.\tag{2.69}$$

As described in Section 2.3.1, this Hamiltonian respects the $\mathbb{Z}_2\times\mathbb{Z}_2$-symmetry,

$$X_{\mathrm{odd}}^{-1}\tilde{V}_{\mathrm{vV}}^2X_{\mathrm{odd}}^{-1}=X_{\mathrm{even}}^{-1}\tilde{V}_{\mathrm{vV}}^2X_{\mathrm{even}}^{-1}=\tilde{V}_{\mathrm{vV}}^2,\tag{2.70}$$

while the original Hamiltonian $H(t)$ does not.

Now, let us discuss what kind of SPT phases are realized in the $\mathbb{Z}_2\times\mathbb{Z}_2$ Hamiltonian $\tilde{V}_{\mathrm{vV}}^2$ given by Eq. (2.68). Here, we employ the Jordan-Wigner transformation, which maps a spin system to a fermionic system [114]. The transformation is defined by

$$\alpha_j\equiv\left(\prod_{k<j}\sigma_k^x\right)\sigma_j^z,\quad \beta_j\equiv-\left(\prod_{k<j}\sigma_k^x\right)\sigma_j^y,\tag{2.71}$$

where $\{\alpha_i\}_{i=1}^L$ and $\{\beta_i\}_i^L$ represent independent Majorana fermions, which satisfy

$$\alpha_i=\alpha_i^\dagger,\quad \beta_i=\beta_i^\dagger,\quad \{\alpha_i,\alpha_j\}=\{\beta_i,\beta_j\}=2\delta_{ij},\quad \{\alpha_i,\beta_j\}=0.\tag{2.72}$$

Under this transformation, the effective Hamiltonian Eq. (2.68) is rewritten by

$$\tilde{V}_{\mathrm{vV}}^2\simeq\left[-i(g+\gamma)\sum_{j:\mathrm{odd}}\alpha_j\beta_j-i\gamma\sum_{j:\mathrm{odd}}\beta_{j-1}\alpha_{j+1}\right]+\left[-i(g+\gamma)\sum_{j:\mathrm{even}}\alpha_j\beta_j-i\gamma\sum_{j:\mathrm{even}}\beta_{j-1}\alpha_{j+1}\right],\tag{2.73}$$

which is equivalent to the Hamiltonian for two decoupled Kitaev chains composed of the odd sites and the even sites. In each Kitaev chain, the SPT phases under a $\mathbb{Z}_2$-symmetry can be classified by the ratio of the coefficient of the intra-coupling $\alpha_j\beta_j$ to that of the inter-coupling $\beta_{j-1}\alpha_{j+1}$. In this case, $\mathrm{sgn}(|(g+\gamma)/\gamma|-1)$ determines the SPT phases. When we assume $h>0$, Eq. (2.69) indicates $\gamma>0$ for $0<\omega\tau<\pi$ and $\gamma<0$ for $\pi<\omega\tau<2\pi$. As a result, we obtain the following relation depending on the sign of γ;

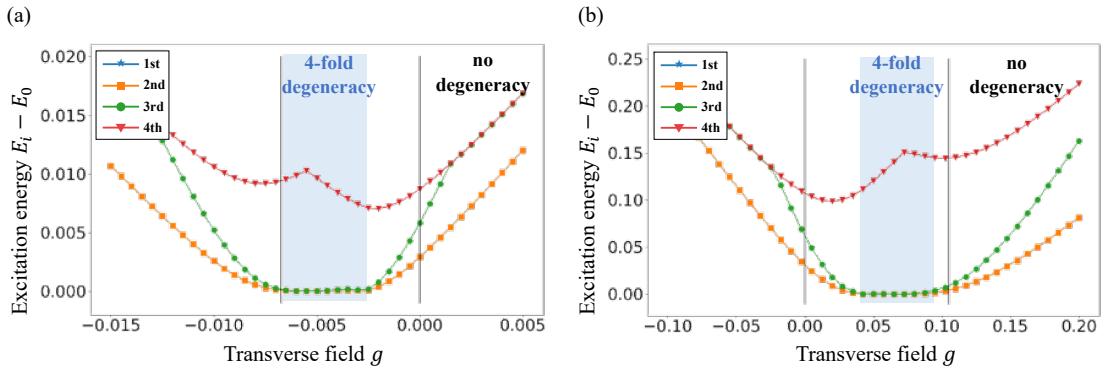

Figure 2.6: Excitation energies from the ground state to low energy excited states of H_{eff} for different choice of switching time (a) $\tau = 1/4$ and (b) $\tau = 3/4$, where the period T is set to 1. In both of the cases, we choose the interaction $J = 0.9$, the amplitude of the oscillating field $h = 0.9$, and the system size $L = 8$. In the gray regions, a four-fold degeneracy appears in the ground states, which is a signature of nontrivial SPT phases. The black lines represent the analytically-obtained topological phase transition points $g = 0$ and $g = -2\gamma$. In the parameter regions shown in both graphs (a) and (b), the first excited state (blue star) and the second excited state (orange square) are degenerate.

When $0 < \tau < T/2$, or equivalently $\gamma > 0$,

$$\begin{aligned} g < -2\gamma,\ 0 < g \quad &: \quad \text{topologically trivial phase,} \\ g = -2\gamma,\ 0 \quad &: \quad \text{topological phase transition point,} \\ -2\gamma < g < 0 \quad &: \quad \text{topologically nontrivial phase.} \end{aligned}$$

When $T/2 < \tau < T$, or equivalently $\gamma < 0$,

$$\begin{aligned} g < 0,\ -2\gamma < g \quad &: \quad \text{topologically trivial phase,} \\ g = 0,\ -2\gamma \quad &: \quad \text{topological phase transition point,} \\ 0 < g < -2\gamma \quad &: \quad \text{topologically nontrivial phase.} \end{aligned}$$

Thus, by properly tuning the parameters J, g, h, τ, we can realize nontrivial topological phases protected by the $\mathbb{Z}_2 \times \mathbb{Z}_2$-symmetry in the $\mathbb{Z}_2$-symmetric setup.

In a Kitaev chain under OBC, a robust two-fold degeneracy appears in its ground state if the system is topologically nontrivial. Since the effective model described by $\tilde{V}_{\text{vV}}^2$ is equivalent to two identical Kitaev chains, it has a robust four-fold degeneracy in its ground state if topologically nontrivial. We numerically examine whether or not this topological nature can appear without resorting to the high-frequency expansion. We compute the exact effective Hamiltonian for the coarse-grained stroboscopic dynamics, defined by

$$\tilde{H}_{\text{eff}} = \frac{i}{2T} \log[U(2T)], \quad U(2T) = \mathcal{T} \exp\left(-i \int_0^{2T} H(t) dt \right), \tag{2.74}$$

where we choose the branch cut at $\pm\pi/(2T)$. In Fig. 2.6, we examine the ground-state degeneracy of $\tilde{H}_{\text{eff}}$. While the parameters experiencing the gap opening deviate from the phase transition points predicted by the high-frequency expansion due to the finite-size effect, we can observe the robust four-fold degeneracy in nontrivial SPT phases.

2.3.3 Control of SPT phases in quasi-steady states

In the previous section, we have discussed how nontrivial SPT phases are realized by tuning the parameters J, g, h, τ. In the two decoupled Kitaev chains under the $\mathbb{Z}_2 \times \mathbb{Z}_2$-symmetry, four distinct

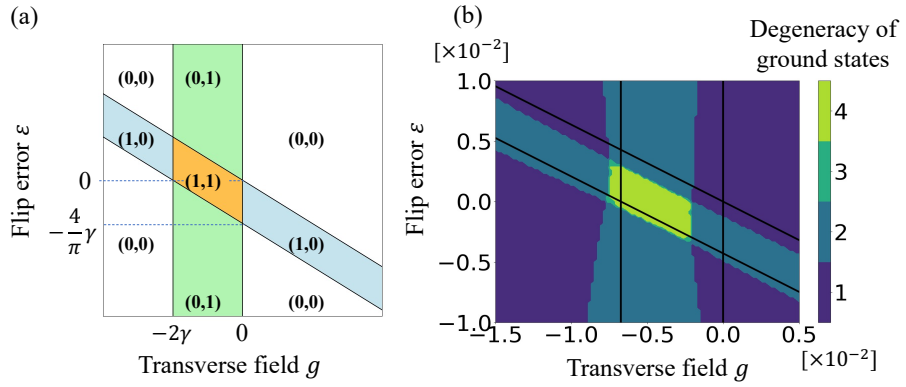

Figure 2.7: (a) Phase diagram of the effective static model Eq. (2.79) based on the van Vleck expansion $\tilde{V}^2_{\rm vV}$. The indices $(Z_{\rm odd}, Z_{\rm even}) \in \mathbb{Z}_2 \times \mathbb{Z}_2$ represent the $\mathbb{Z}_2$ topological numbers of the Kitaev chains composed of the odd and even sites, respectively. (b) The degeneracy of the ground states, calculated in terms of the effective Hamiltonian $\tilde{H}_{\rm eff}$. Here, we define the degeneracy for the n-th excited state with the eigenenergy E_n by satisfying $|E_n - E_0|/|E_0| < 0.01$. The black lines are the boundaries of SPT phases obtained by the analytical calculation of $\tilde{V}^2_{\rm vV}$. This result well reflects the phase diagram based on the van Vleck expansion in (a).

phases are allowed while the previous section has observed two kinds of phases. Here, we provide a way to engineer all the four distinct phases by the additional drive. Let us consider a Floquet system with the deviation of the resonant drive, described by

$$H(t) = H_0(t) + V_\varepsilon(t) + V_{\rm int}(t) + V_h(t) + V_g, \tag{2.75}$$

$$V_\varepsilon(t) = \begin{cases} 0 & (0 \le t < \tau) \\ \dfrac{\pi\varepsilon}{2(T-\tau)} \displaystyle\sum_{j:\rm odd} \sigma^x_j & (\tau \le t < T). \end{cases} \tag{2.76}$$

The additional drive $V_\varepsilon(t)$ represents the deviation imposed on the resonant drive $H_0(t)$, which changes its rotation angle around the x-axis from π to $\pi(1+\varepsilon)$. We again assume that the deviation ε and the transverse field g are much smaller than the local energy scale of the other terms, that is,

$$\frac{\varepsilon}{\lambda(T-\tau)}, \quad \frac{g}{\lambda} = O((\lambda/\omega)^2), \quad \lambda = \max(J, h). \tag{2.77}$$

Then, with redefining the high-frequency drive by $V(t) = V_\varepsilon(t) + V_{\rm int}(t) + V_h(t) + V_g$, we obtain the approximate effective Hamiltonian up to the second order;

$$\tilde{V}^2_{\rm vV} \simeq a_{\rm even} \sum_{j:\rm even} \sigma^x_j + b_{\rm odd} \sum_{j:\rm odd} \sigma^z_{j-1}\sigma^x_j\sigma^z_{j+1} + a_{\rm odd} \sum_{j:\rm odd} \sigma^x_j + b_{\rm even} \sum_{j:\rm even} \sigma^z_{j-1}\sigma^x_j\sigma^z_{j+1} \tag{2.78}$$

$$= \left[-ia_{\rm odd} \sum_{j:\rm odd} \alpha_j\beta_j - ib_{\rm even} \sum_{j:\rm odd} \beta_{j-1}\alpha_{j+1}\right] + \left[-ia_{\rm even} \sum_{j:\rm even} \alpha_j\beta_j - ib_{\rm odd} \sum_{j:\rm even} \beta_{j-1}\alpha_{j+1}\right], \tag{2.79}$$

with $a_{\rm odd} = g + \pi\varepsilon/2T + \gamma$, $a_{\rm even} = g + \gamma$, and $b_{\rm odd} = b_{\rm even} = \gamma$. In the second equality, we again map the system to a fermionic system by the Jordan-Wigner transformation. In the presence of the deviation $V_\varepsilon(t)$, the system becomes equivalent to two decoupled Kitaev chains but they are not identical. The four distinct topological phases are classified by two $\mathbb{Z}_2$ topological numbers, defined by

$$Z_{\rm odd} = \frac{1 + {\rm sgn}(|b_{\rm even}| - |a_{\rm odd}|)}{2}, \quad Z_{\rm even} = \frac{1 + {\rm sgn}(|b_{\rm odd}| - |a_{\rm even}|)}{2}. \tag{2.80}$$

Figure 2.7 (a) shows the phase diagram of the SPT phases which is analytically obtained from the second-order van Vleck effective expansion $\tilde{V}^2_{\rm vV}$. The origin $(g, \varepsilon) = (0, 0)$ lies at the phase

boundary of the four distinct phases, and hence we can control the system among all the four SPT phases by slightly changing the parameters (g, ε) from the origin. These topological characteristics can be found in the ground-state degeneracy of the exact effective Hamiltonian $\tilde{H}_{\text{eff}}$ [See Eq. (2.74)]. Figure 2.7 (b) shows the numerical result, showing that the ground state hosts two-fold or four-fold degeneracy depending on the number of the nonzero $\mathbb{Z}_2$ topological numbers. As mentioned in Section 2.1.2, perturbations to the resonant drive do not harm Floquet prethermalization with the emergent symmetry. On the contrary, they can be useful for the control of phases of matter.

2.4 Summary and outlook of this chapter

Here, we conclude this chapter and discuss some possible future directions, with providing some recent developments in this field. In this chapter, we have formulated Floquet prethermalization in the resonant regime, in which the resonant drive with the local energy scale comparable to the frequency generates a $\mathbb{Z}_N$-symmetry. In contrast to the high-frequency regime, the resonant regime hosts sufficiently-long intermediate dynamics under the $\mathbb{Z}_N$-symmetric van Vleck expansion $\tilde{V}^n_{\text{vV}}$. Importantly, the emergent $\mathbb{Z}_N$-symmetry is robust as long as the time-periodicity is maintained. By applying the formalism, we have also provided prethermal disctrete time crystals (pDTCs) and resonant Floquet engineering, which are inherent in the resonant regime.

Floquet prethermalization in the resonant regime was firstly proposed in Ref. [115], in which they show the existence of a macroscopic quasi-conserved quantity with an emergent $\mathbb{Z}_N$-symmetry in a certain frame. The formulation presented here reveals the explicit formula for the quasi-conserved quantity and the frame including higher-order corrections, which respectively correspond to the van Vleck effective Hamiltonian $\tilde{V}^n_{\text{vV}}$ and the kick operator $\tilde{K}^n_{\text{vV}}$. The accurate effective Hamiltonian with the emergent $\mathbb{Z}_N$-symmetry enables the detailed analysis of pDTCs and resonant Floquet engineering. Recently, while the locality of interactions with a bounded local energy scale and the time-periodicity of the Hamiltonian are essential in these setups, Floquet prethermalization in other nonequilibrium setups, such as long-ranged interacting systems [116, 117], has been vigorously explored. Interestingly, nonequilibrium systems under resonant and high-frequency drives with multiple frequencies incommensurate with each other can also host prethermalization, in which the effective Hamiltonian respects the emergent symmetry more complex than $\mathbb{Z}_N$-symmetries [118]. Prethermalization in the high-frequency regime has been also developed; the existence of the sufficiently-long time scale avoiding heating has been confirmed in quasi-periodic interacting systems by both numerical and analytical ways [119, 120, 121]. Including its extension to the resonant regime, we expect that there exists much room for exploring prethermalization in the resonant regime with some preferable properties coming from the time-dependence such as the emergent symmetries.

As an application of Floquet prethermalization in the resonant drive, we have provided pDTCs, in which robust discrete time crystalline behaviors can be observed in the quasi-steady states. Based on the van Vleck expansion with in the rotating frame, we have shown that the appearance of pDTCs corresponds to spontaneous breaking of the emergent $\mathbb{Z}_N$-symmetry under the van Vleck effective Hamiltonian $\tilde{V}^n_{\text{vV}}$. The van Vleck kick operator $\tilde{K}^n_{\text{vV}}$ is employed for determining the effective temperature under the effective Hamiltonian. While we provide a one-dimensional model as the simplest case for pDTCs, it will be significant to further explore the detailed properties of pDTCs based on the van Vleck effective Hamiltonian, as the experimental developments in Floquet prethermalization [122, 123] and pDTCs [124]. We also note that, the developments in Floquet prethermalization will lead to the novel pDTCs. For example, DTC-like behaviors with nontrivial quasi-periodic oscillations in quasi-steady states have been suggested by the usage of prethermalization under quasi-periodic drive [118]. We expect a variety of pDTCs accompanied by novel Floquet prethermalization.

We have dealt with resonant Floquet engineering as the other application of Floquet prethermalization in the resonant regime. The formalism based on the van Vleck expansion enables the control of phases of matter with adding a $\mathbb{Z}_N$-symmetry. The conventional Floquet engineering exploiting the high-frequency regime has no constraints on the symmetry of the effective Hamiltonian. While the conventional protocol also realizes emergent symmetries in some limited cases only up to low orders with enabling the control of SPT phases [125, 126], resonant Floquet engineering allows the robust emergent symmetry respected up to any truncation order for generic cases. As exemplified in the control of SPT phases, the controlled parameters of both the resonant and

high-frequency drives enable various phases of matter in symmetric setups. With recent studies on the error cancellation and the emergent symmetry by modified resonant drives [127, 128, 129], we expect rapid growth of the control of materials by resonant drives.

2.5 Appendix for this chapter

Rigorous bound in Theorem 2.1.1

Theorem 2.1.1 validates the approximation of the coarse-grained Floquet operator by the van Vleck expansions. Here, we explicitly provide the upper bound in Theorem 2.1.1. To be precise, we evaluate the right hand side of the triangle inequality,

$$\begin{aligned} ||U_f^N - e^{-i\tilde{K}^n_{\rm vV}} e^{-i\tilde{V}^n_{\rm vV}NT} e^{i\tilde{K}^n_{\rm vV}}|| \quad \leq \quad & ||U_f^N - e^{-i\tilde{V}^{n0}_{\rm FM}NT}|| + ||e^{-i\tilde{V}^{n0}_{\rm FM}NT} - e^{-i\tilde{V}^n_{\rm FM}NT}|| \\ & + ||e^{-i\tilde{V}^n_{\rm FM}NT} - e^{-i\tilde{K}^n_{\rm vV}} e^{-i\tilde{V}^n_{\rm vV}NT} e^{i\tilde{K}^n_{\rm vV}}||, \end{aligned} \tag{2.81}$$

where the upper bound for the first two terms is designated by Eqs. (2.18) and (2.20), originating from Theorem 1.3.3. Under the assumption of the k-locality and the J-extensiveness on the high-frequency drive $V(t)$, we evaluate

$$D_n = ||e^{-i\tilde{V}^n_{\rm FM}NT} - e^{-i\tilde{K}^n_{\rm vV}} e^{-i\tilde{V}^n_{\rm vV}NT} e^{i\tilde{K}^n_{\rm vV}}||. \tag{2.82}$$

Upper bound by effective Hamiltonians

The deviation D_n is bounded by

$$D_n \leq 2NT \left|\left| \tilde{V}^n_{\rm FM} - e^{-i\tilde{K}^n_{\rm vV}} \tilde{V}^n_{\rm vV} e^{i\tilde{K}^n_{\rm vV}} \right|\right|, \tag{2.83}$$

with the following lemma. We can confirm Eq. (2.83) by setting $A = -NT\tilde{V}^n_{\rm FM}$ and $B = -NTe^{-i\tilde{K}^n_{\rm vV}} \tilde{V}^n_{\rm vV} e^{i\tilde{K}^n_{\rm vV}}$ in Eq. (2.84).

Lemma 1. (Bound on the deviation of unitary operators)
For any finite-dimensional hermitian matrices A, B, the inequality

$$\left|\left| e^{iA} - e^{iB} \right|\right| \leq 2||A - B|| \tag{2.84}$$

is satisfied.

Proof

For a bounded hermitian operator C and a real number $t \in \mathbb{R}$, we calculate the upper bound of $||F(t) - F(0)||$, where $F(t)$ is a unitary operator defined by $F(t) = \exp\{i(B + Ct)\}$. By denoting $F^{(n)}(t) = d^n F(t)/dt^n$,

$$||F(t) - F(0)|| \leq \left|\left| \sum_{n=1}^{\infty} \frac{1}{n!} F^{(n)}(0) t^n \right|\right| \leq \sum_{n=1}^{\infty} \frac{|t|^n}{n!} ||F^{(n)}(0)|| \tag{2.85}$$

is obtained. By using the formula

$$\frac{d}{dt} e^{X(t)} = \int_0^1 d\alpha e^{\alpha X(t)} \left(\frac{d}{dt} X(t) \right) e^{(1-\alpha)X(t)}, \tag{2.86}$$

we can evaluate $||F^{(1)}(t)||$ as follows:

$$||F^{(1)}(t)|| \leq \left|\left| \int_0^1 d\alpha e^{i\alpha(B+Ct)} iC e^{i(1-\alpha)(B+Ct)} \right|\right| \leq ||C||. \tag{2.87}$$

In a similar way,

$$\begin{aligned} ||F^{(2)}(t)|| &\leq \iint_0^1 \alpha \left|\left| e^{i\beta\alpha(B+Ct)} iC e^{i(1-\beta)\alpha(B+Ct)} iC e^{i(1-\alpha)(B+Ct)} \right|\right| d\alpha d\beta \\ &\quad + \iint_0^1 (1-\alpha) \left|\left| e^{i\alpha(B+Ct)} iC e^{i\beta(1-\alpha)(B+Ct)} iC e^{i(1-\beta)(1-\alpha)(B+Ct)} \right|\right| d\alpha d\beta \\ &\leq ||C||^2 \end{aligned} \tag{2.88}$$

is obtained. By repeating this calculation, $||F^{(n)}(t)|| \leq ||C||^n$ is satisfied. Therefore, if we assume $||C|| \cdot |t| \leq 1$, we get

$$||F(t) - F(0)|| \leq \sum_{n=1}^{\infty} \frac{1}{n!} ||C||^n \cdot |t|^n \leq ||C|| \cdot |t| \sum_{n=1}^{\infty} \frac{1}{n!} \leq 2||C|| \cdot |t|. \tag{2.89}$$

This inequality is satisfied also when $||C|| \cdot |t| \geq 1$, because of

$$||F(t) - F(0)|| = ||e^{i(B+Ct)} - e^{iB}|| \leq ||e^{i(B+Ct)}|| + ||e^{iB}|| \leq 2 \leq 2||C|| \cdot |t|. \tag{2.90}$$

Finally, if we substitute $C = A - B$ and $t = 1$, we obtain the inequality Eq. (2.84). □

Upper bound on the deviation of the effective Hamiltonian

With the usage of Lemma 1, we should evaluate the upper bound of

$$\left|\left| \tilde{V}^n_{\rm FM} - e^{-i\tilde{K}^n_{\rm vV}} \tilde{V}^n_{\rm vV} e^{i\tilde{K}^n_{\rm vV}} \right|\right| = \left|\left| e^{i\tilde{K}^n_{\rm vV}} \tilde{V}^n_{\rm FM} e^{-i\tilde{K}^n_{\rm vV}} - \tilde{V}^n_{\rm vV} \right|\right| \tag{2.91}$$

instead of D_n in Eq. (2.82). Here, we employ the locality and the extensiveness. Let $J(A)$ denote the extensiveness of an operator A, defined by Eq. (1.94). Then, for a series of operators A_i $(i = 1, 2, \ldots, n)$ which are respectively k_i-local and J_i-extensive, the extensiveness of the multi-commutator is bounded from above as follows;

$$\{A_n, A_{n-1}, \ldots, A_1\} \equiv [A_n, [A_{n-1}, \ldots, [A_2, A_1]] \ldots], \tag{2.92}$$

$$J(\{A_n, A_{n-1}, \ldots, A_1\}) \leq J_1 \prod_{i=2}^{n} (2J_i K_i), \tag{2.93}$$

where $K_i = \sum_{m \leq i} k_m$ (See Lemma. 5 in Ref. [28]). With this formula, we obtain the following theorem dictating the bound of Eq. (2.94).

Theorem 2.5.1. (Relation between the two high-frequency expansions)
We consider a Floquet system satisfying all the assumptions in Theorem 2.1.1. Then, for the truncation order n smaller than $n_0 = O((\lambda NT)^{-1})$,

$$\begin{aligned} \left|\left| e^{i\tilde{K}^n_{\rm vV}} \tilde{V}^n_{\rm FM} e^{-i\tilde{K}^n_{\rm vV}} - \tilde{V}^n_{\rm vV} \right|\right| &\leq \frac{L\{4(n+1)\lambda NT\}^{n+2}}{3kNT} \\ &\quad \times \left\{ \frac{j_{{\rm max},n} - (j_{{\rm max,n}})^{n+1}}{1 - j_{{\rm max},n}} + \frac{(j_{{\rm max},n})^{n+1}}{1 - 4(n+1) j_{{\rm max},n} \lambda NT} \right\} \end{aligned} \tag{2.94}$$

is satisfied when the period T is small enough to satisfy $4j_{{\rm max},n}(n+1)\lambda NT < 1$, where the maximal value of the renormalized extensiveness $j_{{\rm max},n}$ is defined as follows:

$$j^{(l)} \equiv \frac{J(\tilde{K}^{(l)}_{\rm vV})}{(\lambda NT)^l JNT(l+1)^{l+1}}, \tag{2.95}$$

$$j_{{\rm max},n} \equiv \max\{j^{(l)} | \, 0 \leq l \leq n\}. \tag{2.96}$$

Proof

By using the Baker-Campbell-Hausdorff formula, we obtain

$$\begin{aligned}\left\|e^{i\tilde{K}^n_{\rm vV}}\tilde{V}^n_{\rm FM}e^{-i\tilde{K}^n_{\rm vV}}-\tilde{V}^n_{\rm vV}\right\| &\le \left\|\sum_{m=0}^{\infty}\frac{i^m}{m!}(\mathrm{ad}_{\tilde{K}^n_{\rm vV}})^m\tilde{V}^n_{\rm FM}-\tilde{V}^n_{\rm FM}\right\| \\ &= \left\|\sum_{m=0}^{\infty}\frac{i^m}{m!}\sum_{l_1,\ldots,l_m=0}^{n}\sum_{l=0}^{n}\{\tilde{K}^{(l_1)}_{\rm vV},\tilde{K}^{(l_2)}_{\rm vV},\ldots,\tilde{K}^{(l_m)}_{\rm vV},\tilde{V}^{(l)}_{\rm FM}\}-\tilde{V}^n_{\rm vV}\right\| \\ &= \left\|\sum_{m=0}^{\infty}\frac{i^m}{m!}\sum_{M=m+1}^{(m+1)(n+1)}\sum_{(l,l_1,\ldots,l_m)\in I_{m,M}}\{\tilde{K}^{(l_1)}_{\rm vV},\tilde{K}^{(l_2)}_{\rm vV},\ldots,\tilde{K}^{(l_m)}_{\rm vV},\tilde{V}^{(l)}_{\rm FM}\}-\tilde{V}^n_{\rm vV}\right\|,\end{aligned} \tag{2.97}$$

where the symbol $\mathrm{ad}_A B$ denotes the commutator $[A,B]$. In the last equality, we recompose the summation so that every term provides the same order M in λNT. Considering that each l-th order term $\tilde{K}^{(l)}_{\rm vV}$ or $\tilde{K}^{(l)}_{\rm FM}$ gives $O((\lambda NT)^{l+1})$ contribution, the set $I_{m,M}$ is defined by

$$I_{m,M}=\left\{(l,l_1,\ldots,l_m)\;\middle|\;\; 0\le l,l_i\le n,\quad \sum_{i=1}^{m}(l_i+1)+(l+1)=M\right\}. \tag{2.98}$$

From the definition of the van Vleck and Floquet-Magnus expansions, low order terms up of the last right hand side in Eq. (2.97) should vanish up to the $(n+1)$-th order, which results in

$$\begin{aligned}[\text{r.h.s of Eq. (2.97)}] &= \left\|\left(\sum_{m=1}^{n}\sum_{M=n+2}^{(m+1)(n+1)}+\sum_{m=n+1}^{\infty}\sum_{M=m+1}^{(m+1)(n+1)}\right)\sum_{(l,l_1,\ldots,l_m)\in I_{m,M}}\frac{i^m}{m!}\{\tilde{K}^{(l_1)}_{\rm vV},\tilde{K}^{(l_2)}_{\rm vV},\ldots,\tilde{K}^{(l_m)}_{\rm vV},\tilde{V}^{(l)}_{\rm FM}\}\right\| \\ &\le \left(\sum_{m=1}^{n}\sum_{M=n+2}^{(m+1)(n+1)}+\sum_{m=n+1}^{\infty}\sum_{M=m+1}^{(m+1)(n+1)}\right)\sum_{(l,l_1,\ldots,l_m)\in I_{m,M}}\frac{1}{m!}\left\|\{\tilde{K}^{(l_1)}_{\rm vV},\tilde{K}^{(l_2)}_{\rm vV},\ldots,\tilde{K}^{(l_m)}_{\rm vV},\tilde{V}^{(l)}_{\rm FM}\}\right\|.\end{aligned} \tag{2.99}$$

Since $\tilde{V}^{(l)}_{\rm FM}$ represents the Floquet-Magnus expansion under the NT-periodic Hamiltonian $\tilde{V}(t)$ with k-locality and J-extensiveness, we can apply Theorem 1.3.2, which gives the following bound on the extensiveness;

$$J(\tilde{V}^{(l)}_{\rm FM})\le\frac{(\lambda NT)^l}{l+1}l!\cdot J. \tag{2.100}$$

Under the k-locality of $\tilde{V}(t)$, the definition of the van Vleck expansion [See Eqs. (2.10)-(2.14)] dictates that the l-th order terms $\tilde{V}^{(l)}_{\rm vV}$ and $\tilde{K}^{(l)}_{\rm vV}$ are at-most $(l+1)k$-local. Thus, by using Eq. (2.93) for the indices $(l,l_1,\ldots,l_m)\in I_{m,M}$, we obtain

$$\begin{aligned}\left\|\{\tilde{K}^{(l_1)}_{\rm vV},\tilde{K}^{(l_2)}_{\rm vV},\ldots,\tilde{K}^{(l_m)}_{\rm vV},\tilde{V}^{(l)}_{\rm FM}\}\right\| &\le LJ(\{\tilde{K}^{(l_1)}_{\rm vV},\tilde{K}^{(l_2)}_{\rm vV},\ldots,\tilde{K}^{(l_m)}_{\rm vV},\tilde{V}^{(l)}_{\rm FM}\}) \\ &\le LJ(\tilde{V}^{(l)}_{\rm FM})\prod_{i=1}^{m}\left[2J(\tilde{K}^{(l_i)}_{\rm vV})k\left\{l+1+\sum_{j=1}^{i}(l_j+1)\right\}\right] \\ &\le LJ\cdot(\lambda NT)^l l!(2k)^m\left[\prod_{i=1}^{m}J(\tilde{K}^{(l_i)}_{\rm vV})\right]\frac{M!}{(M-m)!}.\end{aligned} \tag{2.101}$$

As a dimensionless quantity, we define renormalized extensiveness $j^{(l)}$ by

$$j^{(l)}\equiv\frac{J(\tilde{K}^{(l)}_{\rm vV})}{(\lambda NT)^l JNT(l+1)^{l+1}}, \tag{2.102}$$

which corresponds to Eq. (2.95). As a result, noting that the indices $(l, l_1, \ldots, l_m)$ satisfy $0 \le l \le n$, $0 \le l_i \le n$, and $l + 1 + \sum_i (l_i + 1) = M$, Eq. (1.95) leads to

$$\begin{aligned}
\left|\left|\{\tilde{K}_{\rm vV}^{(l_1)}, \tilde{K}_{\rm vV}^{(l_2)}, \ldots, \tilde{K}_{\rm vV}^{(l_m)}, \tilde{V}_{\rm FM}^{(l)}\}\right|\right| &\le LJ \cdot (\lambda NT)^l l! (2k)^m \left[\prod_{i=1}^{m} (\lambda NT)^{l_i} JNT (l_i+1)^{l_i+1} j^{(l_i)}\right] m!_M C_m \\
&\le LJ \cdot (\lambda NT)^{l+\sum_i l_i + m} (n+1)^l \left[\prod_{i=1}^{m} (n+1)^{l_i+1} j_{\max,n}\right] m! 2^M \\
&\le 2LJ \cdot \{2(n+1)\lambda NT\}^{M-1} (j_{\max,n})^m m!, \qquad (2.103)
\end{aligned}$$

where $j_{\max,n}$ is the maximal value of $\{j^{(l)}\}_{l=0}^n$, defined by Eq. (2.96). By substituting this into Eq. (2.99), when the truncation order n is small enough to satisfy $n < n_0 \le 1/(16\lambda NT)$ and $n < 1/(4j_{\max,n}\lambda NT) - 1$ under the assumption of the sufficiently-small local energy scale $\lambda NT \ll 1$, we arrive at [1]

$$\begin{aligned}
\text{[r.h.s. of Eq. (2.99)]} &\le 2LJ \left(\sum_{m=1}^{n} \sum_{M=n+2}^{(m+1)(n+1)} + \sum_{m=n+1}^{\infty} \sum_{M=m+1}^{(m+1)(n+1)} \right) \sum_{(l,l_1,\ldots,l_m)\in I_{m,M}} \{2(n+1)\lambda NT\}^{M-1} (j_{\max,n})^m \\
&\le 2LJ \left(\sum_{m=1}^{n} \sum_{M=n+2}^{\infty} + \sum_{m=n+1}^{\infty} \sum_{M=m+1}^{\infty} \right) |I_{m,M}| \{2(n+1)\lambda NT\}^{M-1} (j_{\max,n})^m \\
&\le 2LJ \left(\sum_{m=1}^{n} \sum_{M=n+2}^{\infty} + \sum_{m=n+1}^{\infty} \sum_{M=m+1}^{\infty} \right) \{4(n+1)\lambda NT\}^{M-1} (j_{\max,n})^m \\
&= \frac{2LJ\{4(n+1)\lambda NT\}^{n+1}}{1 - 4(n+1)\lambda NT} \left\{ \frac{j_{\max,n} - (j_{\max,n})^{n+1}}{1 - j_{\max,n}} + \frac{(j_{\max,n})^{n+1}}{1 - 4(n+1) j_{\max,n} \lambda NT} \right\} \\
&\le \frac{L}{3kNT} \{4(n+1)\lambda NT\}^{n+2} \left\{ \frac{j_{\max,n} - (j_{\max,n})^{n+1}}{1 - j_{\max,n}} + \frac{(j_{\max,n})^{n+1}}{1 - 4(n+1) j_{\max,n} \lambda NT} \right\}. \qquad (2.104)
\end{aligned}$$

This completes the proof of Theorem 2.5.1. □

As discussed below, the renormalized extensiveness of the kick operator, $j_{\max,n}$, is typically bounded from above by a value of $O(1)$ independent of any parameter other than n, e.g. the system size L. Thus, with Theorem 2.5.1, we obtain the approximate difference between the Floquet operator by the van Vleck expansion and that of the Floquet-Magnus expansion,

$$\begin{aligned}
||e^{-i\tilde{V}_{\rm FM}^n NT} - e^{-i\tilde{K}_{\rm vV}^n} e^{-i\tilde{V}_{\rm vV}^n NT} e^{i\tilde{K}_{\rm vV}^n}|| &\le \frac{2L}{3k} \{4(n+1)\lambda NT\}^{n+2} \\
&\quad \times \left\{ \frac{j_{\max,n} - (j_{\max,n})^{n+1}}{1 - j_{\max,n}} + \frac{(j_{\max,n})^{n+1}}{1 - 4(n+1) j_{\max,n} \lambda NT} \right\} \\
&= O((\lambda NT)^{n+2}) L. \qquad (2.105)
\end{aligned}$$

We hereby employ the upper bounds of $||U_f^N - e^{-i\tilde{V}_{\rm FM}^{n_0} NT}||$ and $||e^{-i\tilde{V}_{\rm FM}^{n_0} NT} - e^{-i\tilde{V}_{\rm FM}^{n} NT}||$, and the triangle inequality Eq. (2.81). Finally, this verifies the validity of the approximation of the coarse-grained Floquet operator by the van Vleck expansion,

$$\left|\left| U_f^N - e^{-i\tilde{K}_{\rm vV}^n} e^{-i\tilde{V}_{\rm vV}^n NT} e^{i\tilde{K}_{\rm vV}^n} \right|\right| = e^{-O(1/(\lambda NT))} L + O((\lambda NT)^{n+2}) L, \qquad (2.106)$$

which reproduces Eq. (2.7) in Theorem 2.1.1.

Renormalized extensiveness of kick operators

Finally, we evaluate the upper bound of $j^{(l)}$ defined by Eq. (2.95), which measures the renormalized extensiveness of the l-th order term of the kick operator $\tilde{K}_{\rm vV}^{(l)}$. This determines the difference

[1] The symbol $|I_{m,M}|$ represents the number of the indices $(l, l_1, \ldots, l_m)$ that satisfy $0 \le l \le n$, $0 \le l_i \le n$, and $l + \sum_i l_i = M - m - 1$. By neglecting the restriction $l, l_i \le n$, it is bounded by

$$|I_{m,M}| \le_{M-1} C_{M-m-1} \le 2^{M-1}.$$

between the van Vleck and the Floquet-Magnus expansions as described by Eq. (2.94) in Theorem 2.5.1 via the maximal value $j_{\max,n} = \max\{j^{(l)}|0 \le l \le n\}$.

Here, we derive the upper bound under the k-locality and the J-extensiveness of the high-frequency drive in the rotating frame $\tilde{V}(t)$, based on the assumptions in Theorem 2.1.1. To this end, we use Eq. (2.93) and the following inequalities;

$$\left|\sum_{m\neq 0}\frac{e^{im\omega t/N}}{m}\right| \leq \pi, \tag{2.107}$$

$$\left|\sum_{m\neq 0}\frac{e^{im\omega t/N}}{m^s}\right| \leq \sum_{m\neq 0}\frac{1}{|m|^s} = 2\zeta(s), \quad \text{for} \quad s\in\mathbb{N}\backslash\{1\}. \tag{2.108}$$

Here, $\zeta(s)$ is the zeta function. The first inequality is derived from the fact that

$$\sum_{m\neq 0}\frac{e^{im\omega t/N}}{m} = \begin{cases} 0 & \text{if} \quad \omega t/N = 0 \mod 2\pi \\ i(\pi-\alpha) & \text{if} \quad \omega t/N = \alpha \ (\in (0,2\pi)) \mod 2\pi. \end{cases} \tag{2.109}$$

We also note that, for a scalar function $f(t)$ bounded by $|f(t)| \le F = \text{Const.}$ and a J_O-extensive operator $O(t)$, the operator $\bar{O} \equiv \int_0^T f(t)O(t)dt$ has extensiveness $J(\bar{O})$ bounded from above as

$$J(\bar{O}) \le FJ_OT, \quad \bar{O} = \int_0^T f(t)O(t)dt. \tag{2.110}$$

This can be derived from the definition of the extensiveness [See Eq. (1.94)] and the inequality

$$\sum_{X:i\in X}||\bar{o}_X|| = \sum_{X:i\in X}\left|\left|\int_0^T f(t)o_X(t)dt\right|\right| \le \int_0^T |f(t)|\sum_{X:i\in X}||o_X(t)||dt \le FJ_OT, \tag{2.111}$$

for each site $i\in\Lambda$, where $O(t)$ and $\bar{O}$ are decomposed by their supports $X\subset\Lambda$ as $O(t) = \sum_{X\subset\Lambda}o_X(t)$, and $\bar{O} = \sum_{X\subset\Lambda}\bar{o}_X$.

For the lowest order, the kick operator Eq. (2.12) is rewritten in the following form,

$$\tilde{K}^{(0)}_{\rm vV} = \frac{i}{\omega T}\int_0^{NT}\left(\sum_{m\neq 0}\frac{e^{im\omega t/N}}{m}\right)\tilde{V}(t)dt. \tag{2.112}$$

By using a series of the above inequalities, we obtain

$$J(\tilde{K}^{(0)}_{\rm vV}) \le \frac{1}{\omega T}\int_0^{NT}\left|\sum_{m\neq 0}\frac{e^{im\omega t/N}}{m}\right|Jdt \le \frac{1}{2}JNT, \tag{2.113}$$

and hence the renormalized extensiveness by Eq. (2.95) satisfies

$$j^{(0)} = \frac{J(\tilde{K}^{(0)}_{\rm vV})}{JNT} \le \frac{1}{2}. \tag{2.114}$$

We can also discuss the first order term $\tilde{K}^{(1)}_{\rm vV}$ given by Eq. (2.13) as follows,

$$\begin{aligned}\tilde{K}^{(1)}_{\rm vV} &= \frac{-i}{2\omega^2T^2}\iint_0^{NT}dt_1dt_2\left(\sum_{m\neq 0}\frac{e^{im\omega t_1/N}}{m^2}\right)[\tilde{V}(t_1),\tilde{V}(t_2)] \\ &\quad + \frac{-i}{2\omega^2T^2}\iint_0^{NT}dt_1dt_2\left(\sum_{m\neq 0}\frac{e^{im\omega(t_1+t_2)/N}}{m}\right)\left(\sum_{n\neq 0}\frac{e^{-in\omega t_2/N}}{n}\right)[\tilde{V}(t_1),\tilde{V}(t_2)].\end{aligned} \tag{2.115}$$

This gives the upper bound of $J(\tilde{K}_{\rm vV}^{(1)})$, which can be described by

$$\begin{aligned} J(\tilde{K}_{\rm vV}^{(1)}) &\leq \frac{1}{2(\omega t)^2}\pi^2 J([\tilde{V}(t_1),\tilde{V}(t_2)])\cdot(NT)^2 + \frac{1}{2(\omega t)^2}2\zeta(2)J([\tilde{V}(t_1),\tilde{V}(t_2)])\cdot(NT)^2 \\ &\leq \frac{1}{3}(\lambda NT)(JNT). \end{aligned} \tag{2.116}$$

This inequality results in the renormalized extensiveness $j^{(1)} \leq 1/12$. In a similar way, by using $\zeta(3) = \pi^3/25.79... < \pi^3/24$, we can obtain the second order results as $J(\tilde{K}_{\rm vV}^{(2)}) \leq 47(\lambda NT)^2 JNT/96$ and $j^{(2)} \leq 47/2592$. To summarize these results, the maximal value $j_{{\rm max},n}$ appearing in Theorem 2.5.1 has the following bounds for low orders;

$$j_{\rm max,0} \leq \frac{1}{2}, \quad j_{\rm max,1} \leq \frac{1}{2}, \quad j_{\rm max,2} \leq \frac{1}{2}. \tag{2.117}$$

In general, the l-th order term of the kick operator $\tilde{K}_{\rm vV}^{(l)}$ can be decomposed into the inverse Fourier transformation of $1/m^s$ and the $(l+1)$-tuple commutators of $\tilde{V}(t_i)$ like Eqs. (2.112) and (2.115). Thus, by using Eqs. (2.93), (2.107), (2.108), and (2.110), we can obtain the upper bounds of $J(\tilde{K}_{\rm vV}^{(l)})$ and thereby $j_{{\rm max},n}$ for any order in principle. We note that the bounds obtained in this way are universal, which depend only on the locality and the extensiveness but not on the detail of models.

Chapter 3

Emergent non-Markovianity in dissipative Floquet systems

In this chapter, we focus on dissipative Floquet many-body systems, affected by the coupling between the system and the external bath. Since Floquet-ETH predicts heating to trivial infinite-temperature states in generic closed Floquet many-body systems, dissipative Floquet many-body systems are expected to host various nontrivial physics with overcoming the heating problem. While this expectation matches the intuition that dissipation suppresses heating caused by energy absorption from periodic drives, it is too difficult to find such intriguing phenomena because of the competition of periodic drives, dissipation, and interactions.

Here, we consider generic dissipative Floquet many-body systems in the high-frequency regime, where the local energy scale of both the Hamiltonian and the dissipation is much smaller than the frequency. In the high-frequency regime, we can analytically understand them with a perturbation theory in the same manner of the high-frequency expansion in closed Floquet systems. They are important also in terms of the correspondence of closed Floquet systems with static systems. In the closed cases, Floquet systems in the high-frequency regime cannot host phenomena inherent in nonequilibrium, but such a correspondence is nontrivial in dissipative cases. We clarify that dissipative Floquet many-body systems generally break this correspondence with static counterparts, interpreted as emergent non-Markovianity in stroboscopic dynamics. This gives the possibility of unique phenomena even in the high-frequency regime.

3.1 Dissipative Floquet systems

3.1.1 Setups

We first introduce how dissipative Floquet systems are described. Throughout this chapter, we assume Markovianity, dictating that the state at time t, $\rho(t)$, is determined by that just before infinitesimal time, $\rho(t-\delta t)$. Combining with the time periodicity, dissipative Floquet systems under Markovianity obeys Floquet-Lindblad equation as follows:

$$\partial_t \rho(t) = \mathcal{L}(t)\rho(t), \quad \mathcal{L}(t) = \mathcal{L}(t+T), \tag{3.1}$$

$$\mathcal{L}(t)\rho = -i[H(t),\rho] + \sum_i L_i(t)\rho L_i(t)^\dagger - \frac{1}{2}\{L_i(t)^\dagger L_i(t),\rho\}. \tag{3.2}$$

Since this is a linear differential equation in a state $\rho(t)$, we can apply Floquet theory as well as closed Floquet systems with replacing $|\psi(t)\rangle \to \rho(t)$ and $H(t) \to i\mathcal{L}(t)$.

Description of dissipative Floquet systems by Floquet-Lindblad equation is valid when the relaxation time of the external bath is much smaller than the time scale of changes in the system and the periodic drive. Then, the bath forgets the history of $\{\rho(t)\}_t$ (referred to as no memory time), resulting in Markovianity and Floquet-Lindblad equation. While Floquet-Lindblad equation is derived only from the time-periodicity, Markovianity and the CPTP (complete-positivity and trace-preserving) property [130, 131, 132, 133], it can be derived also by considering the Hamiltonian $H_{\rm tot}(t) = H(t) + H_{\rm bath}(t) + H_{\rm c}(t)$ including the bath terms and the coupling terms and applying

some approximations such as Markov and the rotating-wave approximations [132, 133, 134, 135, 136]. Experimentally, artificial quantum systems such as cold atoms and cavity-atom systems in approximate vacuum are expected to provide ideal platforms for dissipative Floquet systems under Markovianity [137, 138].

Dissipative Floquet systems with Floquet-Lindblad formalism have been contributed to various nonequilibrium phenomena, such as nonequilibrium steady states [139, 140], heat engines [141, 142], and discrete time crystals [143, 144, 145, 146, 147, 148]. However, despite the applicability of Floquet theory, investigation of dissipative Floquet many-body systems has been quite restricted when compared to closed systems. While a state $|\psi\rangle$ is given in a d^L-dimensional Hilbert space, a state ρ for dissipative systems is defined in a d^{2L}-dimensional system, giving the complexity of dissipative systems. Non-unitarity of the time evolution is also the difficulty of dissipative systems. Thus, exploring universal behaviors in dissipative Floquet many-body systems is difficult due to the competition of dissipation, periodic drives, and interactions, but important to seek for nontrivial nonequilibrium phenomena that overcome the heating problem.

3.1.2 Dissipative Floquet systems in the high-frequency regime

As Floquet theory is applicable also to dissipative cases, generic dissipative Floquet systems can be analyzed by the Floquet operator $\mathcal{U}_f$ or the effective Lindbladian $\mathcal{L}_{\rm eff}$ defined by

$$\mathcal{U}_f = \mathcal{T}\exp\left(\int_0^T \mathcal{L}(t)dt\right), \tag{3.3}$$

$$\mathcal{L}_{\rm eff} = \frac{1}{T}\log\mathcal{U}_f. \tag{3.4}$$

They determine the stroboscopic dynamics as well as closed cases:

$$\rho(mT) = (\mathcal{U}_f)^m\rho(0) = e^{\mathcal{L}_{\rm eff}mT}\rho(0), \quad m = 0, 1, 2, \dots. \tag{3.5}$$

In general, it is difficult to obtain the Floquet operator or the effective Lindbladian due to the larger dimension compared to closed cases in addition to the time-ordered product and the logarithm of operators.

Hereafter, we focus on dissipative Floquet systems in the high-frequency regime for the following two reasons. The first reason is the availability of the high-frequency expansion as well as closed systems. We can discuss generic dissipative Floquet systems in a unified way with the perturbation theory in $||\mathcal{L}(t)||/\omega$. Note that the high-frequency expansions in Chapter 1 are derived only with the fact that $H(t)$ is linear and time-periodic but not using the hermiticity, and hence those for dissipative systems are derived in the same manner. The Floquet-Magnus expansion $\mathcal{L}^n_{\rm FM}$, defined by

$$\mathcal{L}^n_{\rm FM} = \sum_{i=0}^{n}\mathcal{L}^{(i)}_{\rm FM}, \quad \mathcal{L}^{(0)}_{\rm FM} = \frac{1}{T}\int_0^T \mathcal{L}(t)dt, \tag{3.6}$$

$$\mathcal{L}^{(1)}_{\rm FM} = \frac{1}{2T}\int_0^T dt_1\int_0^{t_1} dt_2[\mathcal{L}(t_1), \mathcal{L}(t_2)], \tag{3.7}$$

$$\mathcal{L}^{(2)}_{\rm FM} = \frac{1}{6T}\int_0^T dt_1\int_0^{t_1} dt_2\int_0^{t_2} dt_3\left([\mathcal{L}(t_1), [\mathcal{L}(t_2), \mathcal{L}(t_3)]] + [\mathcal{L}(t_3), [\mathcal{L}(t_2), \mathcal{L}(t_1)]]\right), \tag{3.8}$$

approximately provides the effective Lindbladian $\mathcal{L}_{\rm eff}$ up to the order of $(||\mathcal{L}(t)||/\omega)^n$. Generic m-th order term $\mathcal{L}^{(m)}_{\rm FM}$ is obtained by replacing $H(t) \to i\mathcal{L}(t)$ and $H^{(m)}_{\rm FM} \to i\mathcal{L}^{(m)}_{\rm FM}$ in the Floquet-Magnus expansion for closed systems [See Eqs. (1.27)-(1.29)]. As well as closed cases, the high-frequency expansion enables to analyze Floquet systems as static systems with capturing the time-dependency via higher-order terms $\mathcal{L}^{(m)}_{\rm FM}$ $(m \geq 1)$. In fact, Ref. [149] confirms that the stroboscopic dynamics of local observables is well reproduced by $\mathcal{L}^n_{\rm FM}$ in the high-frequency regime. Refs. [136, 150] consider a wide class of dissipative Floquet systems with time-independent dissipation, and clarify generic steady states up to the first order with the usage of the high-frequency expansion.

The second reason why the high-frequency regime of dissipative Floquet systems is focused on lies in the correspondence of closed Floquet systems with closed static systems, which is directly

related to the aim of this chapter. In closed cases, as discussed in the last of Section 1.3.4, Floquet systems in the high-frequency regime always have counterparts in closed static systems. This is because they are approximately described by the Floquet-Magnus expansion $H^n_{\rm FM}$, which is a static local Hamiltonian. Then, there appears a natural but important question for dissipative cases:

Do dissipative Floquet systems in the high-frequency regime have counterparts in dissipative static systems ?

Tackling this problem will lead to comprehension on what kind of nontrivial steady states unique to Floquet systems is possible.

Aim of this chapter

We aim to resolve the above problem, the correspondence of dissipative Floquet systems in the high-frequency regime with static counterparts. Let us discuss the detail of the problem. We consider dissipative systems under Markovianity. In static cases, a state $\rho(t)$ obeys a time-independent Lindblad equation,

$$\partial_t \rho(t) = \mathcal{L}\rho(t), \tag{3.9}$$

$$\mathcal{L}\rho = -i[H,\rho] + \sum_i L_i \rho L_i^\dagger - \frac{1}{2}\{L_i^\dagger L_i, \rho\}, \tag{3.10}$$

with a Hermitian operator H. The form of $\mathcal{L}$, called a Liouvillian, is derived from the requirement that the time evolution operator $e^{\mathcal{L}t}$ becomes a CPTP map for any $t \geq 0$, and essential to describe dissipative static systems under Markovianity [131]. We refer to it as as Liouvillianity of $\mathcal{L}$, that (or whether) $\mathcal{L}$ is a Liouvillian given by Eq. (3.10). In Floquet cases, their dynamics dominated by a time-periodic Liouvillian $\mathcal{L}(t)$ is approximately described by the static operator $\mathcal{L}^n_{\rm FM}$, given by the Floquet-Magnus expansion. Thus, the problem of interest is interpreted as:

Is the Floquet-Magnus expansion $\mathcal{L}^n_{\rm FM}$, which approximately describes dissipative Floquet systems in the high-frequency regime, a Liouvillian ?

In other words, we analyze Liouvillianity of the Floquet-Magnus expansion $\mathcal{L}^n_{\rm FM}$ for generic systems throughout this chapter, and thereby we aim to clarify whether or not dissipative Floquet systems in the high-frequency regime have static counterparts described by a static Liouvillian.

3.2 Liouvillianity behavior in noninteracting and interacting models

Hereafter, we consider Liouvillianity of the Floquet-Magnus expansion to clarify the correspondence of dissipative Floquet systems with static systems. To this goal we begin with introducing some mathematical tools to judge Liouvillianity in Section 3.2.1. With these tools, we clarify that the behavior of Liovillianity depends on the presence of interactions. Thus, we discuss noninteracting cases and interacting cases respectively in Sections 3.2.2 and 3.2.3.

3.2.1 Method for judging Liouvillianity

We first introduce the Frobenius basis and the doubled Hilbert space representation. After that, we discuss how to judge Liouvillianity. We also derive generic properties of Liouvillianity of each order term in the Floquet-Magnus expansion.

Frobenius basis.—We denote a set of $d \times d$ matrices by $\mathbb{M}_d$ and assume a state $\rho \in \mathbb{M}_d$. We define the Frobenius inner product $\langle A, B\rangle_{\rm F}$ and the Frobenius norm $||A||_{\rm F}$ by

$$\langle A, B\rangle_{\rm F} \equiv {\rm Tr}[A^\dagger B], \quad ||A||_{\rm F} \equiv \sqrt{\langle A, A\rangle_{\rm F}}, \tag{3.11}$$

for $A, B \in \mathbb{M}_d$. The Frobenius basis $\{F_j \in \mathbb{M}_d\}_{j=1}^{d^2}$ is a complete orthonormal set (CONS) for $\mathbb{M}_d$ based on the Frobenius inner product and the Frobenius norm, satisfying

$$\langle F_j, F_k\rangle_{\rm F} = \delta_{jk}, \quad {}^\forall j,k = 1,2,\dots,d^2, \tag{3.12}$$

$$F_{d^2} = I_d/\sqrt{d}. \tag{3.13}$$

Here, I_d denotes the d-dimensional identity matrix. Using the condition $\langle F_j, F_{d^2}\rangle_{\mathrm{F}} = \delta_{jd^2}$, we immediately obtain

$$\mathrm{Tr}[F_j] = 0, \quad j = 1, 2, \ldots, d^2 - 1. \tag{3.14}$$

For the simplest case with $d = 2$, we can choose

$$F_1 = \sigma^x/\sqrt{2}, \quad F_2 = \sigma^y/\sqrt{2}, \quad F_3 = \sigma^z/\sqrt{2}, \quad F_4 = I_2/\sqrt{2} \tag{3.15}$$

as the Frobenius basis.

Doubled Hilbert space representation.—The doubled Hilbert space representation enables to represent linear operators on $\mathbb{M}_d$ by a matrix by associating a state $\rho \in \mathbb{M}_d$ to a d^2-dimensional vector [151, 152]. Let $\{|s\rangle\}_{s=1}^d$ denote a basis for the d-dimensional Hilbert space, and then a state ρ is given by $\rho = \sum_{s,s'} \rho_{ss'} |s\rangle \langle s'|$. We can designate the state ρ by the d^2-dimensional vector $|\rho) = \sum_{ss'} \rho_{ss'} |s\rangle \otimes |s'\rangle$ by the one-to-one correspondence $\rho \leftrightarrow |\rho)$. The representation of the state by $|\rho)$ is called the doubled Hilbert space representation, since $|\rho)$ is defined on a system twice as large as the original system. In the doubled system for $|\rho)$, the system designated by $|s\rangle$ (or $|s'\rangle$) is called a real system (or a fictitious system). When considering linear operators on $\mathbb{M}_d$, they should be written by a d^2-dimensional matrix. In fact, an action $A\rho B$ ($A, B \in \mathbb{M}_d$) is written as $A \otimes B^{\mathrm{T}} \in \mathbb{M}_{d^2}$ due to the following correspondence:

$$A\rho B \leftrightarrow (A \otimes B^{\mathrm{T}})\,|\rho)\,, \quad A, B \in \mathbb{M}_d. \tag{3.16}$$

For instance, a Liouvillian $\mathcal{L}$ given by Eq. (3.10) is given by the d^2-dimensional matrix

$$\mathcal{L} = -i(H \otimes I - I \otimes H^{\mathrm{T}}) + \sum_i \left[L_i \otimes L_i^* - \frac{1}{2}(L_i^\dagger L_i \otimes I + I \otimes L_i^{\mathrm{T}} L_i^*) \right] \tag{3.17}$$

in the doubled Hilbert space representation, where we simply write the correspondence by the equality hereafter.

Judgment of Liouvillianity.—Now, let us discuss how to judge Liouvillianity of the Floquet-Magnus expansion, described by a d^2-dimensional matrix in the doubled Hilbert space representation. By expanding the Lindblad operators with the Frobenius basis as $L_i = \sum_{j=1}^{d^2-1} c_{ij} F_j$ with $c_{ij} \in \mathbb{C}$ (Note that $F_{d^2} \propto I_d$ gives no contribution), we obtain

$$\mathcal{L} = -i(H \otimes I - I \otimes H^{\mathrm{T}}) + \sum_{j,k=1}^{d^2-1} a_{jk} \left[F_j \otimes F_k^* - \frac{1}{2}(F_k^\dagger F_j \otimes I + I \otimes F_j^{\mathrm{T}} F_k^*) \right] \tag{3.18}$$

from Eq. (3.17), where $a_{jk} \equiv \sum_i c_{ij} c_{ik}^*$ ($j, k = 1, 2, \ldots, d^2 - 1$) gives a $(d^2 - 1)$-dimensional positive-semidefinite (all the eigenvalues are non-negative) matrix with the hermiticity $a_{jk} = a_{kj}^*$. Conversely, when a linear operator on $\mathbb{M}_d$ is given in the form of Eq. (3.18) with a hermitian positive-semidefinite matrix $[a_{jk}]_{j,k=1}^{d^2-1}$, we can obtain a Liouvillian of Eq. (3.17) by the spectral decomposition $a_{jk} \equiv \sum_i c_{ij} c_{ik}^*$. Thus, we obtain the following condition: $\mathcal{L}$ is a Liouvillian if and only if $\mathcal{L}$ has the form of Eq. (3.18) with a hermitian matrix $H \in \mathbb{M}_d$ and a hermitian positive-semidefinite matrix $[a_{jk}]_{j,k=1}^{d^2-1} \in \mathbb{M}_{d^2-1}$.

Let us turn to how to judge whether the Floquet-Magnus expansion $\mathcal{L}_{\mathrm{FM}}^n$ is a Liouvillian. While it is difficult to know whether generic matrices in $\mathbb{M}_{d^2}$ can be decomposed in the form of Eq. (3.18), we can do that in the case of the Floquet-Magnus expansion by the following theorem.

Theorem 3.2.1. (Form of the Floquet-Magnus expansion)
Each m-th order term of the Floquet-Magnus expansion, $\mathcal{L}_{\mathrm{FM}}^{(m)}$, is always written in the form of

$$\mathcal{L}_{\mathrm{FM}}^{(m)} = -i(H^{(m)} \otimes I - I \otimes (H^{(m)})^{\mathrm{T}}) + \sum_{j,k=1}^{d^2-1} a_{jk}^{(m)} \left[F_j \otimes F_k^* - \frac{1}{2}(F_k^\dagger F_j \otimes I + I \otimes F_j^{\mathrm{T}} F_k^*) \right] \tag{3.19}$$

where $H^{(m)} \in \mathbb{M}_d$ and $[a_{jk}^{(m)}]_{j,k=1}^{d^2-1} \in \mathbb{M}_{d^2-1}$ are hermitian. The n-th order Floquet-Magnus expansion, $\mathcal{L}_{\mathrm{FM}}^{n} = \sum_{m=0}^{n} \mathcal{L}_{\mathrm{FM}}^{(m)}$, is also written in the form of

$$\mathcal{L}_{\mathrm{FM}}^{n} = -i(H^{n} \otimes I - I \otimes (H^{n})^{\mathrm{T}}) + \sum_{j,k=1}^{d^2-1} a_{jk}^{n} \left[F_j \otimes F_k^* - \frac{1}{2}(F_k^\dagger F_j \otimes I + I \otimes F_j^{\mathrm{T}} F_k^*) \right] \tag{3.20}$$

where $H^{n} \in \mathbb{M}_d$ and $[a_{jk}^{n}]_{j,k=1}^{d^2-1} \in \mathbb{M}_{d^2-1}$ are hermitian.

We can derive Eq. (3.20) by using the fact that the time-periodic Liouvillian $\mathcal{L}(t)$ is given by the form of Eq. (3.2). Since the derivation is done in a similar way of Ref. [153], we provide it in Appendix for this chapter (See Section 3.5). Equation (3.20) soon follows from Eq. (3.19) by giving $H^n = \sum_{m=0}^{n} H^{(m)}$ and $a_{jk}^{n} = \sum_{m=0}^{n} a_{jk}^{(m)}$.

By multiplying $F_j^\dagger \otimes F_k^{\mathrm{T}}$ $(j,k \neq d^2)$ to Eq. (3.20) from the left and taking its trace, we can pick up the matrix elements as

$$a_{jk}^{n} = \mathrm{Tr}[(F_j^\dagger \otimes F_k^{\mathrm{T}}) \mathcal{L}_{\mathrm{FM}}^{n}], \tag{3.21}$$

where we use the orthonormality of the Frobenius basis Eqs. (3.12) and (3.13). While the form of Eq. (3.20) is the same as that of a Liouvillian, Eq. (3.18), we note that the positive-semidefiniteness of $[a_{jk}^{n}]$ is not ensured here. In other words, we obtain the necessary and sufficient condition for the Floquet-Magnus expansion being a Liouvillian as the following theorem says [154].

Theorem 3.2.2. (Judging Liouvillianity of the Floquet-Magnus expansion)
For the Floquet-Magnus expansion $\mathcal{L}_{\mathrm{FM}}^{n}$, the following relation is satisfied:

$$\mathcal{L}_{\mathrm{FM}}^{n} \text{ is a Liouvillian } \Leftrightarrow [a_{jk}^{n}]_{j,k=1}^{d^2-1} \in \mathbb{M}_{d^2-1} \text{ is positive-semidefinite,} \tag{3.22}$$

where the hermitian matrix $[a_{jk}^{n}]_{j,k=1}^{d^2-1}$ is given by

$$a_{jk}^{n} = \mathrm{Tr}[(F_j^\dagger \otimes F_k^{\mathrm{T}}) \mathcal{L}_{\mathrm{FM}}^{n}]. \tag{3.23}$$

Thus, in order to judge Liouvillianity of the Floquet-Magnus expansion, we should confirm that all the eigenvalues of the matrix $[a_{jk}^{n}]_{j,k=1}^{d^2-1}$ is non-negative. When we consider an L-site system having f degrees of freedom at each site, the dimension of $[a_{jk}^{n}]$ exponentially grows with the system size as $d^2 - 1 = f^{2L} - 1$. It is nontrivial that we can rigorously evaluate Liouvillianity for generic systems including interacting cases. In fact, Ref. [154], which provides the way of judging Liouvillianity without specifying the usage of the Frobenius basis, gives an analysis on Liouvillianity of the Floquet-Magnus expansion, but it is limited to noninteracting cases, essentially equivalent to the case $L = 1$. Here, we aim to understand the behavior of Liouvillianity for generic Floquet systems both in noninteracting cases and interacting cases.

Generic properties about Liouvillianity.—Before discussing Liouvillianity of the Floquet-Magnus expansion, we derive a generic property of each m-th order term and reconsider the structure of the problem. As each m-th order term $\mathcal{L}_{\mathrm{FM}}^{(m)}$ is given by Eq. (3.19), we can diagnose its Liouvillianity by

$$\mathcal{L}_{\mathrm{FM}}^{(m)} \text{ is a Liouvillian } \Leftrightarrow [a_{jk}^{(m)}]_{j,k=1}^{d^2-1} \in \mathbb{M}_{d^2-1} \text{ is positive-semidefinite,} \tag{3.24}$$

with $a_{jk}^{(m)} = \mathrm{Tr}[(F_j^\dagger \otimes F_k^{\mathrm{T}})\mathcal{L}_{\mathrm{FM}}^{(m)}]$, as well as the Floquet-Magnus expansion. Then, we derive the following theorem on Liouvillianity of each m-th order term.

Theorem 3.2.3. (Liouvillianity of each order term)
Each m-th order term of the Floquet-Magnus expansion satisfies the following proposition:

(a) $\mathcal{L}_{\mathrm{FM}}^{(0)}$ $(= \mathcal{L}_f^0)$ is always a Liouvillian.

(b) $\mathcal{L}_{\mathrm{FM}}^{(m)}$ $(m \geq 1)$ is a Liouvillian if and only if

$$[a_{jk}^{(m)}] = \left[\mathrm{Tr}[(F_j^\dagger \otimes F_k^{\mathrm{T}})\,\mathcal{L}_f^{(m)}]\right] = O_{d^2-1}, \tag{3.25}$$

where O_d $(\in \mathbb{M}_d)$ represents a zero matrix with the size d.

Proof

From Eq. (3.2), the time-periodic Liouvillian $\mathcal{L}(t)$ is also written in the form of

$$\mathcal{L}(t) = -i(H(t)\otimes I - I \otimes H(t)^{\mathrm{T}}) + \sum_{j,k=1}^{d^2-1} a_{jk}(t)\left[F_j \otimes F_k^* - \frac{1}{2}(F_k^\dagger F_j \otimes I + I \otimes F_j^{\mathrm{T}} F_k^*)\right] \tag{3.26}$$

where the T-periodic matrices $H(t) \in \mathbb{M}_d$ and $[a_{jk}(t)] \in \mathbb{M}_{d^2-1}$ are hermitian. Since the zeroth order term is given by the time-average of $\mathcal{L}(t)$, we obtain

$$a_{jk}^{(0)} = \frac{1}{T}\int_0^T a_{jk}(t)dt. \tag{3.27}$$

The hermitian matrix $[a_{jk}^{(0)}]$ becomes positive-semidefinite since $[a_{jk}(t)]$ is positive-semidefinite, and hence $\mathcal{L}_{\mathrm{FM}}^{(0)}$ is always a Liouvillian. On the other hand, using the fact that each order term $\mathcal{L}_{\mathrm{FM}}^{(m)}$ is composed of m-tuple comutators, each m-th order term is traceless, $\mathrm{Tr}\left[\mathcal{L}_{\mathrm{FM}}^{(m)}\right] = 0$, for $m \geq 1$. We can calculate the trace in another way using Eq. (3.19), and this results in

$$\mathrm{Tr}\left[\mathcal{L}_{\mathrm{FM}}^{(m)}\right] = -\frac{1}{2}\sum_{j,k=1}^{d^2-1} a_{jk}^{(m)}(\mathrm{Tr}[F_j^\dagger F_k \otimes I] + \mathrm{Tr}[I \otimes F_j^{\mathrm{T}} F_k^*]) = -d\cdot\sum_{j=1}^{d^2-1} a_{jj}^{(n)} = -d\cdot\mathrm{Tr}\left([a_{jk}^{(m)}]\right). \tag{3.28}$$

Therefore, $[a_{jk}^{(m)}]$ is also traceless, and hence the summation of the eigenvalues of $[a_{jk}^{(m)}]$ is zero. Since all of the eigenvalues of hermitian positive-semidefinite matrices cannot be negative, $[a_{jk}^{(m)}]$ is positive-semidefinite if and only if $[a_{jk}^{(m)}] = O$. Using the condition for Liouvillianity, we complete the proof of the theorem. □

This theorem says that any higher order term $\mathcal{L}_{\mathrm{FM}}^{(m)}$ cannot be a Liouvllian except for special cases where $\mathcal{L}_{\mathrm{FM}}^{(m)}$ gives no dissipation. Since we use the fact that the zeroth-order term is given by the time-average and that higher-order terms are composed of commutators, this result is also valid for the van Vleck expansion and the Schrieffer-Wolff expansion other than the Floquet-Magnus expansion.

We note that this theorem brings an essential difference from closed cases to the problem of interest. In closed cases, any order term of the Floquet-Magnus expansion $H_{\mathrm{FM}}^{(m)}$, given by Eq. (1.28) is always a Hamiltonian (i.e. a hermitian operator), thereby making the Floquet-Magnus expansion $H_{\mathrm{FM}}^n = \sum_{m=0}^n H_{\mathrm{FM}}^{(m)}$ a Hamiltonian. On the other hand, in dissipative cases, in the Floquet-Magnus expansion $\mathcal{L}_{\mathrm{FM}}^n = \sum_{m=0}^n \mathcal{L}_{\mathrm{FM}}^{(m)}$, only the zeroth-order becomes a Liouvillian while the other terms cannot be Liouvillians in general. That makes Liouvillianity of the Floquet-Magnus expansion nontrivial in contrast to closed systems.

3.2.2 Liouvillianity in noninteracting models

To understand how Liouvillianity of the Floquet-Magnus expansion behaves, we begin with noninteracting cases. For simplicity, we focus on dissipative systems under a binary drive, described by

$$\mathcal{L}(t) = \begin{cases} \mathcal{L}_1 & (0 \le t < \tau) \\ \mathcal{L}_2 & (\tau \le t < 2\tau = T), \end{cases} \tag{3.29}$$

and then the Floquet operator is given by $\mathcal{U}_{\rm eff} = \exp(\mathcal{L}_2\tau)\exp(\mathcal{L}_1\tau) \equiv \exp(\mathcal{L}_{\rm eff}\cdot 2\tau)$. By using the Baker-Campbell-Hausdorff formula, we can directly calculate the Floquet-Magnus expansion as follows:

$$\mathcal{L}^{(0)}_{\rm FM} = \frac{1}{2}(\mathcal{L}_1+\mathcal{L}_2), \quad \mathcal{L}^{(1)}_{\rm FM} = \frac{\tau}{4}[\mathcal{L}_2,\mathcal{L}_1], \tag{3.30}$$

$$\mathcal{L}^{(2)}_{\rm FM} = \frac{\tau^2}{24}[\mathcal{L}_2-\mathcal{L}_1,[\mathcal{L}_2,\mathcal{L}_1]], \quad \mathcal{L}^{(3)}_{\rm FM} = \frac{\tau^3}{48}[\mathcal{L}_1,[\mathcal{L}_2,[\mathcal{L}_1,\mathcal{L}_2]]], \quad \ldots \tag{3.31}$$

Since noninteracting cases can be captured by models with single site, we consider a single-spin system with $S = 1/2$. We provide two models and show that they have different behaviors of Liouvillianity; one always shows breakdown of Liouvillianity of $\mathcal{L}^n_{\rm FM}$ while the other preserves Liouvillianity of $\mathcal{L}^n_{\rm FM}$ in a finite parameter region.

Noninteracting model showing Liouvillianity breaking.—We first consider a single-spin system with $S = 1/2$, described by the time-periodic Hamiltonian

$$\mathcal{L}_A(t)\rho = \begin{cases} -ih[\sigma^z,\rho] & (0 \le t < \tau) \\ \gamma_1(\sigma^x\rho\sigma^x-\rho) & (\tau \le t < 2\tau). \end{cases} \tag{3.32}$$

Here, $h \in \mathbb{R}$ represents the magnetic field in the z-direction, and $\gamma_1 > 0$ is the dephasing in the x-direction. Assuming the high-frequency regime indicates $h\tau, \gamma_1\tau \ll 1$. By using the formula Eqs. (3.30)-(3.31), we obtain the Floquet-Magnus expansion in the doubled Hilbert representation as follows:

$$\begin{aligned} \mathcal{L}^2_{\rm FM} = & -\frac{ih}{2}\left\{1+\frac{(\gamma_1\tau)^2}{3}\right\}(\sigma^z\otimes I - I\otimes\sigma^z) + \frac{\gamma_1}{2}(\sigma^x\otimes\sigma^x - I\otimes I) \\ & -\frac{\gamma_1 h\tau}{2}(\sigma^y\otimes\sigma^x - \sigma^x\otimes\sigma^y) - \frac{\gamma_1(h\tau)^2}{3}(\sigma^x\otimes\sigma^x + \sigma^y\otimes\sigma^y). \end{aligned} \tag{3.33}$$

Remembering that the Frobenius basis for the dimension $d = 2$ is given by Eq. (3.15), we can calculate the matrix $a^2_{jk} = {\rm Tr}[(F^\dagger_j\otimes F^{\rm T}_k)\mathcal{L}^2_{\rm FM}]$ based on Eq. (3.23). This results in

$$[a^2_{jk}] = \gamma_1 \begin{pmatrix} 1-\alpha^{(2)}_A & \alpha^{(1)}_A & 0 \\ \alpha^{(1)}_A & \alpha^{(2)}_A & 0 \\ 0 & 0 & 0 \end{pmatrix}, \tag{3.34}$$

where $\alpha^{(1)}_A = -h\tau$ and $\alpha^{(2)}_A = 2(h\tau)^2/3$ are the first- and the second-order contributions. Substituting $\alpha^{(1)}_A = \alpha^{(2)}_A = 0$ ($\alpha^{(2)}_A = 0$) into Eq. (3.34) reproduces the matrix $[a^0_{jk}]$ ($[a^1_{jk}]$).

Let us evaluate Liouvillianity of the Floquet-Magnus expansion $\mathcal{L}^n_{\rm FM}$, or equivalently, judge the positive-semidefiniteness of $[a^n_{jk}]$ based on Theorem 3.2.2. The zeroth-order $\mathcal{L}^0_{\rm FM}$ is always a Liouvillian since $[a^0_{jk}]$ is positive-semidefinite. This result is rather trivial due to Theorem 3.2.3. On the other hand, for the first-order, the matrix $[a^1_{jk}]$ always has a negative eigenvalue $(1-\sqrt{1+4(h\tau)^2})\gamma_1/2 \simeq -\gamma_1(h\tau)^2 = O((h\tau)^2)$. Thus, the first-order expansion $\mathcal{L}^1_{\rm FM}$ cannot be a Liouvillian regardless of parameters $h, \gamma_1 \neq 0$, which we refer to as Liouvillianity breaking. In a similar manner, for the second-order, the matrix $[a^2_{jk}]$ always has a negative eigenvalue $(1-\sqrt{1+4(h\tau)^2/3+16(h\tau)^4/9})\gamma_1/2 \simeq -\gamma_1(h\tau)^2/3 = O((h\tau)^2)$. As a result, $\mathcal{L}^2_f$ always breaks Liouvillianity.

To summarize, this noninteracting model always shows Liouvillianity breaking of the Floquet-Magnus expansion when we consider higher-order terms coming from the time-dependency of $\mathcal{L}(t)$. This originates from the inevitable negative eigenvalues of $[a^n_{jk}]$. We note that, for the

first-order in this model, it is difficult to observe the effects of Liouvillianity breaking since the negative eigenvalue $\sim (h\tau)^2$ is small when we consider its accuracy. For the higher-orders $n \geq 2$, Liouvillianity breaking of $\mathcal{L}^n_{\rm FM}$ is non-negligible due to the negative eigenvalues $\sim (h\tau)^2$.

Noninteracting model preserving Liouvillianity.—We introduce another noninteracting model showing behaviors different from the above model. Let us consider the time-periodic Liouvillian

$$\mathcal{L}_B(t)\rho = \begin{cases} \gamma_2(\tilde{\sigma}^{xz}\rho\tilde{\sigma}^{xz} - \rho) & (0 \leq t < \tau) \\ \gamma_1(\sigma^x\rho\sigma^x - \rho) & (\tau \leq t < 2\tau), \end{cases} \tag{3.35}$$

with $\tilde{\sigma}^{xz} = (\sigma^x + \sigma^z)/\sqrt{2}$. This model is purely driven by dephasing terms $\gamma_1, \gamma_2 > 0$. Up to the second-order, we obtain the matrix $[a^2_{jk}]$ as

$$[a^2_{jk}] = \begin{pmatrix} \gamma_2/2 + \gamma_1 + \alpha^{(2)}_B\gamma_2 & 0 & \gamma_2/2 + \alpha^{(2)}_B\gamma_1 \\ 0 & 0 & 0 \\ \gamma_2/2 + \alpha^{(2)}_B\gamma_1 & 0 & \gamma_2/2 - \alpha^{(2)}_B\gamma_2 \end{pmatrix} \tag{3.36}$$

with $\alpha^{(2)}_B = (\gamma_1\tau)(\gamma_2\tau)/6$. Here, the first-order contribution $a^{(1)}_{jk}$ disappears as $a^{(1)}_{jk} = 0$, exemplifying the case where $\mathcal{L}^{(1)}_{\rm FM}$ becomes a Liouvillian in Theorem 3.2.3. The zeroth- and the first-order expansions $\mathcal{L}^0_{\rm FM}$ and $\mathcal{L}^1_{\rm FM}$ are Liouvillians under any choice of the parameters γ_1, γ_2, τ. For the second-order, the smallest eigenvalue of $[a^2_{jk}]$ is the smaller one of 0 and

$$\frac{\gamma_1 + \gamma_2}{2} - \frac{1}{6}\sqrt{\gamma_1^2\gamma_2^2\tau^2(\gamma_1^2\tau^2 + \gamma_2^2\tau^2 + 12) + 9\,(\gamma_1^2 + \gamma_2^2)}. \tag{3.37}$$

This suggests that the second-order expansion $\mathcal{L}^2_{\rm FM}$ becomes a Liovillian in the finite parameter range $0 < \tau \leq \tau_{\max}$, where $\tau_{\max}$ is given by

$$\tau_{\max} = \left[\frac{6\left(\sqrt{1 + (\gamma_1^2 + \gamma_2^2)\,/\,(2\gamma_1\gamma_2)} - 1\right)}{\gamma_1^2 + \gamma_2^2}\right]^{1/2} > 0. \tag{3.38}$$

This behavior, preservation of Liouvillianity of $\mathcal{L}^n_{\rm FM}$, is confirmed also when we consider higher-orders $n \geq 3$, while the threshold $\tau_{\max}$ depends on the order.

Non-universal behavior in noninteracting models.—In the above discussion, we discover two different behaviors of noninteracting cases:

1. Liouvillianity breaking of $\mathcal{L}^n_{\rm FM}$ $(n \geq 1)$.

2. Liouvillianity preservation of $\mathcal{L}^n_{\rm FM}$ in a finite parameter range.

This difference comes from the structures of the matrix $[a^n_{jk}]$. In the first case, the higher order terms $[a^{(m)}_{jk}]$ $(m \geq 1)$ appear in the different block from $[a^{(0)}_{jk}]$ [See Eq. (3.34)]. This can be interpreted as that the zero eigenvalue of $[a^{(0)}_{jk}]$ is perturbed by higher-order terms, resulting in the negative eigenvalues of $[a^n_{jk}]$ $(n \geq 1)$. On the other hand, in the second case, the zeroth-order term $[a^0_{jk}]$ and the higher-order terms $[a^{(m)}_{jk}]$ $(m \geq 1)$ are closed within the same block [See Eq. (3.36)]. Since the positive eigenvalues of $[a^0_{jk}]$ are shifted by the higher-order terms, the positive-semidefiniteness of $[a^n_{jk}]$ is maintained. This is why preservation of Liovillianity is observed. Although we focus on two specific models, generic noninteracting models are expected to show these behaviors since the matrix $[a^n_{jk}]$ should be either closed or not with the increasing order n. Thus, noninteracting models have non-universal behaviors of Liouvillianity of the Floquet-Magnus expansion, in that they can either break or preserve it depending on the model.

3.2.3 Liouvillianity in interacting models

Here, we discuss few-body and many-body interacting models and how they behaves in contrast to noninteracting models. We consider an L-site spin chain with $S = 1/2$, and the dimension d

becomes 2^L. Then, the Frobenius basis is composed of 4^L matrices in $\mathbb{M}_{2^L}$. We use a set of labels $J = \{\vec{j} = (j_1, j_2, \ldots, j_L) \,|\, j_l = 0, 1, 2, 3 \quad (l = 1, 2, \ldots, L)\}$, and we can choose $\{F_{\vec{j}}\}_{\vec{j}\in J}$ given by

$$F_{\vec{j}} = \prod_{l=1}^{L} \tilde{F}_{j_l}, \quad \tilde{F}_0 = I_2/\sqrt{2}, \quad \tilde{F}_1 = \sigma^x/\sqrt{2}, \quad \tilde{F}_2 = \sigma^y/\sqrt{2}, \quad \tilde{F}_3 = \sigma^z/\sqrt{2}, \tag{3.39}$$

as the Frobenius basis for $\mathbb{M}_{2^L}$. The matrix $F_{\vec{j}=\vec{0}}$ corresponds to F_{d^2}, having the nonzero trace in Eq. (3.13), and the others $F_{\vec{j}\neq\vec{0}}$ are traceless corresponding to Eq. (3.14).

Interacting model showing Liouvillianity breaking.— We begin with the model analysis based on the following time-periodic Liouvillian

$$\mathcal{L}_C(t)\rho = \begin{cases} -iJ_z \sum_l [\sigma_l^z \sigma_{l+1}^z, \rho] \equiv \mathcal{L}_{C1}\rho & (0 \le t < \tau) \\ \gamma \sum_l (\sigma_l^x \rho \sigma_l^x - \rho) \equiv \mathcal{L}_{C2}\rho & (\tau \le t < 2\tau), \end{cases} \tag{3.40}$$

where $\mathcal{L}_{C1}$ and $\mathcal{L}_{C2}$ are respectively Ising interactions and dephasing. Here, we assume the periodic boundary condition $\sigma_{L+1}^\alpha = \sigma_1^\alpha$ $(\alpha = x, y, z)$, but it is not essential. The zeroth-order expansion

$$\mathcal{L}_{\rm FM}^0 = (\mathcal{L}_{C1} + \mathcal{L}_{C2})/2 = -i\frac{J_z}{2}\sum_l (\sigma_l^z \sigma_{l+1}^z \otimes I - I \otimes \sigma_l^z \sigma_{l+1}^z) + \frac{\gamma}{2}\sum_l (\sigma_l^x \otimes \sigma_l^x - I) \tag{3.41}$$

is trivially a Liouvillian as a result of Theorem 3.2.3. Note that we employ the doubled Hilbert space representation, and then linear operators on $\mathbb{M}_{2^L}$ are represented as non-hermitian Hamiltonians on a $2L$-site spin system.

For the first-order, we obtain the following Floquet-Magnus expansion,

$$\mathcal{L}_{\rm FM}^1 = \mathcal{L}_{\rm FM}^0 + \frac{J_z\gamma\tau}{2}\sum_l \left\{\sigma_l^x \otimes \sigma_l^y(\sigma_{l-1}^z + \sigma_{l+1}^z) - \sigma_l^y(\sigma_{l-1}^z + \sigma_{l+1}^z) \otimes \sigma_l^x\right\}. \tag{3.42}$$

We compute the matrix elements $[a_{\vec{j}\vec{k}}^1]$ for $\vec{j}, \vec{k} \in J\backslash\{\vec{0}\}$. By properly changing the order of the basis, we arrive at the $(4^L - 1)$-dimensional hermitian matrix,

$$[a_{\vec{j}\vec{k}}^1] = \left[\bigoplus_{l=1}^{L} 2^{L-1}\gamma \begin{pmatrix} 1 & \alpha_C^{(1)} & \alpha_C^{(1)} \\ \alpha_C^{(1)} & 0 & 0 \\ \alpha_C^{(1)} & 0 & 0 \end{pmatrix}_l\right] \oplus O_{4^L-3L-1}, \tag{3.43}$$

with the first-order contribution $\alpha_C^{(1)} = -J_z\tau$. The basis of the 3×3 matrices $(\cdots)_l$ is composed of $\vec{j} = (\ldots 0, j_l = 1, 0\ldots), (\ldots 0, 2, j_l = 3, 0\ldots), (\ldots 0, j_l = 3, 2, 0\ldots)$. Here, the component 1 in $(\cdots)_l$ comes from the two-body term $\sigma_l^x \otimes \sigma_l^x$ in $\mathcal{L}_{\rm FM}^{(0)}$ [See Eq. (3.41)], and $\alpha_C^{(1)}$ comes from the three-body terms $\sigma_l^x \otimes \sigma_l^y \sigma_{l\pm1}^z$ and $\sigma_l^y \sigma_{l\pm1}^z \otimes \sigma_l^x$ in $\mathcal{L}_{\rm FM}^{(1)}$. [See Eq. (3.42)]. Due to the block-diagonalization, we can exactly obtain all the eigenvalues of the matrix $[a_{\vec{j}\vec{k}}]$, whose size is exponentially large in the system size L. The smallest eigenvalue of $[a_{\vec{j}\vec{k}}]$ is $\gamma \cdot 2^{L-2}\{1 - \sqrt{1 + 8(J_z\tau)^2}\} \simeq -\gamma(J_z\tau)^2 2^L$, which is always negative. Therefore, the first-order Floquet-Magnus expansion $\mathcal{L}_{\rm FM}^1$ cannot be a Liouvillian regardless of the parameters J_z, γ, τ, indicating Liouvillianity breaking. Note that its order $(J_z\tau)^2$ is small considering the truncation order $n = 1$ in this case.

As well, the second-order is calculated as

$$\begin{aligned} \mathcal{L}_{\rm FM}^2 \quad = \quad & \mathcal{L}_{\rm FM}^1 - \frac{\gamma(J_z\tau)^2}{3}\sum_l \{\sigma_l^x \otimes \sigma_l^x(I + \sigma_{l-1}^z\sigma_{l+1}^z) + \sigma_l^x(I + \sigma_{l-1}^z\sigma_{l+1}^z) \otimes \sigma_l^x \\ & + \sigma_l^y(\sigma_{l-1}^z + \sigma_{l+1}^z) \otimes \sigma_l^y(\sigma_{l-1}^z + \sigma_{l+1}^z)\}, \end{aligned} \tag{3.44}$$

and then, the matrix $[a_{\vec{j}\vec{k}}^2]$ becomes

$$[a_{\vec{j}\vec{k}}^2] = \left[\bigoplus_{l=1}^{L} 2^{L-1}\gamma \begin{pmatrix} 1 - 2\alpha_C^{(2)} & \alpha_C^{(1)} & \alpha^{(1)} & -\alpha_C^{(2)} \\ \alpha_C^{(1)} & \alpha_C^{(2)} & \alpha_C^{(2)} & 0 \\ \alpha_C^{(1)} & \alpha_C^{(2)} & \alpha_C^{(2)} & 0 \\ -\alpha_C^{(2)} & 0 & 0 & 0 \end{pmatrix}_l\right] \oplus O_{4^L-4L-1}, \tag{3.45}$$

with the second-order contribution $\alpha_C^{(2)} = 2(J_z\tau)^2/3$. Here, the first three components of the basis of $(\cdots)_l$ are the same as those for Eq. (3.43), and the fourth is $\vec{j} = (\ldots 0, 3, j_l = 1, 3, 0 \ldots)$. The components $\alpha_C^{(2)}$ appearing in the lower right of $\alpha_C^{(1)}$ in $(\ldots)_l$ originate from the four-body terms in $\mathcal{L}_{\rm FM}^{(2)}$. The matrix $[a^2_{\vec{j}\vec{k}}]$ always has negative eigenvalues, and the smallest one is numerically given by

$$\lambda_{\min}/[\gamma \cdot 2^{L-1}(J_z\tau)^2] \simeq \sum_{m=0}^{3} C_m (J_z\tau)^m, \tag{3.46}$$
$$C_0 = -0.667, C_1 = 0.0197, C_2 = -3.08, C_3 = 2.84,$$

with the root mean square error 3.25×10^{-4} in $0 < J_z\tau < 0.5$ (Although we can obtain its analytical formula, it is too complicated). Thus, the second-order Floquet-Magnus expansion $\mathcal{L}_{\rm FM}^2$ shows Liouvillianity breaking with the non-negligible order $O((J_z\tau)^2)$.

Universal behaviors of Liouvillianity in interacting models ?—In the above discussion, we obtain that the interacting model $\mathcal{L}_C(t)$ show Liouvillianity breaking of the Floquet-Magnus expansion $\mathcal{L}_{\rm FM}^n$ for $n = 1, 2$. What should be tackled next is to examine whether or not the Liouvillianity breaking behavior is common with generic interacting systems. For instance, we consider another model $\mathcal{L}_D(t)$ given by

$$\mathcal{L}_D(t)\rho = \begin{cases} -iJ_x \sum_l [\sigma_l^1 \sigma_{l+1}^1, \rho] \equiv \mathcal{L}_{D1}\rho & (0 \le t < \tau) \\ \gamma \sum_l (\sigma_l^- \rho \sigma_l^+ - \frac{1}{2}\{\sigma_l^+\sigma_l^-, \rho\}) \equiv \mathcal{L}_{D2}\rho & (\tau \le t < 2\tau = T), \end{cases} \tag{3.47}$$

with $\sigma_l^{\pm} = (\sigma_l^x \pm i\sigma_l^y)/2$, which is composed of Ising interactions and dissipation making the down-spin state preferable. The resulting non-positive-semidefinite matrix $[a^1_{\vec{j}\vec{k}}]$, given by

$$[a^1_{\vec{j}\vec{k}}] = \left[\bigoplus_{l=1}^{L} \gamma \cdot 2^{L-3} \begin{pmatrix} 2 & 2i & -i(J_x\tau) & -i(J_x\tau) \\ -2i & 2 & -(J_x\tau) & -(J_x\tau) \\ i(J_x\tau) & -(J_x\tau) & 0 & 0 \\ i(J_x\tau) & -(J_x\tau) & 0 & 0 \end{pmatrix}_l \right] \oplus O_{4^L-4L-1}, \tag{3.48}$$

has a structure similar to Eqs. (3.43) and (3.45), showing Liouvillianity breaking of $\mathcal{L}_{\rm FM}^1$.

We note that the structure of the matrices $[a^n_{\vec{j}\vec{k}}]$ appearing in the interacting models is common with that in the noninteracting case $\mathcal{L}_A(t)$ with Liouvillianity breaking, in that the zeroth-order and the higher-order contributions are not closed in the same block. In contrast to the noninteracting case, higher-order contributions in $[a^n_{\vec{j}\vec{k}}]$ are connected to many-body terms in $\mathcal{L}_{\rm FM}^n$ for interacting systems. In the next chapter, we clarify that this connection holds for generic interacting systems and results in the universal structure of the matrix $[a^n_{\vec{j}\vec{k}}]$, which gives Liouvillianity breaking in generic interacting systems.

3.3 Liouvillianity breaking in generic interacting models

Here, we generalize the result of the interacting models in the previous section, and provide the main assertion in this chapter, saying that the Floquet-Magnus expansion $\mathcal{L}_{\rm FM}^n$ $(n \ge 1)$ cannot be a Liouvillian in generic interacting systems.

We first specify the setup for generic dissipative Floquet systems with interactions. We consider an L-site lattice Λ, where each site has f degrees of freedom. The time-periodic Liouvillian $\mathcal{L}(t) = \mathcal{L}(t+T)$ is given by

$$\mathcal{L}(t) = -i(H(t) \otimes I - I \otimes H(t)^{\rm T}) + \sum_i \left[L_i(t) \otimes L_i(t)^* - \frac{1}{2}(L_i(t)^\dagger L_i(t) \otimes I + I \otimes L_i(t)^{\rm T} L_i(t)^*) \right] \tag{3.49}$$

in the doubled Hilbert space representation. By regarding $\mathcal{L}(t)$ as a non-hermitian Hamiltonian on a $2L$-site lattice $\Lambda_{\rm d} = \{1, 2, \ldots, 2L\}$, we extend the notions of locality and extensiveness for Hamiltonians to Liouvillians (See Definition 1.3.1). The locality k for a Liouvillian is defined by

$$\mathcal{L}(t) \text{ is } k\text{-local} \Leftrightarrow H(t) \text{ and } L_i(t) \text{ respectively have at-most } k\text{-body and } (k/2)\text{-body interactions.} \tag{3.50}$$

This immediately means that $\mathcal{L}(t)$ in the doubled Hilbert space representation has at-most k-body interactions. We decompose a Liouvillian by $\mathcal{L}(t) = \sum_{X\subset\Lambda_{\rm d}} \mathcal{L}|_X(t)$, where $\mathcal{L}|_X(t)$ denotes the terms of $\mathcal{L}(t)$ nontrivially acting on a domain $X \subset \Lambda_{\rm d}$ in the doubled Hilbert space representation. We define the extensiveness of a Liouvillian by

$$\mathcal{L}(t) \text{ is } \mathcal{J}\text{-extensive} \Leftrightarrow \sum_{X:X\ni i} ||\mathcal{L}|_X(t)|| \le \mathcal{J}, \quad {}^\forall i \in \Lambda_{\rm d}, \tag{3.51}$$

which is the natural extension of Eq. (1.94). Under the finite extensiveness $\mathcal{J}$, we obtain the bounded local energy scale $||\mathcal{L}(t)||/L \le 2\mathcal{J}$.

The locality (the extensiveness) of a Liouvillian assumes the locality (the bounded local energy scale) of the Hamiltonian and the dissipation, which is expected to be physically reasonable. For example, when we consider the model $\mathcal{L}_C(t)$ composed of Ising interactions and dephasing dissipation, we obtain the locality $k = 2$ and the extensiveness $\mathcal{J} = 2|J_z| + \gamma$. Thus, we adopt the k-locality and the $\mathcal{J}$-extensiveness as natural assumptions for generic interacting systems.

To discuss Liouvillianity of the Floquet-Magnus expansion, we should consider the matrix $[a^n_{jk}] = \mathrm{Tr}[(F_j^\dagger \otimes F_k^{\rm T})\mathcal{L}^n_{\rm FM}]$. Here, the Frobenius basis for $\mathbb{M}_{f^L}$ is designated by

$$J = \{\vec{j} = (j_1, \dots, j_L) \,|\, j_l = 0, 1, \dots, f-1\}. \tag{3.52}$$

The Frobenius basis is composed of $F_{\vec{j}} = \prod_{l=1}^L \tilde{F}_{j_l}$ with $\tilde{F}_0 = I_f/\sqrt{f}$ and $\tilde{F}_j$ $(j \neq 0)$ given by the Frobenius basis for $\mathbb{M}_f$ other than $\tilde{F}_0$. Judgment of Liouvillianity can be done by the positive-semidefiniteness of the $(f^{2L}-1)$-dimensional matrix $[a^n_{\vec{j}\vec{k}}]_{\vec{j},\vec{k}\in J\setminus\{\vec{0}\}}$. When we assume the locality and the extensiveness, we can obtain the following generic property of this matrix.

Theorem 3.3.1. (Bound on the matrix elements $a^{(m)}_{\vec{j}\vec{k}}$)
For a k-local and $\mathcal{J}$-extensive Liouvillian $\mathcal{L}(t)$, the matrix elements $a^{(m)}_{\vec{j}\vec{k}} = \mathrm{Tr}[(F_{\vec{j}}^\dagger \otimes F_{\vec{k}}^{\rm T})\mathcal{L}^{(m)}_{\rm FM}]$ are bounded by

$$\left|a^{(m)}_{\vec{j}\vec{k}}\right| \le \frac{(2kJT)^m}{m+1} J \cdot m! \cdot f^L. \tag{3.53}$$

Proof

We consider $a^{(m)}_{\vec{j}\vec{k}}$ for fixed $\vec{j}, \vec{k} \neq \vec{0}$, and let $X \in \Lambda_{\rm d}$ be a domain where $F_{\vec{j}} \otimes F^*_{\vec{k}}$ nontrivially acts. Let us define $A^{(m)}_{\vec{j}\vec{k}}$ by

$$A^{(m)}_{\vec{j}\vec{k}} = \sum_{\vec{j}',\vec{k}'} a^{(m)}_{\vec{j}'\vec{k}'} \left(F_{\vec{j}'} \otimes F^*_{\vec{k}'}\right), \tag{3.54}$$

where $\sum_{\vec{j}',\vec{k}'}$ represents the summation over $\vec{j}', \vec{k}'$ such that $F_{\vec{j}'} \otimes F^*_{\vec{k}'}$ nontrivially acts only on the domain X (there exist at-most $(f^2-1)^{|X|}$ terms). Then, $A^{(m)}_{\vec{j}\vec{k}}$ is the unique term nontrivially acting just on X in $\mathcal{L}^{(m)}_f$, and hence we obtain

$$||A^{(m)}_{\vec{j}\vec{k}}|| \le \mathcal{J}^{(m)}, \tag{3.55}$$

where $J^{(m)}$ is the extensiveness of the i-th order term $\mathcal{L}^{(m)}_{\rm FM}$ from the definition of the extensiveness. We note that the bound on the extensiveness of $H^{(m)}_{\rm FM}$ in the Floquet-Magnus effective Hamiltonian, given by Theorem 1.3.2 in Section 1.3.4, is derived without using the hermiticity of $H^{(m)}_{\rm FM}$. This results in the same bound for the non-hermitian Hamiltonian $\mathcal{L}^{(m)}_{\rm FM}$ given by

$$\mathcal{J}^{(m)} \le \frac{(2k\mathcal{J}T)^m}{m+1} \mathcal{J} \cdot m!. \tag{3.56}$$

Using the Schwartz inequality for the Frobenius inner product and the Frobenius norm, we arrive at

$$\left|a^{(m)}_{\vec{j}\vec{k}}\right| = \left|\left\langle \left(F_{\vec{j}} \otimes F^*_{\vec{k}}\right), A^{(m)}_{\vec{j}\vec{k}} \right\rangle_{\rm F}\right| \le \left|\left|\left(F_{\vec{j}} \otimes F^*_{\vec{k}}\right)\right|\right|_{\rm F} \cdot \left|\left|A^{(m)}_{\vec{j}\vec{k}}\right|\right|_{\rm F}. \tag{3.57}$$

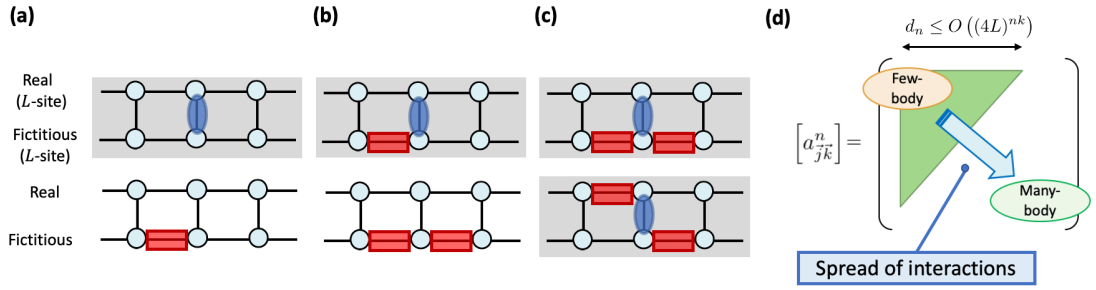

Figure 3.1: (a) Possible local terms appearing in $\mathcal{L}(t)$ or $\mathcal{L}^{(0)}_{\rm FM}$ under the locality $k = 2$. (b,c) Possible local terms appearing in $\mathcal{L}(t)$ and $\mathcal{L}^{(1)}_{\rm FM}$ and $\mathcal{L}^{(2)}_{\rm FM}$ under the locality $k = 2$, respectively. In (a,b,c), red rectangles (closed within either the real or the fictitious system) represent local terms caused by the Hamiltonian $H(t)$, while blue ellipses (connecting the two systems) originate from the dissipation $L_i(t)$. Local terms with gray backgrounds, involving both the real and the fictitious systems, appear as nonzero components in $[a^n_{\vec{j}\vec{k}}]$. (d) Generic form of the matrix $[a^n_{\vec{j}\vec{k}}]$ in few-body or many-body systems with local interactions. It reflects the spread of local interactions seen in (a), (b), and (c).

Since the Frobenius norm $||\cdot||_{\rm F}$ is related to the operator norm $||\cdot||$ by $||A||_{\rm F} \leq \sqrt{{\rm rank}A}\cdot||A||$, we obtain

$$\left|a^{(m)}_{\vec{j}\vec{k}}\right| \leq \sqrt{{\rm rank}\left(A^{(m)}_{\vec{j}\vec{k}}\right)}\cdot\left|\left|A^{(m)}_{\vec{j}\vec{k}}\right|\right| \leq \frac{(2kJT)^m}{m+1}J\cdot m!\cdot f^L. \qquad \square \tag{3.58}$$

This theorem says that the matrix elements $a^{(m)}_{\vec{j}\vec{k}}$ generally decay with the increasing order m up to $1/(2k\mathcal{J}T) = O(\omega/\mathcal{J})$, as the m-th order term $\mathcal{L}^{(m)}_{\rm FM}$ is suppressed. Thus, in generic interacting systems, Liouvillianity of $\mathcal{L}^{(m)}_{\rm FM}$ is determined by whether $a^{(0)}_{\vec{j}\vec{k}}$ can remain positive-semidefinite under perturbations of non-positive-semidefinite matrices $a^{(m)}_{\vec{j}\vec{k}}$ $(m \geq 1)$, as well as noninteracting systems.

However, unlike noninteracting cases, the locality of interactions strongly restricts the form of the matrix $[a^n_{\vec{j}\vec{k}}]$ in interacting cases. Let us consider a k-local Liouvillian $\mathcal{L}(t)$. When we divide $\Lambda_{\rm d}$ into L-site real and fictitious systems, $H(t)\otimes I$ and $I\otimes H(t)^{\rm T}$ in $\mathcal{L}(t)$ give at-most k-body interactions closed within real or fictitious systems. On the other hand, the term $L_i(t)\otimes L_i(t)$, originating from the dissipation, appears as at-most k-body interactions bridging the real and the fictitious systems [See Fig. 3.1 (a)]. The zeroth-order term $\mathcal{L}^{(0)}_{\rm FM}$, given by the time-average of $\mathcal{L}(t)$, involves at-most k-body interactions as well as $\mathcal{L}(t)$. For the first-order, the commutator $[\mathcal{L}(t_1),\mathcal{L}(t_2)]$ in Eq. (3.7) gives at-most $(2k-1)$-body interactions coming from local terms in $\mathcal{L}(t)$ with overlaps on at-least one site. In general, the m-th order term $\mathcal{L}^{(m)}_{\rm FM}$ contains at-most $\{(m+1)k-m\}$-body interactions originating from the m-tuple commutators of $\mathcal{L}(t)$.

Next, we examine how this locality constraint on $\mathcal{L}^{(m)}_{\rm FM}$ affects the form of $[a^n_{\vec{j}\vec{k}}]$. Let $n_{\vec{j}}$ denote the number of l satisfying $j_l \neq 0$ for $\vec{j}\in J$. Then, Eq. (3.20) dictates that nonzero $a^n_{\vec{j}\vec{k}}$ ensures the existence of a $(n_{\vec{j}}+n_{\vec{k}})$-body term $F_{\vec{j}}\otimes F^*_{\vec{k}}$ in $\mathcal{L}^n_{\rm FM}$, involving both the real and the fictitious systems [See Figs. 3.1 (a)-(c)]. Since $\mathcal{L}^n_{\rm FM} = \sum_{m=0}^n \mathcal{L}^{(m)}_{\rm FM}$ contains at-most $\{(n+1)k-n\}$-body interactions, the locality constraint results in

$$a^n_{\vec{j}\vec{k}} = 0 \quad \text{if} \quad (n_{\vec{j}}+n_{\vec{k}}) > \{(n+1)k-n\}. \tag{3.59}$$

We rearrange the labels of the Frobenius basis $\vec{j}\in J$ in the ascending order of the locality $n_{\vec{j}}$, and then we obtain the following block-diagonalized form:

$$\left[a^n_{\vec{j}\vec{k}}\right] = A_{d_n}\oplus O_{f^{2L}-d_n-1}, \quad A_{d_n}\in\mathbb{M}_{d_n}. \tag{3.60}$$

The basis of the nontrivial part A_{d_n} is composed of $\vec{j} \in J$ that satisfies $1 \leq n_{\vec{j}} \leq (n+1)k-n$, and the number of such $\vec{j}$ gives its dimension d_n. The dimension d_n is bounded by

$$d_n \leq {}_L C_{(n+1)k-n} \cdot (f^2)^{(n+1)k-n} \sim \frac{(f^2 L)^{(n+1)k-n}}{\{(n+1)k-n\}!}, \tag{3.61}$$

which is usually much smaller than the whole size f^{2L} when $nk \ll L$. Furthermore, Eq. (3.59) also indicates that the nontrivial part A_{d_n} becomes the triangular form,

$$A_{d_n} = \begin{pmatrix} \tilde{A}_{e_n} & \tilde{B} \\ \tilde{B}^\dagger & O_{d_n - e_n} \end{pmatrix}, \quad \tilde{A}_{e_n} \in \mathbb{M}_{e_n} : \text{hermitian}, \tag{3.62}$$

where we assume $d_n \leq f^{2L} - 1$. Here, the dimension e_n is the number of $\vec{j} \in J$ such that $n_{\vec{j}}$ exceeds $\lceil (n+1)k/2 - n/2 \rceil$ ($\lceil x \rceil$: the ceil function), having the upper bound,

$$e_n \leq {}_L C_{\lceil (n+1)k/2 - n/2 \rceil} \cdot 4^{\lceil (n+1)k/2 - n/2 \rceil}. \tag{3.63}$$

When the interactions are neighboring (The ranges of interactions of $H(t)$ and $L_i(t)$ are respectively k and $k/2$), the size d_n and e_n respectively reduce to $O((f^2)^{(n+1)k-n} L)$ and $O((f^2)^{\lceil (n+1)k/2 - n/2 \rceil} L)$ since the Floquet-Magnus expansion $\mathcal{L}^n_{\rm FM}$ also involves neighboring interactions whose range is at-most $(n+1)k-n$ sites. Finally, we summarize the generic form as follows.

Theorem 3.3.2. (Generic form of $[a^n_{\vec{j}\vec{k}}]$)
For a k-local time-periodic Liouvillian $\mathcal{L}(t)$, the matrix $[a^n_{\vec{j}\vec{k}}]$ has the generic form

$$[a^n_{\vec{j}\vec{k}}] = \begin{pmatrix} \tilde{A}_{e_n} & \tilde{B} \\ \tilde{B}^\dagger & O_{d_n - e_n} \end{pmatrix} \otimes O_{f^{2L} - d_n - 1} \tag{3.64}$$

when the order n is smaller than L/k.

The triangular form of the matrix $[a^n_{\vec{j}\vec{k}}]$ can be attributed to the spread of local interactions in the Floquet-Magnus expansion. In fact, each m-th order contribution $[a^{(m)}_{\vec{j}\vec{k}}]$ ($m \leq n$) appears in the upper left triangular of the nontrivial part satisfying $n_{\vec{j}} + n_{\vec{k}} \leq (m+1)k - m$, and spreads from the upper left to the lower right with increasing m [See Fig. 3.1 (d)]. Thus, the matrix $[a^n_{\vec{j}\vec{k}}]$ generally has a structure where the zeroth-order and the higher-order contributions are not closed within the same block, which is common with the interacting models $\mathcal{L}_C(t)$ and $\mathcal{L}_D(t)$ discussed in the previous section. Intuitively, the higher-order terms perturb the zero eigenvalues in the block where $[a^{(0)}_{\vec{j}\vec{k}}]$ does not appear, and can shift them negative as discussed in the previous section. Here, we conclude more rigorously with employing the following theorem derived by technique of the Schur complements (See Theorem 1.11 in Ref. [155]).

Theorem. Let A denote a hermitian square matrix represented by

$$A = \begin{pmatrix} \tilde{A} & \tilde{B} \\ \tilde{B}^\dagger & O \end{pmatrix}, \tag{3.65}$$

with hermitian square matrices $\tilde{A} = \tilde{A}^\dagger$. Then, the number of positive (negative) eigenvalues of A, denoted by $p(A)$ ($n(A)$), satisfies

$$p(A) \geq \mathrm{rank}(\tilde{B}), \quad n(A) \geq \mathrm{rank}(\tilde{B}). \tag{3.66}$$

With the usage of this theorem, we rigorously conclude that the matrix $[a^n_{\vec{j}\vec{k}}]$ with the triangular form always becomes non-positive-semidefinite as long as $\tilde{B} \neq 0$ [1]. Finally, we obtain the following generic result on Liouvillianity of the Floquet-Magnus expansion.

[1] We show some trivial exceptions for this result. The first example is a commutative Liouvillian $\mathcal{L}(t)$ [153], which satisfies $[\mathcal{L}(t_1), \mathcal{L}(t_2)] = 0$ for any t_1 and t_2. In this case, we obtain the exact Floquet-Magnus expansion by $\mathcal{L}^n_{\rm FM} = \mathcal{L}^0_{\rm FM}$ at any order n, preserving the Liouvillianity. The second example is a time-periodic Liouvillian with time-independent Lindblad operators $L_i(t) = L_i$. The first-order van Vleck expansion $\mathcal{L}^1_{\rm vV}$ does not break Liouvillianity since the first-order term $\mathcal{L}^{(1)}_{\rm vV}$ does not include dissipation. For higher-order expansions, Liouvillianity breaking takes place in general.

Remark. (Liouvillianity breaking in generic interacting systems)
In generic few-body or many-body dissipative Floquet systems with local interactions, described by a time-periodic Liouvillian $\mathcal{L}(t)$, the Floquet-Magnus expansion $\mathcal{L}^n_{\rm FM}$ $(n \geq 1)$ cannot be a Liouvillian (Liouvillianity breaking).

This result answers the question delivered as the aim of this chapter, "*Do dissipative Floquet systems in the high-frequency regime have static counterparts described by a Liouvillian ?*", in Section 3.1.2. We clarify that, in generic interacting cases, dissipative Floquet systems in the high-frequency regime are approximately described by a static operator $\mathcal{L}^n_{\rm FM}$ that cannot be a Liouvillian. This implies the breakdown of the correspondence between Floquet systems in the high-frequency regime and static systems under dissipation in contrast to closed cases, where Floquet systems in this regime are described by a static Hamiltonian.

3.4 Conclusions and outlook of this chapter

Here, we conclude this chapter and provide possible future directions. In this chapter, we consider dissipative Floquet systems described by a time-periodic Liouvillian $\mathcal{L}(t)$. While dissipative Floquet systems are expected to host unique nonequilibrium many-body phenomena with overcoming Floquet-ETH or the heating problem, there are hardly such universal many-body phenomena found due to the difficulty of the analysis by the competition of dissipation, periodic drive, and interactions. We focus on the high-frequency regime, which can be addressed by the perturbation theory in a unified way, and tackle the fundamental question whether or not dissipative Floquet systems in the high-frequency regime correspond to static dissipative systems. As closed Floquet systems in the high-frequency regime cannot host unique nonequilibrium phenomena due to the correspondence with closed static systems, this question is of importance in that it determines the identity of dissipative Floquet systems in the high-frequency regime.

With the usage of the Floquet-Magnus expansion, the question is interpreted as whether the Floquet-Magnus expansion $\mathcal{L}^n_{\rm FM}$ is a static Liouvillian or not. The main assertion in this chapter is that the Floquet-Magnus expansion universally shows Liouvillianity breaking in generic interacting systems, while noninteracting systems can either preserve or break its Liouvillianity depending on models. Liouvillianity breaking in generic interacting systems can be attributed to the spread of local interactions lying in the Floquet-Magnus expansion with the increasing order. As a result, we clarify that dissipative Floquet systems can host phenomena having no static counterparts even in the high-frequency regime as opposed to closed cases. We also note that Liouvillianity breaking of the Floquet-Magnus expansion can be regarded as emergent non-Markovianity in the stroboscopic dynamics. The Liouvillianity of $\mathcal{L}(t)$ means that the time evolution microscopically reflects Markovianity. Nevertheless, when we focus on the stroboscopic dynamics, the dynamics effectively looks non-Markov due to Liouvillainity breaking of $\mathcal{L}^n_{\rm FM}$.

Next, we show some possible future directions. First, it should be interesting to clarify what kind of non-Markovian dynamics is realized in dissipative Floquet systems. Liouvillianity breaking is the signature of non-Markovian dynamics. For instance, Ref. [156] confirms that finite memory time unique to non-Markovian dynamics effectively appears in noninteracting dissipative Floquet systems under Markovianity, with the numerical calculation of the effective Lindbladian $\mathcal{L}_{\rm eff}$ [Eq. (3.4)]. Thus, identifying the effective non-Markovian dynamics by some ways such as memory time will be necessary to further characterize interacting dissipative Floquet systems. Second, as one of the most promising directions, we should seek for what kind of phenomena can be brought by Liouvillianity breaking. While we clarify that the stroboscopic dynamics is described by a static operator different from a Liouvillian, it is still unclear how this affects steady states, dynamics, and observables. For instance, in contrast to closed cases where we can employ the knowledge of time-independent Hamiltonians for Floquet systems, dissipative Floquet systems fail to have some properties of time-independent Liouvillians, such as the existence of steady states and the validity of the trajectory method (See Section 3.5 for the detail). Uncovering phenomena brought by these properties will contribute to the comprehension on the essential difference between Floquet systems and static systems. We expect that this direction will also lead to Floquet engineering in dissipative Floquet systems. Liouvillianity breaking in generic interacting systems implies that we can engineer steady states or dynamics which are not reproducible in static dissipative systems.

3.5 Appendix for this chapter

Proof of Theorem 3.2.1

Here, we prove Theorem 3.2.1 for each m-th order term $\mathcal{L}_{\rm FM}^{(m)}$ in a way similar to Ref. [153].

Theorem. (Form of each m-th order term)
Each m-th order term of the Floquet-Magnus expansion, $\mathcal{L}_{\rm FM}^{(m)}$, is always written in the form of

$$\mathcal{L}_{\rm FM}^{(m)} = -i(H^{(m)} \otimes I - I \otimes (H^{(m)})^{\rm T}) + \sum_{j,k=1}^{d^2-1} a_{jk}^{(m)} \left[F_j \otimes F_k^* - \frac{1}{2}(F_k^\dagger F_j \otimes I + I \otimes F_j^{\rm T} F_k^*) \right] \tag{3.67}$$

where $H^{(m)} \in \mathbb{M}_d$ and $[a_{jk}^{(m)}]_{j,k=1}^{d^2-1} \in \mathbb{M}_{d^2-1}$ are hermitian.

Proof

The time-periodic Liouvillain $\mathcal{L}(t)$, given by Eq. (3.2), satisfies the following conditions at each time t:

$$\mathrm{Tr}(\mathcal{L}(t)[\rho]) = 0, \quad (\mathcal{L}(t)[\rho])^\dagger = \mathcal{L}(t)[\rho^\dagger], \quad {}^\forall\rho. \tag{3.68}$$

The first condition represents that the time evolution operator is trace-preserving, and the second one represents that $\mathcal{L}(t)$ is hermiticity-preserving. Then, the sum, difference, and product of $\mathcal{L}(t)$ satisfy the same properties. For example,

$$(\mathcal{L}(t_1)\mathcal{L}(t_2)[\rho])^\dagger = \mathcal{L}(t_1)[(\mathcal{L}(t_2)[\rho])^\dagger] = \mathcal{L}(t_1)\mathcal{L}(t_2)[\rho^\dagger] \tag{3.69}$$

is obtained. Each m-th order term of the Floquet-Magnus expansion $\mathcal{L}_{\rm FM}^{(m)}$, composed of m-tuple multi-commutators of $\mathcal{L}(t)$, possesses the same properties:

$$\mathrm{Tr}(\mathcal{L}_{\rm FM}^{(m)}[\rho]) = 0, \quad {}^\forall\rho, \tag{3.70}$$

$$(\mathcal{L}_{\rm FM}^{(m)}[\rho])^\dagger = \mathcal{L}_{\rm FM}^{(m)}[\rho^\dagger], \quad {}^\forall\rho. \tag{3.71}$$

We show that linear operators satisfying Eqs. (3.70) and (3.71) result in Eq. (3.67). The structure theorem [157] says that a linear operator satisfying Eq (3.71) is always given by

$$\mathcal{L}_{\rm FM}^{(m)}[\rho] = \sum_i x_i X_i \rho X_i^\dagger, \quad x_i \in \mathbb{R},\, X_i \in \mathbb{M}_d. \tag{3.72}$$

By expanding $X_i \in \mathbb{M}_d$ by the Frobenius basis as $X_i = \sum_{j=1}^{d^2} t_{ij} F_j$, we arrive at

$$\mathcal{L}_{\rm FM}^{(m)}[\rho] = \sum_{j,k=1}^{d^2} a_{jk}^{(m)} F_j \rho F_k^\dagger, \quad a_{jk}^{(m)} = \sum_i x_i t_{ij} t_{ik}^* = (a_{kj}^{(m)})^*, \tag{3.73}$$

with the hermitian matrix $[a_{jk}^{(m)}]_{j,k=1}^{d^2-1}$. Using the fact $F_{d^2} = I_d/\sqrt{d}$ and defining $M^{(m)} \equiv (a_{d^2d^2}^{(m)}/2d) I_d + \sum_{j=1}^{d^2-1} a_{jd^2}^{(m)} F_j$ result in

$$\mathcal{L}_{\rm FM}^{(m)}[\rho] = M^{(m)}\rho + \rho(M^{(m)})^\dagger + \sum_{j,k=1}^{d^2-1} a_{jk}^{(m)} F_j \rho F_k^\dagger = i[\mathrm{Im}(M^{(m)}), \rho] + \{\mathrm{Re}(M^{(m)}), \rho\} + \sum_{j,k=1}^{d^2-1} a_{jk}^{(m)} F_j \rho F_k^\dagger. \tag{3.74}$$

In the last equality, we have defined two hermitian matrices $\mathrm{Re}(M) = (M + M^\dagger)/2$ and $\mathrm{Im}(M) = (M - M^\dagger)/2i$. Then,

$$\mathrm{Tr}(\mathcal{L}_{\rm FM}^{(m)}[\rho]) = \mathrm{Tr}[\{\mathrm{Re}(M^{(m)}), \rho\}] + \sum_{j,k=1}^{d^2-1} a_{jk}^{(m)} \mathrm{Tr}[F_j \rho F_k^\dagger] = \mathrm{Tr}\left[\left(2\mathrm{Re}(M^{(m)}) + \sum_{j,k=1}^{d^2-1} a_{jk}^{(m)} F_k^\dagger F_j \right) \rho \right]$$

should be zero regardless of ρ from Eq. (3.70). Therefore, $\mathrm{Re}(M^n)$ is given by

$$\mathrm{Re}(M^{(m)}) = -\frac{1}{2}\sum_{j,k=1}^{d^2-1} a_{jk}^{(m)} F_k^\dagger F_j, \tag{3.75}$$

where the hermiticity of $\mathrm{Re}(M^{(m)})$ is ensured by Eq. (3.73). Finally, by defining $H^{(m)} = -\mathrm{Im}(M^{(m)})$ and using the doubled Hilbert space representation, we obtain Eq. (3.67) □.

As discussed in Section 3.2.1, the Floquet-Magnus expansion $\mathcal{L}_{\mathrm{FM}}$ is also written in the same form. By expanding the hermitian term H^n by the Frobenius basis as $H^n = \sum_{j=1}^{d^2-1} h_j^n F_j$ (The $j = d^2$ component is irrelevant in the commutator), we obtain

$$\mathcal{L}_{\mathrm{FM}}^n = -i\sum_{j=1}^{d^2-1} h_j^n (F_j \otimes I - I \otimes F_j^{\mathrm{T}}) + \sum_{j,k=1}^{d^2-1} a_{jk}^n \left[F_j \otimes F_k^* - \frac{1}{2}(F_k^\dagger F_j \otimes I + I \otimes F_j^{\mathrm{T}} F_k^*)\right]. \tag{3.76}$$

While the matrix elements a_{jk}^n are given by $\mathrm{Tr}[(F_j^\dagger \otimes F_k^{\mathrm{T}})\mathcal{L}_{\mathrm{FM}}^n]$, we can also extract the effective Hamiltonian terms H^n from Eq. (3.76). We multiply $(F_j \otimes I)$ from the left and take the trace with assuming the hermiticity of F_j (This is satisfied in generic spin systems):

$$\mathrm{Tr}[(F_j \otimes I)\,\mathcal{L}_{\mathrm{FM}}^n] = -ih_j^n \mathrm{Tr}I - \frac{1}{2}\sum_{j'k'} a_{j'k'}^n \mathrm{Tr}[F_j F_{k'} F_{j'}] \cdot \mathrm{Tr}I. \tag{3.77}$$

We obtain the effective Hamiltonian terms $H^n = \sum_j h_j^n F_j$, characterized by the coefficients

$$h_j^n = \frac{i}{d}\mathrm{Tr}[(F_j \otimes I)\,\mathcal{L}_{\mathrm{FM}}^n] + \frac{i}{2}\sum_{j'k'} \mathrm{Tr}[(F_{j'}^\dagger \otimes F_{k'}^T)\,\mathcal{L}_{\mathrm{FM}}^n] \cdot \mathrm{Tr}[F_j F_{k'} F_{j'}]. \tag{3.78}$$

We emphasize that Theorem 3.2.1 is proven only using the fact that $\mathcal{L}_{\mathrm{FM}}^{(m)}$ is given by the integrals of polynomial functions of the Liouvillian $\mathcal{L}(t)$. Therefore, other types of high-frequency expansions such as the van Vleck expansion and the Schrieffer-Wolff expansion [158] also satisfy this theorem, and we can check their Liouvillianity in the same way.

Properties of the Floquet-Magnus expansion breaking Liouvillianity

Here, we discuss generic properties of the Floquet-Magnus expansion $\mathcal{L}_{\mathrm{FM}}^n$ in the presence of Liouvillianity breaking. In closed cases, the Floquet-Magnus expansion H_{FM}^n is always a static Hamiltonian, and hence we can employ all the conventional methods for closed static systems. For instance, when we apply ETH of the static Hamiltonian H_{FM}^n, we can predict prethermalization in Floquet systems. Floquet engineering for controlling phases of matter considers topological phases or ordered phases under the static Hamiltonian H_{FM}^n. Clarifying the difference between the Floquet-Magnus expansion breaking Liouvillianity and a static Liouvillian is important to understand what kind of conventional methods or what kind of novel properties are possible in Floquet systems.

We employ the spectral decomposition of the hermitian matrix $[a_{jk}^n]$, which results in $a_{jk}^n = \sum_{i=1}^{d^2-1} \tilde{x}_i \tilde{t}_{ij} \tilde{t}_{jk}^*$ ($\tilde{x}_i \in \mathbb{R}$). By substituting this into Eq. (3.20) and defining $\tilde{L}_i = \sum_{j=1}^{d^2-1} \sqrt{|\tilde{x}_i|}\tilde{t}_i j F_j$, we obtain

$$\mathcal{L}_{\mathrm{FM}}^n \rho = -i[H^n, \rho] + \sum_i s_i \left(\tilde{L}_i \rho \tilde{L}_i^\dagger - \{\tilde{L}_i^\dagger \tilde{L}_i, \rho\}\right), \quad s_i = \mathrm{sgn}(\tilde{x}_i) = \pm 1, \tag{3.79}$$

and the approximate time evolution operator $e^{\mathcal{L}_{\mathrm{FM}}^n mT}$. Thus, the Floquet-Magnus expansion breaking Liouvillianity is different from a static Liouvillian in that it has some negative signs s_i in dissipative terms. We note that this difference does not necessarily mean that the Floquet-Magnus expansion is unphysical. Liouvillianity of $\mathcal{L}$ is equivalent to that the time evolution operator $e^{\mathcal{L}t}$ becomes a CPTP map for any $t \geq 0$. On the other hand, the approximate one $e^{\mathcal{L}_{\mathrm{FM}}^n mT}$ is valid solely at discrete time $t = mT$, thereby imposing weaker constraints on $\mathcal{L}_{\mathrm{FM}}^n$.

With the usage of Eq. (3.79), we obtain the trace-preserving property,

$$\mathrm{Tr}\left[e^{\mathcal{L}_{\mathrm{FM}}^n mT}\rho\right] = \mathrm{Tr}[\rho], \quad {}^\forall\rho \in \mathbb{M}_d. \tag{3.80}$$

The approximate dynamics satisfies the conservation of probability as well as that under a static Liouvillian. However, Eq. (3.79) implies that the Floquet-Magnus expansion can break two important generic notions of a static Liouvillian, the existence of nonequilibrium steady states (NESS) and the validity of the trajectory method.

Existence of NESS.— It is proven from Eq. (3.10) that any static Liouvillian $\mathcal{L}$ has at-least one eigenstate with zero eigenvalue, and that all the eigenvalues of $\mathcal{L}$ have non-positive real parts. Then, the right-eigenstates with zero eigenvalue are called nonequilibrium steady states (NESS) ρ_{NESS}, which appear after sufficiently long-time dynamics due to the other vanishing eigenstates. The existence of NESS is proven with the usage of Liouvillianity, Eq. (3.10), and hence it is nontrivial whether it holds under Eq. (3.79) breaking Liouvillianity. Using Eq. (3.79), we can show that $\mathcal{L}_{\mathrm{FM}}^n$ has a left-eigenstate with zero eigenvalue, described by

$$(\mathcal{L}_{\mathrm{FM}}^n)^\dagger[I_d] = O_d. \tag{3.81}$$

This ensures that $\mathcal{L}_{\mathrm{FM}}^n$ has also a right-eigenstate with zero eigenvalue, which survives after long-time dynamics. However, eigenvalues of $\mathcal{L}_{\mathrm{FM}}^n$ do not always have non-positive eigenvalues, and hence $\mathcal{L}_f^n$ which breaks Liouvillianity does not ensure the existence of NESS in general.

In our models $\mathcal{L}_\alpha(t)$ ($\alpha = A, B, C, D$), NESS becomes ill-defined under $\mathcal{L}_{\mathrm{FM}}^n$ ($n \geq 1$) when the frequency is comparable to the energy scale, although such an anomalous effect is not physically accessible. However, we expect that, when the NESS of the Liouvillian $\mathcal{L}_f^0$ is degenerated or the Liouvillian gap $\Delta = \min\{\mathrm{Re}\lambda \neq 0 \,|\, \lambda : \text{eigenvalue of } \mathcal{L}_f^0\}$ is small enough, NESS will disappear in the high-frequency regime. While such a situation where some eigenstates become divergent might be unphysical, we expect some anomalous behaviors related to Liouviilianity breaking around that situation.

Validity of trajectory method.— Next, we discuss the validity of trajectory method, with which we can efficiently calculate the nonequilibrium dynamics [159]. In static Liouvillian systems, the Lindblad equation is rewritten as

$$\partial_t\rho = -i(H_{\mathrm{eff}}\rho - \rho H_{\mathrm{eff}}^\dagger) + \sum_i L_i\rho L_i^\dagger \tag{3.82}$$

with a non-hermitian Hamiltonian $H_{\mathrm{eff}} = H - (i/2)\sum_i L_i^\dagger L_i$. A single trajectory dynamics is a stochastic dynamics composed of non-unitary time evolution under H_{eff} and quantum jumps by L_i. Let us assume the initial state $\rho_0 = |\psi_0\rangle\langle\psi_0|$ and consider the dynamics of $|\psi_0\rangle$ for infinitesimal duration δt. Up to the first order of δt, the state is stochastically updated by $\exp(-iH_{\mathrm{eff}}\delta t)|\psi_0\rangle/\sqrt{1-p}$ with the probability $1-p$ (non-hermitian dynamics) or by $L_i|\psi_0\rangle/\sqrt{p_i}$ with the probability p_i (quantum jumps). Here, the propabilities p_i and p are given by $p_i = \langle\psi_0|L_i^\dagger L_i|\psi_0\rangle$ and $p = 1 - \sum_i p_i$ respectively. A series of states $|\psi(t)\rangle$ obtained by repeating this procedure m times up to $t = m\delta t$ is called a trajectory. By taking the statistical ensemble of $|\psi(t)\rangle\langle\psi(t)|$ over many trajectories with small δt, we can reproduce the density operator $\rho(t)$ obeying the Lindblad equation Eq. (3.82). We note that all the eigenvalues of H_{eff} have nonpositive imaginary parts, indicating that the non-unitary time evolution by H_{eff} is always lossy. The lost probability due to this non-unitary dynamics corresponds to the probabilities of quantum jumps by L_i.

On the other hand, if $\mathcal{L}_{\mathrm{FM}}^n$ breaks Liouvillianity, the corresponding non-hermitian Hamiltonian becomes $H_{\mathrm{eff}} = H - (i/2)\sum s_i L_i^\dagger L_i$ ($s_i = \pm 1$) where some of $\{s_i\}$ are -1. Thus, H_{eff} can have eigenvalues with positive imaginary parts, and then stochastic dynamics composed of the non-hermitian Hamiltonian time evolution and quantum jumps becomes ill-defined (some of the probabilities p_i become negative). This represents the breakdown of the trajectory method in the absence of Liouvillianity for $\mathcal{L}_f^n$. Each trajectory of the dissipative dynamics is also often in the context of realizing non-hermitian physics under H_{eff} [160]. The Floquet-Magnus expansion $\mathcal{L}_{\mathrm{FM}}^n$ which breaks Liouvillianity can provide broader non-hermitian Hamiltonians compared to static Liouvillians, maybe leading to one of the advantages in Floquet systems.

Chapter 4

Exact Floquet quantum many-body scars under Rydberg blockade

In the previous chapters, we explore Floquet many-body systems that violate some assumptions of Floquet-ETH or the heating problem to find nontrivial phenomena. Chapter 2 considers long-lived quasi-steady states which appear before the trivial steady states, and Chapter 3 deals with dissipative systems which violate the isolation assumed in Floquet-ETH. On the other hand, Floquet-ETH is an empirical law numerically and experimentally confirmed in closed nonintegrable Floquet many-body systems, and hence it has been still a significant task to seek for nontrivial steady states when all the assumptions of Floquet-ETH are satisfied.

In this chapter, we explore closed nonintegrable Floquet systems, expected to satisfy Floquet-ETH. Here, using quantum many-body scars (QMBS) in static systems, we find a series of Floquet setups rigorously violating Floquet-ETH. We consider a periodically-driven one-dimensional chain under Rydberg blockade, and prove the existence of athermal Floquet eigenstates, dubbed Floquet QMBS eigenstates. Our model becomes a counterexample to Floquet-ETH, giving the possibility of nontrivial phenomena even in nonintegrable Floquet systems.

4.1 Periodically-driven model under Rydberg blockade

4.1.1 Setups

The aim of this chapter is to construct nonintegrable counterexamples to Floquet-ETH. In other words, we will find a series of nonintegrable time-periodic Hamiltonian $H(t)$, such that there exists a eigenstate of the Floquet operator $U_f = U(T)$, denoted by $|\varepsilon\rangle$, satisfying

$$\langle\varepsilon|O|\varepsilon\rangle \neq \frac{1}{\dim(\mathcal{H})}\mathrm{Tr}[O] \tag{4.1}$$

for a certain local operator O. The right hand side is the expectation value of infinite temperature states $\rho_\infty = I/\dim(\mathcal{H})$, and this inequality indicates the breakdown of Floquet-ETH (See Section 1.3.3 for the detail). Since counterexamples to ETH are referred to as hosting quantum many-body scars (QMBS), we call their Floquet versions Floquet QMBS.

For simplicity, we first consider a binary drive described by the following Hamiltonian $H(t) = H(t+T)$:

$$H(t) = \begin{cases} H_1 & 0 \leq t < T_1 \\ H_2 & T_1 \leq t < T_1 + T_2 = T. \end{cases} \tag{4.2}$$

In that case, the Floquet operator U_f is given by

$$U_f = e^{-iH_2T_2}e^{-iH_1T_1}. \tag{4.3}$$

For the binary drive, what distinguishes Floquet systems from static systems is to assume the incommutability

$$[H_1, H_2] \neq 0. \tag{4.4}$$

In order to construct nonintegrable Floquet models showing Floquet QMBS, we take a strategy in which we employ two different static Hamiltonians H_1 and H_2 showing static QMBS.

To achieve the above strategy, we first consider static QMBS that can be candidates for the binary drive. Here, we focus on the PXP model realized on a one-dimensional system under Rydberg blockade as the first candidate, and construct other static models inequivalent to the PXP model, named the PY_4P model and the PZ_4P model. Following this strategy for Floquet QMBS, the rest of this chapter is organized as follows. In Section 4.1.2, we discuss some properties of one-dimensional systems under under Rydberg blockade, which are platforms of both the PXP model and the time-periodic model showing Floquet QMBS. In Sections 4.1.3 and 4.1.4, we introduce some static models for the binary drive. The construction of Floquet QMBS begins from Section 4.2. We consider the binary drive composed of different static Hamiltonians hosting QMBS, and mainly focus on two key ingredients for the model to be a nontrivial counterexample to Floquet-ETH, "nonintegrability" and "existence of eigenstates inequivalent to infinite-temperature states." In Section 4.3, we generalize the result, and construct generic time-periodic drives other than the binary drive, which host Floquet QMBS.

4.1.2 Preliminary: One-dimensional system under Rydberg blockade

First, we discuss one-dimensional systems under Rydberg blockade. We consider a L-site chain where each site has two degrees of freedom $|\uparrow\rangle$ and $|\downarrow\rangle$ under OBC. Throughout this chapter, we consider Rydberg atoms, which have been developed as programmable quantum simulators [161, 162]. Then, the two states $|\uparrow\rangle$ and $|\downarrow\rangle$ respectively represent the Rydberg state and the ground state, where the former is a highly-excited state with a large quantum number $n \sim 100$. The dimension of the whole Hilbert space $\mathcal{H}_L$ is 2^L. In Rydberg atom systems, two atoms in Rydberg states feel the van der Waals repulsive interactions $V_{ij} \sim C/|r_i - r_j|^6$ $(C > 0)$, which are controllable by arranging the atom-atom distance with the optical lattice. In the limit of the extremely strong repulsive interactions, pairs of neighboring atoms in Rydberg states are prohibited, referred to as Rydberg blockade. In other words, some configurations which include adjacent excited atoms $|\uparrow\uparrow\rangle$ are excluded from the whole Hilbert space $\mathcal{H}_L$. In one-dimensional systems under Rydberg blockade, we consider such a constrained Hilbert space $\mathcal{H}_{\mathrm{Ryd},L}$ instead of the whole one $\mathcal{H}_L$.

Both the PXP model and the time-periodic models showing QMBS are defined on the constrained space $\mathcal{H}_{\mathrm{Ryd},L}$. Before going to QMBS and Floquet QMBS, we briefly discuss some properties of $\mathcal{H}_{\mathrm{Ryd},L}$. Let $\mathcal{D}_L$ denote the dimension of $\mathcal{H}_{\mathrm{Ryd},L}$, giving the number of possible configurations prohibiting adjacent pairs of $\uparrow$. Under OBC, the number of such configurations satisfies the following recursive relation:

$$\mathcal{D}_1 = 2, \quad \mathcal{D}_2 = 3, \quad \mathcal{D}_{L+2} = \mathcal{D}_{L+1} + \mathcal{D}_L. \tag{4.5}$$

This is nothing but the definition of the Fibonacci sequence, and hence we obtain

$$\mathcal{D}_L = \frac{1}{\sqrt{5}} \left\{ \phi^{L+2} - (1-\phi)^{L+2} \right\}, \quad \phi = \frac{1+\sqrt{5}}{2}. \tag{4.6}$$

Next, with the dimension $\mathcal{D}_L$, we derive some properties of infinite temperature states ρ_∞, which are determined only from the constrained Hilbert space $\mathcal{H}_{\mathrm{Ryd},L}$.

Local observables

The expectation value of a certain observable O at infinite temperature is given by

$$\langle O \rangle_{T=\infty} \equiv \frac{1}{\mathcal{D}_L} \mathrm{Tr}_{\mathcal{H}_{\mathrm{Ryd},L}}[O] = \frac{1}{\mathcal{D}_L} \sum_{\vec{\sigma} \in \mathcal{K}_L} \langle \vec{\sigma}|O|\vec{\sigma}\rangle, \tag{4.7}$$

where $\mathcal{K}_L$ represents a set of classical spin configurations of an L-site chain which includes no adjacent excited states $|\uparrow\uparrow\rangle$. The basis $\{|\vec{\sigma}\rangle\}$ is composed of eigenstates of Pauli z operators,

satisfying $\sigma_i^z |\vec{\sigma}\rangle = \sigma_i |\vec{\sigma}\rangle$ with $\vec{\sigma} = (\sigma_1, \ldots, \sigma_L) \in \mathcal{K}_L$. Here, we focus on the expectation values of the Pauli operators σ_i^x and σ_i^z, and that of the domain wall density $D_b = (1 - \sigma_{2b-1}^z \sigma_{2b}^z)/2$.

Since the operator σ_i^x has only off-diagonal elements in the basis $\{|\vec{\sigma}\rangle\}_{\vec{\sigma}\in\mathcal{K}_L}$, we obtain

$$\langle \sigma_i^x \rangle_{T=\infty} = \frac{1}{\mathcal{D}_L} \sum_{\vec{\sigma}\in\mathcal{K}_L} \langle \vec{\sigma} | \sigma_i^x | \vec{\sigma} \rangle = 0. \tag{4.8}$$

Let us consider the expectation value of σ_i^z, which is diagonal in the basis $\{|\vec{\sigma}\rangle\}_{\vec{\sigma}\in\mathcal{K}_L}$. When we fix the i-th site's state by $|\uparrow\rangle$ (or $|\downarrow\rangle$), the number of possible configurations of the other sites excluding neighboring $\uparrow\uparrow$ is $\mathcal{D}_{i-2} \times \mathcal{D}_{L-i-1}$ (or $\mathcal{D}_{i-1} \times \mathcal{D}_{L-i}$). This results in the following expectation value for finite and infinite systems:

$$\langle \sigma_i^z \rangle_{T=\infty} = \frac{1}{\mathcal{D}_L} \sum_{\vec{\sigma}\in\mathcal{K}_L} \langle \vec{\sigma} | \sigma_i^z | \vec{\sigma} \rangle = \frac{\mathcal{D}_{i-2}\mathcal{D}_{L-i-1} - \mathcal{D}_{i-1}\mathcal{D}_{L-i}}{\mathcal{D}_L}, \quad \lim_{L\to\infty} \left\langle \sigma_{L/2}^z \right\rangle_{T=\infty} = -\frac{1}{\sqrt{5}}. \tag{4.9}$$

In a similar way, we obtain the expectation value of the domain wall density D_b by counting the possible configurations $\vec{\sigma}$ as follows:

$$\langle D_b \rangle_{T=\infty} = \frac{1}{\mathcal{D}_L} \sum_{\vec{\sigma}\in\mathcal{K}_L} \langle \vec{\sigma} | D_b | \vec{\sigma} \rangle = \frac{\mathcal{D}_{2b-3}\mathcal{D}_{2L_b-2b} + \mathcal{D}_{2b-2}\mathcal{D}_{2L_b-2b-1}}{\mathcal{D}_{2L_b}}, \quad \lim_{L_b\to\infty} \left\langle D_{L_b/2} \right\rangle_{T=\infty} = \frac{2}{\sqrt{5}\phi}. \tag{4.10}$$

Here, $L_b \equiv L/2$ represents the number of pairs in the system.

We rigorously derive expectation values of some local observables in infinite temperature states, $\langle \sigma_i^x \rangle_{T=\infty}$, $\langle \sigma_i^z \rangle_{T=\infty}$, and $\langle D_b \rangle_{T=\infty}$. These values are important to confirm the inequivalence between eigenstates and infinite temperature states. We will see that the Floquet operator of the model has some eigenstates $|\varepsilon\rangle$ with the expectation values $\langle \varepsilon | O | \varepsilon \rangle$ ($O = \sigma_i^x, \sigma_i^z, D_b$), different from those at infinite temperature.

Entanglement entropy

For a certain pure state $|\psi\rangle$, whether or not it is thermal can be detected by its entanglement entropy. To see the similarity and difference between the eigenstates $|\varepsilon\rangle$ and (thermal) infinite temperature states in terms of entanglement, we hereby introduce the entanglement entropy of the infinite temperature states. The infinite temperature state of the L-site system is given by $\rho_\infty = I_{\mathcal{D}_L}/\mathcal{D}_L$. Let the left half (the right half) of the system A (B), and then we define the entanglement entropy at infinite temperature S_∞ by

$$S_\infty \equiv -\mathrm{Tr}_A[\rho_\infty^A \log \rho_\infty^A] = -\mathrm{Tr}_B[\rho_\infty^B \log \rho_\infty^B], \tag{4.11}$$

$$\rho_\infty^A \equiv \mathrm{Tr}_B[\rho_\infty], \quad \rho_\infty^B \equiv \mathrm{Tr}_A[\rho_\infty]. \tag{4.12}$$

This definition is chosen so that it can be operationally equivalent to the entanglement entropy for pure states, and we note that the entanglement entropy is not available for generic mixed states and other partitions A, B. From the above definition, we obtain the reduced density matrix as

$$\rho_\infty^A = \frac{1}{\mathcal{D}_L} \left(\mathcal{D}_{L/2-1} \sum_{\vec{\sigma}\in\mathcal{K}_\uparrow} |\vec{\sigma}\rangle \langle\vec{\sigma}| + \mathcal{D}_{L/2} \sum_{\vec{\sigma}\in\mathcal{K}_\downarrow} |\vec{\sigma}\rangle \langle\vec{\sigma}| \right). \tag{4.13}$$

Here, we define $\mathcal{K}_\uparrow$ ($\mathcal{K}_\downarrow$) by a set of configurations of $L/2$ sites having $\uparrow$ ($\downarrow$) at the right edge. Using the equations $|\mathcal{K}_\uparrow| = \mathcal{D}_{L/2-2}$ and $|\mathcal{K}_\downarrow| = \mathcal{D}_{L/2-1}$, we obtain S_∞ as follows:

$$S_\infty = -\frac{\mathcal{D}_{L/2-2}\mathcal{D}_{L/2-1}}{\mathcal{D}_L} \log\left(\frac{\mathcal{D}_{L/2-1}}{\mathcal{D}_L}\right) - \frac{\mathcal{D}_{L/2-2}\mathcal{D}_{L/2-1}}{\mathcal{D}_L} \log\left(\frac{\mathcal{D}_{L/2-1}}{\mathcal{D}_L}\right). \tag{4.14}$$

In particular, when we focus on the thermodynamic limit $L \to \infty$, it obeys the volume law described by

$$\lim_{L\to\infty} \frac{S_\infty}{L} = \frac{1}{2} \log \phi. \tag{4.15}$$

Thus, infinite temperature states, which are thermal, have the volume-law entanglement entropy $S_\infty \sim O(L)$. We will numerically calculate the entanglement entropy of all the eigenstates of the Floquet operator, and compare them with infinite temperature states.

4.1.3 Preliminary: Static PXP model

To construct a periodically-driven model showing Floquet QMBS, we employ multiple static models showing static QMBS, inequivalent to each other. Here, we introduce the PXP model as the first candidate of the static models [46]. We assume the even system size L and OBC. As briefly discussed in Section 1.3.2, the PXP model is given by

$$H_{\mathrm{PXP}} = \sum_{i=2}^{L-1} P_{i-1}\sigma_i^x P_{i+1} + \sigma_1^x P_2 + P_{L-1}\sigma_L^x, \quad P_i = (I - |\uparrow\rangle\langle\uparrow|)_i, \tag{4.16}$$

defined on the constrained Hilbert space $\mathcal{H}_{\mathrm{Ryd},L}$. For the later discussion, we focus on the exact QMBS eigenstates of the PXP model. We can rigorously derive some eigenstates of the PXP model as follows [47].

Theorem 4.1.1. (Exact QMBS eigenstates of the PXP model [47])
Let us define four matrix product states $|\Gamma^x_{\alpha\beta}\rangle$ $(\alpha,\beta = 1,2)$ by

$$|\Gamma^x_{\alpha\beta}\rangle = \sum_{\vec{\sigma}\in\mathcal{K}_L} \vec{u}_\alpha^\dagger B^{\sigma_1}C^{\sigma_2}\dots B^{\sigma_{L-1}}C^{\sigma_L}\vec{u}_\beta\,|\vec{\sigma}\rangle \tag{4.17}$$

$$B^\uparrow = \sqrt{2}\begin{pmatrix} 0 & 0 & 0 \\ 1 & 0 & 1 \end{pmatrix}, \quad B^\downarrow = \begin{pmatrix} 1 & 0 & 0 \\ 0 & 1 & 0 \end{pmatrix}, \tag{4.18}$$

$$C^\uparrow = \sqrt{2}\begin{pmatrix} 1 & 0 \\ 0 & 0 \\ -1 & 0 \end{pmatrix}, \quad C^\downarrow = \begin{pmatrix} 0 & -1 \\ 1 & 0 \\ 0 & 0 \end{pmatrix}, \tag{4.19}$$

$$\vec{u}_1 = \frac{1}{\sqrt{2}}\begin{pmatrix} 1 \\ 1 \end{pmatrix}, \qquad \vec{u}_2 = \frac{1}{\sqrt{2}}\begin{pmatrix} 1 \\ -1 \end{pmatrix}. \tag{4.20}$$

Then, these four states become exact eigenstates of the PXP Hamiltonian H_{PXP} as

$$\begin{aligned} &H_{\mathrm{PXP}}\,|\Gamma^x_{11}\rangle = 0, \quad H_{\mathrm{PXP}}\,|\Gamma^x_{12}\rangle = \sqrt{2}\,|\Gamma^x_{12}\rangle\,, \\ &H_{\mathrm{PXP}}\,|\Gamma^x_{22}\rangle = 0, \quad H_{\mathrm{PXP}}\,|\Gamma^x_{21}\rangle = -\sqrt{2}\,|\Gamma^x_{21}\rangle\,. \end{aligned} \tag{4.21}$$

While the original proof of this theorem is given in Ref. [47], we provide another simple proof in Appendix of this chapter (See Section 4.5). In Eq. (4.17), we can replace the summation over $\mathcal{K}_L$ by the one over all the configurations of $\vec{\sigma}$, since configurations which include neighboring up states $\uparrow\uparrow$ have no contribution due to $B^\uparrow C^\uparrow = O$ and $C^\uparrow B^\uparrow = O$.

With the numerical calculation of the level statistics, the PXP model is considered to be nonintegrable [46], thereby expected to satisfy ETH. Nevertheless, as discussed later, the four eigenstates $|\Gamma^x_{\alpha\beta}\rangle$ are inequivalent to thermal equilibrium states in terms of some local observable, which indicates the breakdown of ETH. These four eigenstates, having athermal properties, $|\Gamma^x_{\alpha\beta}\rangle$ are called exact QMBS eigenstates while other typical eigenstates are thermal as expected from ETH.

4.1.4 Static $\mathrm{PY_4P}$ model and $\mathrm{PZ_4P}$ model

In order to realize Floquet QMBS, we prepare another static model H_2 showing static QMBS, which is inequivalent to the PXP model in that $[H_{\mathrm{PXP}}, H_2] \neq 0$ is satisfied. Although there exist various types of static QMBS, a tactless choice without considering the property of the PXP model leads to the satisfaction of Floquet-ETH. As promising candidates for realizing Floquet-QMBS with the breakdown of Floquet-ETH, we construct two static models, dubbed the $\mathrm{PY_4P}$ model and the $\mathrm{PZ_4P}$ models.

$\mathrm{PY_4P}$ model

We first introduce the $\mathrm{PY_4P}$ model, showing static QMBS. We assume that the number of the sites L is a multiple of 4. Then, the $\mathrm{PY_4P}$ Hamiltonian, defined on the constrained Hilbert space

$\mathcal{H}_{\mathrm{Ryd},L}$, is given by

$$H_{\mathrm{PY_4P}} = \sum_{i=2}^{L-1} c_i P_{i-1}\sigma_i^y P_{i+1} + \sigma_1^y P_2 + P_{L-1}\sigma_L^y, \tag{4.22}$$

$$c_i = \sqrt{2}\cos\left(\frac{i\pi}{2} - \frac{\pi}{4}\right). \tag{4.23}$$

This model possesses quadruple lattice-periodicity, different from the PXP model. In a similar way to the PXP model, we derive exact eigenstates of the $\mathrm{PY_4P}$ model as follows.

Theorem 4.1.2. (Exact QMBS eigenstates of the $\mathrm{PY_4P}$ model)
We define four states $|\Gamma^y_{\alpha\beta}\rangle$ $(\alpha,\beta = 1,2)$ by

$$|\Gamma^y_{\alpha\beta}\rangle = \sum_{\vec{\sigma}} \vec{v}_\alpha^\dagger B^{\sigma_1}C^{\sigma_2}\dots B^{\sigma_{L-1}}C^{\sigma_L}\vec{v}_\beta\,|\vec{\sigma}\rangle\,, \tag{4.24}$$

$$\vec{v}_1 = \frac{1}{\sqrt{2}}\begin{pmatrix}1\\ i\end{pmatrix}, \qquad \vec{v}_2 = \frac{1}{\sqrt{2}}\begin{pmatrix}1\\ -i\end{pmatrix}, \tag{4.25}$$

where B^σ and C^σ are given by Eqs. (4.18) and (4.19). Then, these are exact eigenstates of the $\mathrm{PY_4P}$ Hamiltonian $H_{\mathrm{PY_4P}}$, that is,

$$\begin{aligned} &H_{\mathrm{PY_4P}}\,|\Gamma^y_{11}\rangle = 0, \quad H_{\mathrm{PY_4P}}\,|\Gamma^y_{12}\rangle = \sqrt{2}\,|\Gamma^y_{12}\rangle\,,\\ &H_{\mathrm{PY_4P}}\,|\Gamma^y_{22}\rangle = 0, \quad H_{\mathrm{PY_4P}}\,|\Gamma^y_{21}\rangle = -\sqrt{2}\,|\Gamma^y_{21}\rangle\,. \end{aligned} \tag{4.26}$$

Proof

We provide the proof of Eq. (4.26). Let us consider the projection to the constrained Hilbert space $\mathcal{H}_{\mathrm{Ryd},L}$, given by

$$P_{\mathrm{Ryd},L} = \prod_{i=1}^{L-1}\left(1 - |\uparrow\uparrow\rangle\langle\uparrow\uparrow|\right)_{i,i+1}. \tag{4.27}$$

In the constrained Hilbert space, each term of the $\mathrm{PY_4P}$ Hamiltonian is represented by

$$\begin{aligned} P_{\mathrm{Ryd},L}P_{i-1}\sigma_i^y P_{i+1}P_{\mathrm{Ryd},L} &= iP_{\mathrm{Ryd},L}(1-|\uparrow\rangle\langle\uparrow|)_{i-1}(|\downarrow\rangle\langle\uparrow| - |\uparrow\rangle\langle\downarrow|)_i(1-|\uparrow\rangle\langle\uparrow|)_{i+1}P_{\mathrm{Ryd},L}\\ &= iP_{\mathrm{Ryd},L}(|\downarrow\rangle\langle\uparrow| - |\uparrow\rangle\langle\downarrow|)_i P_{\mathrm{Ryd},L}. \end{aligned} \tag{4.28}$$

in the bulk. The edge terms $\sigma_1^y P_2$ and $P_{L-1}\sigma_L^y$ give the same results. Thus, we should show that the four states $|\Gamma^y_{\alpha\beta}\rangle$ are the eigenstates of the $\mathrm{PY_4P}$ Hamiltonian in the constrained Hilbert space, given by

$$P_{\mathrm{Ryd},L}H_{\mathrm{PY_4P}}P_{\mathrm{Ryd},L} = \sum_{i=1}^{L} c_i P_{\mathrm{Ryd},L}\sigma_i^y P_{\mathrm{Ryd},L}, \quad c_i = \sqrt{2}\cos\left(\frac{i\pi}{2} - \frac{\pi}{4}\right). \tag{4.29}$$

On the other hand, the four states $|\Gamma^y_{\alpha\beta}\rangle$ given by Eq. (4.24) can be written in the following form:

$$|\Gamma^y_{\alpha\beta}\rangle = \vec{v}_\alpha^\dagger B'_1 C'_2 \dots B'_{L-1}C'_L\vec{v}_\beta, \tag{4.30}$$

$$B'_i = \begin{pmatrix} |\downarrow\rangle_i & 0 & 0\\ \sqrt{2}\,|\uparrow\rangle_i & |\downarrow\rangle_i & \sqrt{2}\,|\uparrow\rangle_i\end{pmatrix}, \quad C'_i = \begin{pmatrix} \sqrt{2}\,|\uparrow\rangle_i & -|\downarrow\rangle_i\\ |\downarrow\rangle_i & 0\\ -\sqrt{2}\,|\uparrow\rangle_i & 0\end{pmatrix}. \tag{4.31}$$

Considering the relations $B^\uparrow C^\uparrow = 0$ and $C^\uparrow B^\uparrow = 0$ from Eqs. (4.18) and (4.19), the states $|\Gamma^y_{\alpha\beta}\rangle$ do not include $\uparrow\uparrow$, which ensures $P_{\mathrm{Ryd},L}\,|\Gamma^y_{\alpha\beta}\rangle = |\Gamma^y_{\alpha\beta}\rangle$. Let us compute the action of $P_{\mathrm{Ryd},L}\sigma_i^y P_{\mathrm{Ryd},L}$

on $|\Gamma^y_{\alpha\beta}\rangle$. For an odd integer i, we obtain

$$\begin{aligned} P_{\mathrm{Ryd},L}\sigma^y_i P_{\mathrm{Ryd},L}\,|\Gamma^y_{\alpha\beta}\rangle &= P_{\mathrm{Ryd},L}\vec{v}^\dagger_\alpha B'_1\dots C'_{i-1}(\sigma^y_i B'_i C'_{i+1})B'_{i+2}\dots C'_L\vec{v}_\beta \\ &= P_{\mathrm{Ryd},L}\vec{v}^\dagger_\alpha B'_1\dots C'_{i-1}F^y_{i,i+1}B'_{i+2}\dots C'_L\vec{v}_\beta, \qquad (4.32) \\ F^y_{i,i+1} &= \begin{pmatrix} 0 & i\,|{\uparrow\downarrow}\rangle_{i,i+1} \\ -i\,|{\uparrow\downarrow}\rangle_{i,i+1} & -\sqrt{2}\,|{\downarrow\downarrow}\rangle_{i,i+1} \end{pmatrix} \\ &= YB'_iC'_{i+1} - B_i\tilde{Y}C'_{i+1}, \qquad (4.33) \\ Y &= \frac{1}{\sqrt{2}}\begin{pmatrix} 0 & -i \\ i & 0 \end{pmatrix}, \quad \tilde{Y} = \frac{1}{\sqrt{2}}\begin{pmatrix} 0 & -i & 0 \\ -i & 0 & -2i \\ 0 & 2i & 0 \end{pmatrix}. \qquad (4.34) \end{aligned}$$

In a similar way, for an even integer i,

$$\begin{aligned} P_{\mathrm{Ryd},L}\sigma^y_i P_{\mathrm{Ryd},L}\,|\Gamma^y_{\alpha\beta}\rangle &= P_{\mathrm{Ryd},L}\vec{v}^\dagger_\alpha B'_1\dots C'_{i-2}(B'_{i-1}\sigma^y_i C'_i)B'_{i+1}\dots C'_L\vec{v}_\beta \\ &= P_{\mathrm{Ryd},L}\vec{v}^\dagger_\alpha B'_1\dots C'_{i-2}\tilde{F}^y_{i-1,i}B'_{i+1}\dots C'_L\vec{v}_\beta, \qquad (4.35) \\ \tilde{F}^y_{i-1,i} &= \begin{pmatrix} \sqrt{2}i\,|{\downarrow\downarrow}\rangle_{i-1,i} & i\,|{\downarrow\uparrow}\rangle_{i-1,i} \\ -i\,|{\downarrow\uparrow}\rangle_{i-1,i} & 0 \end{pmatrix} \\ &= -B'_{i-1}\tilde{Y}C'_i - B'_{i-1}C'_iY \qquad (4.36) \end{aligned}$$

is obtained. When the size of the system L is a multiple of 4, the alternately varying coefficients $\{c_i\}_{i=1}^L$ ($c_1 = c_5 = \ldots = 1, c_2 = c_6 = \ldots = -1, c_3 = c_7 = \ldots = -1, c_4 = c_8 = \ldots = 1$) lead to the cancellation of the middle terms in $\sum_{i=1}^L c_i P_{\mathrm{Ryd},L}\sigma^y_i P_{\mathrm{Ryd},L}\,|\Gamma^y_{\alpha\beta}\rangle$ under the expansion of $F^y_{i,i+1}$ and $\tilde{F}^y_{i-1,i}$ by Eqs. (4.33) and (4.36). As a result, we arrive at

$$\begin{aligned} P_{\mathrm{Ryd},L}H_{\mathrm{PY_4P}}P_{\mathrm{Ryd},L}\,|\Gamma^y_{\alpha\beta}\rangle &= P_{\mathrm{Ryd},L}\vec{v}^\dagger_\alpha(YB'_1C'_2\dots B'_{L-1}C'_L - B'_1C'_2\dots B'_{L-1}C'_LY)\vec{v}_\beta \\ &= \frac{1}{\sqrt{2}}\left\{(-1)^{\alpha-1} - (-1)^{\beta-1}\right\}|\Gamma^x_{\alpha\beta}\rangle\,, \qquad (4.37) \end{aligned}$$

where we have used the fact that the vectors $\vec{v}_\alpha$ (α) [See Eq. (4.25)] are eigenvectors of Y [See Eq. (4.34)] with eigenvalues $(-1)^{\alpha-1}$. This completes the proof of Eq. (4.26). □

The $\mathrm{PY_4P}$ Hamiltonian $H_{\mathrm{PY_4P}}$ is related to the PXP Hamiltonian H_{PXP} by a unitary transformation as follows:

$$H_{\mathrm{PY_4P}} = \mathcal{U}_Z H_{\mathrm{PXP}}\mathcal{U}_Z^\dagger, \quad H_{\mathrm{PXP}} = -\mathcal{U}_Z H_{\mathrm{PY_4P}}\mathcal{U}_Z^\dagger, \quad \mathcal{U}_Z = \exp\left(-i\frac{\pi}{4}\sum_{i=1}^L c_i\sigma^z_i\right). \qquad (4.38)$$

Thus, properties of the PXP model as a static QMBS are inherited to the $\mathrm{PY_4P}$ model, including ithe nonintegrability, the violation of ETH, and the anomalously long athermal oscillation from a $\mathbb{Z}_2$-ordered state.

$\mathrm{PZ_4P}$ model

We introduce another static model dubbed the $\mathrm{PZ_4P}$ model. The $\mathrm{PZ_4P}$ Hamiltonian under OBC is defined by

$$\begin{aligned} H_{\mathrm{PZ_4P}} &= -\sqrt{2}\left(\sum_{i=2}^{L-1} c_i P_{i-1}Q_iP_{i+1} + Q_1P_2 + P_{L-1}Q_L\right), \qquad (4.39) \\ Q_i &= I_i - P_i = (1+\sigma^z_i)/2, \qquad (4.40) \end{aligned}$$

where the coefficient c_i is given by Eq. (4.23). As well as the $\mathrm{PY_4P}$ model, it has the following four eigenstates which satisfy

$$\begin{aligned} &H_{\mathrm{PZ_4P}}\,|\Gamma^z_{11}\rangle = 0, \quad H_{\mathrm{PZ_4P}}\,|\Gamma^z_{12}\rangle = \sqrt{2}\,|\Gamma^z_{12}\rangle\,, \\ &H_{\mathrm{PZ_4P}}\,|\Gamma^z_{22}\rangle = 0, \quad H_{\mathrm{PZ_4P}}\,|\Gamma^z_{21}\rangle = -\sqrt{2}\,|\Gamma^z_{21}\rangle\,, \end{aligned} \qquad (4.41)$$

where the four eigenstates $|\Gamma^z_{\alpha\beta}\rangle$ $(\alpha,\beta=1,2)$ are given by

$$|\Gamma^z_{\alpha\beta}\rangle = \sum_{\vec{\sigma}} \vec{w}^\dagger_\alpha B^{\sigma_1} C^{\sigma_2} \dots B^{\sigma_{L-1}} C^{\sigma_L} \vec{w}_\beta \, |\vec{\sigma}\rangle \,, \quad \vec{w}_1 = \begin{pmatrix} 1 \\ 0 \end{pmatrix}, \quad \vec{w}_2 = \begin{pmatrix} 0 \\ 1 \end{pmatrix}. \tag{4.42}$$

The derivation is done in the same way as that for the $\mathrm{PY_4P}$ model. While the PXP model and the $\mathrm{PY_4P}$ model are referred to as static QMBS, the $\mathrm{PZ_4P}$ model is not due to its integrability. It has a macroscopic number of conserved quantities $\{\sigma^z_i\}_{i=1}^L$, satisfying $[\sigma^z_i, H_{\mathrm{PZ_4P}}]=0$. Although the $\mathrm{PZ_4P}$ model is a trivial model in terms of QMBS, the four eigenstates $|\Gamma^z_{\alpha\beta}\rangle$ gives properties similar to $|\Gamma^x_{\alpha\beta}\rangle$ and $|\Gamma^y_{\alpha\beta}\rangle$. Thus, we refer to $|\Gamma^z_{\alpha\beta}\rangle$ as the exact QMBS eigenstates. The $\mathrm{PZ_4P}$ model can provide a variety of nontrivial Floquet QMBS when combined with the PXP model and the $\mathrm{PY_4P}$ model, as we will discuss later in Section 4.3.

4.1.5 Local observables in the exact QMBS eigenstates

Let us calculate expectation values of some local observables in the exact QMBS eigenstates $|\Gamma^\nu_{\alpha\beta}\rangle$ $(\nu = x,y,z)$. The results are used to confirm that the PXP model and the $\mathrm{PY_4P}$ model violate ETH, giving static QMBS. In addition, they are also necessary for rigorously concluding the violation of Floquet-ETH in the periodically-driven model.

To compute local observables, we first introduce the block description, where the b-th block is composed of the $(2b-1)$-th and the $2b$-th sites for $b=1,2,\dots,L_b$ $(L_b=L/2)$. Each block has three states $l=\uparrow\downarrow$, $o=\downarrow\downarrow$, $r=\downarrow\uparrow$, while $\uparrow\uparrow$ is excluded by Rydberg blockade. Then, the exact QMBS eigenstates are rewritten in the following form,

$$|\Gamma^\nu_{\alpha\beta}\rangle = \sum_{\vec{s}} (\vec{u}^\nu_\alpha)^\dagger A^{s_1} \dots A^{s_{L_b}} \vec{u}^\nu_\beta \, |\vec{s}\rangle \,, \tag{4.43}$$

$$A^l = \begin{pmatrix} 0 & 0 \\ 0 & -\sqrt{2} \end{pmatrix}, \quad A^o = \begin{pmatrix} 0 & -1 \\ 1 & 0 \end{pmatrix}, \quad A^r = \begin{pmatrix} \sqrt{2} & 0 \\ 0 & 0 \end{pmatrix}, \tag{4.44}$$

with $\vec{u}^x_\alpha = \vec{u}_\alpha$, $\vec{u}^y_\alpha = \vec{v}_\alpha$, and $\vec{u}^z_\alpha = \vec{w}_\alpha$. The vector $\vec{s}=(s_1,\dots,s_{L_b})$ designates the basis of each block by $s_b = l,o,r$. The relation $A^r A^l = 0$ indicates the exclusion of $\uparrow\uparrow$.

We consider a local observable O_b, acting on the b-th block, and its expectation value. Then, we define

$$F^s = \sum_{s'=l,o,r} (O_b)_{ss'} A^{s'}. \tag{4.45}$$

The matrix elements $\langle\Gamma^\nu_{\alpha\beta}|O_b|\Gamma^\nu_{\alpha'\beta'}\rangle$ can be computed by

$$\begin{aligned}
\langle\Gamma^\nu_{\alpha\beta}|O_b|\Gamma^\nu_{\alpha'\beta'}\rangle &= \sum_{\vec{s}} \{(\vec{u}^\nu_\alpha)^\dagger A^{s_1} \dots A^{s_{L_b}} \vec{u}^\nu_\beta\}^* \{(\vec{u}^\nu_{\alpha'})^\dagger A^{s_1} \dots F^{s_b} \dots A^{s_{L_b}} \vec{u}^\nu_{\beta'}\} \\
&= (\vec{U}^\nu_{\alpha\alpha'})^\dagger (E_{AA})^b E_{AF} (E_{AA})^{L_b-b-1} (\vec{U}^\nu_{\beta\beta'}), \qquad (4.46) \\
E_{AA} &\equiv \sum_s (A^s)^* \otimes A^s = \begin{pmatrix} 2 & 0 & 0 & 1 \\ 0 & 0 & -1 & 0 \\ 0 & -1 & 0 & 0 \\ 1 & 0 & 0 & 2 \end{pmatrix}, \qquad (4.47) \\
E_{AF} &\equiv \sum_s (A^s)^* \otimes F^s, \quad \vec{U}^\nu_{\alpha\alpha'} \equiv (\vec{u}^\nu_\alpha)^* \otimes \vec{u}^\nu_{\alpha'}. \qquad (4.48)
\end{aligned}$$

The norm and the overlap of $\{|\Gamma^\nu_{\alpha\beta}\rangle\}_{\alpha,\beta=1,2}$ are evaluated by setting $O_b = I_b$, which results in

$$\langle\Gamma^\nu_{11}|\Gamma^\nu_{11}\rangle = \langle\Gamma^\nu_{22}|\Gamma^\nu_{22}\rangle = \frac{1}{2}(3^{L_b}+1), \quad \langle\Gamma^\nu_{12}|\Gamma^\nu_{12}\rangle = \langle\Gamma^\nu_{21}|\Gamma^\nu_{21}\rangle = \frac{1}{2}(3^{L_b}-1), \tag{4.49}$$

$$\langle\Gamma^\nu_{11}|\Gamma^\nu_{12}\rangle = \langle\Gamma^\nu_{11}|\Gamma^\nu_{21}\rangle = \langle\Gamma^\nu_{22}|\Gamma^\nu_{12}\rangle = \langle\Gamma^\nu_{22}|\Gamma^\nu_{21}\rangle = \langle\Gamma^\nu_{12}|\Gamma^\nu_{21}\rangle = 0, \quad \langle\Gamma^\nu_{11}|\Gamma^\nu_{22}\rangle = 1 \tag{4.50}$$

for even L_b and $\nu = x,y,z$. Thus, under the renormalization by $|\tilde{\Gamma}^\nu_{\alpha\beta}\rangle \equiv |\Gamma^\nu_{\alpha\beta}\rangle / || \, |\Gamma^\nu_{\alpha\beta}\rangle \, ||$, the four eigenstates $|\tilde{\Gamma}^\nu_{\alpha\beta}\rangle$ $(\alpha,\beta=1,2)$ become orthonormal with one another.

Here, we focus on the Pauli operators σ_i^x, σ_i^z and the domain wall density D_b. The Pauli x [z] operator for the b-th block is represented by $O_b = \sigma_{2b-1}^x + \sigma_{2b}^x = (|l\rangle\langle o| + |r\rangle\langle o| + \text{h.c.})_b$ [$O_b = \sigma_{2b-1}^x + \sigma_{2b}^x = -2(|o\rangle\langle o|)_b$]. Using Eqs. (4.45)-(4.50), their matrix elements in the renormalized eigenstates $|\tilde{\Gamma}_{\alpha\beta}^x\rangle$, which include their expectation values, are given by

$$\lim_{L\to\infty}\sum_{i=1}^{L}\langle\tilde{\Gamma}_{\alpha\beta}^x|\sigma_i^x|\tilde{\Gamma}_{\alpha'\beta'}^x\rangle = \frac{1}{\sqrt{2}}\{(-1)^{\alpha-1}-(-1)^{\beta-1}\}\delta_{\alpha\alpha'}\delta_{\beta\beta'}, \tag{4.51}$$

$$\lim_{L\to\infty}\frac{1}{L}\sum_{i=1}^{L}\langle\tilde{\Gamma}_{\alpha\beta}^x|\sigma_i^z|\tilde{\Gamma}_{\alpha'\beta'}^x\rangle = -\frac{1}{6}\delta_{\alpha\alpha'}\delta_{\beta\beta'}, \tag{4.52}$$

in the thermodynamic limit. The matrix elements in $|\tilde{\Gamma}_{\alpha\beta}^\nu\rangle$ for $\nu = y, z$ are computed in the same way. On the other hand, the domain wall density, given by $D_b = (1-\sigma_{2b-1}^z\sigma_{2b}^z)/2 = (|l\rangle\langle l| + |r\rangle\langle r|)_b$, has the following matrix elements,

$$\lim_{L_b\to\infty}\langle\tilde{\Gamma}_{\alpha\beta}^\nu|D_b|\tilde{\Gamma}_{\alpha'\beta'}^\nu\rangle = \frac{2}{3}\delta_{\alpha\alpha'}\delta_{\beta\beta'}, \quad \nu = x, y, z. \tag{4.53}$$

We compare these results with the infinite-temperature values in Section 4.2.2. We focus on the PXP model $H_{\rm PXP}$ and one of the renormalized exact QMBS eigenstates, $|\tilde{\Gamma}_{11}^x\rangle$, which has zero energy $\langle\tilde{\Gamma}_{11}^x|H_{\rm PXP}|\tilde{\Gamma}_{11}^x\rangle = 0$. On the other hand, when the thermal state $\rho_\beta = e^{-\beta H_{\rm PXP}}/\mathrm{Tr}[e^{-\beta H_{\rm PXP}}]$ has zero energy with satisfying $\mathrm{Tr}[H_{\rm PXP}\rho_\beta] = 0$, the temperature $1/\beta$ should be infinite due to $\mathrm{Tr}[H_{\rm PXP}] = 0$. Then, ETH predicts that the eigenstate $|\tilde{\Gamma}_{11}^x\rangle$ should be indistinguishable from the infinite temperature state ρ_∞ in any local observable. However, considering the infinite-temperature results Eqs. (4.9) and (4.10), the eigenstate $|\tilde{\Gamma}_{11}^x\rangle$ has expectation values different from those of ρ_∞ in the local observables σ_i^x and D_b, suggesting the breakdown of ETH. In the same way, the $\mathrm{PY_4P}$ model also possesses eigenstates which are distinguishable from the corresponding thermal states, exemplifying a static model violating ETH, referred to as QMBS.

4.2 Exact Floquet quantum many-body scars (Floquet QMBS)

In this section, we construct a periodically-driven model composed of static Hamiltonians showing QMBS, and prove that it shows Floquet QMBS, exemplifying a counterexample to Floquet-ETH.

We consider a L-site chain, where L is a multiple of 4. Based on the strategy in Section 4.1.1, we focus on the following time-periodic Hamiltonian,

$$H(t) = \begin{cases} H_{\rm PXP} & 0 \le t < T_1 \\ H_{\rm PY_4P} & T_1 \le t < T_1 + T_2 = T, \end{cases} \tag{4.54}$$

defined on the constrained Hilbert space $\mathcal{H}_{\mathrm{Ryd},L}$. The Floquet operator is written by

$$U_f = e^{-iH_{\rm PY_4P}T_2}e^{-iH_{\rm PXP}T_1}. \tag{4.55}$$

Here, T_1 and T_2 are arbitrary except for the case where either one of them is zero (there is no need for fine-tuning of them).

We specify the symmetries underlying in the model. First, the model has an inversion symmetry I, which maps each i-th site to the $(L-i+1)$-th site. Since both the PXP and $\mathrm{PY_4P}$ models are invariant under I, the Floquet operator satisfies $[I, U_f] = 0$, which dictates that U_f can be block-diagonalized in the eigenvalues of $I = \pm 1$. Second, a nonlocal chiral symmetry $\mathcal{C}$, designated by

$$\mathcal{C}U_f\mathcal{C}^\dagger = U_f^\dagger, \quad \mathcal{C} = \left(\prod_i \sigma_i^z\right)e^{iH_{\rm PY_4P}T_2}, \tag{4.56}$$

is also respected. The chiral symmetry $\mathcal{C}$ makes the spectrum of quasienergy $\{\varepsilon\}$ symmetric to $\varepsilon = 0$. In addition, in the case of $T_1 = T_2$, the model also respects a time-reversal symmetry (TRS), described by

$$\mathcal{U}_Z U_f^* \mathcal{U}_Z^\dagger = U_f^\dagger, \quad \mathcal{U}_Z = \exp\left(-i\frac{\pi}{4}\sum_{i=1}^{L} c_i\sigma_i^z\right), \tag{4.57}$$

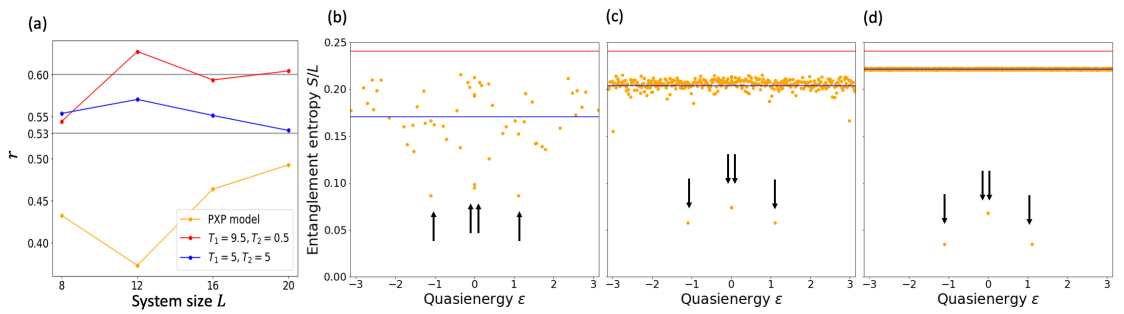

Figure 4.1: (a) Level statistics of the PXP model (the yellow line) and the periodically driven model (the red and blue lines). In the Floquet case, it rapidly approaches a value close to 0.6 ($T_1 = 9.5, T_2 = 0.5$) or 0.53 ($T_1 = T_2 = 5$, with TRS) as the system size grows. Both results imply the nonintegrability of the driven model. (b)-(d): Entanglement entropy per length for each Floquet eigenstate of a different system size (b) $L = 8$, (c) $L = 12$, and (d) $L = 20$. We use $T_1 = 9.5$ and $T_2 = 0.5$ as the parameters. The blue (lower solid) lines, representing the mean values of entanglement entropy, approach the red (upper solid) lines which denote the one at infinite temperature as the system size increases. The four marked states designated by the arrows (two points are degenerated at $\varepsilon = 0$) remain low-entangled since they are exact scar eigenstates of the periodically driven model within the embedded subspace $\mathcal{S}$.

This comes from the fact that the PY_4P model is unitarily equivalent to the PXP model [See Eq. (4.38)].

Floquet-ETH is believed to be valid for nonintegrable systems, dictating that any eigenstate of the Floquet-operator becomes equivalent to infinite temperature states. Thus, in the following subsections, we examine the nonintegrablity of the model and explore the existence of athermal eigenstates of the Floquet operator, so that the model can be regarded as a nontrivial example rigorously violating Floquet-ETH.

4.2.1 Spectrum and entanglement as a signature of nonintegrablity

Here, we numerically confirm that the Floquet system described by the Hamiltonian Eq. (4.54) is nonintegrable. As discussed in Section 1.3.3, we compute the level spacing ratio

$$r_n = \min\left(\frac{s_n}{s_{n+1}}, \frac{s_{n+1}}{s_n}\right), \quad s_n = \varepsilon_{n+1} - \varepsilon_n. \tag{4.58}$$

from the quasienergy spectrum $\{\varepsilon_n\}_n$, determined by the Floquet operator U_f. Considering the inversion symmetry I, we pick up the eigenstates $|\varepsilon\rangle$ in the inversion-plus sector, satisfying $I|\varepsilon\rangle = |\varepsilon\rangle$, and compute r_n from them. The level statistics $\{r_n\}_n$ determines whether or not the model is integrable.

Figure 4.1 shows the numerical results calculated by the exact diagonalization for finite-size systems. The red solid line shows the spectrally-averaged value $r = \langle r_n \rangle$ in the case of $T_1 = 9.5$, $T_2 = 0.5$ without TRS. As the system size L increases, it approaches the Circular Unitary Ensemble (CUE) value 0.6, supporting that the model is nonintegrable. On the other hand, the time-reversal symmetric case with $T_1 = T_2 = 5$, has the average r approaching 0.53, as described by the blue solid line. This is the Circular Orthogonal Ensemble (COE) value, which ensures the nonintegrability of systems with TRS.

We also demonstrate the nonintegrability in terms of entanglement entropy of each Floquet eigenstate. Entanglement entropy of a given state $|\psi\rangle$ is defined by

$$S[\psi] = -\mathrm{Tr}_A[\rho_A \log \rho_A], \quad \rho_A = \mathrm{Tr}_B |\psi\rangle\langle\psi|, \tag{4.59}$$

where the subsystem A (B) represents the left (right) half of the system. We numerically compute entanglement entropy for all the eigenstates of the Floquet operator by the exact diagonalization. Figures 4.1 (b)-(d) show the results for the different system size $L = 8, 12, 20$. Each yellow point

shows quasienergy and entanglement entropy of each eigenstate $|\varepsilon\rangle$, and the averaged value of the entanglement entropy is represented by the blue solid line. We see that, with the increasing system size, almost all the eigenstates become featureless in terms of entanglement entropy with approaching the infinite temperature value computed in Section 4.1.2 (the red solid line). This behavior, showing the volume law of entanglement entropy, is consistent with other generic nonintegrable systems. We note that there exist four eigenstates which do not obey the volume law, designated by the black arrows in Figs. 4.1 (b)-(d). As discussed later, these are the exact Floquet QMBS eigenstates which are inequivalent to infinite temperature states.

Based on the above calculation of the level statistics, the Floquet system $H(t)$, described by Eq. (4.54), is nonintegrable. Thus, by showing that this nonintegrable model has athermal eigenstates, it is proven to be a nontrivial counterexample to Floquet-ETH in contrast to trivial ones which are integrable or localized. We show this, with referring to it as the exact Floquet QMBS.

4.2.2 Exact Floquet QMBS eigenstates

Now, we prove the existence of athermal eigenstates of the Floquet operator U_f, indicating the violation of Floquet-ETH. In addition, we also discuss the real-time dynamics of the model. We show that it shows thermal or athermal steady states depending on the initial states accompanied by the exact Floquet QMBS eigenstates, while other generic nonintegrable models always show relaxation to infinite temperature regardless of the initial states.

Existence of the exact Floquet QMBS eigenstates

Let us derive the exact Floquet QMBS eigenstates by using the properties of the PXP and the PY_4P models in Sections 4.1.3 and 4.1.4. We define the four-dimensional embedded subspace $\mathcal{S}$ by

$$\mathcal{S} = \mathrm{span}(\{|\Gamma^x_{11}\rangle, |\Gamma^x_{12}\rangle, |\Gamma^x_{21}\rangle, |\Gamma^x_{22}\rangle\}). \tag{4.60}$$

Within the subspace $\mathcal{S}$, thermalization does not take place under $\exp(-iH_{\mathrm{PXP}}T_1)$ by its definition. On the other hand, using Eqs. (4.17) and (4.24), we obtain

$$\begin{aligned}
|\Gamma^y_{11}\rangle &= \frac{1}{2}(|\Gamma^x_{11}\rangle + i\,|\Gamma^x_{12}\rangle - i\,|\Gamma^x_{21}\rangle + |\Gamma^x_{22}\rangle),\\
|\Gamma^y_{12}\rangle &= \frac{1}{2}(i\,|\Gamma^x_{11}\rangle + |\Gamma^x_{12}\rangle + |\Gamma^x_{21}\rangle - i\,|\Gamma^x_{22}\rangle),\\
|\Gamma^y_{21}\rangle &= \frac{1}{2}(-i\,|\Gamma^x_{11}\rangle + |\Gamma^x_{12}\rangle + |\Gamma^x_{21}\rangle + i\,|\Gamma^x_{22}\rangle),\\
|\Gamma^y_{22}\rangle &= \frac{1}{2}(|\Gamma^x_{11}\rangle - i\,|\Gamma^x_{12}\rangle + i\,|\Gamma^x_{21}\rangle + |\Gamma^x_{22}\rangle).
\end{aligned} \tag{4.61}$$

Since this transformation is invertible, the subspace $\mathcal{S}$ is identical to the one spanned by $\{|\Gamma^y_{\alpha\beta}\rangle\}_{\alpha,\beta=1,2}$. Thus, thermalization does not take place in the subspace $\mathcal{S}$ also under $\exp(-iH_{\mathrm{PY_4P}}T_2)$, and hence we can conclude the absence of thermalization in the subspace $\mathcal{S}$ under the Floquet operator U_f.

The above discussion shows that the dynamics under the Floquet operator U_f is completely closed within the embedded subspace $\mathcal{S}$. As obtained from Eqs. (4.49) and (4.50), the renormalized exact QMBS eigenstates $|\tilde{\Gamma}^x_{\alpha\beta}\rangle$ $(\alpha,\beta=1,2)$ become orthonormal with each other in the thermodynamic limit, giving an orthonormal basis of the subspace $\mathcal{S}$. By using this basis and the relation Eq. (4.61), we obtain the matrix representation of the Floquet operator restricted to $\mathcal{S}$,

$$U_f|_{\mathcal{S}} = \begin{pmatrix} p & qr & qr^* & 1-p \\ -q & pr & -(1-p)r^* & q \\ -q & -(1-p)r & pr^* & q \\ 1-p & -qr & -qr^* & p \end{pmatrix}, \tag{4.62}$$

$$p = \frac{1+\cos\sqrt{2}T_2}{2}, \quad q = \frac{\sin\sqrt{2}T_2}{2}, \quad r = e^{-i\sqrt{2}T_1}, \tag{4.63}$$

Thus, the Floquet operator U_f has four eigenstates $|\varepsilon\rangle_{\mathcal{S}}$ within the subspace $\mathcal{S}$. Equation (4.53) suggests that the domain wall density D_b is diagonal within $\mathcal{S}$, ensuring the following relation

$$\lim_{L_b\to\infty} \langle\varepsilon|D_b|\varepsilon\rangle_{\mathcal{S}} = \frac{2}{3} \neq \frac{2}{\sqrt{5}\phi} = 0.542\ldots, \tag{4.64}$$

for all the four eigenstates $|\varepsilon\rangle_{\mathcal{S}} \in \mathcal{S}$. Considering the deviation from the infinite temperature value $2/(\sqrt{5}\phi)$ [See Eq. (4.10)], the four eigenstates $|\varepsilon\rangle_{\mathcal{S}}$ are distingushable from infinite temperature states in terms of a local observable D_b. Thus, we rigorously show that the model violates Floquet-ETH in spite of its nonintegrability, which is the main result of this chapter. We call the four special eigenstates $|\varepsilon\rangle_{\mathcal{S}}$ "the exact Floquet QMBS eigenstates."

Let us discuss the detailed properties of the exact Floquet QMBS eigenstates. The explicit form of them can be obtained by diagonalizing the Floquet operator within $\mathcal{S}$, given by Eq. (4.62). Two of them have the following simple form:

$$|\Gamma_0\rangle = |\Gamma^x_{11}\rangle + |\Gamma^x_{22}\rangle\,, \tag{4.65}$$

$$|\Gamma'_0\rangle = \sin\frac{T_1}{\sqrt{2}}\cos\frac{T_2}{\sqrt{2}}(|\Gamma^x_{11}\rangle - |\Gamma^x_{22}\rangle) + i\sin\frac{T_2}{\sqrt{2}}(e^{iT_1/\sqrt{2}}\,|\Gamma^x_{12}\rangle - e^{-iT_1/\sqrt{2}}\,|\Gamma^x_{21}\rangle). \tag{4.66}$$

Both of the two have the quasienergy $\varepsilon = 0$, and are invariant under the nonlocal chiral symmetry operation $\mathcal{C}$ [See Eq. (4.56)]. The other two athermal eigenstates are too complex to write down. Instead, from the chiral symmetry $\mathcal{C}$, we can mention that they are related to each other by $\mathcal{C}$ and have quasienergy with the opposite sign.

All the four exact Floquet scar eigenstates appear in Fig. 4.1 (b)-(d) as the four marked low-entangled states. As discussed above, the two of them, lying in $\varepsilon \neq 0$, appear symmetrically with respect to $\varepsilon = 0$. Since each of the Floquet scar eigenstates is a superposition of the four states $|\Gamma^x_{\alpha\beta}\rangle$ with bond dimension 2, they are represented by matrix product states with at-most bond dimension 8 using the direct sum of matrices. Thus, their entanglement entropy per length decays with $O(1/L)$, which implies the nonthermal behavior of them. This result also corresponds to the numerical result [See Fig. 4.1 (b)-(d)].

Dynamics in and out of the embedded subspace

Floquet-ETH is a sufficient condition for the system relaxing to infinite temperature states from any initial state. Thus, the violation of Floquet-ETH in the model implies that it can relax to or avoid such trivial steady states depending on initial states. Here, we analyze the dynamics for initial states in and out of the embedded subspace $\mathcal{S}$, and clarify that the former case shows a persistent motion with avoiding trivial steady states.

First, let us consider the dynamics within the embedded subspace $\mathcal{S}$. Once the initial state $|\psi(t)\rangle$ is in $\mathcal{S}$, the state evolving under the Hamiltonian $H(t)$ remains in $\mathcal{S}$. The stroboscopic dynamics is given by

$$|\psi(nT)\rangle = (U_f|_{\mathcal{S}})^n\,|\psi(0)\rangle \in \mathcal{S}, \quad |\psi\rangle \in \mathcal{S}. \tag{4.67}$$

Here, the Floquet operator $U_f|_{\mathcal{S}}$ is given by Eq. (4.62) with the orthonormal basis $\{|\tilde{\Gamma}^x_{\alpha\beta}\rangle\}$ in the thermodynamic limit. For any local observable O, its expectation value can be computed by $\langle\psi(0)|(U_f|^\dagger_{\mathcal{S}})^n O|_{\mathcal{S}}(U_f|_{\mathcal{S}})^n|\psi(0)\rangle$ with the matrix elements in the restricted subspace $\mathcal{S}$, denoted by $O|_{\mathcal{S}}$. For instance, from Eqs. (4.51), the total magnetization in the x-direction, $\lim_{L\to\infty}\sum_i \sigma^x_i$, is given by $\mathrm{diag}(0, \sqrt{2}, -\sqrt{2}, 0)$ and shows a persistent oscillation in general, while the local Pauli operator σ^z_i and the domain-wall density D_b remain constant since they are proportional to identity in $\mathcal{S}$. On the other hand, concerning the microscopic dynamics, generic initial states in $\mathcal{S}$, different from $|\Gamma_0\rangle$, show some persistent motion since $|\Gamma_0\rangle$ is the unique simultaneous eigenstate of H_{PXP} and $H_{\mathrm{PY_4P}}$ in $\mathcal{S}$. We show typical real-time dynamics in Fig. 4.2 (a).

Next, we demonstrate the dynamics outside of the embedded subspace $\mathcal{S}$. Following the non-integrability of the model, generic initial states are expected to relax to infinite temperature, and we numerically confirm it by ED [See Fig. 4.2 (b), (c)]. We consider two different initial states $|\psi_1\rangle \equiv |\downarrow\downarrow\ldots\rangle$ and $|\psi_2\rangle \equiv \mathcal{P}_{\mathrm{Ryd},L}\,|-\rangle^{\otimes L}/\sqrt{\mathcal{D}_L}$ with $|-\rangle = (|\uparrow\rangle - |\downarrow\rangle)/\sqrt{2}$ and the projection to the constrained Hilbert space $\mathcal{P}_{\mathrm{Ryd},L}$. They have an exponentially small overlap with $\mathcal{S}$ in the system size, and have energy under the PXP Hamiltonian H_{PXP}, given by

$$\langle\psi_1|H_{\mathrm{PXP}}|\psi_1\rangle = 0, \quad \langle\psi_2|H_{\mathrm{PXP}}|\psi_2\rangle = -2L/\sqrt{5}\phi. \tag{4.68}$$

By solving the energy conservation

$$\frac{\langle\psi|H_{\mathrm{PXP}}|\psi\rangle}{\langle\psi|\psi\rangle} = \frac{\mathrm{Tr}[H_{\mathrm{PXP}}e^{-\beta H_{\mathrm{PXP}}}]}{\mathrm{Tr}[e^{-\beta H_{\mathrm{PXP}}}]} \tag{4.69}$$

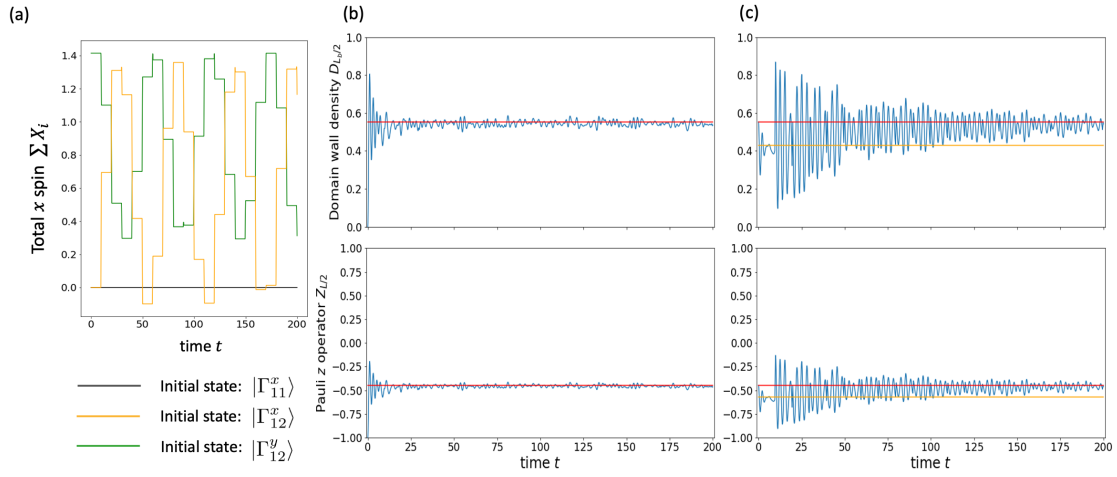

Figure 4.2: (a) Real-time dynamics of total x spin $\sum_i \sigma_i^x$ under the initial states within $\mathcal{S}$ at $T_1 = 9.5, T_2 = 0.5$. The states $|\Gamma^x_{12}\rangle$ and $|\Gamma^y_{12}\rangle$ show a persistent oscillation. (b) Real-time dynamics under the initial state $|\psi_1\rangle$, which is at infinite temperature under H_{PXP}. The red lines represent the values at infinite temperature. (c) Real-time dynamics under the initial state $|\psi_2\rangle$, which is at finite temperature β_{eff} under H_{PXP}. The lower solid yellow lines represent the finite-temperature-equilibrium values under H_{PXP} [β_{eff} is obtained by numerically solving Eq. (4.69)]. The Floquet drive breaks such a feature of the initial state, and makes the observable approach the values at infinite temperature (the upper solid red lines).

in terms of β, the initial state $|\psi_1\rangle$ ($|\psi_2\rangle$) corresponds to infinite temperature $\beta = 0$ (finite temperature $\beta > 0$) under the PXP Hamiltonian H_{PXP}. Figure 4.2 (b) and (c) show the dynamics at $T_1 = 9.5$ and $T_2 = 0.5$, which we choose so that pre-equilibration under an effective static Hamiltonian in the high-frequency regime can be avoided (See Section 1.3.4). The model shows thermalization to infinite temperature regardless of initial states outside of the embedded subspace in contrast to the static PXP model and the $\mathrm{PY_4P}$ model, where the system relaxes to thermal states with a certain temperature depending on its initial states.

Local conserved quantities in the embedded subspace

To summarize the behavior of the model showing Floquet-QMBS, any initial state spanned by the exact Floquet QMBS eigenstates avoids thermalization while the other initial states experience the relaxation to trivial infinite temperature states as well as conventional nonintegrable Floquet systems. Here, we aim to understand the dynamics within the embedded subspace $\mathcal{S}$ in terms of emergent local conserved quantities.

Let us reconsider the PXP Hamiltonian and the $\mathrm{PY_4P}$ Hamiltonian in the embedded subspace. The PXP model is proven to have an extensive number of conserved quantities when restricted to the embedded subspace [163], and we show that the $\mathrm{PY_4P}$ model also does in a similar way. We employ the block description provided in Section 4.1.5, where the b-th block is composed of the $(2b-1)$-th and $2b$-th sites. In the $\mathrm{PY_4P}$ Hamiltonian [See Eq. (4.22)], the nontrivial terms acting on the b-th and $(b+1)$-th blocks, $h^y_{b,b+1}$, are given by

$$\begin{aligned} h^y_{b,b+1} &= (-1)^b(P_{2b-1}\sigma^y_{2b}P_{2b+1} + P_{2b}\sigma^y_{2b+1}P_{2b+2}) \\ &= i(-1)^b(|o\rangle\langle r| - |r\rangle\langle o|)_b(I - |l\rangle\langle l|)_{b+1} + i(-1)^b(I - |r\rangle\langle r|)_b(|o\rangle\langle l| - |l\rangle\langle o|)_{b+1} \\ &\equiv h^{y,(2)}_{b,b+1} + h^{y,(1)}_{b,b+1}, \end{aligned} \tag{4.70}$$

$$h^{y,(1)}_{b,b+1} = i(-1)^b(|o\rangle\langle r| - |r\rangle\langle o|)_b + i(-1)^b(|o\rangle\langle l| - |l\rangle\langle o|)_{b+1} \tag{4.71}$$

$$h^{y,(2)}_{b,b+1} = i(-1)^b\{|rl\rangle(\langle ol| + \langle ro|) - \mathrm{h.c.}\}_{b,b+1}, \tag{4.72}$$

for the bulk $b = 2, 3, \ldots, L_b - 1$. The terms $h^{y,(1)}_{b,b+1}$ and $h^{y,(2)}_{b,b+1}$ respectively represent one-body

noninteracting terms and two-body interacting terms in the block description. The boundary terms of the PY_4P Hamiltonian is also computed as

$$\sigma_1^y P_2 = i(|o\rangle\langle l| - |l\rangle\langle o|)_1, \qquad P_{L-1}\sigma_L^y = -i(|r\rangle\langle o| - |o\rangle\langle r|)_{L_b}. \tag{4.73}$$

Using these results, the PY_4P Hamiltonian is written in the following form:

$$H_{PY_4P} = \sum_{b=2}^{L_b-1} h_{b,b+1}^{y,(2)} + \sum_{b=1}^{L_b} h_b^{y,(1)} \tag{4.74}$$

$$h_b^{y,(1)} = i(-1)^b(|o\rangle\langle r| + |l\rangle\langle o| - \text{h.c.})_b. \tag{4.75}$$

From the matrix elements of A^s $(s = l, o, r)$ in Eq. (4.44), we can confirm $A^r A^l = 0$ and $A^o A^l + A^r A^o = 0$. As a result, we obtain

$$H_{PY_4P}|\Gamma_{\alpha\beta}^{\nu}\rangle = \sum_{b=1}^{L_b} h_b^{y,(1)}|\Gamma_{\alpha\beta}^{\nu}\rangle \tag{4.76}$$

for $\alpha, \beta = 1, 2$ and $\nu = x, y, z$, where we have used Eq. (4.24). In addition, as discussed in Section 4.1.4, the PY_4P Hamiltonian is completely closed within the embedded subspace $\mathcal{S}$ spanned by $|\Gamma_{\alpha\beta}^{\nu}\rangle$, and hence this equation gives the PY_4P Hamiltonian restricted to $\mathcal{S}$,

$$H_{PY_4P}|_{\mathcal{S}} = \sum_{b=1}^{L_b} h_b^{y,(1)}, \quad h_b^{y,(1)} = i(-1)^b(|o\rangle\langle r| + |l\rangle\langle o| - \text{h.c.})_b. \tag{4.77}$$

Since each term $h_b^{y,(1)}$ is closed in each block, the PY_4P Hamiltonian has an extensive number of local conserved quantities $\{h_b^{y,(1)}\}_{b=1}^{L_b}$ within the subspace $\mathcal{S}$.

In a similar way, according to Ref. [163], the PXP Hamiltonian also has a macroscopic number of local conserved quantities $\{h_b^{x,(1)}\}_{b=1}^{L_b}$ within the same subspace $\mathcal{S}$, as described by

$$H_{PXP}|_{\mathcal{S}} = \sum_{b=1}^{L_b} h_b^{x,(1)}, \quad h_b^{x,(1)} = (|o\rangle\langle l| + |o\rangle\langle r| + \text{h.c.})_b \tag{4.78}$$

in $\mathcal{S}$. Based on the conserved quantities, we can reinterpret the dynamics of the model showing Floquet-QMBS. Within the embedded subspace $\mathcal{S}$, the Floquet operator $U_f = e^{-iH_{PY_4P}T_2}e^{-iH_{PXP}T_1}$ becomes equivalent to

$$U_f|_{\mathcal{S}} = \prod_{b=1}^{L_b}\left(e^{-iT_2 h_b^{y,(1)}}e^{-iT_1 h_b^{x,(1)}}\right). \tag{4.79}$$

due to Eqs. (4.77) and (4.78). This indicates that the model emergently possesses a macroscopic number of local conserved quantities $\{-i\log(\exp(-iT_2 h_b^{y,(1)})\exp(-iT_1 h_b^{x,(1)}))\}_b$ within $\mathcal{S}$ as well as integrable systems. Therefore, any state in $\mathcal{S}$ does not experience thermalization to infinite temperature. On the other hand, in the other states out of $\mathcal{S}$, such local conserved quantities do not appear like conventional nonintegrable systems, leading to thermalization to trivial steady states.

We also note that the emergent local conserved quantities in $\mathcal{S}$ make the nonlocal chiral symmetry $\mathcal{C}$ local. To be precise, the nonlocal operator $\mathcal{C}$ defined by Eq. (4.56) can be rewritten by

$$\mathcal{C} = \left(\prod_i \sigma_i^z\right)\exp\left(i\sum_b h_b^{y,(1)}T_2\right), \tag{4.80}$$

within the embedded subspace $\mathcal{S}$ using Eq. (4.77). This suggests that the two Floquet QMBS eigenstates which are related to each other by $\mathcal{C}$ possess the same entanglement entropy, while other pairs outside of $\mathcal{S}$ do not due to the nonlocality of $\mathcal{C}$. We can confirm this signature of the conserved quantities from Figs. 4.1 (b)-(d), in which the pair of the Floquet QMBS eigenstates having nonzero quasienergy symmetrically appears in the entanglement spectrum.

4.3 Generalized time-periodic models for Floquet QMBS

In the above discussion, we construct a model under binary drive, which rigorously shows Floquet QMBS. Here, we generalize the binary drive to generic time-periodic models by combining the PXP, PY_4P, and PZ_4P models. First, we consider the following time-independent Hamiltonian on the constrained Hilbert space:

$$H_{\vec{a}} = \vec{a} \cdot \vec{H}, \quad \vec{H} = (H_{\mathrm{PXP}}, H_{\mathrm{PY_4P}}, H_{\mathrm{PZ_4P}}), \tag{4.81}$$

with $\vec{a} \in \mathbb{R}^3$. While the PY_4P model is unitarily equivalent to the PXP model, this generalized static model is no longer equivalent to either the PXP, PY_4P, or PZ_4P models. With the polar display $\vec{a} = |\vec{a}|(\sin\theta\cos\varphi, \sin\theta\sin\varphi, \cos\theta)$, we can compose four exact QMBS eigenstates by

$$|\Gamma^{\vec{a}}_{\alpha\beta}\rangle \quad = \quad \sum_{\vec{\sigma}} \vec{u}^{a,\dagger}_{\alpha} B^{\sigma_1} C^{\sigma_2} \dots B^{\sigma_{L-1}} C^{\sigma_L} \vec{u}^{a}_{\beta} \, |\vec{\sigma}\rangle \, , \tag{4.82}$$

$$\vec{u}^{a}_{1} = \begin{pmatrix} \cos(\theta/2) \\ e^{i\varphi}\sin(\theta/2) \end{pmatrix}, \quad \vec{u}^{a}_{2} = \begin{pmatrix} -e^{-i\varphi}\sin(\theta/2) \\ \cos(\theta/2) \end{pmatrix}. \tag{4.83}$$

By using the action of the PY_4P Hamiltonian on the embedded subspace $\mathcal{S}$, given by Eq. (4.37), and the similar relations for the PXP model [See Eq. (4.100)] and the PZ_4P model, we obtain

$$H_{\vec{a}} \, |\Gamma^{\vec{a}}_{\alpha\beta}\rangle = \sum_{\vec{\sigma}} \vec{u}^{a,\dagger}_{\alpha} \left\{ (\vec{a}\cdot\vec{\Sigma}) D^{\vec{\sigma}} - D^{\vec{\sigma}} (\vec{a}\cdot\vec{\Sigma}) \right\} \vec{u}^{a}_{\beta} \, |\vec{\sigma}\rangle \, , \tag{4.84}$$

in which we define $\vec{\Sigma} = (\sigma^x, \sigma^y, \sigma^z)/\sqrt{2}$ and $D^{\vec{\sigma}} = B^{\sigma_1} C^{\sigma_2} \dots B^{\sigma_{L-1}} C^{\sigma_L}$. Considering the fact that the vectors $\vec{u}^{a}_{\alpha}$ $(\alpha = 1, 2)$ are eigenvectors of the 2×2 matrix $\vec{a}\cdot\vec{\Sigma}$, we confirm that the four states $|\Gamma^{\vec{a}}_{\alpha\beta}\rangle$ $(\alpha, \beta = 1, 2)$ are the exact eigenstates of the generalized Hamiltonian $H_{\vec{a}}$ as follows:

$$H_{\vec{a}} \, |\Gamma^{\vec{a}}_{\alpha\beta}\rangle = \frac{1}{\sqrt{2}} \left\{ (-1)^{\alpha-1} - (-1)^{\beta-1} \right\} |\Gamma^{\vec{a}}_{\alpha\beta}\rangle \, . \tag{4.85}$$

Now, we give the generalized time-periodic Hamiltonian for Floquet QMBS as follows:

$$H(t) = \vec{a}(t) \cdot \vec{H}, \quad \vec{a}(t+T) = \vec{a}(t) \in \mathbb{R}^3. \tag{4.86}$$

Since it is composed of a series of nonintergable static Hamiltonians such as H_{PXP} and $H_{\mathrm{PY_4P}}$, the time-periodic model also becomes nonintegrable in general. Since $|\Gamma^{\vec{a}}_{\alpha\beta}\rangle$ is represented by a linear combination of $\{|\Gamma^{x}_{\alpha\beta}\rangle\}$ for arbitrary $\vec{a}$, the dynamics under $H(t)$ is closed within the subspace spanned by $\{|\Gamma^{x}_{\alpha\beta}\rangle\}_{\alpha,\beta=1,2}$. Therefore, this generalized Floquet model has at-least four Floquet eigenstates $|\varepsilon\rangle$ in the embedded subspace $\mathcal{S}$, indicating the breakdown of Floquet-ETH. Using the fact that $\{\vec{u}^{a}_{\alpha}\}_{\alpha=1,2}$ is a complete orthonormal basis of $\mathbb{C}^2$, the static Hamiltonian $H_{\vec{a}}$ always has the following eigenstates,

$$|\Gamma_0\rangle \equiv |\Gamma^{\vec{a}}_{11}\rangle + |\Gamma^{\vec{a}}_{22}\rangle = \sum_{\vec{\sigma}} \mathrm{Tr}\left[B^{\sigma_1} C^{\sigma_2} \dots B^{\sigma_{L-1}} C^{\sigma_L} \right] |\vec{\sigma}\rangle \, , \tag{4.87}$$

with zero eigenvalue independent of $\vec{a}$. This means that we can obtain the exact description for one of the Floquet QMBS eigenstates by

$$U_f \, |\Gamma_0\rangle = |\Gamma_0\rangle \, , \quad U_f = \mathcal{T} \exp\left(-i \int_0^T H_{\vec{a}(t)} dt \right). \tag{4.88}$$

While the Floquet QMBS eigenstate $|\Gamma_0\rangle$ is invariant during the dynamics, any initial state in the subspace spanned by the other three Floquet QMBS eigenstates show persistent oscillation since the Hamiltonians $H_{\vec{a}(t)}$ for different time t do not have simultaneous eigenstates other than $|\Gamma_0\rangle$ in general.

4.4 Discussion and conclusion for this chapter

Before concluding this chapter, we briefly discuss how to realize the time-periodic Hamiltonian Eq. (4.54), which hosts Floquet QMBS, in experiments. As discussed in Section 1.3.2, the PXP Hamiltonian can be realized in Rydberg-atom experiments, where the Rabi oscillation takes place under the strong repulsive atom-atom interactions [45]. Once the PXP Hamiltonian is realized, the time-periodic model $H(t)$ is also realizable by implementing the potential with quadruple periodicity of the lattice:

$$H_{\mathbb{Z}_4} = \sum_{i=1}^{L} c_i \sigma_i^z, \quad c_i = \sqrt{2}\cos\left(\frac{i\pi}{2} - \frac{\pi}{4}\right). \tag{4.89}$$

Then, using the unitary equivalence Eq. (4.38), the Floquet operator for the binary drive is

$$\begin{aligned} U_f &= e^{-iH_{\mathrm{PY_4P}}T_2} e^{-iH_{\mathrm{PXP}}T_1} \\ &= e^{-iH_{\mathbb{Z}_4}(\pi/4)} e^{-iH_{\mathrm{PXP}}T_2} e^{-i(-H_{\mathbb{Z}_4})(\pi/4)} e^{-iH_{\mathrm{PXP}}T_1}. \end{aligned} \tag{4.90}$$

Thus, switching of the PXP Hamiltonian and the potential enables the realization of the time-periodic model. We can realize the $\mathrm{PZ_4P}$ model in a similar setting since the potential $Q_i = (|\uparrow\rangle\langle\uparrow|)_i = (1+\sigma_i^z)/2$ becomes equivalent to each term $P_{i-1}Q_iP_{i+1}$ in the constrained Hilbert space $\mathcal{H}_{\mathrm{Ryd},L}$. This is confirmed by the relation

$$\mathcal{P}_{\mathrm{Ryd},L} H_{\mathrm{PZ_4P}} \mathcal{P}_{\mathrm{Ryd},L} = \sum_{i=1}^{L} c_i \mathcal{P}_{\mathrm{Ryd},L} Q_i \mathcal{P}_{\mathrm{Ryd},L}, \tag{4.91}$$

with the projection to the constrained Hilbert space $\mathcal{P}_{\mathrm{Ryd},L}$. Thus, the time-periodic models for Floquet QMBS, including the generalized versions Eq. (4.86), can be realized in Rydberg atoms. While our model does not require the fine-tuning of the parameters T_1, T_2, or $a(t)$ in Eqs. (4.54) and (4.86), what seems to be difficult is to prepare the initial state in the embedded subspace $\mathcal{S}$. However, considering that the states in the embedded subspace $\mathcal{S}$ are equivalent to the well-known topologically nontrivial state under certain symmetries called the Affleck-Kennedy-Lieb-Tasaki state [47, 163], there are some proposals for preparing such low-entangled states in AMO experiments, such as the dissipative preparation [164].

In summary, we have constructed a nonintegrable model which hosts Floquet QMBS, driven by uniformly imposed Hamiltonians on the constrained Hilbert space prohibiting adjacent pairs of excited Rydberg states. We have rigorously shown that the model violates Floquet-ETH with the fact that instantaneous Hamiltonians share a subspace immune to thermalization although their QMBS eigenstates do not correspond to one another. We note that the violation of Floquet-ETH results in the initial-state-dependent behavior of relaxation; The initial states in the embedded subspace generally show persistent oscillation avoiding the heating. On the other hand, the entanglement spectrum of Floquet eigenstates and the real-time dynamics of the model indicate that any initial state outside of the embedded subspace is thermalized to infinite temperature.

Finally, we provide some future directions for Floquet QMBS with discussing recent progress in QMBS. Throughout this chapter, we focus on the PXP-type static models, which are realized under Rydberg blockade, and construct Floquet QMBS based on their properties. While such PXP-type Hamiltonians are experimentally feasible in Rydberg atoms, they have only a few QMBS eigenstates rigorously found, which have not been directly observed yet. Recent studies have revealed a series of static QMBS, such as models with local constraints by local projections [51, 163, 165, 166] and models relying on algebraic structures [52, 167, 168, 169, 170, 171]. In the latter case, there exist a series of exact QMBS eigenstates composing a tower-like structure. It will be interesting to seek for the interplay between various static QMBS and Floquet systems, e.g. whether we can find some Floquet-intrinsic dynamics dependent on initial states, which emerges from the algebraic structures of the Floquet operator U_f instead of static Hamiltonians. It should be of interest to find out the relation between special scar states in static systems [See Section 1.3.2] and Floquet QMBS. In the PXP models, there exist some special initial states such as $|\mathbb{Z}_2\rangle = |\uparrow\downarrow\ldots\rangle$ showing long-lived athermal oscillation, other than the exact QMBS eigenstates [45, 46, 47, 48, 172, 173]. Although the Floquet systems discussed here do not show such an anomalous oscillation other

than the exact Floquet QMBS eigenstates [See Section 4.5], recent theoretical and experimental studies have reported athermal behaviors from some special initial states in other time-periodic models [174, 175, 176]. It is also important to clarify what kind of Floquet systems has special initial states with long-lived athermal oscillation and how the special states are related to the exact Floquet QMBS eigenstates, in parallel to static systems.

We also introduce recent developments in Floquet QMBS. In terms of the exact Floquet QMBS eigenstates, Ref. [177] have reported a periodically-driven model rigorously showing Floquet QMBS, composed of PXP-type but integrable instantaneous Hamiltonians. Since it is realized by the quasienergy degeneracy modulo $2\pi/T$, they call it "Floquet-intrinsic QMBS." As Floquet QMBS, the Hilbert space shattering [54, 178] has attracted much interest, which is realized in local random unitary circuits with macroscopic conserved quantities. Ref. [54, 178] has reported that locality of interactions and the conservation of macroscopic charge and dipole moment prevent some initial states from relaxing to infinite temperature. Ref. [54] also suggests that a large number of exact Floquet QMBS eigenstates in the model, immune to thermalization under the presence of the locality and the macroscopic symmetries, may be applicable to quantum information storage. While Floquet QMBS is originally introduced to find out counterexamples to Floquet-ETH and the resulting nontrivial dynamics in interacting Floquet systems, now it may be time to seek for intriguing or useful condensed matter properties of Floquet many-body systems such as response and robustness upon Floquet QMBS.

4.5 Appendix for this chapter

Exact QMBS eigenstates of the PXP model

Here, we prove Theorem 4.1.1, dictating that the PXP Hamiltonian H_{PXP} has four eigenstates $|\Gamma^x_{\alpha\beta}\rangle$ $(\alpha,\beta=1,2)$ satisfying

$$\begin{aligned} &H_{\mathrm{PXP}}\,|\Gamma^x_{11}\rangle = 0, \quad H_{\mathrm{PXP}}\,|\Gamma^x_{12}\rangle = \sqrt{2}\,|\Gamma^x_{12}\rangle\,, \\ &H_{\mathrm{PXP}}\,|\Gamma^x_{22}\rangle = 0, \quad H_{\mathrm{PXP}}\,|\Gamma^x_{21}\rangle = -\sqrt{2}\,|\Gamma^x_{21}\rangle\,. \end{aligned} \tag{4.92}$$

See Eq. (4.16) for H_{PXP} and Eq. (4.17) for $|\Gamma^x_{\alpha\beta}\rangle$ respectively. We take a strategy different from the original way provided in Ref. [47, 163], but in a similar way to the $\mathrm{PY_4P}$ model in Section 4.1.4.

Proof

We consider the PXP Hamiltonian $P_{\mathrm{Ryd},L}H_{\mathrm{PXP}}P_{\mathrm{Ryd},L}=\sum_{i=1}^{L}P_{\mathrm{Ryd},L}\sigma^x_iP_{\mathrm{Ryd},L}$, where $P_{\mathrm{Ryd},L}=\prod_{i=1}^{L-1}\left(1-|\uparrow\uparrow\rangle\langle\uparrow\uparrow|\right)_{i,i+1}$ denotes the projection to the constrained Hilbert space $\mathcal{H}_{\mathrm{Ryd},L}$. This representation is nothing but the result of perturbation theory where Rabi oscillation takes place under strong repulsive interactions causing Rydberg blockade (See Section 1.3.2).

As well as Eqs. (4.30) and (4.31) for the $\mathrm{PY_4P}$ model, the four states $|\Gamma^x_{\alpha\beta}\rangle$ given by Eq. (4.17) can be written in the following form:

$$|\Gamma^x_{\alpha\beta}\rangle = \vec{u}^{\dagger}_{\alpha}B'_1C'_2\ldots B'_{L-1}C'_L\vec{u}_{\beta}, \tag{4.93}$$

$$B'_i = \begin{pmatrix} |\downarrow\rangle_i & 0 & 0 \\ \sqrt{2}\,|\uparrow\rangle_i & |\downarrow\rangle_i & \sqrt{2}\,|\uparrow\rangle_i \end{pmatrix}, \quad C'_i = \begin{pmatrix} \sqrt{2}\,|\uparrow\rangle_i & -|\downarrow\rangle_i \\ |\downarrow\rangle_i & 0 \\ -\sqrt{2}\,|\uparrow\rangle_i & 0 \end{pmatrix}. \tag{4.94}$$

We apply $P_{\mathrm{Ryd},L}\sigma^x_iP_{\mathrm{Ryd},L}$ to $|\Gamma^x_{\alpha\beta}\rangle$ with the relation $P_{\mathrm{Ryd},L}\,|\Gamma^x_{\alpha\beta}\rangle=|\Gamma^x_{\alpha\beta}\rangle$. We obtain

$$P_{\mathrm{Ryd},L}\sigma^x_iP_{\mathrm{Ryd},L}\,|\Gamma^x_{\alpha\beta}\rangle = P_{\mathrm{Ryd},L}\vec{u}^{\dagger}_{\alpha}B'_1\ldots C'_{i-1}F^x_{i,i+1}B'_{i+2}\ldots C'_L\vec{u}_{\beta}, \tag{4.95}$$

$$\begin{aligned} F^x_{i,i+1} &= \begin{pmatrix} 0 & -|\uparrow\downarrow\rangle_{i,i+1} \\ |\downarrow\uparrow\rangle_{i,i+1} & -\sqrt{2}\,|\downarrow\downarrow\rangle_{i,i+1} \end{pmatrix} \\ &= XB'_iC'_{i+1} - B'_i\tilde{X}C'_{i+1}, \end{aligned} \tag{4.96}$$

$$X = \frac{1}{\sqrt{2}}\begin{pmatrix} 0 & 1 \\ 1 & 0 \end{pmatrix}, \quad \tilde{X} = \frac{1}{\sqrt{2}}\begin{pmatrix} 0 & 1 & 0 \\ -1 & 0 & -2 \\ 0 & -2 & 0 \end{pmatrix}. \tag{4.97}$$

for an odd integer i, and obtain

$$\begin{aligned} P_{\mathrm{Ryd},L}\sigma_i^x P_{\mathrm{Ryd},L}\,|\Gamma^x_{\alpha\beta}\rangle &= P_{\mathrm{Ryd},L}\vec{u}_\alpha^\dagger B'_1\dots C'_{i-2}\tilde{F}^x_{i-1,i}B'_{i+1}\dots C'_L\vec{u}_\beta, \qquad (4.98)\\ \tilde{F}^x_{i-1,i} &= \begin{pmatrix} \sqrt{2}\,|{\downarrow\downarrow}\rangle_{i-1,i} & -|{\downarrow\uparrow}\rangle_{i-1,i} \\ |{\uparrow\downarrow}\rangle_{i-1,i} & 0 \end{pmatrix} \\ &= B'_{i-1}\tilde{X}C'_i - B'_{i-1}C'_iX. \qquad (4.99)\end{aligned}$$

for an even integer i. Finally, when the system size L is even, we arrive at

$$\begin{aligned} P_{\mathrm{Ryd},L}H_{\mathrm{PXP}}P_{\mathrm{Ryd},L}\,|\Gamma^x_{\alpha\beta}\rangle &= P_{\mathrm{Ryd},L}\vec{u}_\alpha^\dagger(XB'_1\dots C'_L - B'_1\dots C'_LX)\vec{u}_\beta \\ &= \frac{1}{\sqrt{2}}\left\{(-1)^{\alpha-1}-(-1)^{\beta-1}\right\}|\Gamma^x_{\alpha\beta}\rangle\,, \qquad (4.100)\end{aligned}$$

where we have used Eq. (4.20) for the vectors $\vec{u}_\alpha$ ($\alpha = 1, 2$). Thus, the four states $|\Gamma^x_{\alpha\beta}\rangle$ are exact eigenstates of the PXP Hamiltonian. □

Dynamics of $\mathbb{Z}_2$ scar states

As introduced in Section 1.3.2, the static PXP model can show anomalously-long athermal oscillation from some special initial states such as $\mathbb{Z}_n$-ordered states $|\mathbb{Z}_n\rangle$. Although it has been still unclear whether or not this behavior gives rigorous violation of ETH in the thermodynamic limit, the approximate relation to the exact static QMBS is pointed out [47]. From the unitarily equivalence, the PY_4P model also shows such an athermal oscillation from the same special initial states. Here, we examine the Floquet dynamics from such special initial states found in the static models, and explore the possibility of special athermal behaviors related to the exact Floquet QMBS eigenstates.

We consider the binary drive,

$$H(t) = \begin{cases} H_{\mathrm{PXP}} & 0 \le t < T_1 \\ H_{\mathrm{PY_4P}} & T_1 \le t < T_1 + T_2 = T, \end{cases} \qquad (4.101)$$

which shows Floquet QMBS as discussed in Section 4.2. Here, instead of the embedded subspace $\mathcal{S}$, rigorously avoiding the thermalization, we consider the $\mathbb{Z}_2$-ordered state $|\mathbb{Z}_2\rangle = |{\uparrow\downarrow\uparrow\downarrow}\dots\rangle$ as an initial state. Figure 4.3 (a) shows the corresponding dynamics of the domain wall density and the Pauli Z operator under the PY_4P Hamiltonian $H_{\mathrm{PY_4P}}$, or equivalently the above binary model with $T_1 = 0$. As far as we can numerically simulate, the static model shows a long-lived oscillation with avoiding the thermalization to the corresponding equilibrium states. The similar behavior from the $\mathbb{Z}_2$-ordered initial state is also observed for the PXP model both in experiments [45] and numerical simulations [46, 172].

Let us discuss what happens if we add time-periodic modulation like Eq. (4.54), where the instantaneous static Hamiltonians show the above anomalous long-lived athermal behaviors from $|\mathbb{Z}_2\rangle$. Figures 4.3 (b) and (c) show the numerical results for the periodically-driven model with (b) $T_1 = 9.5, T_2 = 0.5$ (c) $T_1 = 0.95, T_2 = 0.05$. First, we identify the athermal behavior observed in (c). In the case of $T_1 = 0.95, T_2 = 0.05$, the frequency of the binary drive, given by $\omega = 2\pi/(T_1 + T_2) = 2\pi$, is relatively larger than the local energy scale of the Hamiltonian $H(t)$, given by $O(1)$. Thus, the system lies in the high-frequency regime which hosts pre-thermalization, justifying the description by the Floquet-Magnus expansion [See Section 1.3.4]. Up to the lowest order in the period T, the static effective Hamiltonian for the model is given by the time-averaged one over one period,

$$H_{\mathrm{eff}} = \frac{T_1}{T_1+T_2}H_{\mathrm{PXP}} + \frac{T_2}{T_1+T_2}H_{\mathrm{PY_4P}} + O(T). \qquad (4.102)$$

This static model is unitarily equivalent to the PXP model, and hence show anomalous long-lived athermal behavior from the initial state $|\mathbb{Z}_2\rangle$. The long-lived oscillation in Fig. 4.3 (c) originates from the static model H_{eff}, which is not inherent in Floquet systems.

On the other hand, in the case of $T_1 = 9.5, T_2 = 0.5$ corresponding to Fig. 4.3 (b), the local energy scale of the system is larger than the frequency, where the system is deeply affected by the time-dependency. As shown in Fig. 4.3 (b), both the domain-wall density $D_{L_b/2}$ and the Pauli

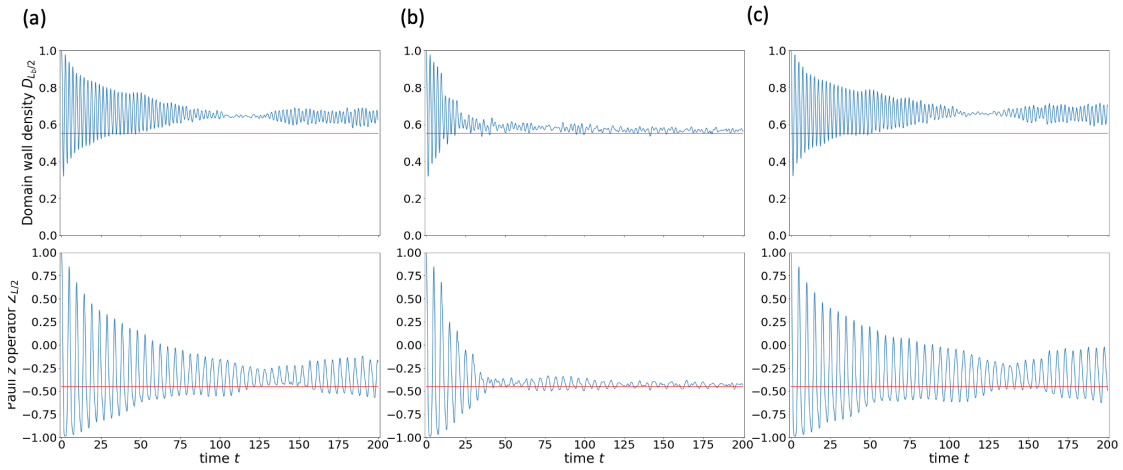

Figure 4.3: Real-time dynamics under the special initial state $|\mathbb{Z}_2\rangle = |\uparrow\downarrow\uparrow\downarrow\ldots\rangle$: (a) under the static PY_4P Hamiltonian, or equivalently at $T_1 = 10, T_2 = 0$; (b) under the binary drive at $T_1 = 9.5, T_2 = 0.5$; and (c) under the binary drive at $T_1 = 0.95, T_2 = 0.05$. (a) Both the domain-wall density and the Pauli Z operator show long-lasting oscillations without approaching their thermal equilibrium values at the temperature $T = \infty$. (b) The observables rapidly approach those of the infinite temperature due to the drive. (c) Athermal behaviors of the observables are observed as in the static case in spite of the existence of the drive. These are brought by pre-equilibration under an effective static Hamiltonian in the high-frequency regime of Floquet systems.

operator $\sigma^z_{L/2}$ with the initial state $|\mathbb{Z}_2\rangle$ quickly relax to the values of infinite temperature states as well as other usual initial states. This behavior is also confirmed by the entanglement spectrum of the Floquet eigenstates $\{|\varepsilon\rangle\}$ [See Figs. 4.1 (b)-(d)]. In the static models showing QMBS such as H_{PXP}, there exist a large number of low-entangled eigenstates, which are distinguishable from volume-law entangled thermal equilibrium states, other than the exact QMBS eigenstates such as $|\Gamma^x_{\alpha\beta}\rangle$. The special initial state $|\mathbb{Z}_2\rangle$ (and also other scar states) has a large overlap with these low-entangled eigenstates, thereby leading to the long-lived athermal oscillation in the static models [47]. However, when we focus on the entanglement spectrum of the Floquet eigenstates in Figs. 4.1 (b)-(d), only the four Floquet QMBS eigenstates in the embedded subspace $\mathcal{S}$ are low-entangled. This suggests that all the other Floquet eigenstates, having volume-law entanglement entropy, are indistinguishable from infinite temperature states. Considering that the initial state $|\mathbb{Z}_2\rangle$ is a superposition of the four Floquet QMBS eigenstates and a comparably large number of Floquet eigenstates equivalent to infinite temperature, the system shows relaxation to infinite temperature even under the preparation of $|\mathbb{Z}_2\rangle$.

Thus, we can conclude that some special scar states having long-lived oscillations vanish in the periodically-driven case. This indicates that the exact Floquet QMBS eigenstates have no relationship with anomalously long athermal behavior in contrast to the static models, where such an athermal behavior is also dubbed "quantum many-body scars."

Chapter 5

Conclusion

In this thesis, we have focused on nonequilibrium phenomena in periodically-driven or Floquet many-body systems. As introduced in Chapter 1, isolated Floquet many-body systems generally suffer from trivial steady states at infinite temperature predicted by Floquet-ETH or the heating problem. Motivated by recent developments of novel nonequilibrium phenomena and their applications, such as discrete time crystals (DTCs) and Floquet engineering, we have aimed to find out nontrivial dynamics or steady states in Floquet many-body systems with avoiding Floquet-ETH. Based on the assumptions in Floquet-ETH, we have explored Floquet many-body systems in quasi-steady states, those breaking the isolation, and those directly violating Floquet-ETH.

In Chapter 2, we have explored quasi-steady states in Floquet systems under resonant drive, giving the effective Hamiltonians for their coarse-grained stroboscopic dynamics. Floquet systems in the regime can host unique nonequilibrium phenomena such as DTCs and anomalous Floquet topological phases, while those in the high-frequency regime cannot. Motivated by this, we have extended the van Vleck expansion to the resonant regime, and have shown that Floquet systems effectively acquire an emergent $\mathbb{Z}_N$-symmetry up to any perturbation order when the resonant drive realizes a $\mathbb{Z}_N$-symmetry operation. Furthermore, the emergent $\mathbb{Z}_N$-symmetry is robust against any local perturbation that does not break the time-periodicity. As the applications of quasi-steady states with the emergent symmetry, we have proposed a way to analyze DTCs in quasi-steady states (prethermal DTCs, pDTCs) and Floquet engineering in the resonant regime (resonant Floquet engineering). In particular, in the latter case, we can simultaneously control phases of matter and symmetries of the system, enabling us to realize and control symmetry-protected topological phases even when the required symmetries are absent in the original system.

In Chapter 3, we have explored dissipative Floquet interacting systems, and in particular we have discussed the high-frequency regime.One of the central questions in dissipative Floquet systems is whether those in the high-frequency regimes have static counterparts, since isolated Floquet systems cannot host unique nonequilibrium phenomena in the high-frequency regime. Focusing on the Floquet-Magnus expansion for the time-periodic Liouvillians, we have proven that the generator for the stroboscopic dynamics cannot be a Liouvillian in generic interacting systems. This implies that dissipative Floquet interacting systems cannot have no counterparts in static systems even in the high-frequency regime unlike isolated Floquet systems, which we call Liouvillianity breaking. While noninteracting systems can either preserve or break Liouvillianity depending on model, Liouvillianity breaking is a universal phenomenon caused by interactions, and hence we expect novel dynamics or steady states in dissipative Floquet interacting systems.

In Chapter 4, we have proposed Floquet quantum many-body scars (QMBS) realized under Rydberg blockade. Floquet-ETH or the heating problem is a conjecture for nonintegrable Floquet systems giving the sufficient condition of thermalization. It is of great importance to ask wherer there exists a nonintegrable counterexample to Floquet-ETH, which can avoid trivial infinite-temperature steady states. By extending the static QMBS, which provides counterexamples to static ETH, we have composed a periodically-driven model which rigorously violates Floquet-ETH. We have first extended the PXP model, and have constructed the Floquet models composed of static Hamiltonians hosting the static QMBS. Exploiting the overlap of the embedded subspace avoiding thermalization, we have delivered the exact Floquet eigenstates inequivalent to infinite-temperature states, suggesting the violation of Floquet-ETH. Accompanied by the breakdown of

Floquet-ETH, the models show either thermalization to trivial steady states or persistent oscillation depending on their initial states. Our proposal, dubbed Floquet QMBS, will elucidate nontrivial dynamics and steady states in Floquet many-body systems without local conserved quantities.

Although each of Chapters 2,3, and 4 has dealt with different Floquet setups, all the topics have been devoted to understanding nontrivial dynamics and steady states in Floquet many-body systems beyond Floquet-ETH or the heating problem. As well as several future tasks discussed in each chapter, it is also a fundamental and interesting issue to further seek for what kind of phases of matter can exist upon (quasi-)steady states with resonant drives, dissipation, or Floquet-QMBS.

References

[1] J. W. McIver, B. Schulte, F. U. Stein, T. Matsuyama, G. Jotzu, G. Meier, and A. Cavalleri. Light-induced anomalous hall effect in graphene. *Nature Physics*, 16:38–41, 2020. URL https://doi.org/10.1038/s41567-019-0698-y.

[2] C. Monroe, W. C. Campbell, L.-M. Duan, Z.-X. Gong, A. V. Gorshkov, P. W. Hess, R. Islam, K. Kim, N. M. Linke, G. Pagano, P. Richerme, C. Senko, and N. Y. Yao. Programmable quantum simulations of spin systems with trapped ions. *Rev. Mod. Phys.*, 93:025001, 2021. URL https://link.aps.org/doi/10.1103/RevModPhys.93.025001.

[3] Gross Christian and Bloch Immanuel. Quantum simulations with ultracold atoms in optical lattices. *Science*, 357:995–1001, 2017. URL https://doi.org/10.1126/science.aal3837.

[4] Mikael C. Rechtsman, Julia M. Zeuner, Yonatan Plotnik, Yaakov Lumer, Daniel Podolsky, Felix Dreisow, Stefan Nolte, Mordechai Segev, and Alexander Szameit. Photonic floquet topological insulators. *Nature*, 496:196–200, 2013. URL https://doi.org/10.1038/nature12066.

[5] Sebabrata Mukherjee, Alexander Spracklen, Manuel Valiente, Erika Andersson, Patrik Öhberg, Nathan Goldman, and Robert R. Thomson. Experimental observation of anomalous topological edge modes in a slowly driven photonic lattice. *Nature Communications*, 8:13918, 2017. URL https://doi.org/10.1038/ncomms13918.

[6] L. Xiao, X. Zhan, Z. H. Bian, K. K. Wang, X. Zhang, X. P. Wang, J. Li, K. Mochizuki, D. Kim, N. Kawakami, W. Yi, H. Obuse, B. C. Sanders, and P. Xue. Observation of topological edge states in parity–time-symmetric quantum walks. *Nature Physics*, 13:1117–1123, 2017. URL https://doi.org/10.1038/nphys4204.

[7] Chao Chen, Xing Ding, Jian Qin, Yu He, Yi-Han Luo, Ming-Cheng Chen, Chang Liu, Xi-Lin Wang, Wei-Jun Zhang, Hao Li, Li-Xing You, Zhen Wang, Da-Wei Wang, Barry C. Sanders, Chao-Yang Lu, and Jian-Wei Pan. Observation of topologically protected edge states in a photonic two-dimensional quantum walk. *Phys. Rev. Lett.*, 121:100502, 2018. URL https://link.aps.org/doi/10.1103/PhysRevLett.121.100502.

[8] Michael A. Nielsen and Isaac L. Chuang. *Quantum Computation and Quantum Information, 10th Anniversary Edition*. Cambridge University Press, 2010.

[9] T. D. Ladd, F. Jelezko, R. Laflamme, Y. Nakamura, C. Monroe, and J. L. O'Brien. Quantum computers. *Nature*, 464:45–53, 2010. URL https://doi.org/10.1038/nature08812.

[10] Morten Kjaergaard, Mollie E. Schwartz, Jochen Braumüller, Philip Krantz, Joel I. J. Wang, Simon Gustavsson, and William D. Oliver. Superconducting qubits: Current state of play. *Annual Review of Condensed Matter Physics*, 11:369–395, 2020. URL https://doi.org/10.1146/annurev-conmatphys-031119-050605.

[11] Takuya Kitagawa, Erez Berg, Mark Rudner, and Eugene Demler. Topological characterization of periodically driven quantum systems. *Phys. Rev. B*, 82:235114, 2010. URL https://link.aps.org/doi/10.1103/PhysRevB.82.235114.

[12] B. Andrei Bernevig. *Topological Insulators and Topological Superconductors*. Princeton University Press, 2013.

[13] Mark S. Rudner, Netanel H. Lindner, Erez Berg, and Michael Levin. Anomalous edge states and the bulk-edge correspondence for periodically driven two-dimensional systems. *Phys. Rev. X*, 3:031005, 2013. URL https://link.aps.org/doi/10.1103/PhysRevX.3.031005.

[14] Liang Jiang, Takuya Kitagawa, Jason Alicea, A. R. Akhmerov, David Pekker, Gil Refael, J. Ignacio Cirac, Eugene Demler, Mikhail D. Lukin, and Peter Zoller. Majorana fermions in equilibrium and in driven cold-atom quantum wires. *Phys. Rev. Lett.*, 106:220402, 2011. URL https://link.aps.org/doi/10.1103/PhysRevLett.106.220402.

[15] Masaya Nakagawa, Robert-Jan Slager, Sho Higashikawa, and Takashi Oka. Wannier representation of floquet topological states. *Phys. Rev. B*, 101:075108, 2020. URL https://link.aps.org/doi/10.1103/PhysRevB.101.075108.

[16] Krzysztof Sacha. Modeling spontaneous breaking of time-translation symmetry. *Phys. Rev. A*, 91:033617, 2015. URL https://link.aps.org/doi/10.1103/PhysRevA.91.033617.

[17] Haruki Watanabe and Masaki Oshikawa. Absence of quantum time crystals. *Phys. Rev. Lett.*, 114:251603, 2015. URL https://link.aps.org/doi/10.1103/PhysRevLett.114.251603.

[18] Takahiro Morimoto, Hoi Chun Po, and Ashvin Vishwanath. Floquet topological phases protected by time glide symmetry. *Phys. Rev. B*, 95:195155, 2017. URL https://link.aps.org/doi/10.1103/PhysRevB.95.195155.

[19] Ken Mochizuki, Takumi Bessho, Masatoshi Sato, and Hideaki Obuse. Topological quantum walk with discrete time-glide symmetry. *Phys. Rev. B*, 102:035418, 2020. URL https://link.aps.org/doi/10.1103/PhysRevB.102.035418.

[20] Ofer Neufeld, Daniel Podolsky, and Oren Cohen. Floquet group theory and its application to selection rules in harmonic generation. *Nature Communications*, 10:405, 2019. URL https://doi.org/10.1038/s41467-018-07935-y.

[21] Kohei Nagai, Kento Uchida, Naotaka Yoshikawa, Takahiko Endo, Yasumitsu Miyata, and Koichiro Tanaka. Dynamical symmetry of strongly light-driven electronic system in crystalline solids. *Communications Physics*, 3:137, 2020. URL https://doi.org/10.1038/s42005-020-00399-x.

[22] J. Struck, C. Ölschläger, M. Weinberg, P. Hauke, J. Simonet, A. Eckardt, M. Lewenstein, K. Sengstock, and P. Windpassinger. Tunable gauge potential for neutral and spinless particles in driven optical lattices. *Phys. Rev. Lett.*, 108:225304, 2012. URL https://link.aps.org/doi/10.1103/PhysRevLett.108.225304.

[23] Gregor Jotzu, Michael Messer, Rémi Desbuquois, Martin Lebrat, Thomas Uehlinger, Daniel Greif, and Tilman Esslinger. Experimental realization of the topological haldane model with ultracold fermions. *Nature*, 515:237–240, 2014. URL https://doi.org/10.1038/nature13915.

[24] Takashi Oka and Hideo Aoki. Photovoltaic hall effect in graphene. *Phys. Rev. B*, 79:081406, 2009. URL https://link.aps.org/doi/10.1103/PhysRevB.79.081406.

[25] Kazuaki Takasan, Akito Daido, Norio Kawakami, and Youichi Yanase. Laser-induced topological superconductivity in cuprate thin films. *Phys. Rev. B*, 95:134508, 2017. URL https://link.aps.org/doi/10.1103/PhysRevB.95.134508.

[26] Hiroomi Chono, Kazuaki Takasan, and Youichi Yanase. Laser-induced topological s-wave superconductivity in bilayer transition metal dichalcogenides. *Phys. Rev. B*, 102:174508, 2020. URL https://link.aps.org/doi/10.1103/PhysRevB.102.174508.

[27] I Bialynicki-Birula, B Mielnik, and J Plebański. Explicit solution of the continuous baker-campbell-hausdorff problem and a new expression for the phase operator. *Annals of Physics*, 51:187–200, 1969. URL https://www.sciencedirect.com/science/article/pii/0003491669903510.

[28] Tomotaka Kuwahara, Takashi Mori, and Keiji Saito. Floquet–magnus theory and generic transient dynamics in periodically driven many-body quantum systems. *Annals of Physics*, 367:96–124, 2016. URL https://www.sciencedirect.com/science/article/pii/S0003491616000142.

[29] Takahiro Mikami, Sota Kitamura, Kenji Yasuda, Naoto Tsuji, Takashi Oka, and Hideo Aoki. Brillouin-wigner theory for high-frequency expansion in periodically driven systems: Application to floquet topological insulators. *Phys. Rev. B*, 93:144307, 2016. URL https://link.aps.org/doi/10.1103/PhysRevB.93.144307.

[30] Tierry Giamarchi. *Quantum Physics in One Dimension*. Clarendon Press, Oxford, 2003.

[31] Naoto Shiraishi. Proof of the absence of local conserved quantities in the XYZ chain with a magnetic field. *EPL (Europhysics Letters)*, 128:17002, 2019. URL https://doi.org/10.1209/0295-5075/128/17002.

[32] Vadim Oganesyan and David A. Huse. Localization of interacting fermions at high temperature. *Phys. Rev. B*, 75:155111, 2007. URL https://link.aps.org/doi/10.1103/PhysRevB.75.155111.

[33] Y. Y. Atas, E. Bogomolny, O. Giraud, and G. Roux. Distribution of the ratio of consecutive level spacings in random matrix ensembles. *Phys. Rev. Lett.*, 110:084101, 2013. URL https://link.aps.org/doi/10.1103/PhysRevLett.110.084101.

[34] J. M. Deutsch. Quantum statistical mechanics in a closed system. *Phys. Rev. A*, 43:2046–2049, 1991. URL https://link.aps.org/doi/10.1103/PhysRevA.43.2046.

[35] Mark Srednicki. Chaos and quantum thermalization. *Phys. Rev. E*, 50:888–901, 1994. URL https://link.aps.org/doi/10.1103/PhysRevE.50.888.

[36] Marcos Rigol, Vanja Dunjko, and Maxim Olshanii. Thermalization and its mechanism for generic isolated quantum systems. *Nature*, 452:854–858, 2008. URL https://doi.org/10.1038/nature06838.

[37] S. Trotzky, Y-A. Chen, A. Flesch, I. P. McCulloch, U. Schollwöck, J. Eisert, and I. Bloch. Probing the relaxation towards equilibrium in an isolated strongly correlated one-dimensional bose gas. *Nature Physics*, 8:325–330, 2012. URL https://doi.org/10.1038/nphys2232.

[38] Adam M. Kaufman, M. Eric Tai, Alexander Lukin, Matthew Rispoli, Robert Schittko, Philipp M. Preiss, and Markus Greiner. Quantum thermalization through entanglement in an isolated many-body system. *Science*, 353:794–800, 2016. URL https://science.sciencemag.org/content/353/6301/794.

[39] Luca D'Alessio, Yariv Kafri, Anatoli Polkovnikov, and Marcos Rigol. From quantum chaos and eigenstate thermalization to statistical mechanics and thermodynamics. *Advances in Physics*, 65:239–362, 2016. URL https://doi.org/10.1080/00018732.2016.1198134.

[40] Takashi Mori, Tatsuhiko N Ikeda, Eriko Kaminishi, and Masahito Ueda. Thermalization and prethermalization in isolated quantum systems: a theoretical overview. *Journal of Physics B: Atomic, Molecular and Optical Physics*, 51:112001, 2018. URL https://doi.org/10.1088/1361-6455/aabcdf.

[41] J. M. Deutsch. Eigenstate thermalization hypothesis. *Rep. Prog. Phys.*, 80:082001, 2018. URL https://doi.org/10.1088/1361-6633/aac9f1.

[42] Giulio Biroli, Corinna Kollath, and Andreas M. Läuchli. Effect of rare fluctuations on the thermalization of isolated quantum systems. *Phys. Rev. Lett.*, 105:250401, 2010. URL https://link.aps.org/doi/10.1103/PhysRevLett.105.250401.

[43] Eiki Iyoda, Kazuya Kaneko, and Takahiro Sagawa. Fluctuation theorem for many-body pure quantum states. *Phys. Rev. Lett.*, 119:100601, 2017. URL https://link.aps.org/doi/10.1103/PhysRevLett.119.100601.

[44] Hyungwon Kim and David A. Huse. Ballistic spreading of entanglement in a diffusive nonintegrable system. *Phys. Rev. Lett.*, 111:127205, 2013. URL https://link.aps.org/doi/10.1103/PhysRevLett.111.127205.

[45] Hannes Bernien, Sylvain Schwartz, Alexander Keesling, Harry Levine, Ahmed Omran, Hannes Pichler, Soonwon Choi, Alexander S. Zibrov, Manuel Endres, Markus Greiner, Vladan Vuletić, and Mikhail D. Lukin. Probing many-body dynamics on a 51-atom quantum simulator. *Nature*, 551:579–584, 2017. URL https://doi.org/10.1038/nature24622.

[46] C. J. Turner, A. A. Michailidis, D. A. Abanin, M. Serbyn, and Z. Papić. Weak ergodicity breaking from quantum many-body scars. *Nature Physics*, 14:745–749, 2018. URL https://doi.org/10.1038/s41567-018-0137-5.

[47] Cheng-Ju Lin and Olexei I. Motrunich. Exact quantum many-body scar states in the rydberg-blockaded atom chain. *Phys. Rev. Lett.*, 122:173401, 2019. URL https://link.aps.org/doi/10.1103/PhysRevLett.122.173401.

[48] Wen Wei Ho, Soonwon Choi, Hannes Pichler, and Mikhail D. Lukin. Periodic orbits, entanglement, and quantum many-body scars in constrained models: Matrix product state approach. *Phys. Rev. Lett.*, 122:040603, 2019. URL https://link.aps.org/doi/10.1103/PhysRevLett.122.040603.

[49] Maksym Serbyn, Dmitry A. Abanin, and Zlatko Papić. Quantum many-body scars and weak breaking of ergodicity. *Nature Physics*, 17:675–685, 2021. URL https://doi.org/10.1038/s41567-021-01230-2.

[50] Sanjay Moudgalya, B. Andrei Bernevig, and Nicolas Regnault. Quantum many-body scars and hilbert space fragmentation: A review of exact results, 2021. URL https://arxiv.org/abs/2109.00548.

[51] Naoto Shiraishi and Takashi Mori. Systematic construction of counterexamples to the eigenstate thermalization hypothesis. *Phys. Rev. Lett.*, 119:030601, 2017. URL https://link.aps.org/doi/10.1103/PhysRevLett.119.030601.

[52] Sanjay Moudgalya, Stephan Rachel, B. Andrei Bernevig, and Nicolas Regnault. Exact excited states of nonintegrable models. *Phys. Rev. B*, 98:235155, 2018. URL https://link.aps.org/doi/10.1103/PhysRevB.98.235155.

[53] Pablo Sala, Tibor Rakovszky, Ruben Verresen, Michael Knap, and Frank Pollmann. Ergodicity breaking arising from hilbert space fragmentation in dipole-conserving hamiltonians. *Phys. Rev. X*, 10:011047, 2020. URL https://link.aps.org/doi/10.1103/PhysRevX.10.011047.

[54] Vedika Khemani, Michael Hermele, and Rahul Nandkishore. Localization from hilbert space shattering: From theory to physical realizations. *Phys. Rev. B*, 101:174204, 2020. URL https://link.aps.org/doi/10.1103/PhysRevB.101.174204.

[55] Luca D'Alessio and Marcos Rigol. Long-time behavior of isolated periodically driven interacting lattice systems. *Phys. Rev. X*, 4:041048, 2014. URL https://link.aps.org/doi/10.1103/PhysRevX.4.041048.

[56] Achilleas Lazarides, Arnab Das, and Roderich Moessner. Equilibrium states of generic quantum systems subject to periodic driving. *Phys. Rev. E*, 90:012110, 2014. URL https://link.aps.org/doi/10.1103/PhysRevE.90.012110.

[57] Pedro Ponte, Anushya Chandran, Z. Papić, and Dmitry A. Abanin. Periodically driven ergodic and many-body localized quantum systems. *Annals of Physics*, 353:196–204, 2015. doi: https://doi.org/10.1016/j.aop.2014.11.008. URL https://www.sciencedirect.com/science/article/pii/S0003491614003212.

[58] Bruno Bertini, Pavel Kos, and Toma ž Prosen. Exact spectral form factor in a minimal model of many-body quantum chaos. *Phys. Rev. Lett.*, 121:264101, 2018. URL https://link.aps.org/doi/10.1103/PhysRevLett.121.264101.

[59] Bruno Bertini, Pavel Kos, and Toma ž Prosen. Entanglement spreading in a minimal model of maximal many-body quantum chaos. *Phys. Rev. X*, 9:021033, 2019. URL https://link.aps.org/doi/10.1103/PhysRevX.9.021033.

[60] Bruno Bertini, Pavel Kos, and Toma ž Prosen. Exact correlation functions for dual-unitary lattice models in 1 + 1 dimensions. *Phys. Rev. Lett.*, 123:210601, 2019. URL https://link.aps.org/doi/10.1103/PhysRevLett.123.210601.

[61] Lorenzo Piroli, Bruno Bertini, J. Ignacio Cirac, and Toma ž Prosen. Exact dynamics in dual-unitary quantum circuits. *Phys. Rev. B*, 101:094304, 2020. URL https://link.aps.org/doi/10.1103/PhysRevB.101.094304.

[62] Ryotaro Suzuki, Kosuke Mitarai, and Keisuke Fujii. Computational power of one- and two-dimensional dual-unitary quantum circuits. arXiv:2103.09211, 2021. URL https://arxiv.org/abs/2103.09211.

[63] Felix Fritzsch and Toma ž Prosen. Eigenstate thermalization in dual-unitary quantum circuits: Asymptotics of spectral functions. *Phys. Rev. E*, 103:062133, 2021. URL https://link.aps.org/doi/10.1103/PhysRevE.103.062133.

[64] Takashi Mori, Tomotaka Kuwahara, and Keiji Saito. Rigorous bound on energy absorption and generic relaxation in periodically driven quantum systems. *Phys. Rev. Lett.*, 116:120401, 2016. URL https://link.aps.org/doi/10.1103/PhysRevLett.116.120401.

[65] Dmitry A. Abanin, Wojciech De Roeck, Wen Wei Ho, and Fran çois Huveneers. Effective hamiltonians, prethermalization, and slow energy absorption in periodically driven many-body systems. *Phys. Rev. B*, 95:014112, 2017. URL https://link.aps.org/doi/10.1103/PhysRevB.95.014112.

[66] Dmitry Abanin, Wojciech De Roeck, Wen Wei Ho, and François Huveneers. A rigorous theory of many-body prethermalization for periodically driven and closed quantum systems. *Communications in Mathematical Physics*, 354:809–827, 2017. URL https://doi.org/10.1007/s00220-017-2930-x.

[67] D. H. Dunlap and V. M. Kenkre. Dynamic localization of a charged particle moving under the influence of an electric field. *Phys. Rev. B*, 34:3625–3633, 1986. URL https://link.aps.org/doi/10.1103/PhysRevB.34.3625.

[68] F. Grossmann, T. Dittrich, P. Jung, and P. Hänggi. Coherent destruction of tunneling. *Phys. Rev. Lett.*, 67:516–519, 1991. URL https://link.aps.org/doi/10.1103/PhysRevLett.67.516.

[69] Takahiro Ishikawa, Yuto Sagae, Yota Naitoh, Yohei Kawakami, Hirotake Itoh, Kaoru Yamamoto, Kyuya Yakushi, Hideo Kishida, Takahiko Sasaki, Sumio Ishihara, Yasuhiro Tanaka, Kenji Yonemitsu, and Shinichiro Iwai. Optical freezing of charge motion in an organic conductor. *Nature Communications*, 5:5528, 2014. URL https://doi.org/10.1038/ncomms6528.

[70] Takashi Oka and Sota Kitamura. Floquet engineering of quantum materials. *Annual Review of Condensed Matter Physics*, 10:387–408, 2019. URL https://doi.org/10.1146/annurev-conmatphys-031218-013423.

[71] Masahiro Sato, Shintaro Takayoshi, and Takashi Oka. Laser-driven multiferroics and ultrafast spin current generation. *Phys. Rev. Lett.*, 117:147202, 2016. URL https://link.aps.org/doi/10.1103/PhysRevLett.117.147202.

[72] Kazuaki Takasan, Masaya Nakagawa, and Norio Kawakami. Laser-irradiated kondo insulators: Controlling the kondo effect and topological phases. *Phys. Rev. B*, 96:115120, 2017. URL https://link.aps.org/doi/10.1103/PhysRevB.96.115120.

[73] Marko Žnidarič, Toma ž Prosen, and Peter Prelovšek. Many-body localization in the heisenberg *xxz* magnet in a random field. *Phys. Rev. B*, 77:064426, 2008. URL https://link.aps.org/doi/10.1103/PhysRevB.77.064426.

[74] Arijeet Pal and David A. Huse. Many-body localization phase transition. *Phys. Rev. B*, 82: 174411, 2010. URL https://link.aps.org/doi/10.1103/PhysRevB.82.174411.

[75] Schreiber Michael, Hodgman Sean S., Bordia Pranjal, Lüschen Henrik P., Fischer Mark H., Vosk Ronen, Altman Ehud, Schneider Ulrich, and Bloch Immanuel. Observation of many-body localization of interacting fermions in a quasirandom optical lattice. *Science*, 349: 842–845, 2015. URL https://doi.org/10.1126/science.aaa7432.

[76] J. Smith, A. Lee, P. Richerme, B. Neyenhuis, P. W. Hess, P. Hauke, M. Heyl, D. A. Huse, and C. Monroe. Many-body localization in a quantum simulator with programmable random disorder. *Nature Physics*, 12(10):907–911, 2016. URL https://doi.org/10.1038/nphys3783.

[77] Fabien Alet and Nicolas Laflorencie. Many-body localization: An introduction and selected topics. *Comptes Rendus Physique*, 19(6):498–525, 2018. URL https://www.sciencedirect.com/science/article/pii/S163107051830032X.

[78] Dmitry A. Abanin, Ehud Altman, Immanuel Bloch, and Maksym Serbyn. Colloquium: Many-body localization, thermalization, and entanglement. *Rev. Mod. Phys.*, 91:021001, 2019. URL https://link.aps.org/doi/10.1103/RevModPhys.91.021001.

[79] Pedro Ponte, Z. Papić, Fran çois Huveneers, and Dmitry A. Abanin. Many-body localization in periodically driven systems. *Phys. Rev. Lett.*, 114:140401. doi: 10.1103/PhysRevLett.114.140401. URL https://link.aps.org/doi/10.1103/PhysRevLett.114.140401.

[80] Achilleas Lazarides, Arnab Das, and Roderich Moessner. Fate of many-body localization under periodic driving. *Phys. Rev. Lett.*, 115:030402, 2015. URL https://link.aps.org/doi/10.1103/PhysRevLett.115.030402.

[81] Dmitry A. Abanin, Wojciech De Roeck, and François Huveneers. Theory of many-body localization in periodically driven systems. *Annals of Physics*, 372:1–11, 2016. URL https://www.sciencedirect.com/science/article/pii/S000349161630001X.

[82] Pranjal Bordia, Henrik Lüschen, Ulrich Schneider, Michael Knap, and Immanuel Bloch. Periodically driving a many-body localized quantum system. *Nature Physics*, 13:460–464, 2017. URL https://doi.org/10.1038/nphys4020.

[83] Hoi Chun Po, Lukasz Fidkowski, Takahiro Morimoto, Andrew C. Potter, and Ashvin Vishwanath. Chiral floquet phases of many-body localized bosons. *Phys. Rev. X*, 6:041070, 2016. URL https://link.aps.org/doi/10.1103/PhysRevX.6.041070.

[84] Dominic V. Else and Chetan Nayak. Classification of topological phases in periodically driven interacting systems. *Phys. Rev. B*, 93:201103, 2016. URL https://link.aps.org/doi/10.1103/PhysRevB.93.201103.

[85] Andrew C. Potter, Takahiro Morimoto, and Ashvin Vishwanath. Classification of interacting topological floquet phases in one dimension. *Phys. Rev. X*, 6:041001, 2016. URL https://link.aps.org/doi/10.1103/PhysRevX.6.041001.

[86] C. W. von Keyserlingk and S. L. Sondhi. Phase structure of one-dimensional interacting floquet systems. i. abelian symmetry-protected topological phases. *Phys. Rev. B*, 93:245145, 2016. URL https://link.aps.org/doi/10.1103/PhysRevB.93.245145.

[87] Fenner Harper and Rahul Roy. Floquet topological order in interacting systems of bosons and fermions. *Phys. Rev. Lett.*, 118:115301, 2017. URL https://link.aps.org/doi/10.1103/PhysRevLett.118.115301.

[88] Frank Wilczek. Quantum time crystals. *Phys. Rev. Lett.*, 109:160401, 2012. URL https://link.aps.org/doi/10.1103/PhysRevLett.109.160401.

[89] Dominic V. Else, Bela Bauer, and Chetan Nayak. Floquet time crystals. *Phys. Rev. Lett.*, 117:090402, 2016. URL https://link.aps.org/doi/10.1103/PhysRevLett.117.090402.

[90] C. W. von Keyserlingk and S. L. Sondhi. Phase structure of one-dimensional interacting floquet systems. ii. symmetry-broken phases. *Phys. Rev. B*, 93:245146, 2016. URL https://link.aps.org/doi/10.1103/PhysRevB.93.245146.

[91] Vedika Khemani, Achilleas Lazarides, Roderich Moessner, and S. L. Sondhi. Phase structure of driven quantum systems. *Phys. Rev. Lett.*, 116:250401, 2016. URL https://link.aps.org/doi/10.1103/PhysRevLett.116.250401.

[92] C. W. von Keyserlingk, Vedika Khemani, and S. L. Sondhi. Absolute stability and spatiotemporal long-range order in floquet systems. *Phys. Rev. B*, 94:085112, 2016. URL https://link.aps.org/doi/10.1103/PhysRevB.94.085112.

[93] Vedika Khemani, C. W. von Keyserlingk, and S. L. Sondhi. Defining time crystals via representation theory. *Phys. Rev. B*, 96:115127, 2017. URL https://link.aps.org/doi/10.1103/PhysRevB.96.115127.

[94] N. Y. Yao, A. C. Potter, I.-D. Potirniche, and A. Vishwanath. Discrete time crystals: Rigidity, criticality, and realizations. *Phys. Rev. Lett.*, 118:030401, 2017. URL https://link.aps.org/doi/10.1103/PhysRevLett.118.030401.

[95] J. Zhang, P. W. Hess, A. Kyprianidis, P. Becker, A. Lee, J. Smith, G. Pagano, I. D. Potirniche, A. C. Potter, A. Vishwanath, N. Y. Yao, and C. Monroe. Observation of a discrete time crystal. *Nature*, 543(7644):217–220, 2017. URL https://doi.org/10.1038/nature21413.

[96] Soonwon Choi, Joonhee Choi, Renate Landig, Georg Kucsko, Hengyun Zhou, Junichi Isoya, Fedor Jelezko, Shinobu Onoda, Hitoshi Sumiya, Vedika Khemani, Curt von Keyserlingk, Norman Y. Yao, Eugene Demler, and Mikhail D. Lukin. Observation of discrete time-crystalline order in a disordered dipolar many-body system. *Nature*, 543:221–225, 2017. URL https://doi.org/10.1038/nature21426.

[97] Krzysztof Sacha and Jakub Zakrzewski. Time crystals: a review. *Reports on Progress in Physics*, 81:016401, nov 2017. URL https://doi.org/10.1088/1361-6633/aa8b38.

[98] Vedika Khemani, Roderich Moessner, and S. L. Sondhi. A brief history of time crystals. arXiv:1910.10745, 2019. URL https://arxiv.org/abs/1910.10745.

[99] Dominic V. Else, Christopher Monroe, Chetan Nayak, and Norman Y. Yao. Discrete time crystals. *Annual Review of Condensed Matter Physics*, 11:467–499, 2020. URL https://doi.org/10.1146/annurev-conmatphys-031119-050658.

[100] Jared Rovny, Robert L. Blum, and Sean E. Barrett. Observation of discrete-time-crystal signatures in an ordered dipolar many-body system. *Phys. Rev. Lett.*, 120:180603, 2018. URL https://link.aps.org/doi/10.1103/PhysRevLett.120.180603.

[101] Jared Rovny, Robert L. Blum, and Sean E. Barrett. ^{31}P nmr study of discrete time-crystalline signatures in an ordered crystal of ammonium dihydrogen phosphate. *Phys. Rev. B*, 97: 184301, 2018. URL https://link.aps.org/doi/10.1103/PhysRevB.97.184301.

[102] Wen Wei Ho, Soonwon Choi, Mikhail D. Lukin, and Dmitry A. Abanin. Critical time crystals in dipolar systems. *Phys. Rev. Lett.*, 119:010602, 2017. URL https://link.aps.org/doi/10.1103/PhysRevLett.119.010602.

[103] Matteo Ippoliti, Kostyantyn Kechedzhi, Roderich Moessner, S.L. Sondhi, and Vedika Khemani. Many-body physics in the nisq era: Quantum programming a discrete time crystal. *PRX Quantum*, 2:030346, 2021. URL https://link.aps.org/doi/10.1103/PRXQuantum.2.030346.

[104] Philipp Frey and Stephan Rachel. Simulating a discrete time crystal over 57 qubits on a quantum computer. arXiv:2105.06632, 2021. URL https://arxiv.org/abs/2105.06632.

[105] Xiao Mi, Matteo Ippoliti, Chris Quintana, Ami Greene, Zijun Chen, Jonathan Gross, Frank Arute, Kunal Arya, Juan Atalaya, Ryan Babbush, Joseph C. Bardin, Joao Basso, Andreas Bengtsson, Alexander Bilmes, Alexandre Bourassa, Leon Brill, Michael Broughton, Bob B. Buckley, David A. Buell, Brian Burkett, Nicholas Bushnell, Benjamin Chiaro, Roberto Collins, William Courtney, Dripto Debroy, Sean Demura, Alan R. Derk, Andrew Dunsworth, Daniel Eppens, Catherine Erickson, Edward Farhi, Austin G. Fowler, Brooks Foxen, Craig Gidney, Marissa Giustina, Matthew P. Harrigan, Sean D. Harrington, Jeremy Hilton, Alan Ho, Sabrina Hong, Trent Huang, Ashley Huff, William J. Huggins, L. B. Ioffe, Sergei V. Isakov, Justin Iveland, Evan Jeffrey, Zhang Jiang, Cody Jones, Dvir Kafri, Tanuj Khattar, Seon Kim, Alexei Kitaev, Paul V. Klimov, Alexander N. Korotkov, Fedor Kostritsa, David Landhuis, Pavel Laptev, Joonho Lee, Kenny Lee, Aditya Locharla, Erik Lucero, Orion Martin, Jarrod R. McClean, Trevor McCourt, Matt McEwen, Kevin C. Miao, Masoud Mohseni, Shirin Montazeri, Wojciech Mruczkiewicz, Ofer Naaman, Matthew Neeley, Charles Neill, Michael Newman, Murphy Yuezhen Niu, Thomas E. O'Brien, Alex Opremcak, Eric Ostby, Balint Pato, Andre Petukhov, Nicholas C. Rubin, Daniel Sank, Kevin J. Satzinger, Vladimir Shvarts, Yuan Su, Doug Strain, Marco Szalay, Matthew D. Trevithick, Benjamin Villalonga, Theodore White, Z. Jamie Yao, Ping Yeh, Juhwan Yoo, Adam Zalcman, Hartmut Neven, Sergio Boixo, Vadim Smelyanskiy, Anthony Megrant, Julian Kelly, Yu Chen, S. L. Sondhi, Roderich Moessner, Kostyantyn Kechedzhi, Vedika Khemani, and Pedram Roushan. Time-crystalline eigenstate order on a quantum processor. *Nature*, 2021. URL `https://doi.org/10.1038/s41586-021-04257-w`.

[106] Huikai Xu, Jingning Zhang, Jiaxiu Han, Zhiyuan Li, Guangming Xue, Weiyang Liu, Yirong Jin, and Haifeng Yu. Realizing discrete time crystal in an one-dimensional superconducting qubit chain. arXiv:2108.00942, 2021. URL `https://arxiv.org/abs/2108.00942`.

[107] J. Randall, C. E. Bradley, F. V. van der Gronden, A. Galicia, M. H. Abobeih, M. Markham, D. J. Twitchen, F. Machado, N. Y. Yao, and T. H. Taminiau. Many-body localized discrete time crystal with a programmable spin-based quantum simulator. *Science*, 374(6574):1474–1478, 2021. URL `https://www.science.org/doi/abs/10.1126/science.abk0603`.

[108] Paraj Titum, Erez Berg, Mark S. Rudner, Gil Refael, and Netanel H. Lindner. Anomalous floquet-anderson insulator as a nonadiabatic quantized charge pump. *Phys. Rev. X*, 6:021013, 2016. URL `https://link.aps.org/doi/10.1103/PhysRevX.6.021013`.

[109] A Quelle, C Weitenberg, K Sengstock, and C Morais Smith. Driving protocol for a floquet topological phase without static counterpart. *New Journal of Physics*, 19:113010, 2017. doi: 10.1088/1367-2630/aa8646. URL `https://doi.org/10.1088/1367-2630/aa8646`.

[110] Guifré Vidal. Efficient classical simulation of slightly entangled quantum computations. *Phys. Rev. Lett.*, 91:147902, 2003. URL `https://link.aps.org/doi/10.1103/PhysRevLett.91.147902`.

[111] Guifré Vidal. Efficient simulation of one-dimensional quantum many-body systems. *Phys. Rev. Lett.*, 93:040502, 2004. URL `https://link.aps.org/doi/10.1103/PhysRevLett.93.040502`.

[112] U. Schollwöck. The density-matrix renormalization group. *Rev. Mod. Phys.*, 77:259–315, 2005. URL `https://link.aps.org/doi/10.1103/RevModPhys.77.259`.

[113] Lorenza Viola, Emanuel Knill, and Seth Lloyd. Dynamical decoupling of open quantum systems. *Phys. Rev. Lett.*, 82:2417–2421, 1999. URL `https://link.aps.org/doi/10.1103/PhysRevLett.82.2417`.

[114] P. Jordan and E. Wigner. Über das paulische äquivalenzverbot. *Zeitschrift für Physik*, 47: 631–651, 1928. URL `https://doi.org/10.1007/BF01331938`.

[115] Dominic V. Else, Bela Bauer, and Chetan Nayak. Prethermal phases of matter protected by time-translation symmetry. *Phys. Rev. X*, 7:011026, 2017. URL `https://link.aps.org/doi/10.1103/PhysRevX.7.011026`.

[116] Francisco Machado, Gregory D. Kahanamoku-Meyer, Dominic V. Else, Chetan Nayak, and Norman Y. Yao. Exponentially slow heating in short and long-range interacting floquet systems. *Phys. Rev. Research*, 1:033202, 2019. URL https://link.aps.org/doi/10.1103/PhysRevResearch.1.033202.

[117] Francisco Machado, Dominic V. Else, Gregory D. Kahanamoku-Meyer, Chetan Nayak, and Norman Y. Yao. Long-range prethermal phases of nonequilibrium matter. *Phys. Rev. X*, 10: 011043, 2020. URL https://link.aps.org/doi/10.1103/PhysRevX.10.011043.

[118] Dominic V. Else, Wen Wei Ho, and Philipp T. Dumitrescu. Long-lived interacting phases of matter protected by multiple time-translation symmetries in quasiperiodically driven systems. *Phys. Rev. X*, 10:021032, 2020. URL https://link.aps.org/doi/10.1103/PhysRevX.10.021032.

[119] Philipp T. Dumitrescu, Romain Vasseur, and Andrew C. Potter. Logarithmically slow relaxation in quasiperiodically driven random spin chains. *Phys. Rev. Lett.*, 120:070602, 2018. URL https://link.aps.org/doi/10.1103/PhysRevLett.120.070602.

[120] Hongzheng Zhao, Florian Mintert, Roderich Moessner, and Johannes Knolle. Random multipolar driving: Tunably slow heating through spectral engineering. *Phys. Rev. Lett.*, 126: 040601, 2021. URL https://link.aps.org/doi/10.1103/PhysRevLett.126.040601.

[121] Takashi Mori, Hongzheng Zhao, Florian Mintert, Johannes Knolle, and Roderich Moessner. Rigorous bounds on the heating rate in thue-morse quasiperiodically and randomly driven quantum many-body systems. *Phys. Rev. Lett.*, 127:050602, 2021. URL https://link.aps.org/doi/10.1103/PhysRevLett.127.050602.

[122] Antonio Rubio-Abadal, Matteo Ippoliti, Simon Hollerith, David Wei, Jun Rui, S. L. Sondhi, Vedika Khemani, Christian Gross, and Immanuel Bloch. Floquet prethermalization in a bose-hubbard system. *Phys. Rev. X*, 10:021044, 2020. URL https://link.aps.org/doi/10.1103/PhysRevX.10.021044.

[123] Pai Peng, Chao Yin, Xiaoyang Huang, Chandrasekhar Ramanathan, and Paola Cappellaro. Floquet prethermalization in dipolar spin chains. *Nature Physics*, 17:444–447, 2021. URL https://doi.org/10.1038/s41567-020-01120-z.

[124] A. Kyprianidis, F. Machado, W. Morong, P. Becker, K. S. Collins, D. V. Else, L. Feng, P. W. Hess, C. Nayak, G. Pagano, N. Y. Yao, and C. Monroe. Observation of a prethermal discrete time crystal. *Science*, 372:1192–1196, 2021. URL https://www.science.org/doi/abs/10.1126/science.abg8102.

[125] Thomas Iadecola, Luiz H. Santos, and Claudio Chamon. Stroboscopic symmetry-protected topological phases. *Phys. Rev. B*, 92:125107, 2015. URL https://link.aps.org/doi/10.1103/PhysRevB.92.125107.

[126] I.-D. Potirniche, A. C. Potter, M. Schleier-Smith, A. Vishwanath, and N. Y. Yao. Floquet symmetry-protected topological phases in cold-atom systems. *Phys. Rev. Lett.*, 119:123601, 2017. URL https://link.aps.org/doi/10.1103/PhysRevLett.119.123601.

[127] Joonhee Choi, Hengyun Zhou, Helena S. Knowles, Renate Landig, Soonwon Choi, and Mikhail D. Lukin. Robust dynamic hamiltonian engineering of many-body spin systems. *Phys. Rev. X*, 10:031002, 2020. URL https://link.aps.org/doi/10.1103/PhysRevX.10.031002.

[128] Hengyun Zhou, Joonhee Choi, Soonwon Choi, Renate Landig, Alexander M. Douglas, Junichi Isoya, Fedor Jelezko, Shinobu Onoda, Hitoshi Sumiya, Paola Cappellaro, Helena S. Knowles, Hongkun Park, and Mikhail D. Lukin. Quantum metrology with strongly interacting spin systems. *Phys. Rev. X*, 10:031003, 2020. URL https://link.aps.org/doi/10.1103/PhysRevX.10.031003.

[129] Kartiek Agarwal and Ivar Martin. Dynamical enhancement of symmetries in many-body systems. *Phys. Rev. Lett.*, 125:080602, 2020. URL https://link.aps.org/doi/10.1103/PhysRevLett.125.080602.

[130] Vittorio Gorini, Andrzej Kossakowski, and E. C. G. Sudarshan. Completely positive dynamical semigroups of n-level systems. *Journal of Mathematical Physics*, 17:821–825, 1976. URL https://aip.scitation.org/doi/abs/10.1063/1.522979.

[131] G. Lindblad. On the generators of quantum dynamical semigroups. *Communications in Mathematical Physics*, 48:119, 1976. URL https://doi.org/10.1007/BF01608499.

[132] Heinz-Peter Breuer and Francesco Petruccione. *The Theory of Open Quantum Systems*. Oxford University Press, Oxford, 2002.

[133] Angel Rivas and Susana F. Huelga. *Open Quantum Systems An Introduction*. Springer, Berlin, Heidelberg, 2012.

[134] Sigmund Kohler, Thomas Dittrich, and Peter Hänggi. Floquet-markovian description of the parametrically driven, dissipative harmonic quantum oscillator. *Phys. Rev. E*, 55:300–313, 1997. URL https://link.aps.org/doi/10.1103/PhysRevE.55.300.

[135] Frederik Nathan and Mark S. Rudner. Universal lindblad equation for open quantum systems. *Phys. Rev. B*, 102:115109, 2020. URL https://link.aps.org/doi/10.1103/PhysRevB.102.115109.

[136] Tatsuhiko N. Ikeda, Koki Chinzei, and Masahiro Sato. Nonequilibrium steady states in the floquet-lindblad systems: van vleck's high-frequency expansion approach. arXiv:2107.07911, 2021. URL https://arxiv.org/abs/2107.07911.

[137] Jiaming Li, Andrew K. Harter, Ji Liu, Leonardo de Melo, Yogesh N. Joglekar, and Le Luo. Observation of parity-time symmetry breaking transitions in a dissipative floquet system of ultracold atoms. *Nature Communications*, 10:855, 2019. URL https://doi.org/10.1038/s41467-019-08596-1.

[138] Hans Keßler, Phatthamon Kongkhambut, Christoph Georges, Ludwig Mathey, Jayson G. Cosme, and Andreas Hemmerich. Observation of a dissipative time crystal. *Phys. Rev. Lett.*, 127:043602, 2021. URL https://link.aps.org/doi/10.1103/PhysRevLett.127.043602.

[139] Tomaz Prosen and Enej Ilievski. Nonequilibrium phase transition in a periodically driven *xy* spin chain. *Phys. Rev. Lett.*, 107:060403, 2011. URL https://link.aps.org/doi/10.1103/PhysRevLett.107.060403.

[140] M Hartmann, D Poletti, M Ivanchenko, S Denisov, and P Hanggi. Asymptotic floquet states of open quantum systems: the role of interaction. *New J. Phys.*, 19:083011, 2017. URL https://iopscience.iop.org/article/10.1088/1367-2630/aa7ceb/meta.

[141] Stefano Scopa, Gabriel T. Landi, and Dragi Karevski. Lindblad-floquet description of finite-time quantum heat engines. *Phys. Rev. A*, 97:062121, 2018. URL https://link.aps.org/doi/10.1103/PhysRevA.97.062121.

[142] Stefano Scopa, Gabriel T. Landi, Adam Hammoumi, and Dragi Karevski. Exact solution of time-dependent lindblad equations with closed algebras. *Phys. Rev. A*, 99:022105, 2019. URL https://link.aps.org/doi/10.1103/PhysRevA.99.022105.

[143] Zongping Gong, Ryusuke Hamazaki, and Masahito Ueda. Discrete time-crystalline order in cavity and circuit qed systems. *Phys. Rev. Lett.*, 120:040404, 2018. URL https://link.aps.org/doi/10.1103/PhysRevLett.120.040404.

[144] F. M. Gambetta, F. Carollo, M. Marcuzzi, J. P. Garrahan, and I. Lesanovsky. Discrete time crystals in the absence of manifest symmetries or disorder in open quantum systems. *Phys. Rev. Lett.*, 122:015701, 2019. URL https://link.aps.org/doi/10.1103/PhysRevLett.122.015701.

[145] Bihui Zhu, Jamir Marino, Norman Y Yao, Mikhail D Lukin, and Eugene A Demler. Dicke time crystals in driven-dissipative quantum many-body systems. *New Journal of Physics*, 21:073028, 2019. URL https://doi.org/10.1088/1367-2630/ab2afe.

[146] Achilleas Lazarides, Sthitadhi Roy, Francesco Piazza, and Roderich Moessner. Time crystallinity in dissipative floquet systems. *Phys. Rev. Research*, 2:022002, 2020. URL https://link.aps.org/doi/10.1103/PhysRevResearch.2.022002.

[147] Andreu Riera-Campeny, Maria Moreno-Cardoner, and Anna Sanpera. Time crystallinity in open quantum systems. *Quantum*, 4:270, 2020. URL http://dx.doi.org/10.22331/q-2020-05-25-270.

[148] Koki Chinzei and Tatsuhiko N. Ikeda. Time crystals protected by floquet dynamical symmetry in hubbard models. *Phys. Rev. Lett.*, 125:060601, 2020. URL https://link.aps.org/doi/10.1103/PhysRevLett.125.060601.

[149] C. M. Dai, Z. C. Shi, and X. X. Yi. Floquet theorem with open systems and its applications. *Phys. Rev. A*, 93:032121, 2016. URL https://link.aps.org/doi/10.1103/PhysRevA.93.032121.

[150] Tatsuhiko N. Ikeda and Masahiro Sato. General description for nonequilibrium steady states in periodically driven dissipative quantum systems. *Science Advances*, 6:eabb4019, 2020. URL https://advances.sciencemag.org/content/6/27/eabb4019.

[151] A Jamiołkowski. Linear transformations which preserve trace and positive semidefiniteness of operators. *Reports on Mathematical Physics*, 3:275, 1973. URL https://www.sciencedirect.com/science/article/pii/0034487772900110.

[152] Man-Duen Choi. Completely positive linear maps on complex matrices. *Linear Algebra and its Applications*, 10:285, 1975. URL https://www.sciencedirect.com/science/article/pii/0024379575900750.

[153] Krzysztof Szczygielski. On the floquet analysis of commutative periodic lindbladians in finite dimension. *Linear Algebra and its Applications*, 609:176–202, 2021. URL https://www.sciencedirect.com/science/article/pii/S0024379520304201.

[154] Farhang Haddadfarshi, Jian Cui, and Florian Mintert. Completely positive approximate solutions of driven open quantum systems. *Phys. Rev. Lett.*, 114:130402, 2015. URL https://link.aps.org/doi/10.1103/PhysRevLett.114.130402.

[155] F Zhang. *The Schur Complement and Its Applications*. Springer Science, New York, 2005.

[156] Alexander Schnell, André Eckardt, and Sergey Denisov. Is there a floquet lindbladian? *Phys. Rev. B*, 101:100301, 2020. URL https://link.aps.org/doi/10.1103/PhysRevB.101.100301.

[157] John de Pillis. Linear transformations which preserve hermitian and positive semidefinite operators. *Pac. J. Math.*, 23:129, 1967. URL https://msp.org/pjm/1967/23-1/p14.xhtml.

[158] Marin Bukov, Luca D'Alessio, and Anatoli Polkovnikov. Universal high-frequency behavior of periodically driven systems: from dynamical stabilization to floquet engineering. *Advances in Physics*, 64:139–226, 2015. URL https://doi.org/10.1080/00018732.2015.1055918.

[159] Andrew J. Daley. Quantum trajectories and open many-body quantum systems. *Advances in Physics*, 63:77–149, 2014. URL https://doi.org/10.1080/00018732.2014.933502.

[160] Yuto Ashida, Zongping Gong, and Masahito Ueda. Non-hermitian physics. *Advances in Physics*, 69:249–435, 2020. URL https://doi.org/10.1080/00018732.2021.1876991.

[161] M. Saffman, T. G. Walker, and K. Mølmer. Quantum information with rydberg atoms. *Rev. Mod. Phys.*, 82:2313–2363, 2010. URL https://link.aps.org/doi/10.1103/RevModPhys.82.2313.

[162] Antoine Browaeys and Thierry Lahaye. Many-body physics with individually controlled rydberg atoms. *Nature Physics*, 16:132–142, 2020. URL https://doi.org/10.1038/s41567-019-0733-z.

[163] Naoto Shiraishi. Connection between quantum-many-body scars and the affleck–kennedy–lieb–tasaki model from the viewpoint of embedded hamiltonians. *Journal of Statistical Mechanics: Theory and Experiment*, 2019:083103, 2019. doi: 10.1088/1742-5468/ab342e. URL https://doi.org/10.1088/1742-5468/ab342e.

[164] B. Kraus, H. P. Büchler, S. Diehl, A. Kantian, A. Micheli, and P. Zoller. Preparation of entangled states by quantum markov processes. *Phys. Rev. A*, 78:042307, 2008. URL https://link.aps.org/doi/10.1103/PhysRevA.78.042307.

[165] Yoshihito Kuno, Tomonari Mizoguchi, and Yasuhiro Hatsugai. Flat band quantum scar. *Phys. Rev. B*, 102:241115, 2020. URL https://link.aps.org/doi/10.1103/PhysRevB.102.241115.

[166] Federica Maria Surace, Giuliano Giudici, and Marcello Dalmonte. Weak-ergodicity-breaking via lattice supersymmetry. *Quantum*, 4:339, 2020. URL http://dx.doi.org/10.22331/q-2020-10-07-339.

[167] Sanjay Moudgalya, Nicolas Regnault, and B. Andrei Bernevig. Entanglement of exact excited states of affleck-kennedy-lieb-tasaki models: Exact results, many-body scars, and violation of the strong eigenstate thermalization hypothesis. *Phys. Rev. B*, 98:235156, 2018. URL https://link.aps.org/doi/10.1103/PhysRevB.98.235156.

[168] Michael Schecter and Thomas Iadecola. Weak ergodicity breaking and quantum many-body scars in spin-1 xy magnets. *Phys. Rev. Lett.*, 123:147201, 2019. URL https://link.aps.org/doi/10.1103/PhysRevLett.123.147201.

[169] Daniel K. Mark, Cheng-Ju Lin, and Olexei I. Motrunich. Unified structure for exact towers of scar states in the affleck-kennedy-lieb-tasaki and other models. *Phys. Rev. B*, 101:195131, 2020. URL https://link.aps.org/doi/10.1103/PhysRevB.101.195131.

[170] Thomas Iadecola and Michael Schecter. Quantum many-body scar states with emergent kinetic constraints and finite-entanglement revivals. *Phys. Rev. B*, 101:024306, 2020. URL https://link.aps.org/doi/10.1103/PhysRevB.101.024306.

[171] Naoyuki Shibata, Nobuyuki Yoshioka, and Hosho Katsura. Onsager's scars in disordered spin chains. *Phys. Rev. Lett.*, 124:180604, 2020. URL https://link.aps.org/doi/10.1103/PhysRevLett.124.180604.

[172] C. J. Turner, A. A. Michailidis, D. A. Abanin, M. Serbyn, and Z. Papić. Quantum scarred eigenstates in a rydberg atom chain: Entanglement, breakdown of thermalization, and stability to perturbations. *Phys. Rev. B*, 98:155134, 2018. URL https://link.aps.org/doi/10.1103/PhysRevB.98.155134.

[173] C. J. Turner, J.-Y. Desaules, K. Bull, and Z. Papić. Correspondence principle for many-body scars in ultracold rydberg atoms. *Phys. Rev. X*, 11:021021, 2021. URL https://link.aps.org/doi/10.1103/PhysRevX.11.021021.

[174] Bhaskar Mukherjee, Sourav Nandy, Arnab Sen, Diptiman Sen, and K. Sengupta. Collapse and revival of quantum many-body scars via floquet engineering. *Phys. Rev. B*, 101:245107, 2020. URL https://link.aps.org/doi/10.1103/PhysRevB.101.245107.

[175] Asmi Haldar, Diptiman Sen, Roderich Moessner, and Arnab Das. Dynamical freezing and scar points in strongly driven floquet matter: Resonance vs emergent conservation laws. *Phys. Rev. X*, 11:021008, 2021. URL https://link.aps.org/doi/10.1103/PhysRevX.11.021008.

[176] D. Bluvstein, A. Omran, H. Levine, A. Keesling, G. Semeghini, S. Ebadi, T. T. Wang, A. A. Michailidis, N. Maskara, W. W. Ho, S. Choi, M. Serbyn, M. Greiner, V. Vuletić, and M. D. Lukin. Controlling quantum many-body dynamics in driven rydberg atom arrays. *Science*, 371:1355–1359, 2021. URL https://science.sciencemag.org/content/371/6536/1355.

[177] Sho Sugiura, Tomotaka Kuwahara, and Keiji Saito. Many-body scar state intrinsic to periodically driven system. *Phys. Rev. Research*, 3:L012010, 2021. URL `https://link.aps.org/doi/10.1103/PhysRevResearch.3.L012010`.

[178] Shriya Pai and Michael Pretko. Dynamical scar states in driven fracton systems. *Phys. Rev. Lett.*, 123:136401, 2019. URL `https://link.aps.org/doi/10.1103/PhysRevLett.123.136401`.

Acknowledgments

First, I would like to express my gratitude to Prof. Norio Kawakami for his kind help during my master and doctoral courses. His support ranges from his insightful suggestions on physics to his advice on everyday life. His supervision is essential for the completion of my works so far.

I am grateful to Dr. Kazuaki Takasan, Dr. Ken Mochizuki, and Prof. Masaya Nakagawa for the collaboration in my studies on Floquet physics so far. They have deep insight into Floquet systems in terms of solid materials and artificial quantum systems, and the fruitful discussion with them stimulated me, leading to the motivations of my studies. I also thank Mr. Yoshihiro Michishita and Prof. Hosho Katsura for having discussion on dissipative quantum systems (Chapter 3) and quantum many-body scars (Chapter 4) respectively.

In terms of my daily life in Condensed Matter Theory group of Kyoto University, I would like to thank the staffs, Prof. Youichi Yanase, Prof. Ryusuke Ikeda, Prof. Robert Peters, Prof. Masaki Tezuka, and Prof. Akito Daido for their support. I have enjoyed various discussions on physics and other topics with my colleagues, Mr. Kazuhiro Kimura, Mr. Shota Kanasugi, Mr. Yoshihiro Michishita, Mr. Kenta Irikawa, Mr. Naoki Sakamoto, Mr. Taiki Matsushita, and all the other members in my group. I acknowledge the financial supports from JSPS Research Fellowship for Young Scientists (JSPS KAKENHI No. 2020J12930) and WISE program of MEXT.

Last bu not least, I would like to express my deepest gratitude to my family for their continuous support during my life from the birth to the present.